Full Scale Test of a SSP 34m box girder 1. Data report

Jensen, Find Mølholt; Branner, Kim; Nielsen, Per Hørlyk; Berring, Peter; Antvorskov, Troels Skieller; Nielsen, Magda; Lindahl, Morten Michael; Lund, Brian; Jensen, Christian; Reffs, Joan Højsholm Humble Ascanius

Total number of authors:
27

Publication date:
2008

Document Version
Publisher's PDF, also known as Version of record

RISØ

Risø-R-Report

Full Scale Test of a SSP 34m box girder 1. Data report

Find M. Jensen, Kim Branner, Per H. Nielsen,
Peter Berring, Troels S. Antvorskov, Magda Nielsen,
Morten Lindahl, Brian Lund, Christian Jensen,
Joan H. Reffs, Rune F. Nielsen, Peter H. Jensen
Risø DTU - Wind Energy Department

Malcolm McGugan, Kaj K. Borum
Risø DTU - Materials Research Department

Rene S. Hansen
Risø DTU - Optics and Plasma Research Department

Carsten Skamris
Blaest Test Center

Flemming Sørensen, Rune Schytt-Nielsen
SSP-Technology A/S

Jeppe H. Laursen, Marcus Klein
Zebicon – GOM

Andy Morris,
E.ON-UK

Andy Gwayne
Laser Optical Engineering

Henrik Stang
DTU – Department of Civil Engineering

Jakob Wedel-Heinen
DNV

John P. Dear, Amit Puri, Alexander Fergusson
Imperial College London
UK Department of Mechanical Engineering

Risø-R-1622(EN)

Risø National Laboratory for Sustainable Energy
Technical University of Denmark
Roskilde, Denmark
March 2008

DTU

Author: Find M. Jensen, Kim Branner, Per H. Nielsen, Peter Berring, Troels S. Antvorskov, Magda Nielsen, Morten Michael Lindahl, Brian Lund, Christian Jensen, Joan H. Reffs, Rune F. Nielsen, Peter H. Jensen, Malcolm McGugan[1], Kaj K. Borum[1], Rene S. Hansen[2], Carsten Skamris[3], Flemming Sørensen[4], Rune Schytt-Nielsen[4], Jeppe H. Laursen[5], Markus Klein[5], Andy Morris[6], Andy Gwayne[7], Henrik Stang[8], Jakob Wedel-Heinen[9], John P. Dear[10], Amit Puri[10], Alexander Fergusson[10]

Title: Full Scale Test of a SSP 34m box girder 1. Data report

Division: Wind Energy Division

1 Risø – Materials Research Department
2 Risø - Optical Department
3 Blaest Test Center
4 SSP-Technology A/S
5 Zebicon – GOM
6 E.ON – UK
7 Laser Optical Engineering
8 DTU – Department of Civil Engineering
9 DNV
10 Imperial College London, Department of Mechanical Engineering - UK

Risø-R-1622(EN)
March 2008

Abstract:

This report presents the setup and result of a full-scale test of a reinforced glass fibre/epoxy box girder used in 34m wind turbine blade. The tests were performed at the Blaest test facility in August 2006.

The test is an important part of a research project established in cooperation between Risø DTU, the National Laboratory for Sustainable Energy at the Technical University of Denmark -, SSP-Technology A/S and Blaest (Blade test centre A/S) and it has been performed as a part of Find Mølholt Jensen's PhD study.

This report contains the complete test data for the final test, in which the box girder was loaded until failure. A comprehensive description of the test setup is given. This report deals only with tests and results. There are no conclusions on the data in this report, but references are given to publications, where the data are used and compared with FEM etc.

Various kinds of measuring equipment have been used during these tests: acoustic emission, 330 strain gauges, 24 mechanical displacement devices and two optical deformation measuring systems. The mechanical displacement devices measured both global (absolute) and local (relative) deflection and the optical systems measured surface deformation. A prediction was made on the location of the failure of the girder. At this location the majority of the measuring equipment was concentrated. The prediction was proved to be correct and valuable information of the behaviour of the box girder prior to failure was obtained.

The experimental investigation consisted of the following load configurations:

-Flapwise bending

-Torsion

Ultrasonic scanning of the box girder was performed before, during and after the test the box girder. This was done to investigate whether the girder was damaged by the load or imperfection (productions defects) growth.

ISSN 0106-2840
ISBN 978-87-550-3636-9

Pages: 151

Information Service Department
Risø National Laboratory for Sustainable Energy
Technical University of Denmark
P.O.Box 49
DK-4000 Roskilde
Denmark
Telephone +45 46774004
bibl@risoe.dk
Fax +45 46774013
www.risoe.dtu.dk

Table of Contents

Terms and Definitions

The tested box girder has the following terms

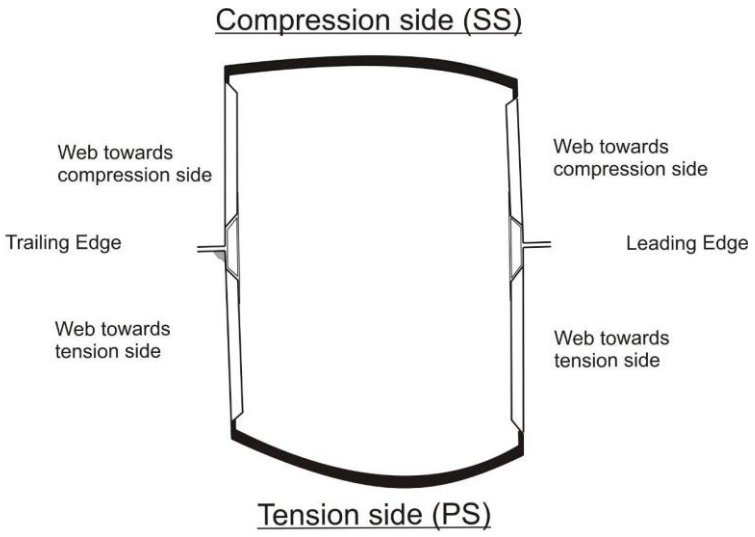

Figure 1. Simplified cross-section of the box girder

Strain gauges definition

(UD) Uni Directional (0° in longitudinal direction)
(Bx) Biax (0^o/90°)
(Tx) Triax-Rosette (0^o/45^o/90^o)

Terms on measuring equipment used in the report

Strain Gauge Unidirectional - Used in 0° and 90°

Strain Gauge Rosette – 0° ; 45° and 90° degree directions

Linear transducers:

LT-ASM Length Transducer from ASM – Cable actuated positions sensors

LT-LVDT Length Linear Variable Differential Transformer – Transducers

DIC: Digital image coloration.

Blade root: Part of the wind turbine blade that is closest to the hub

Box girder: Primary lengthwise structural member of a wind turbine blade

Design loads: Loads that the turbine is designed to withstand. They are obtained by applying the appropriate partial load factors to the characteristic values. [13]

Edgewise: Direction that is parallel to the local chord of the blade

FEM: Finite Element Method

Flapwise: Direction that is perpendicular to the surface swept by the non-deformed rotor blade axis

Strain: Ratio of the elongation (in shear displacement of a material subjected to stress) to the original length of the material.

Trailing edge: Edge of blade pointing opposite travelling direction.

Ultimate strength: Measure of the maximum (static) load-bearing capacity of a material or structural element

1 Introduction

Risø DTU, the National Laboratory for Sustainable Energy at the Technical University of Denmark has initiated full-scale tests of two 34 m glass fibre/epoxy box girders made by SSP-Technology A/S. The box girder is the main load carrying element of a wind turbine blade. This report deals with the test of the first box girder. Test results from the second box girder, will be published later in 2008 in a separate data report, see ref.[2].

The research project is performed in cooperation with SSP-Technology A/S Blaest (Blade test centre A/S), Risø DTU and is a part of Find Mølholt Jensen PhD-Project, see ref [1]. The main goal is to detect elastic and failure mechanics. The experimental results are presented but no conductions about failure model etc. are drawn in this data report. These can be found in [3]-[8]. A comprehensive description of both full-scale tests and the observed elastic and failure mechanisms is given in Find Mølholt Jensen's PhD-thesis [1].

Another purpose of the full-scale test is to test new Digital image coloration (DIC)-techniques and to compare different Non Destructive Testing (NDT) and measuring techniques.

Researchers from three departments at Risø DTU have been involved in the verification of new test methods and NDT-techniques. Since Risø DTU does not cover all relevant measuring techniques, external partners have been invited to participate. These partners are E.ON-UK, Laser optical Engineering, Zebicon, GOM, and Imperial College London – Department of Mechanical Engineering. Work done together with Imperial College London and E.ON is reported in ref. [7]-[12]

Two static tests were performed with different load configurations on the full-scale wind turbine blade box girder:

- Torsion
- Flapwise bending.

The flapwise bending full-scale test consists of eight subtests. The test schedule, with an overview of applied loads and measuring equipment used in the different tests, is given in detail in appendix A.
Chapters one to six give a description of the test setup for the flapwise load configuration. This report also describes the DIC-measurements and NDT–scanning conducted under the flapwise full-scale test.
Chapter seven contains picture of the box girder after failure.
Chapter eight gives summary of the flapwise loading.
Chapter nine describes briefly the torsion load configuration and some selected results from this test are presented in this report.
Chapter ten presents the references and chapter eleven the appendices. Results from the torsion load configuration can be found in appendix F.

A brief overview of the structure of this report is presented below.

1) Loads and supports.

Definitions of the test setup
Implemented loads' supports (Roller-skate)

2) Deformation measurements

Strain Gauge measurements
Local deflection measurements
- LT-ASM inside measurement
- LT-LVDT Outer cap measurement

Global deflection measurement

3) Digital image coloration

ARAMIS system-optical measurement equipment (DIC)
- Fringe projection – optical measurement (DIC)

4) Structural health monitoring

Acoustic emission
Vacuum hood (NDT)
Ultrasonic scanning (NDT)

2 Test specification, loads and supports

2.1. General information

The tested box girder is an essential part of a 34m blade designed for a 1,5MW wind turbine and is manufactured by SSP Technology A/s. The box girder is made of prepreg glass fibre/epoxy and most of the fibres are orientated in the longitudinal direction to carry the flapwise loads and limit tip deflection. The box girder is the load carrying part of the wind turbine blade and is bonded between aerodynamic shells during the manufacturing process.

The box girder was shortened to 25.4m and tested, see Figure 2.

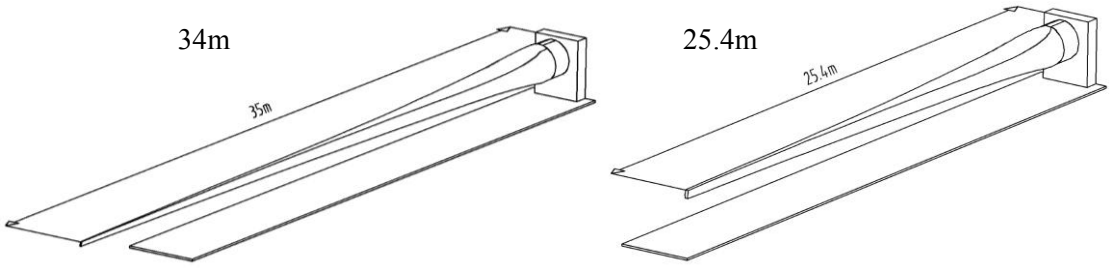

Figure 2. Sketch of box girder: left- not shortened 34m, right- shortened to 25.4m

The box girder was shortened because failure in the tip is not critical and in order to minimise transport costs.

The test of the box girder was made at Blaest test facility in Sparkær (Denmark). The main purpose of this centre is to perform commercial tests of wind turbine blades for Danish and international blade manufacturing companies. Both static and fatigue tests of blades are performed and used to verify the design of the blades to obtain approval from authorities.
Figure 3 shows a typical flapwise bending test. The blade is fixed to the test rig and forces are applied in the clamps.

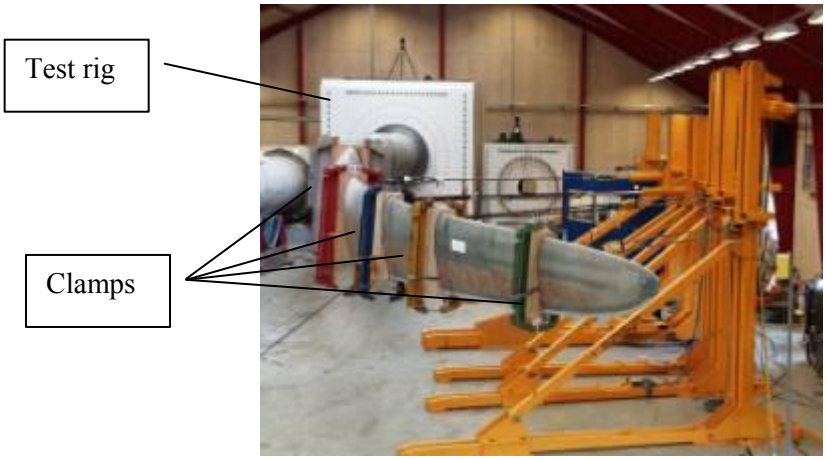

Figure 3. Flapwise bending test of a wind turbine blade performed at Blade test centre. Photo from www.blaest.com.

Figure 4. Box girder no 1 ready to be tested, view of the compression side.

Figure 5. The shortened box girder mounted in the test rig.

The box girder mounted in the test rig is presented in Figure 4 and Figure 5. A previous full-scale test of a complete 34m wind turbine blade from SSP- Technology (box girder including the aerodynamic shells) has shown that it was able to withstand the required loads defined by the Authorities. After the box girder had passed all static and dynamic tests required by the classifications it was tested to failure. This has shown that the shear webs were the most critical part of the blade and therefore they have been reinforced in these new tests. These reinforcements are shown in Figure 1. Due to them, other failure mechanisms could be studied, see [4] and [8].
The tophat reinforcement was introduced in the root section to avoid unwanted buckling failure in the region, see Figure 6. Failure in this region is unrealistic as explained in [2].

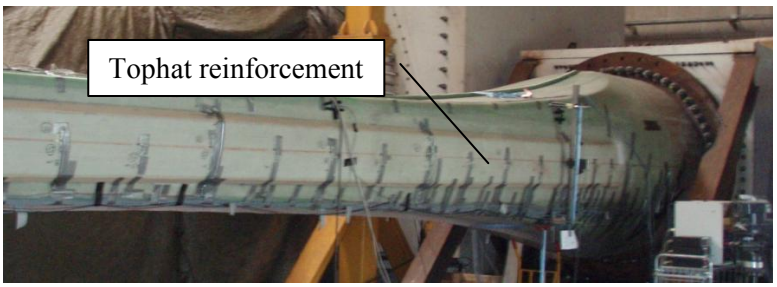

Fig. 6a

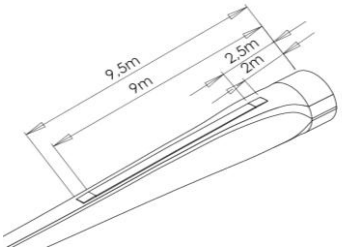

Fig. 6b

Figure 6. Fig. a: Tophat reinforcement on compression side. Fig. b: Sketch of the tophat

The tophat reinforcement went from 2 to 9.5 m, measured from the root. From 2 m till 2.5 m the reinforcement was slightly slanted so it increased from slim to full thickness. From 9m to 9.5m it was decreased, see Figure 6.

2.2. Loads

This section will explain in what manner and position the blade was loaded.

The percentage of load used in this report refers to the ultimate failure load of the complete original wind turbine blade. This is implemented for confidential and comparison reasons.

Since the tip was cut off, the moment transferred from the tip is compensated at distance of 25 m. The loads were applied at 13.2m, 19m and 25m from the root, see Figure 7.

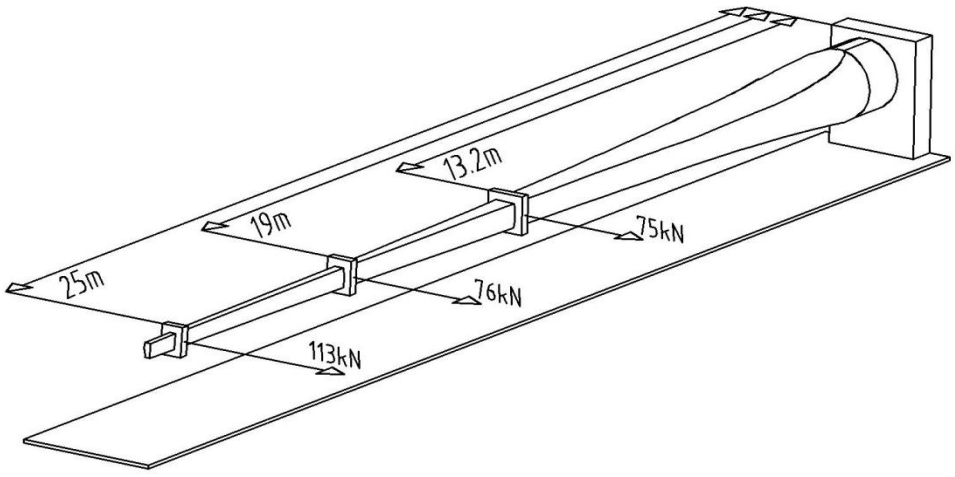

Figure 7. Sketch of box girder with applied forces.

The stroke length of the hydraulic pistons was insufficient due to the fact that the maximum tip deflection was greater than the stroke length of the pistons, see Figure 5. The box girder was loaded (to around 30%) in all places except the tip. Afterwards the tip piston was connected to the box girder. The pistons were moved until the loading on the box girder was 20%. Therefore the test results measurements start at 20%.

This will be apparent on the plots of the strain gauges measurement results as they have their starting point at 20%. As the measurements were collected with only two loading points used, they are not presented in the final plots.

2.3. Roller-skate support

Three simple supports mounted with roller-skates were used to eliminate twisting and distortion of the box girder during the flapwise test, see Figure 8. They were placed at distance of 9m, 13.2m and 19m from the root, Figure 9.

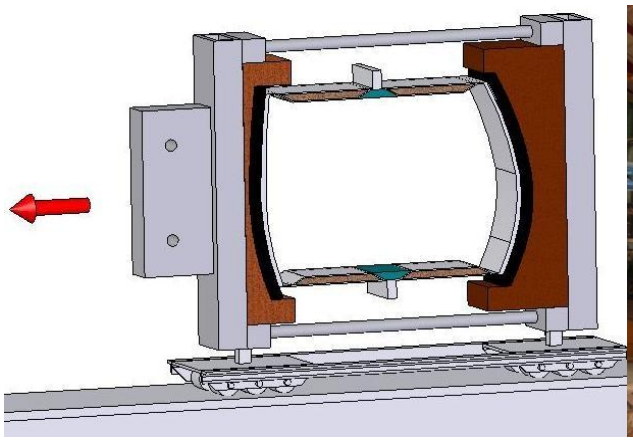

Fig. 8a

Fig. 8b

Figure 8. Fig. a: Sketch of roller-skate support; Fig. b: Roller-skate support at 13.2m

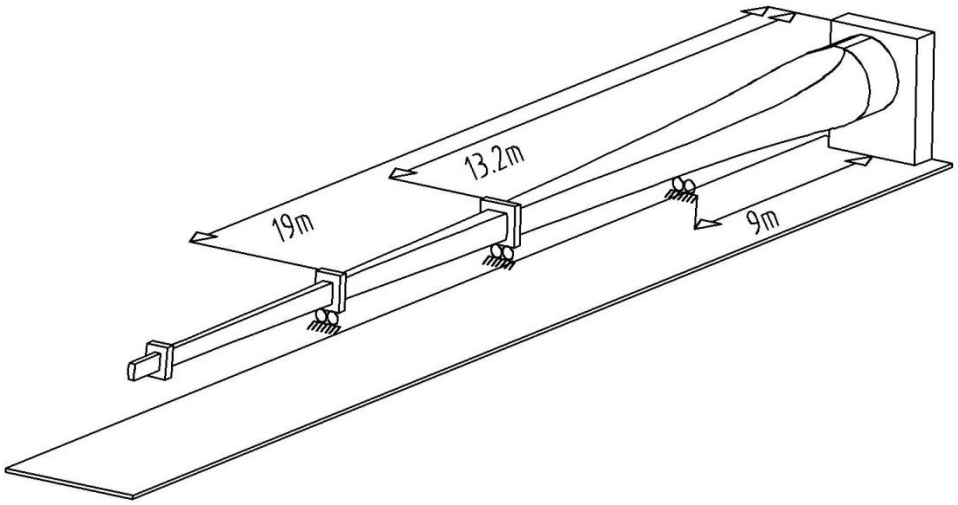

Figure 9. Positions of the roller-skate supports.

In the trial tests only section 13.2 and 19m were supported. Due to experience from the trial tests an extra support at 9m was found necessary.

3 Strain gauges

In this chapter, strain gauges positions and measurements are described and selected results are presented. A complete list of strain gauge measurements from the flapwise test can be found in the appendix E and measurements from the torsional test can be found in appendix F.

3.1. Strain gauge placement

The box girder was instrumented with 330 strain gauges measuring strain in different positions and directions. All strain gauges were placed "back to back" i.e. one strain gauge on each (inner and outer) side of the box girder, (see Figure 10). The strain gauges were numbered with odd numbers on the outside, and even number on the inner side. Their positions and directions can be found in appendices E and F. See Figure 10 for a section through the box girder at 10m from the root, showing the strain gauge positions.

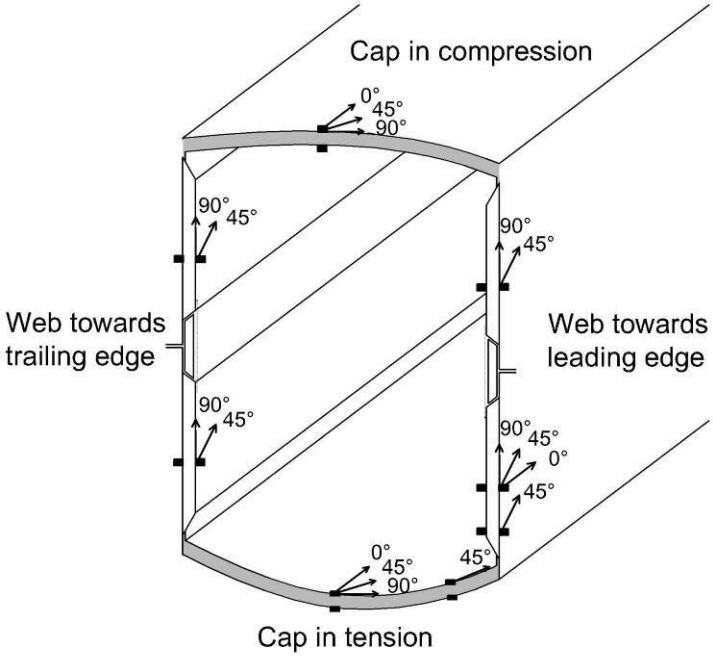

Figure 10. Strain gauge positions at section 10m from root. View from the box girder tip.

Because of the large number of strain gauges and limitations in the capacity of the data acquisition system, a small number of sensors were omitted in the final test (test 8). In these places the results were taken from test 7 and plotted with test 8.

3.2. Strain gauge measurements

All the strain gauge results can be found in appendices E and F. Here only a few results are shown. Explanation of the behaviour of the box girder and conclusions of the test are not included in this data report. These can be found in [1], [3], [4].

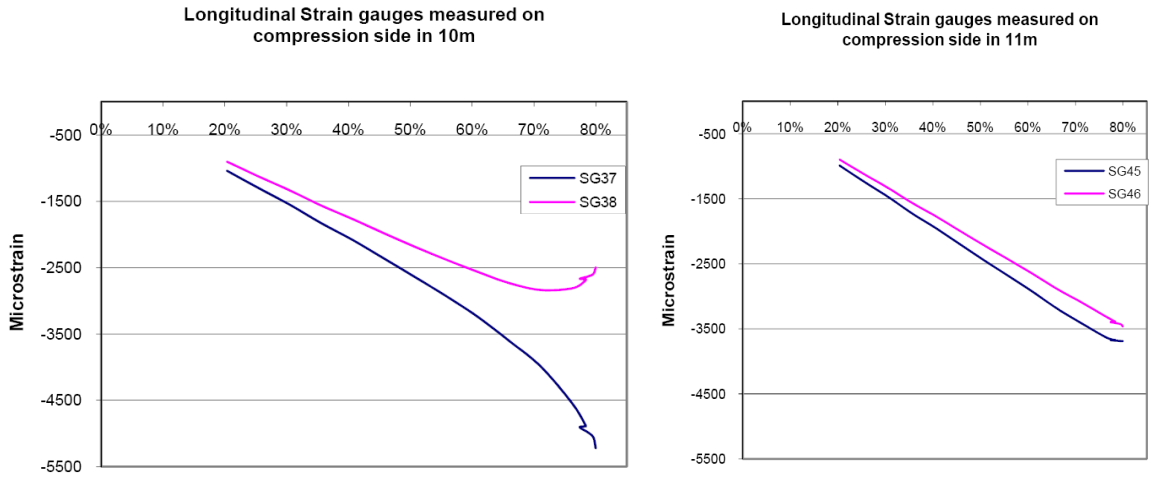

Figure 11. Longitudinal strain gauge measurements (back to back) -compression side.

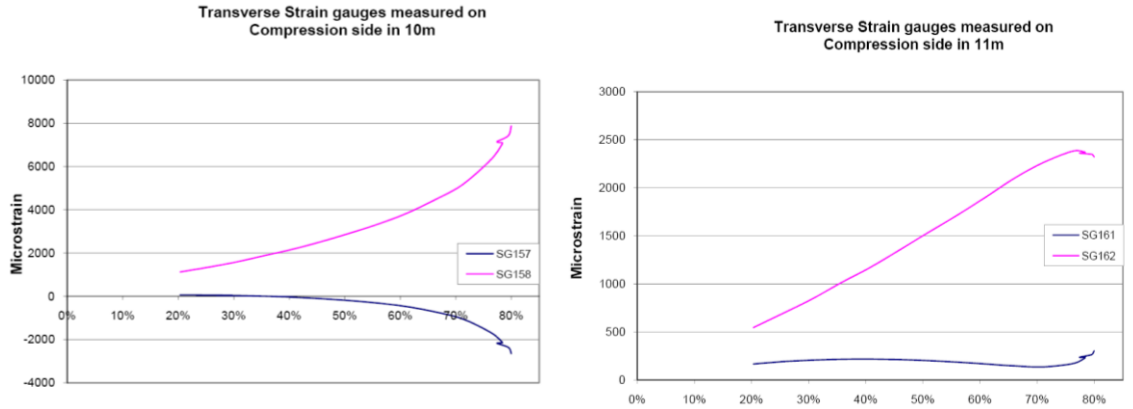

Figure 12. Transverse strain gauge measurements (back to back) - compression side.

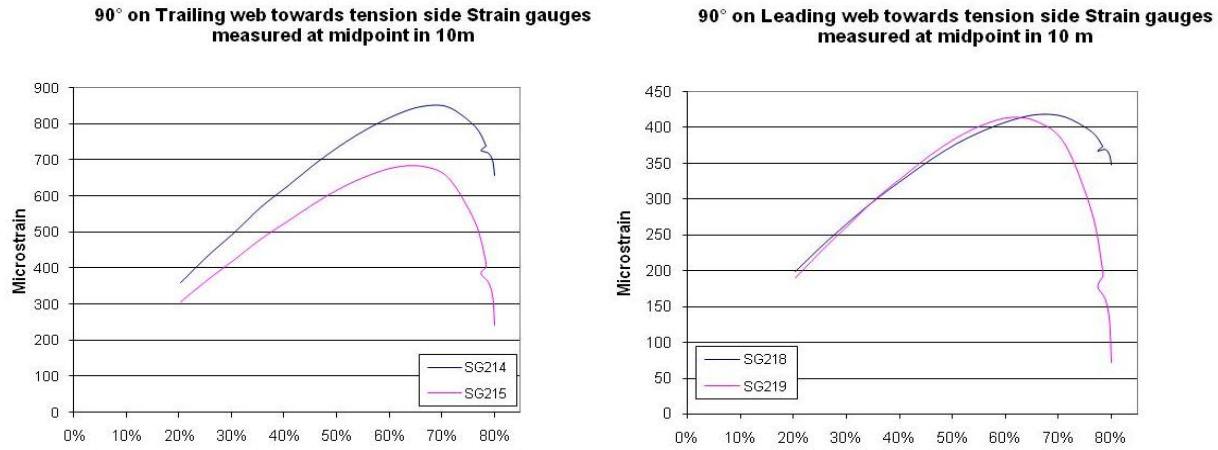

Figure 13. Vertical (90°) strain gauge measurements (back to back) on shear webs.

4 Mechanical measured deflections

Deformation measurement devices have been divided into mechanical and optical (DIC). This chapter gives an overview of the different mechanical devices used in the full-scale test. The optical equipment is described in chapter 5.

Among the mechanical measurement devices, linear transducers LT-LVDT and LT-ASM were used, see Figure 14. These measured both local (relative in a small area) and global (absolute on a global scale) deflections.

4.1. Local deformation measurements

Distortion of the box girder section was measured with displacement sensors, which is sketched in Figure 14. Inside the box girder LT-ASMs have been used, whereas at the outer side of the caps the LT-LVDTs were applied. To measure the individual cap deflection special reference frames have been used.

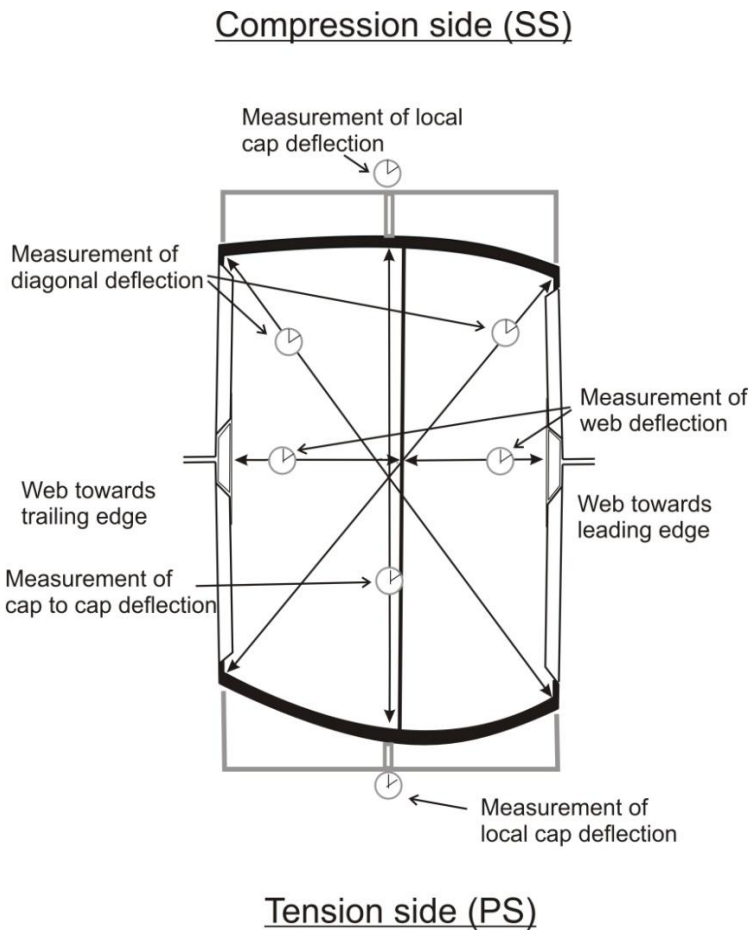

Figure 14. 2D sketch of deformations sensors at the inner and outer side. View from the blade root.

Deformations sensors inside box girder.

LT-ASMs were mounted at both shear webs to measure individual deflection between the web and the reference frame in the centreline, shown in Figure 15. Measurements were performed at 8.6m, 10.1m, 10.6m, 11.1m and 12.1m.

Diagonal LT-ASMs were mounted inside the box girder in 10.2m from the root and measured distance from corner to corner. At the distance of 10.4m a cap-to-cap LT-ASM was mounted, measuring from compression to tension cap.

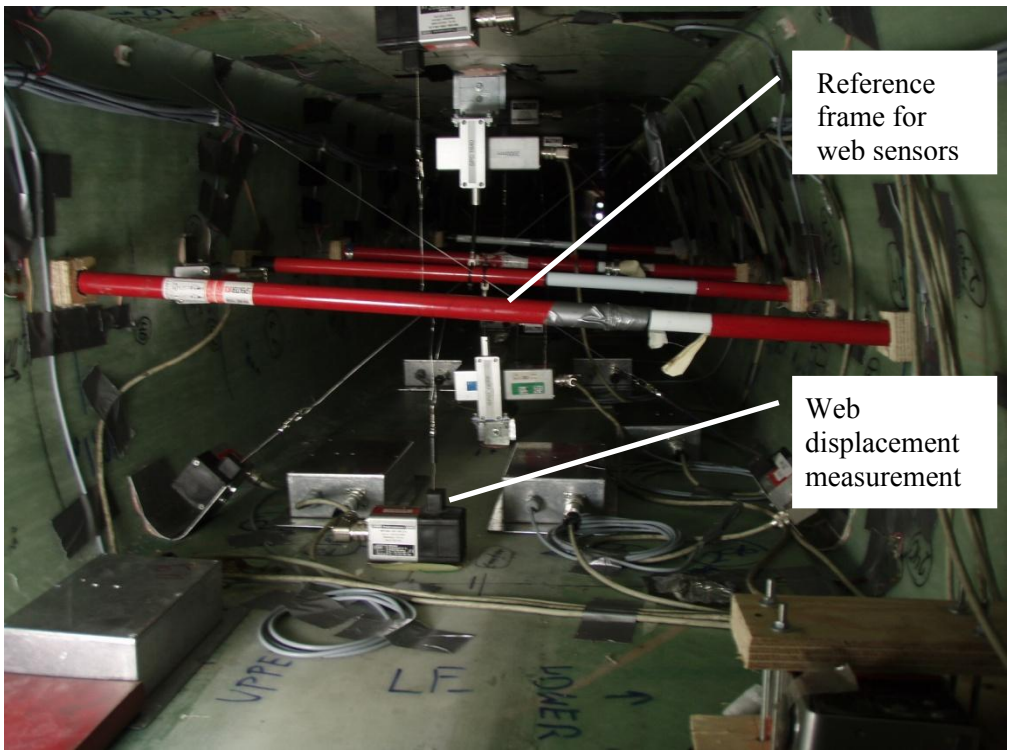

Figure 15. Displacement sensors mounted inside the box girder shown from position looking towards the tip. The sketch of measuring equipment in Figure 14 on page 11 is rotated by 90° with respect to this photo.

The results from LT-ASM are presented in the Figure 16 and in Figure 17. The graph in Figure 16 presents measurements performed from the leading (L) and the trailing (T) web to the centre reference frame. The reference frames are shown in Figure 15.

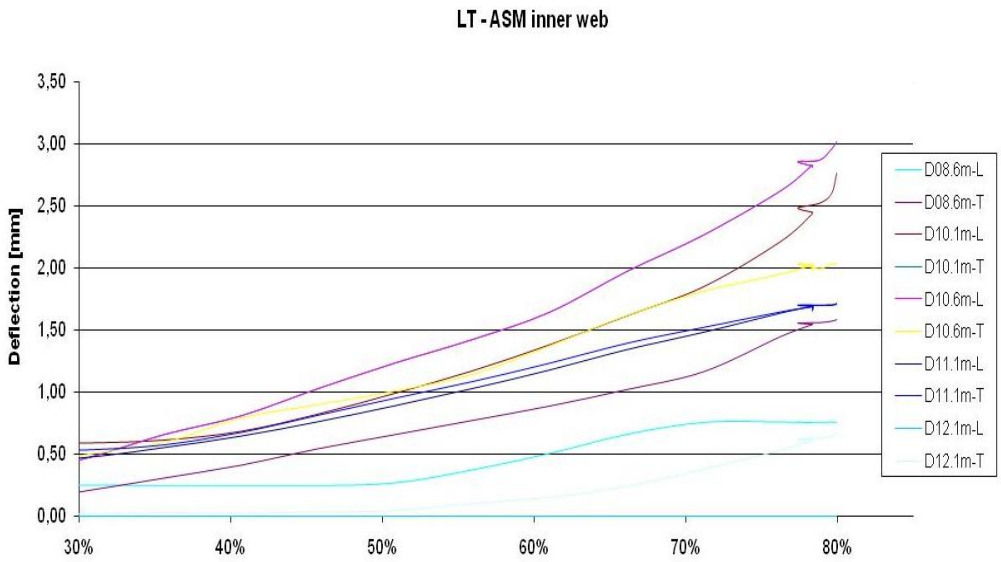

Figure 16. LT-ASM measurements inside the box girder.

The non-linear behaviour is similar to observations during previous full-scale test, see [1] and [4]. The only difference is that the amplitude is reduced due to the reinforced shear webs, see Figure 16.

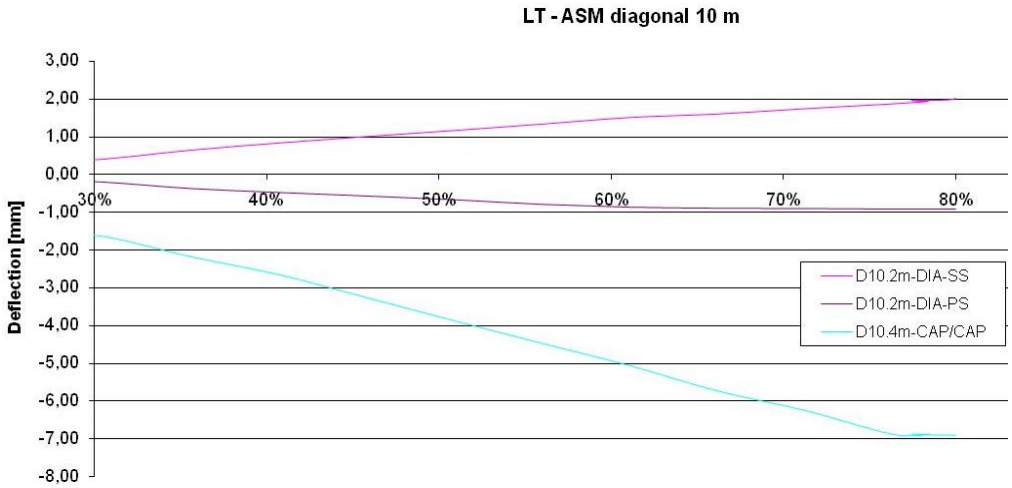

Figure 17. Diagonal LT-ASMs transverse shear distortion and the cap-cap LT-ASM sensor gave the cross-section's compression.

The transverse shear distortion, measured by the diagonal ASM sensors, is small (1-2mm) because of the roller-skates, see Figure 17.

Deflection sensors outside of the box girder.

On the outer side of the box girder, seven LT-LVDTs were mounted to measure local deflections of the compression cap centreline, see Figure 18.

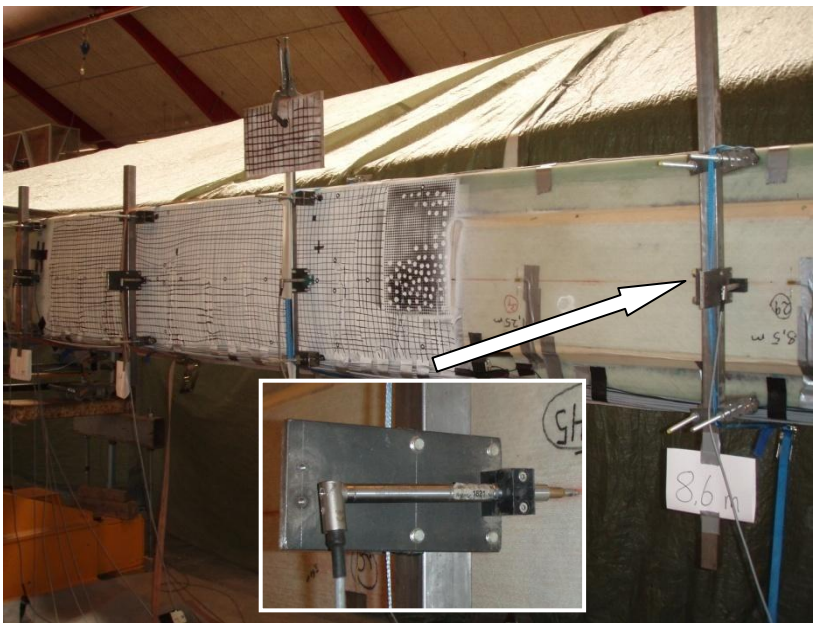

Figure 18. LT-LVDT equipment on the outer compression side of the box girder.

Results given by the cap displacement sensors are shown in Figure 19. The non-linear behaviour description is given in reference [2] and [3].

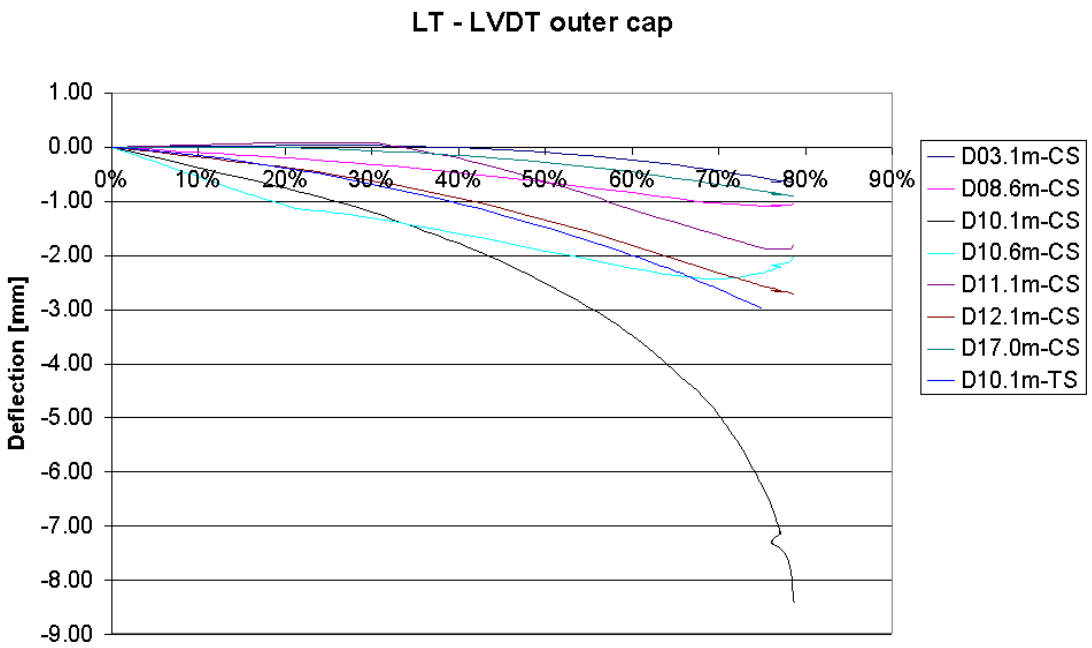

Figure 19. Measurements of cap deformation taken on the compression and tension side.

Since the cap in tension was not expected to be critical, only one displacement sensor was placed on it; see Figure 19 the results for sensor D10.1m TS.

Before the final test the displacement sensor on the tension side was removed and placed at 10.1m on the compression side. This is the reason why the tension sensor (D10.1mTS) in Figure 19 gives data up to only 75% load.

Global deflections

Global deflections in flapwise direction were measured by means of three LT-ASMs. The deformations were measured at a distance of 14.0m, 19.4m and 25.4m from the root. The measuring positions are illustrated in the Figure 20.

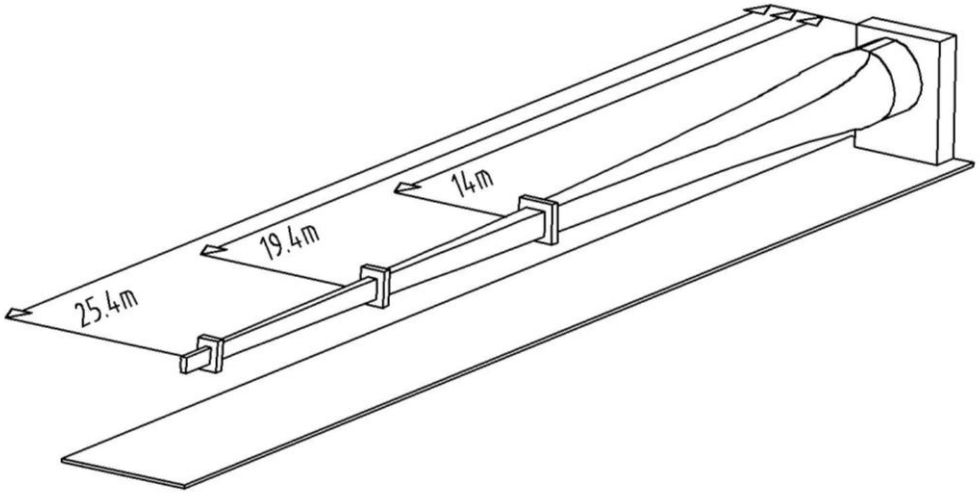

Figure 20. Positions where the global deflections were measured.

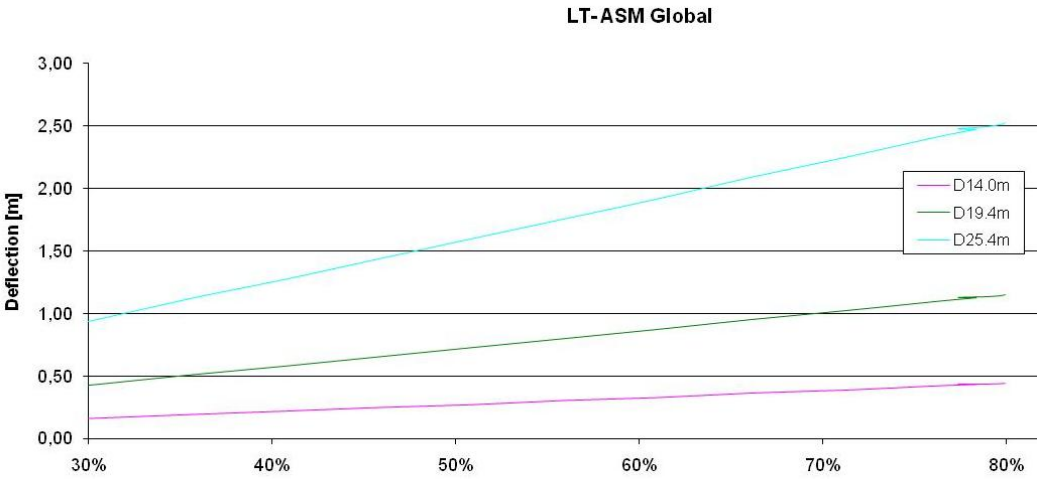

Figure 21. Measured deflections given as functions of load applied to the box girder.

It can be observed that global deflections behave linearly and the local deflections are mainly non-linear. The global deflection is presented in Figure 21 and the local measurement in Figure 16 to Figure 19.

5 Optical measurement - Digital Image Coloration

Two different optical measuring devices were also utilized. One was the ARAMIS system, which is a Digital Image Coloration (DIC). The other system used was the Fringe Projection system. In both systems the local surface deformation was measured. A brief summary of the ARAMIS and the fringe projection results is presented in chapters 5.1 and 5.2. For further information on the two systems, see appendices B and C.

5.1. ARAMIS 3D digital optical measurement

The ARAMIS performed measurements on the box girder's compression side in the distance of 9 to 12 meters from the root. ARAMIS system is an optical measurement system, able to measure 3D displacement and surface strain of an object by image processing. The system uses two CCD cameras detecting the difference in measured pattern. In Figure 22 the measuring equipment is shown from behind, facing the compression side of the box girder. Note the painted speckle/random pattern on the box girder compression side.

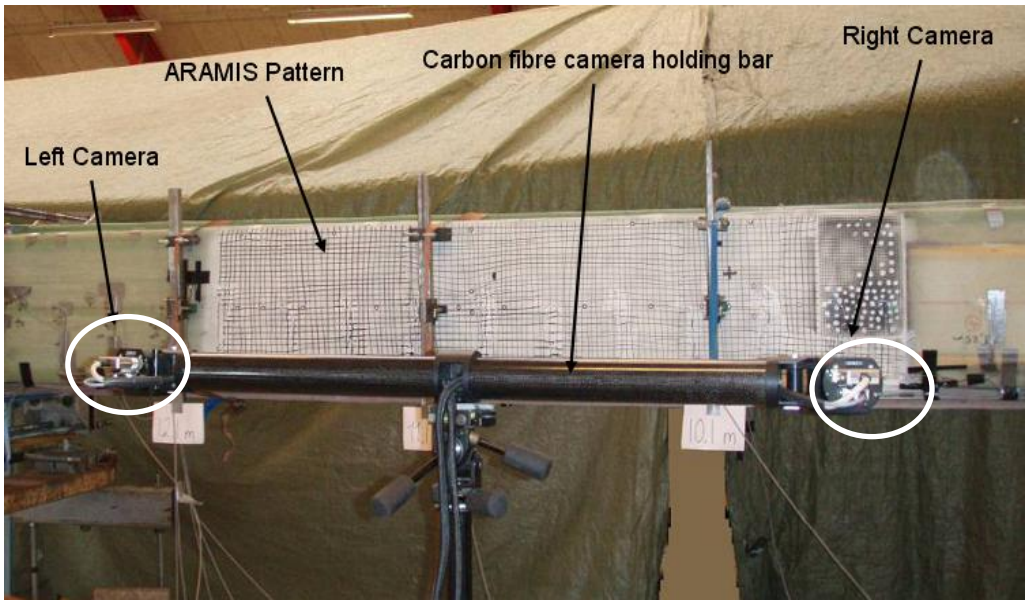

Figure 22. ARAMIS equipment positioned in front of the measuring area.

The measured ARAMIS results are measured during tests no 7 with a load up to 75%. The local deflection during 75% load is shown in Figure 23.

The local deformation is the out-of-plane displacement of the compression side of the box girder. It is determined by subtracting the global deflection (rigid body movement) from all measured points/coordinates (the entire measuring area) and thereby getting fairly good estimates of local deformation.

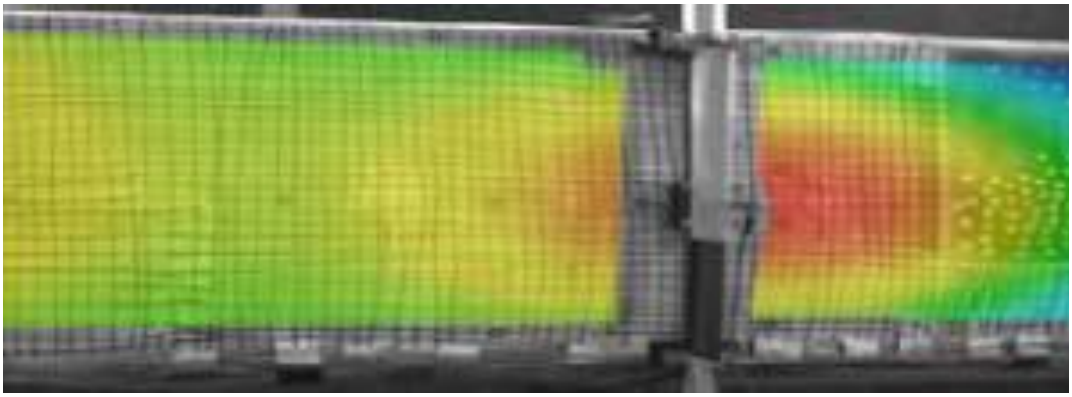

Figure 23. Out-of-plane displacement results from ARAMIS measurement are transferred to the specimen's surface with a rigid body movement correction.

The results of ARAMIS' measurement and further information regarding the system can be found in appendix B.

5.2. Fringe projection

The Fringe projection system can measure out of plane deformations. Measurement system consists of a projector and a camera, both connected to a computer. The deflection can be calculated by illumination of a cosine stripe pattern on the measuring area. The fringe projection system was used to measure deflection on the inside cap in compression side and the web trailing web during the full-scale-test, see appendix C.

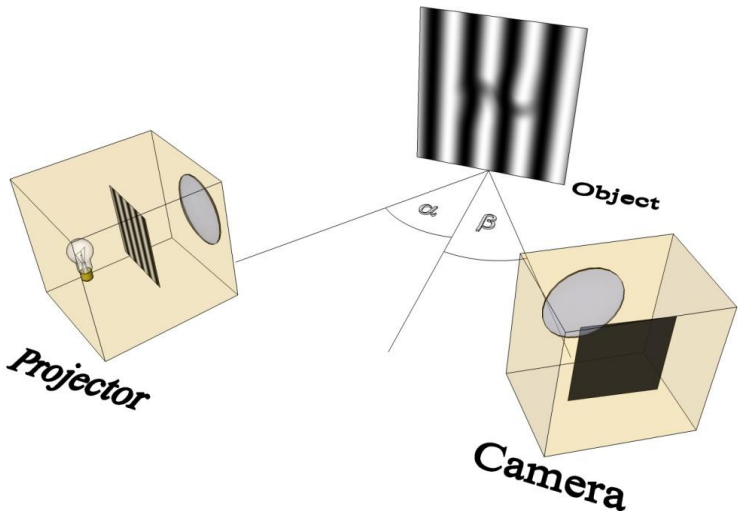

Figure 24. Measurements' set-up. A projector, connected to a computer is illuminating the object surface with a cosine fringe pattern.

Test setup inside the compression cap

The measurements on the compression cap were performed from the inside the box girder. For this measurement the fringe projection equipment was placed inside the box girder, see Figure 25.

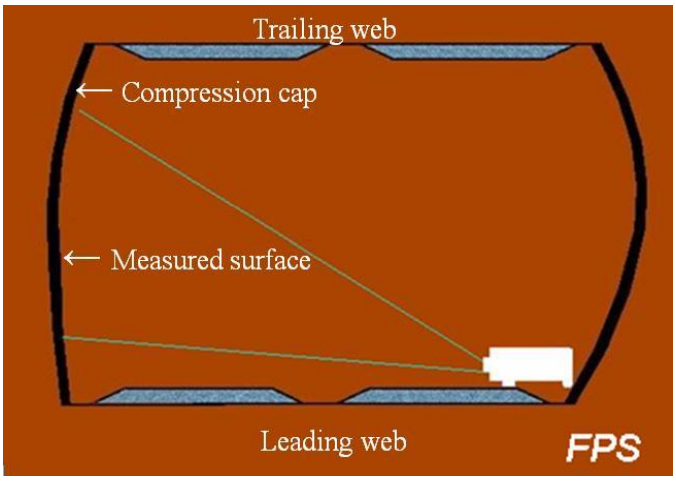

Figure 25. Fringe projection setup inside box girder in 9.5m measuring local deflection; view from the root facing the tip.

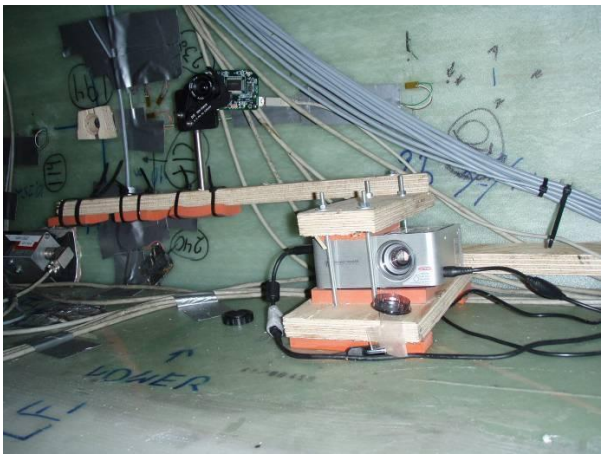

Fig. 26a

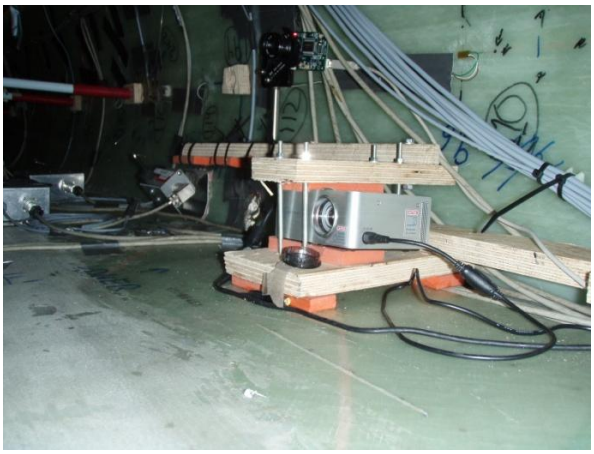

Fig. 26b

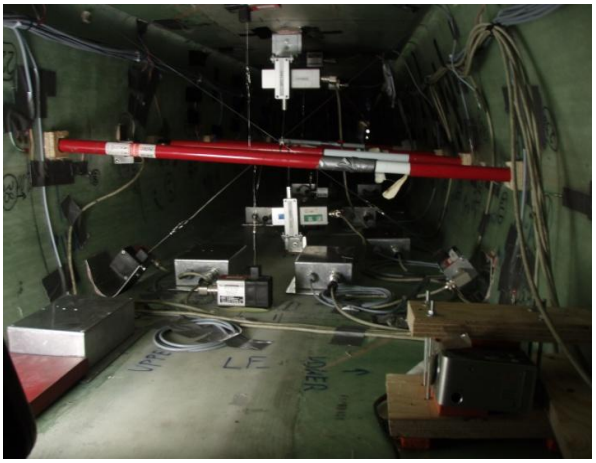

Fig. 26c

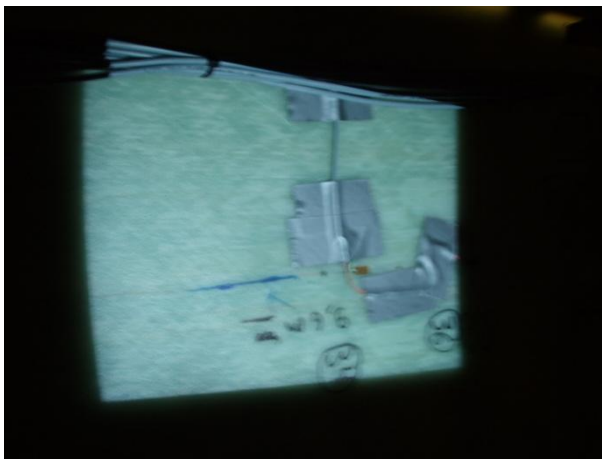

Fig. 26d

Figure 26. Pictures a-c: The fringe projection system seen from the front; d: The measuring area inside the compression cap at 9.5m

Fringe projection results measured inside the compression cap.

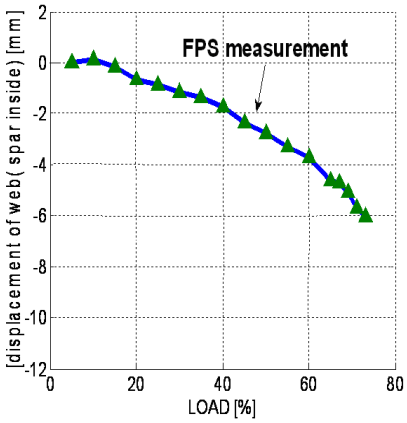

Figure 27. Deflection measured inside the box girder on compression side at 9.5m (minus indicates in the outward direction).

The fringe projection results measured inside the box girder on the compression cap are shown in Figure 27. The results of measurement show that the cap was moving away from the measuring equipment. The surface was moving towards the outer side.

Test setup outside the trailing web

The test setup for the measurements of the deflection of the trailing web is presented in the Figure 28. The projector, illustrated in Figure 28, was placed over the trailing web. It measured the local deflection as it followed the box girder.

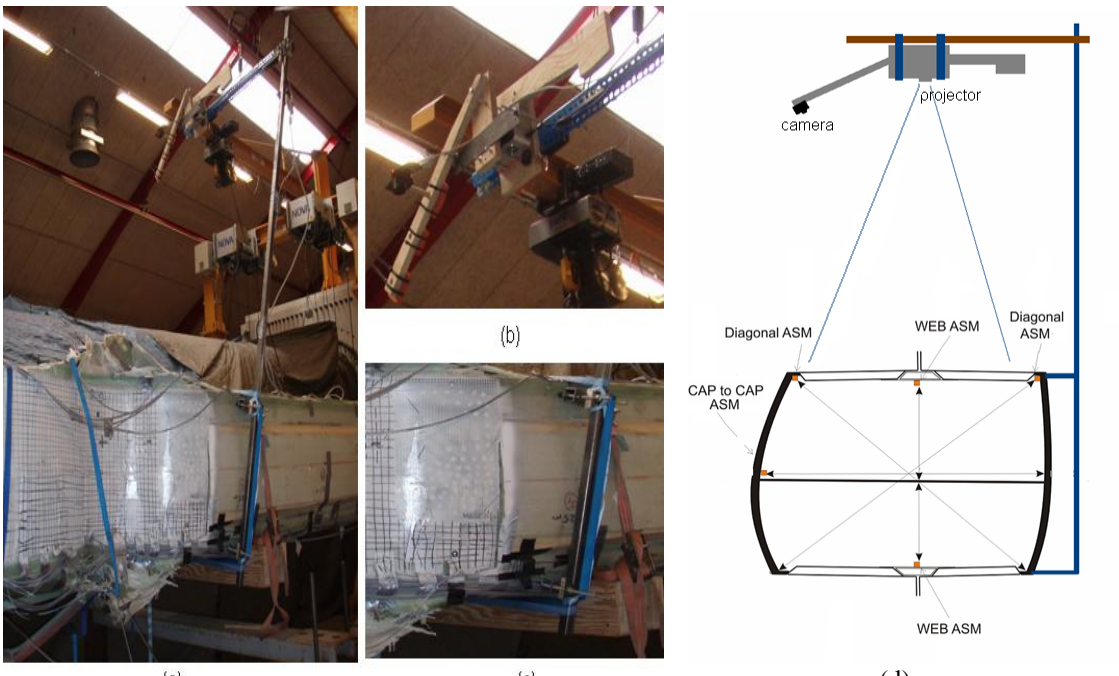

Figure 28: Trailing web deflection measurement. a-c: Photos of measuring setup. d: Sketch (from tip towards the root)

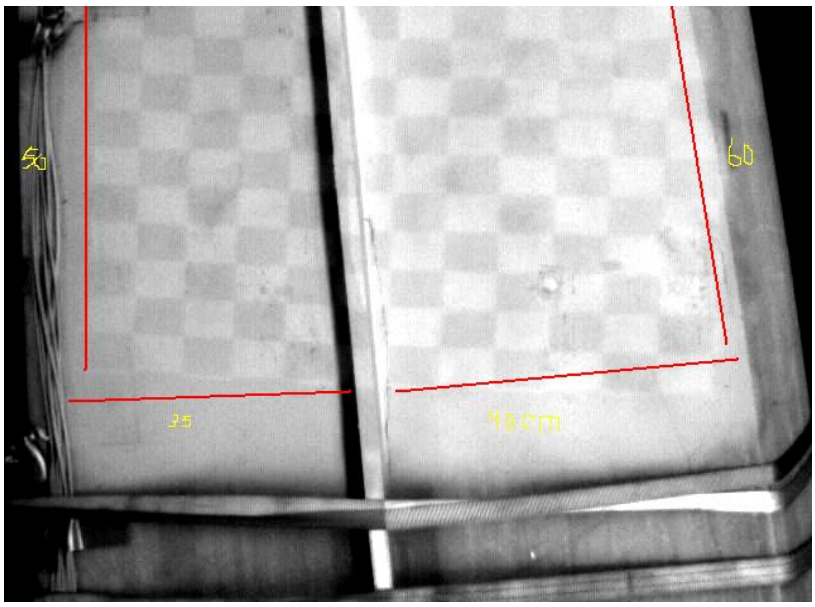

Figure 29. Surface of the web on the trailing edge with projected measuring pattern.

The measurements on the trailing web were not as accurate as the ones performed on the inside of the compression cap. The results are shown in Figure 30, notice the large variations. By means of a geometrical estimation the trailing web's centreline at the 9.6m, a local deflection between 2 or 3-mm was found. More comprehensive explanation is given in [5].

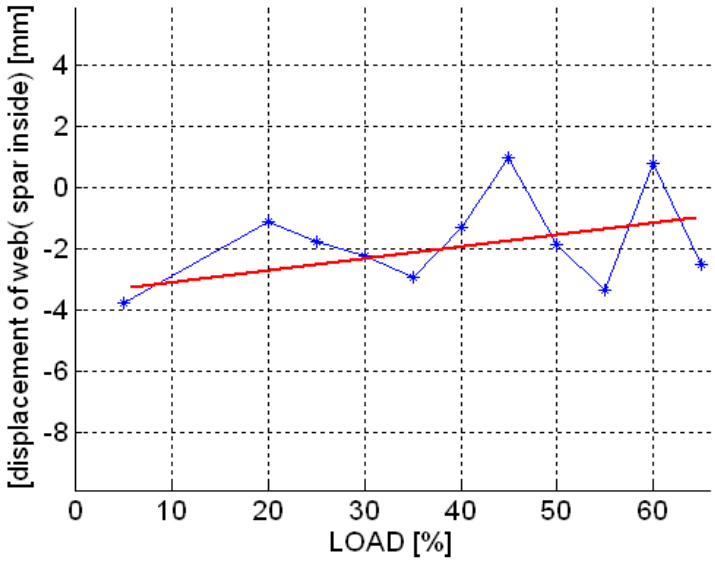

Figure 30. The deflection of the trailing web centreline of the 9.6-meter segment given as a function of the load.

For further information visit appendix C.

6 Structural health monitoring

This chapter covers the following Non Destructive Test techniques:

- Acoustic Emission
- Vacuum hood
- Ultrasonic scanning - air coupled ultrasonic.

6.1. Acoustic Emission measurement

When certain dynamic processes occur in the material, some of the released energy generates elastic stress waves, we might say vibrations. These stress waves are propagated from the source and can be detected by sensitive transducers. Once amplified, the signal from these transducers is available for further analysis. Information about the location, severity and nature of the event causing the stress wave emission can be deduced from the received signals.

When loaded, a structural polymer composite material emits a huge number of these transient stress waves as a result of non-reversible (plastic) micro-damage events such as matrix cracking, tribology at delaminations, fibre fracture, etc. This multitude of small-scale events is detectable long before a reduction in structure stiffness and/or the appearance of visible (macro-scale) crack.

Figure 31. Acoustic emission sensors used Holroyd instrument AE- SS1

When a composite structure is loaded up to critical levels, a significant increase in general stress wave activity can be expected. In the case of a structure loaded within working limits, any area which has already sustained local damage (as the result of for instance an impact, static overload, or severe fatigue) will also return an increase in local stress wave emission activity relative to the structurally unchanged ambient material.

Therefore it is possible to locate defects and damaged areas in composite structures, by monitoring the transient stress waves, before they become threatening to the structure integrity. In this manner we may also chart the progress of structural response to loading towards ultimate failure.

As the signal frequency generally does not fall in the human audible range, the term acoustic emission (AE) is a misnomer and the alternative term stress wave emission (SWE) would be a more accurate description of the phenomenon. Both of them are valid but acoustic emission is the expression in more widespread use.

Application (mounting)

The Acoustic Monitoring Systems used by Risø DTU within the Wind Energy Industry have provided:

- Blade monitoring during testing
    1. Standard (industry approved) testing
    2. Specialty (one-off) testing
    3. Static testing
    4. Fatigue testing
- In-service blade monitoring
    1. Applied on the wind turbine blade and tested while the blade is still mounted on the turbine
    2. During regular operation over an extended period (12 months +)

For further information visit appendix D.

6.2. Vacuum hood.

A measuring technique called Vacuum Hood was introduced in the full-scale test. The purpose of the Vacuum Hood method is to identify any possible imperfections in the composite panels of the box girder. This measuring method was applied to the cap. The cap thickness is approx 30 mm and this was the first time this measuring method was applied to panels of that thickness. That is why another important issue in this experiment was to investigate if it could give reasonable results.

The measurements were performed by Laser Optical Engineering Ltd. (LOE) in cooperation with E-ON UK. More information about this technique can be found on www.laseroptical.co.uk.
The Vacuum Hood method was used before and after the tests, on the suction side at distance of 9 to 13.5 meters from the root, as indicated in Figure 32.

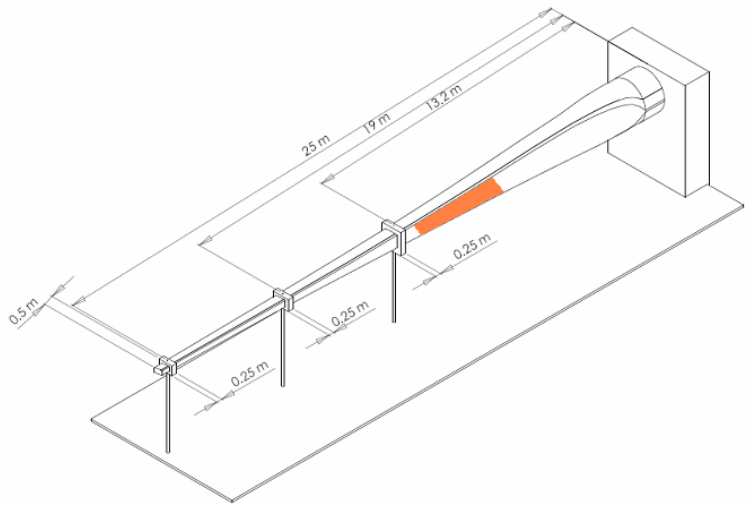

Figure 32. The Vacuum Hood technique was applied on the suction side of the box girder in the area marked with orange.

In Figure 33 the results from the Vacuum Hood are shown. The top figure shows the delamination detected before the test whereas the bottom one gives the detected delaminations after the box girder was loaded to failure.

It appears that the delaminations vanish after the box girder failure, which is not realistic. The most reasonable explanation for this is that the precision of the equipment was inadequate for the specified thickness see Figure 33. According to E-ON UK, equipment with higher precision is under development.

6.3. Ultrasonic scanning - air coupled ultrasonic.

To verify the Vacuum Hood method it was decided to cut out some panels after the full-scale test was performed. Then the ultrasonic scanning was used to see if the delaminations were located in the same areas.

Two panels were cut out and used for standard of reference:

- Panel A – 800 × 600 mm – from 11.3 to 12.1 m – suction side
- Panel B – 600 × 400 mm – from 12.1 to 12.7 m – suction side

At both panels several delaminations were detected. The results are presented graphically in Figure 33.

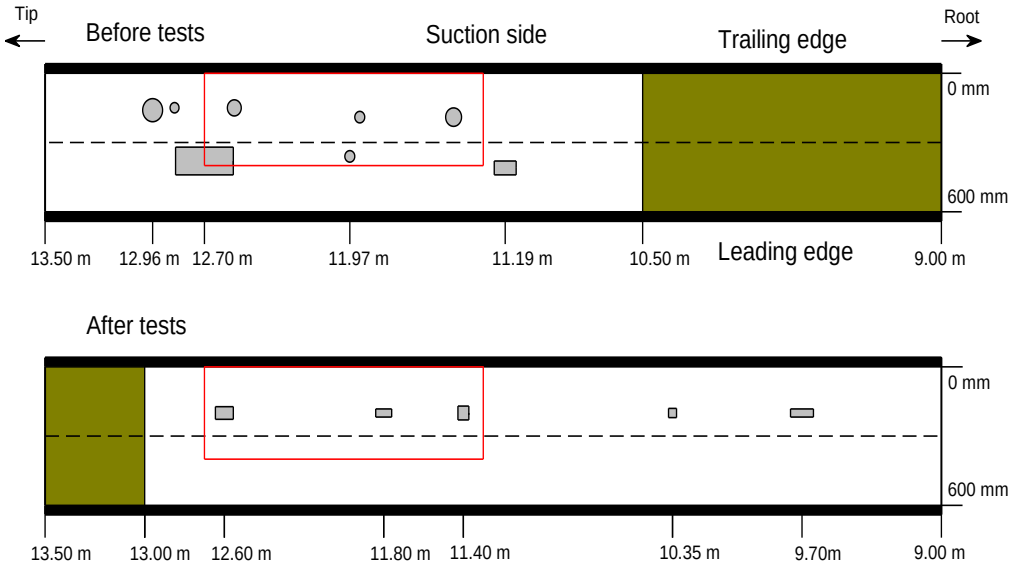

Figure 33. Results from the Vacuum Hood. Delaminations are marked with grey. The pre-test results are presented in the top figure, the post-test in the bottom one. The red lines mark the area where the cut-out panels are taken from.

The two panels were scanned by means of air-coupled ultrasonic through-transmission (TT) technique. This technique has the big advantage of only using atmospheric air as coupling media.

The equipment is called AirTech 2400 and is produced by Ingeniurbüro Dr. Wolfgang Hillger in Germany. It consists of an ultrasonic device with an integrated pc, preamplifier and scanner consisting of two motor driven guides with a scanning area up to 1m x 1,5m. The frequency used was 120 kHz and the scanning resolution was 2 mm. The scans were performed in the Materials Research Department, Risø DTU.

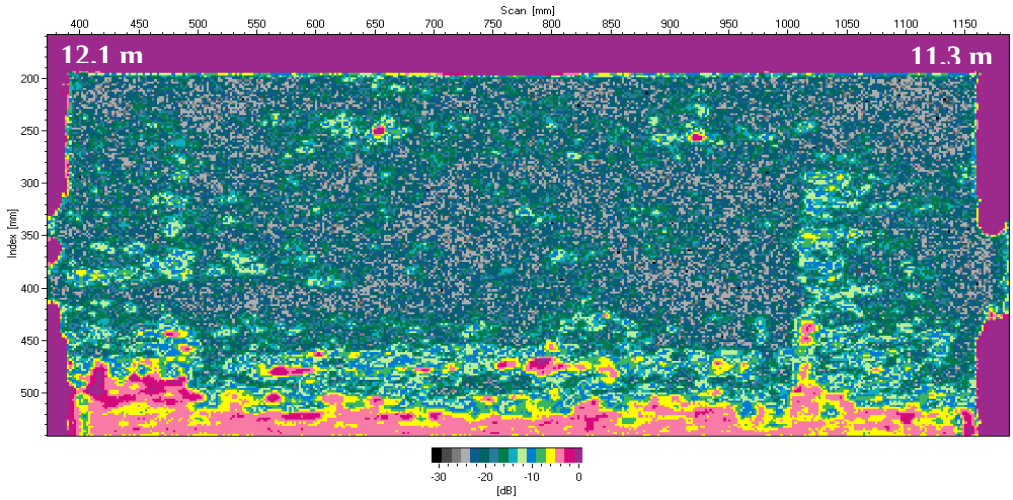

Figure 34. Result of the ultrasonic scanning of panel A. The red areas represent locations where no or only small delaminations occur.

The results are presented in Figure 34 and Figure 35. The colour scale for the scans is in dB and the highest transmitted signal is to the right on the scale (yellow/red colours). During the scanning the transmitted signal from the transmitter to the receiving transducer is measured in each scanning point. In case of a delamination (or other severe defect), the transmitted signal will be damped compared to a defect-free area. The red areas are defect-free area and the grey/green areas have severe ultrasonic damping caused by delaminations.

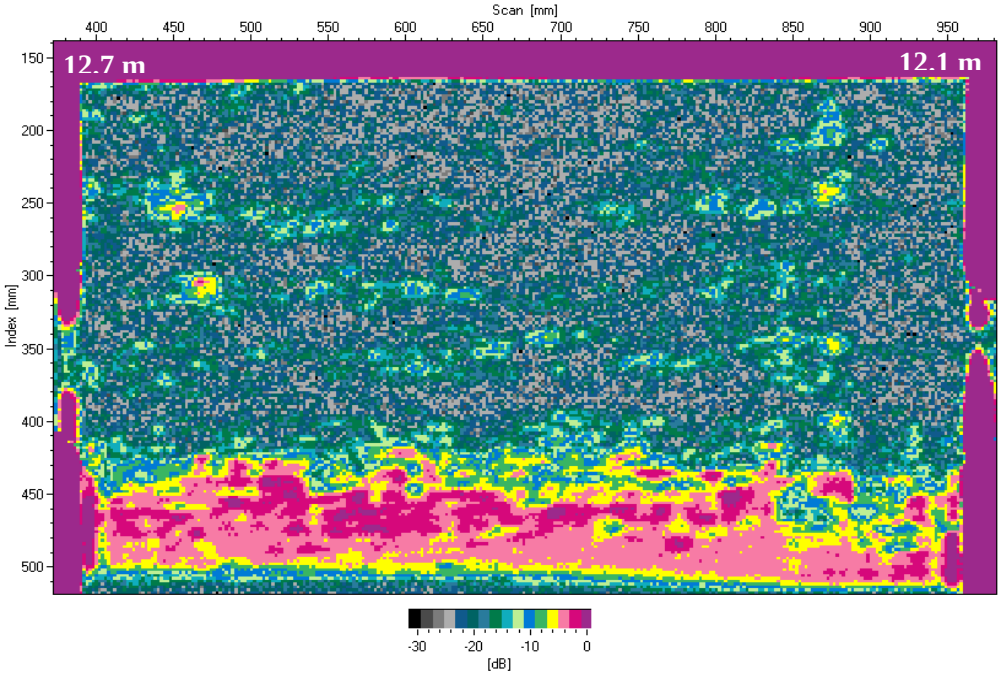

Figure 35. Result of the ultrasonic scanning of panel B. The red areas represent locations where no or only small delaminations occur.

In Figure 34 and Figure 35 it can be easily noticed that the two panels are almost completely delaminated, which was expected since they were taken from an area close to where the box girder failed.

Another panel was cut out from the box girder. As the two previous, this panel was taken from the suction side. The panel dimensions are:

- Panel C – 700 × 600 mm – from 10.6 to 11.3 m – suction side

The panel was tested using ultrasonic scanning technique with the same equipment, frequency and resolution as described earlier. The scan was carried out by the Materials Research Department, Risø DTU. The result is shown in Figure 36.

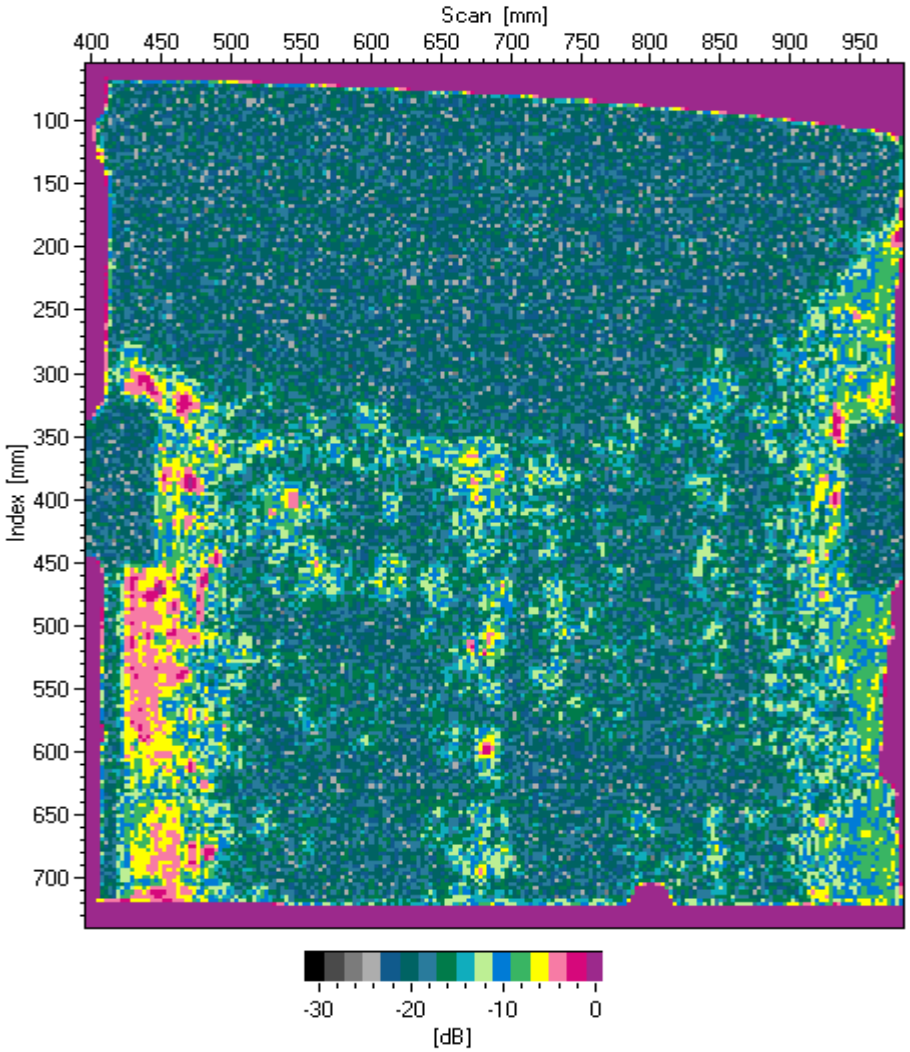

Figure 36: Result of the ultrasonic scanning of panel C. The red areas represent locations where no or only small delaminations occur.

It is visible that the panel is almost entirely delaminated, which is indicated by the blue and grey spots. This plot does not reveal where the delaminations are located through the thickness. However, the visual inspections have shown delaminations in various thickness locations.

7 Failure Description

This chapter only contains pictures done after the final test.
First part includes pictures outside followed by pictures inside the box girder.

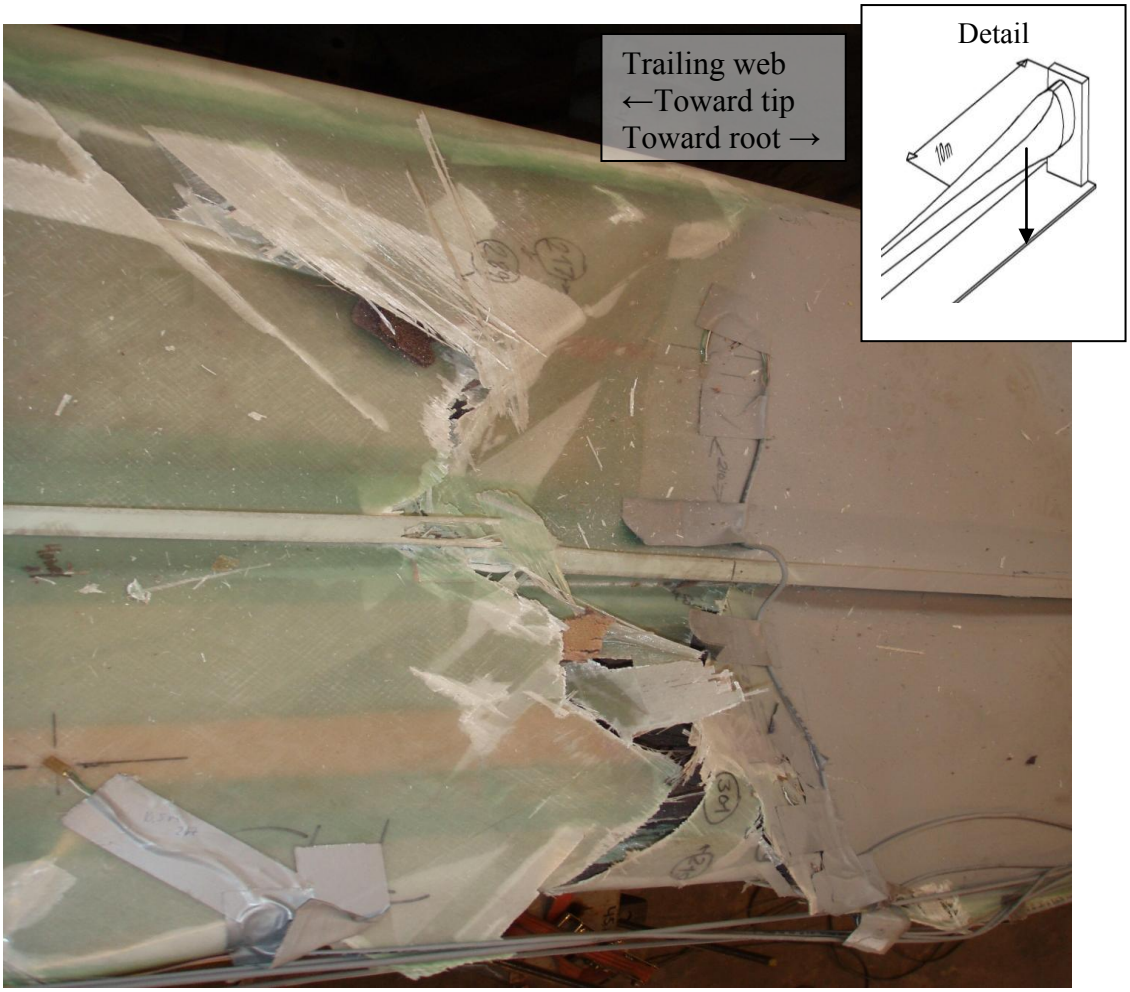

Figure 37. Failure outside box girder in 10.1m

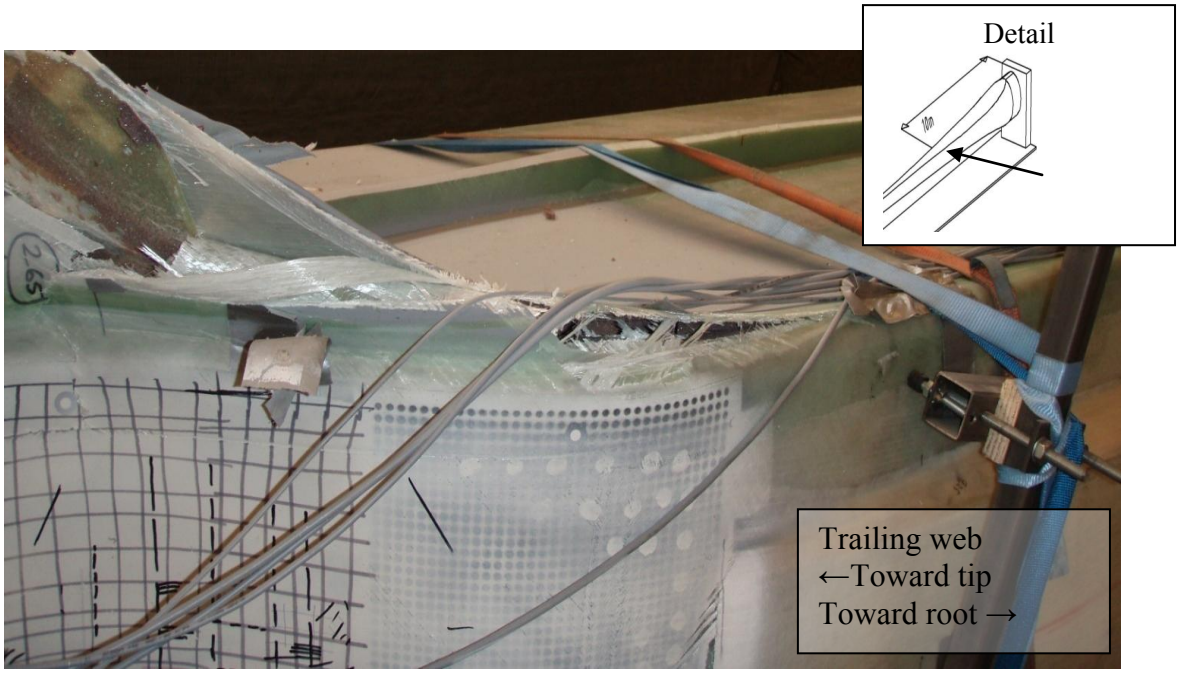

Figure 38. Compression side of box girder in 10m.

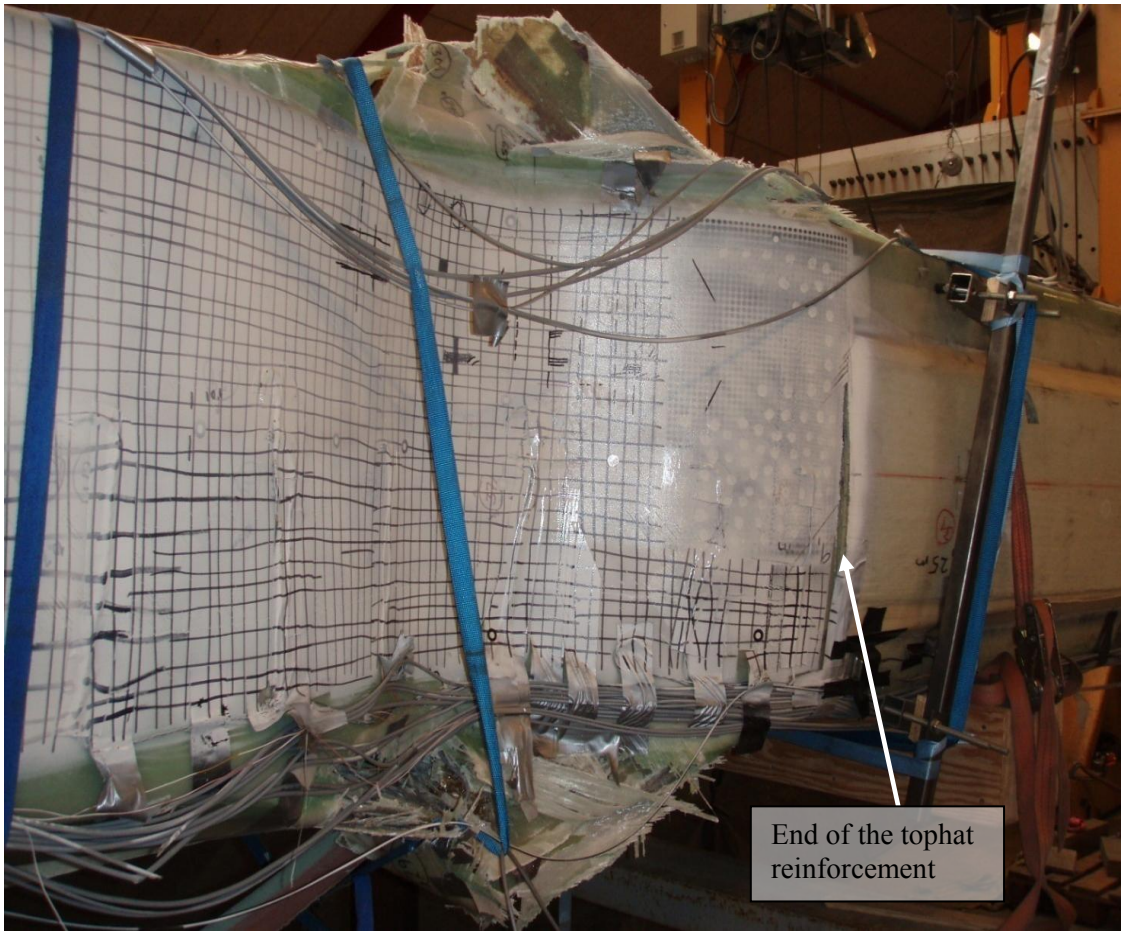

Figure 39. 10.1m section. Compression side of the box girder.

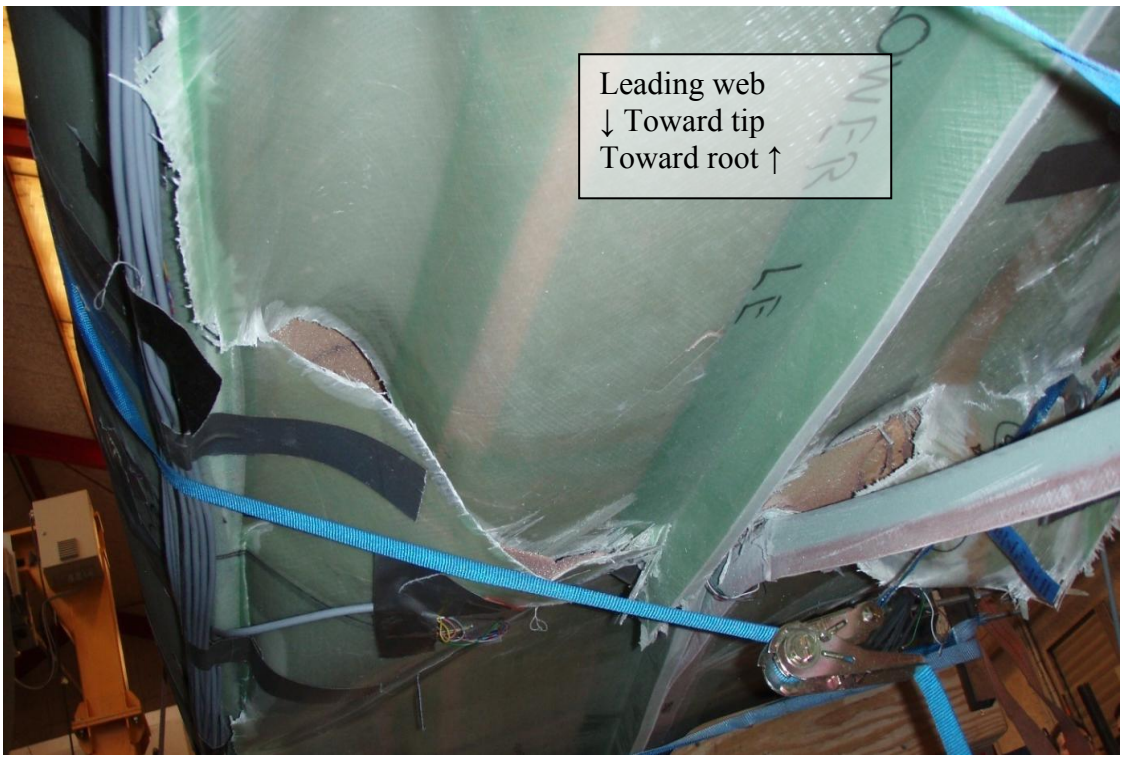

Figure 40. Box girder seen from leading side

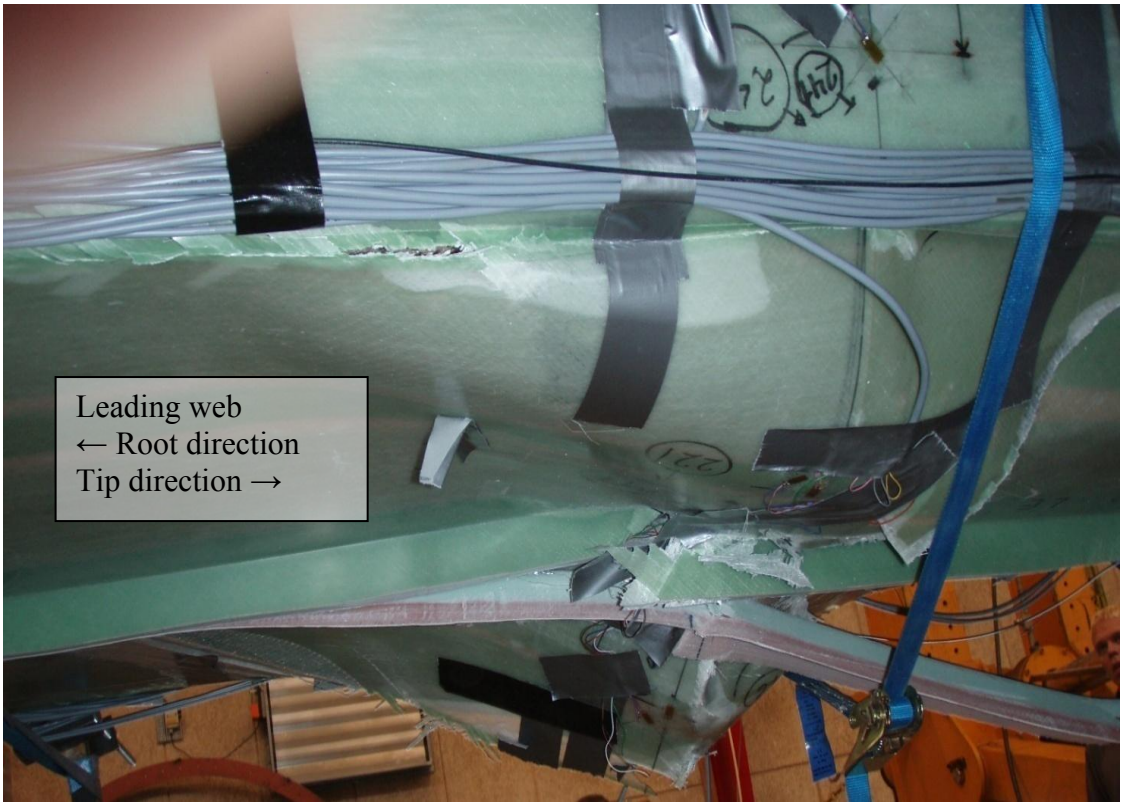

Figure 41. Box girder seen from the tension side, view of the leading web.

Figure 42. Inside the box girder.

8 Summary – flapwise loading

The box girder failed in 10.1m which was expected to be the critical region. Therefore the majority of the measuring equipment was placed in this area.

The ARAMIS system gave satisfactory results for measuring local deformations. The fringe projection system has not reached the same level of precision, but has shown promising results if improvements are implemented.
With ARAMIS and other DIC systems the measuring of the local deformations is an effective way to validate surface deformation in the FE models of blades.
Strain gauge measurements give an indication of how close the box girder is to failure, by studying non-linear behaviour when the blade approaches the failure. However it is required that a large number of strain gauges are positioned in the critical region. Failure in this region has been predictable only due to a comprehensive FE- studies and tests conducted in advance.

During the tests, acoustic emission from the blade was also measured. It was proved to be a very promising method to apply during static tests of box girders. The measurement gave information concerning the severity of the load, as well as zonal localization of the damages in the box girder. In general the global displacement sensors revealed linearity while the local displacement sensors show non-linear deformation behaviour.

Fig. 43a Fig. 43b

Figure 43. Failure: Box girder 1 collapsed.
Fig. a: the outer surface, trailing edge. Fig. b: the inner surface.

9 Description of the torsion test

The torsion test was carried out with a confidential load. The box girder was mounted on the test rig, as it was done under the flapwise bending test. However it was not supported in the same way. This is presented in Figure 44a.

Test setup

Sketch in figure 44 illustrates the test setup.
The test was performed with a counter-clockwise (CCW) and clockwise (CW) torsional moment. The definition of the counter-clockwise direction is shown in Figure 44 looking from the tip towards the root.

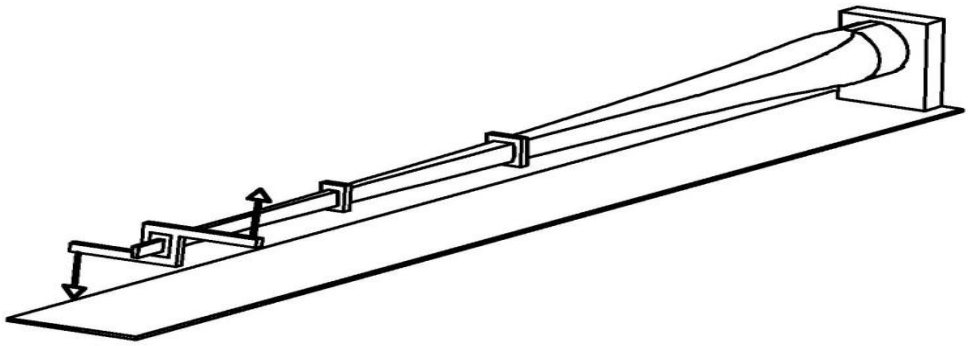

Fig. 44a

Fig. 44b

Fig. 44c

Figure 44. a: The torsional test set up in CCW direction. b: Close up of the outer) loading clamp. b: Close up of loading setup seen from behind, the bending moment applied CW.

Loads

The torsional test consisted of three subtests:
One test conducted with the torsional moment applied in counter-clockwise (CCW) direction at 19m and two tests with moment applied at 25m both clockwise (CW) and counter-clockwise (CCW).

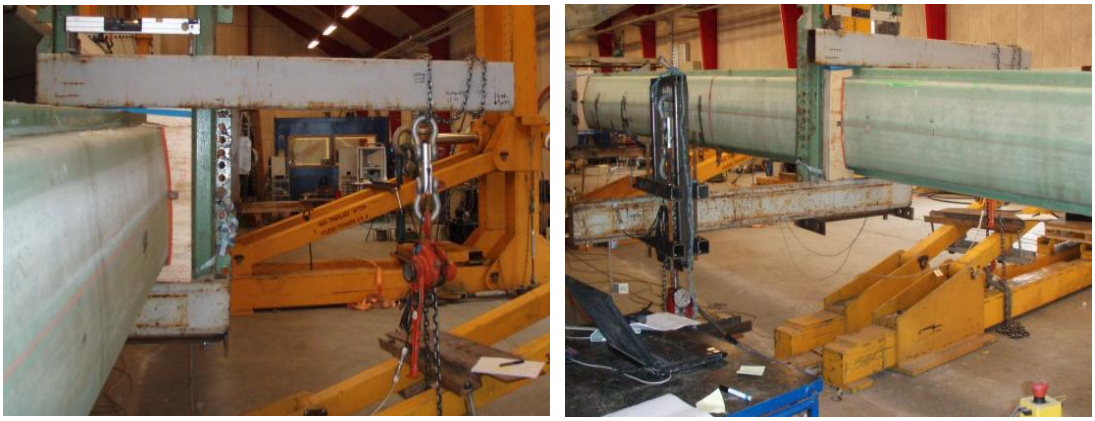

Figure 45. Left: Loading in 19m at compression side. Right: Loading at tension side

Results

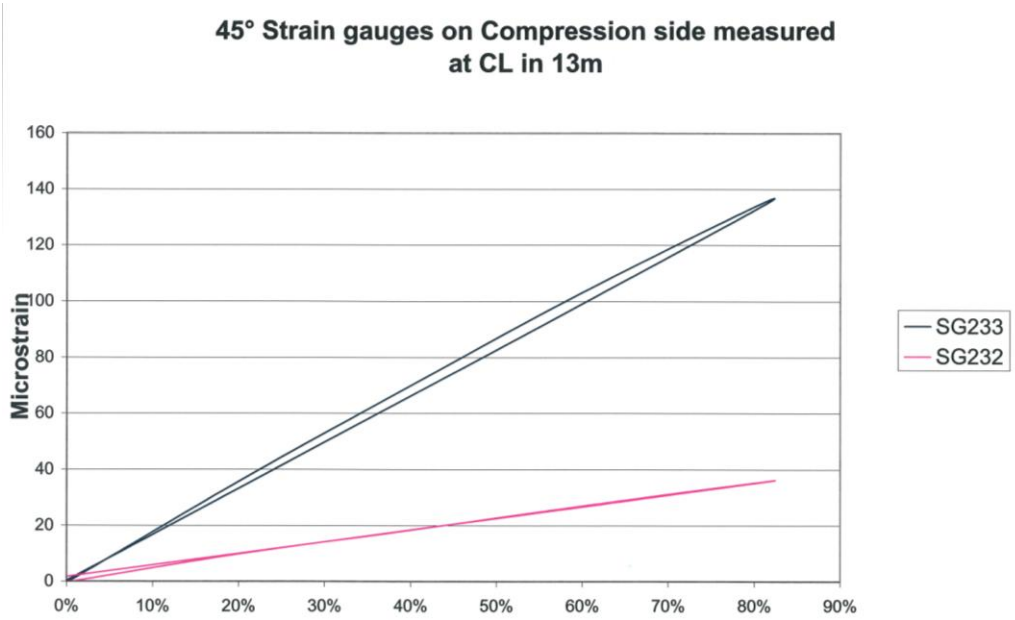

Figure 46. 45° strain gauge clockwise measurement in 13m on compression side

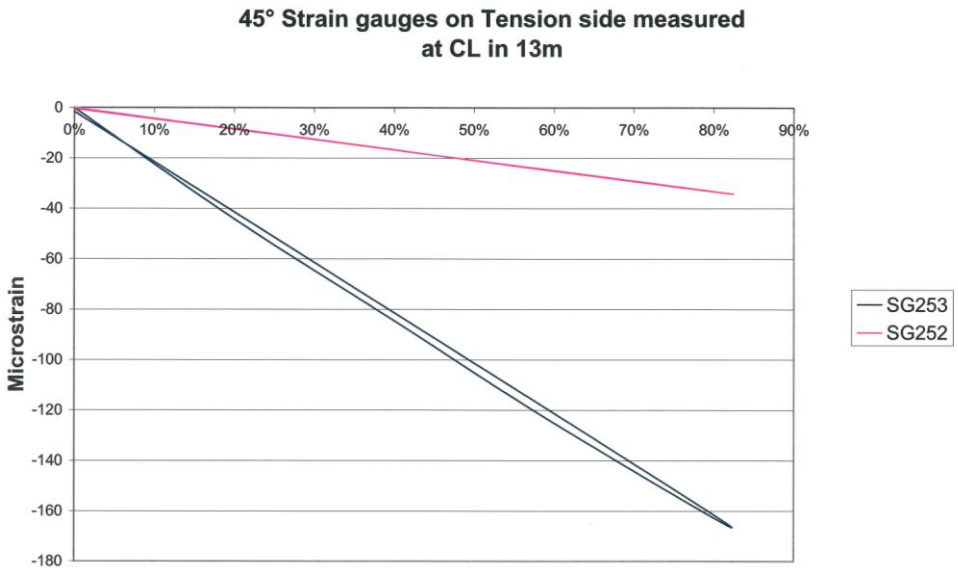

Figure 47. 45° strain gauge clockwise measurement in 13m on tension side

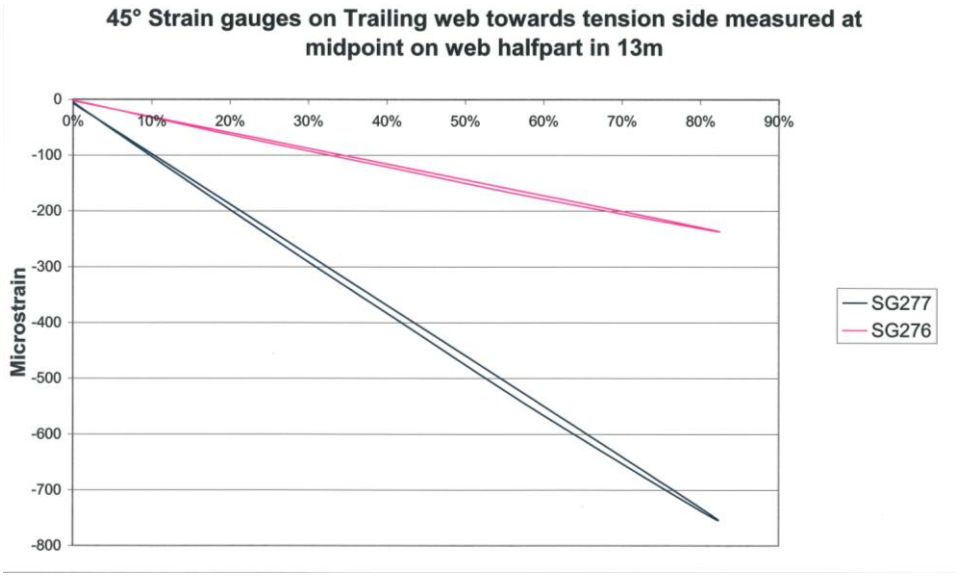

Figure 48. 45° strain gauge clockwise measurement in 13m on trailing web towards tension side

One selected measurement section is shown in Figure 46 to Figure 48. The box girder was loaded and unloaded. Complete results from the three tests can be found in appendix F.

10 References

[1] "*Ultimate strength of a large wind turbine blade*" Find M. Jensen. Ph.D thesis. Risø Nartional Laboratory, Technical University of Denmark. Submitted May 2008.

[2] "*Full-scale Test of a SSP34m box girder 2 – Data Report*" F. M. Jensen, K. Branner, P. H. Nielsen, P. Berring, T. S. Antvorskov, M. Nielsen, J. H. Reffs, P. H. Jensen, M. McGugan. C. Skamris, F. Sørensen, R. S. Nielsen, J. H. Laursen, M. Klein, A. Morris, H. Stang, J. Wedel-Heinen, J. P. Dear, A. Puri, A. Fergusson Risø-R-1588(EN) in progress (April 2008)

[3] *"Full-scale testing and finite element simulation of a 34 metre long wind turbine blade"* Find M. Jensen, Andy Morris. NAFEMS World Congress – Vancouver (April 2007)

[4] *"The Brazier effect in Wind-Turbine Blades and its Influence on Design"* F.M. Jensen, P.M. Weaver, L.S. Cecchini, H. Stang, R.F. Nielsen, Department of Wind Energy – Risoe National Laboratory, Technical University of Denmark. Department of Aerospace Engineering – University of Bristol – Bristol, UK DeepSea. Department of Civil Engineering – Technical University of Denmark.

[5] *"Optics measurement and numerical simulation of a wind turbine blade"* Weitao Ma. Risø National Laboratory, Roskilde, and Technical University of Denmark, Lyngby, Denmark, (30th July 2007)

[6] *"Keynotepresentation bending behaviour of a wind-turbine blade under full-scale testing"* Find M. Jensen. NAFEMS-UK Seminar in UK, November Abstract (2006)

[7] "*Resultat behandling fra fuldskalaforsøg*". Troels S. Antvorskov. Final Project. Engineerschool in Copenhagen (December 2006)

[8] "*Effect of sandwich core properties on ultimate strength of a wind turbine blade*" 8thedition K. Branner, F. M. Jensen, P. Berring, A. Puri, A. Morris and J. Dear International Conference on sandwich Structures. (April 2008)

[9] *"Digital image correlation based failure examination of sandwich structures for wind turbine blades"* J. Dear, A. Puri, A. Fergusson, A. Morris, I. Dear, K. Branner and F. M. Jensen. International conference on sandwich Structures. (April 2008)

[10] *"Experimental techniques for improving life assessment and qualification of wind turbine blades"* A. Puri, A. Fergusson, J. Dear, A. Morris, Find. M. Jensen. T12 Structural Design and Matrials EWEC in progress (2008). Abstract only

[11] "*Digital image correlation and finite element analysis of wind turbine blade structural components*" A. Puri, A. Fergusson, J. Dear, A. Morris, F. M. Jensen 2007 European Offshore Wind Energy Association conference. Germany, (December 2007)

[12] *"Analysis of Wind Turbine Material using Digital Image Correlation"* Amit Puri, Jon P. Dear, Andrew Morris & Find M. Jensen. EWEC conference (2008)

[13] Guidelines for Design of Wind Turbines – DNV/ Risø 2nd Edition

11 Appendices.

A: Test schedule

B: ARAMIS

C: Fringe Projection – optical measurement on local deflection

D: Acoustic Emission measurement

E: Measured strain gauge results flapwise bending

Strain gauge plan

Strain gauge longitudinal 0°

Strain gauge transverse 90°

Strain gauge transverse 45°

Appendix A: Test Schedule

Test schedule

This appendix reveals the period when the tests have been performed and gives comments on the testing process.

Test 1

Date: Tuesday 11 August 2006 — **P**erformed to verify the test equipment.
Time: 18:15-19:00
Test setup: Supports to eliminate torsion: 2
Load range: 0% to 60%
Strain gauge list: Appendix E

Acoustic Noise Emission
Date: Tuesday 11 August 2006 — This test was performed to check the measuring and logging equipment output.
Time: 17:45-18:10
Test setup: Supports to eliminate torsion: 2
Load range: 0% to 50%
Strain gauge list: No Data
Acoustic Noise Emission: Appendix D – Burst rating =20.4
Fringe Projection (Optical measuring): Appendix C - Testing and calibration
Test note:
Problems with the Strain Gauge/LT-LVDT/LT-ASM data logger, test performed without the system working properly.

Test 2

Date: Wednesday 12 August 2006 — The test was performed to verify the test equipment.
Time: 09:00-09:20
Test setup: Supports to eliminate torsion: 2
Load range: 0% to 69%
Strain gauge list: Appendix E
Acoustic Noise Emission: Appendix D – Burst rating = 256
Fringe Projection: Appendix C - Testing and calibration
Test note:
Problems with the Strain Gauge/LT-LVDT/LT-ASM data logger fixed.

Test 3

Date: Wednesday 12 August 2006 — **P**erformed to verify the test equipment.
Time: 12:20-12:50
Test setup: Supports to eliminate torsion: 2
Load range: 0% to 75% (target 77%)
Strain gauge list: Appendix E
Acoustic Noise Emission: Appendix D – Burst rating = 319
ARAMIS: Appendix B
Fringe Projection: Appendix C - Testing and calibration
Test note:
Tip actuator reached its maximum travel after as much as 75% load, the test setup had to be modified. During the data processing it was discovered that an extra support needs to be added to eliminate torsion.

Test 4

Date: Wednesday 12 August 2006 This test was performed to verify the test equipment and setup.

Time: 14:30-15:00
Test setup: Supports to eliminate torsion: 2
Load range: 20% to 77%
Strain gauge list: Appendix E
Acoustic Noise Emission: Appendix D – Burst rating = 265
ARAMIS: Appendix B
Fringe Projection: Appendix C - Inside Box girder 10m
Test note:
To obtain loads higher than 75%, the blade is loaded up to 20 % and a link is removed from the tip actuator. Therefore in the following tests the load has its starting point at value 20%. The additional support has not been completed yet.

Test 5

Confidential test

Test 6

Date: Wednesday 23 August 2006
Time: 08:30-09:30
Test setup: Supports to eliminate torsion: 2
Load range: 20% to 65%
Strain gauge list: Appendix E
Acoustic Noise Emission: Appendix D – Burst rating = 13
Fringe Projection: Appendix C - Inside Box 10m
Test note:
To enable reaching loads higher than 75%, the blade is loaded up to 20 % and a link is removed from the tip actuator. Therefore in the following tests the load has its starting point at 20%. The additional support has not been completed yet.

Test 7

Date: Wednesday 23 August 2006
Time: 10:30-11:15
Test setup: Supports to eliminate torsion: 3
Load range: 20% to 77% (target 79%)
Strain gauge list: Appendix E
Acoustic Noise Emission: Appendix D – Burst rating = 1130
Fringe Projection: Appendix C - Outside the Box girder 10m
Test note:
Test stopped due to high acoustic emission level.

Test 8 Ultimate test

Date: Wednesday 23 August 2006
Time: 11:30-12:20
Test setup: Supports to eliminate torsion: 3
Load range: 20% to failure (79 %)
Strain gauge list: Appendix E
Acoustic Noise Emission: Appendix D – Burst rating = 7800
Fringe Projection: Appendix C - Outside the Box girder 10m
Test note: Test recorded on video tape. Blade failure

Appendix B: Aramis

Aramis

In principle the ARAMIS system works by analysis of the acquired images. Undeformed stage is used as a reference and multiple deformed stages are recorded during a test.
Multiple subsets of image pixels are analyzed by a grey-value correlation technique in the undeformed and the deformed state.

Figure 49. ARAMIS equipment (facing towards the tip).

Aramis is an optical measurement system which can measure deflection in three directions at the same time. The system uses two cameras detecting the difference in measured pattern. This technique can measure the deflection in an area of 2.5m by 2.5m for a four Mega pixel system.
The ARAMIS equipment is produced by GOM and the measurements were performed by GOM / Zebicon.

In the Figure 50 the measuring equipment is shown from behind, facing the compression side of the box girder. Note the painted speckle/ random pattern on the box girder compression side.

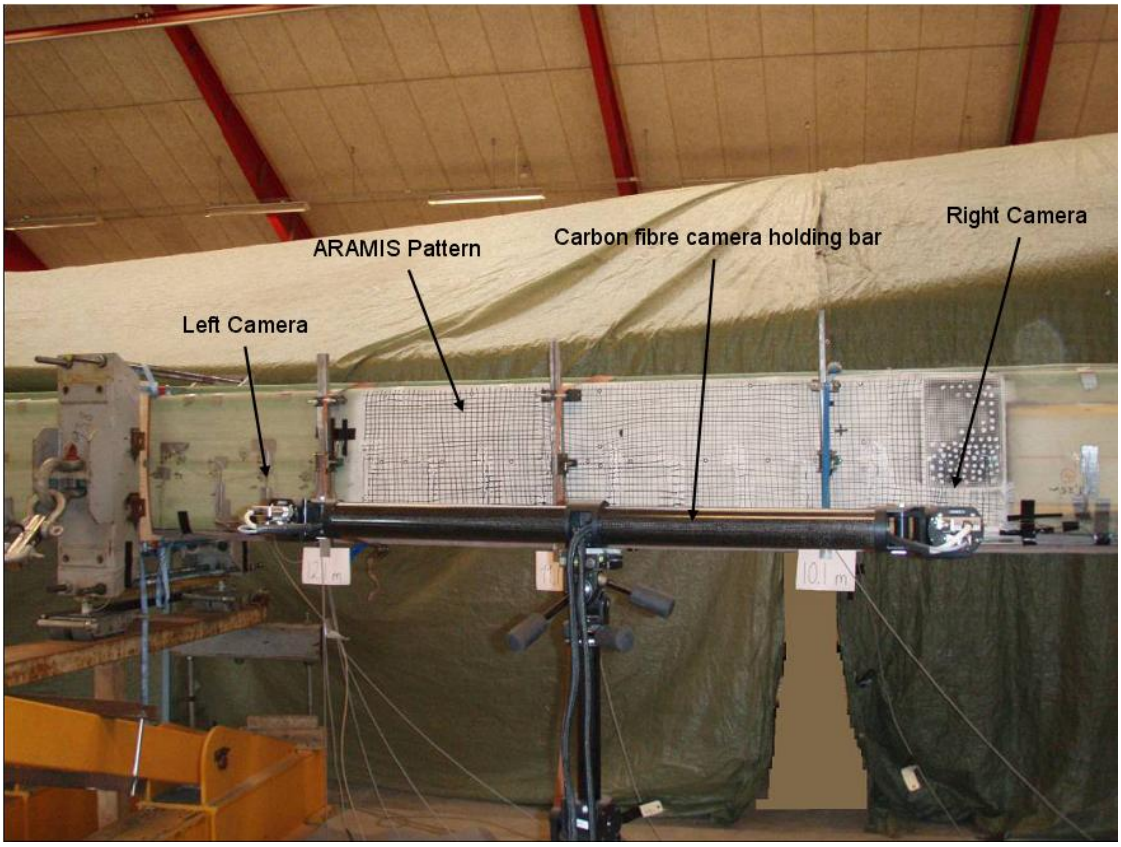

Figure 50. ARAMIS equipment positioned in front of the measuring area.

The ARAMIS performed measurements on the box girder's compression side in the distance of 9 to 12 meters from the root. The results from these measurements are presented in the following figure.

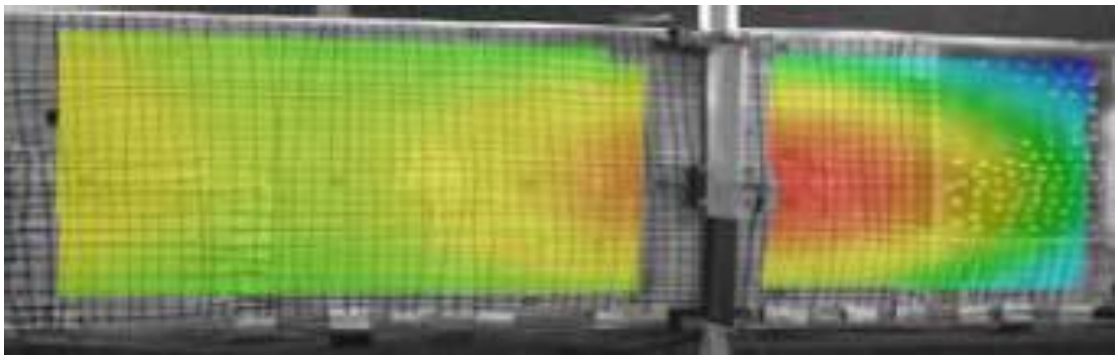

Figure 51. Out-of-plane displacement results from the ARAMIS measurements are transferred to the specimen's surface with a rigid body movement correction.

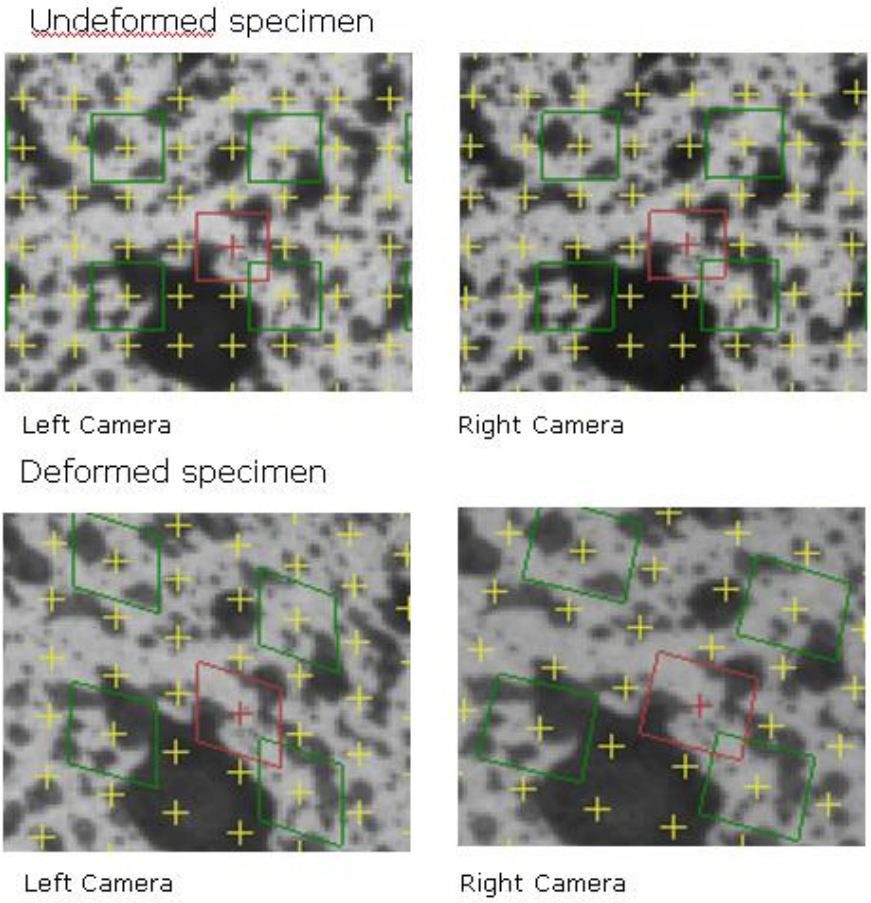

Figure 52. Changing of a random pattern during deformation

From each of the shown centres of the subsets 3D coordinates with X-, Y- and Z-coordinates are triangulated.

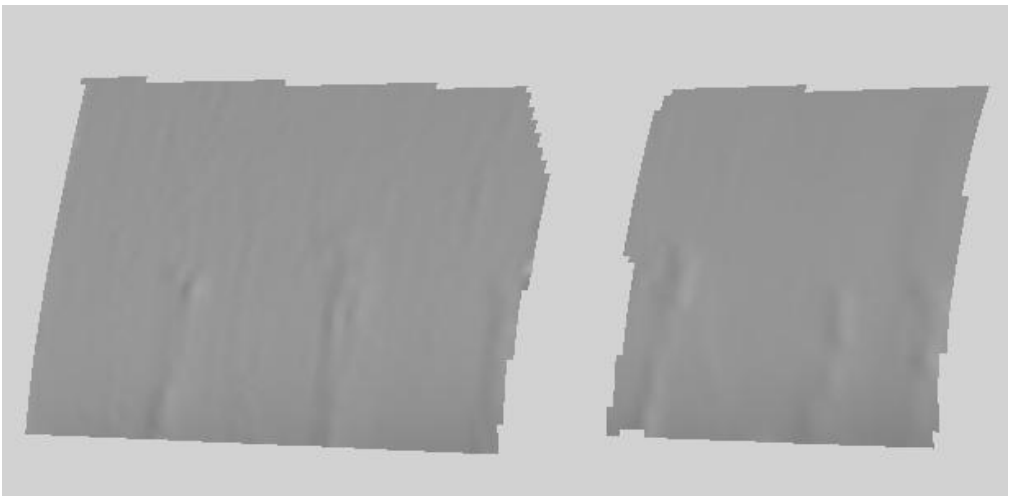

Figure 53. 3D-coordinate data from specimens surface in deformed state

3D-displacements and surface strain values were computed by means of comparison of the coordinates between reference and deformed stages of the test specimen.

Appendix C: Fringe Projection

Fringe Projection – optical measurement on local deflection

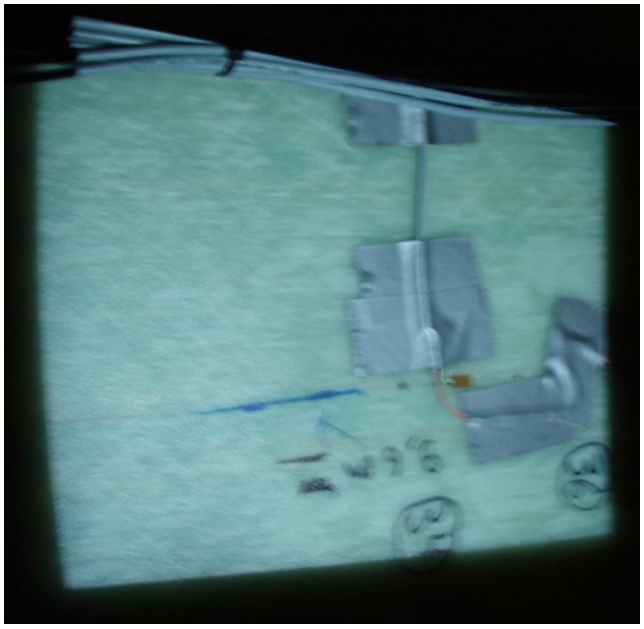

Figure 54. Fringe projection on the inner side of the compression side

Measurement of surface deflections using Fringe Projection

René Skov Hansen (OPL), Weitao Ma (student, VEA)

The fringe projection technique is a non-contact optical method for measuring out-of-plane surface deflections of whole 2D-surfaces. The system is based on a multi-channel triangulation technique, where the surface of interest is illuminated by a fringe pattern consisting of straight stripes with a cosine intensity variation, see Figure 55.

Figure 55. The surface of interest is illuminated by a cosine intensity pattern. For illustration, a computer mouse is inserted as an object in the fringe pattern.

When the illuminated surface is viewed from a certain angle, different from the illumination angle, all surface shapes and/or displacements generate a related displacement of the observed fringe position. Images of the illuminated surface are captured by a digital camera and stored in a computer for further processing. By measuring the phase distribution across the captured cosine fringe pattern using general phase-shifting techniques, the system is able to measure local displacements of the fringe pattern down to $\Lambda/20$. Here, Λ is the spacing between the fringes, measured in unit of meters across the object surface. With typical values for the measurement setup, this corresponds to a measuring resolution on the out-of-plane surface position of approximately 0.1mm. The measured phase distribution of the captured fringe pattern is called a phase image. When used for measuring out-of-plane surface displacements, the system first measures and stores a reference phase image of the cosine pattern, seen on the non-deformed object surface. Afterwards, the reference phase image is subtracted from the phase images, measured with the object under load. For small deformations, the out-of-plane surface displacement, Δh, at position $\vec{r}$ is related to a displacement of the corresponding fringe, Δx, by

$$\Delta x\ \vec{r}\ = \Delta h\ \vec{r}\ \quad \tan\alpha + \tan\beta \qquad \text{(C.1)}$$

where, α, and β are the angle of illumination and observation respectively, see Figure 56. The corresponding shift of the phase to be measured by the system is determined by

$$\Delta\theta\ \vec{r}\ = \frac{2\pi}{\Lambda}\ \tan\alpha + \tan\beta\ \ \Delta h\ \vec{r} \qquad \text{(C.2)}$$

Thus, the relation between the measured phase, $\Delta\theta$ and the surface displacement is given by:

$$\Delta h\ \vec{r}\ = \frac{\Delta\theta\ \vec{r}\ \ \frac{\Lambda}{2\pi}}{\tan\alpha + \tan\beta} \qquad \text{(C.3)}$$

It is seen that the sensitivity of the system i.e. the amount of phase change per surface displacement, is determined by the angles of illumination and observation (camera) and the fringe spacing. A normal image projector, connected to a secondary graphics card in a PC-computer, is employed as the illuminating source. In this way, the computer can easily and dynamically create the fringe patterns needed for the measurement.

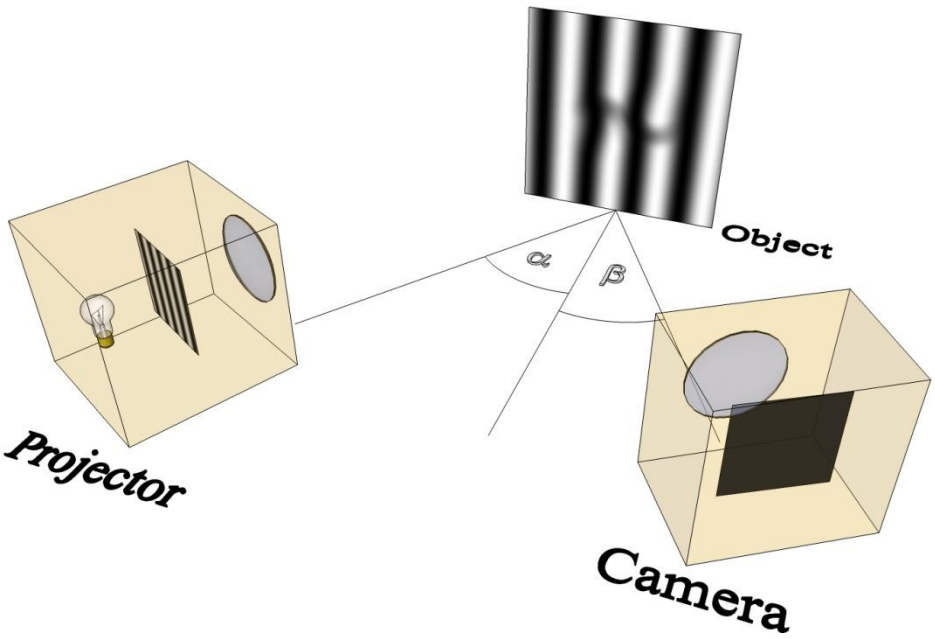

Figure 56. The measurements set-up. A normal projector, connected to a PC-computer is illuminating the object surface with a cosine fringe pattern. The projector is positioned in an angle α with respect to the normal surface. A digital camera, also connected to the PC-computer, is capturing images of the resulting fringe pattern. The camera is located at an angle β from the object surface.

For illustrative purposes, the resulting phase image of the above computer mouse is recalculated to a height image which is shown in Figure 57.

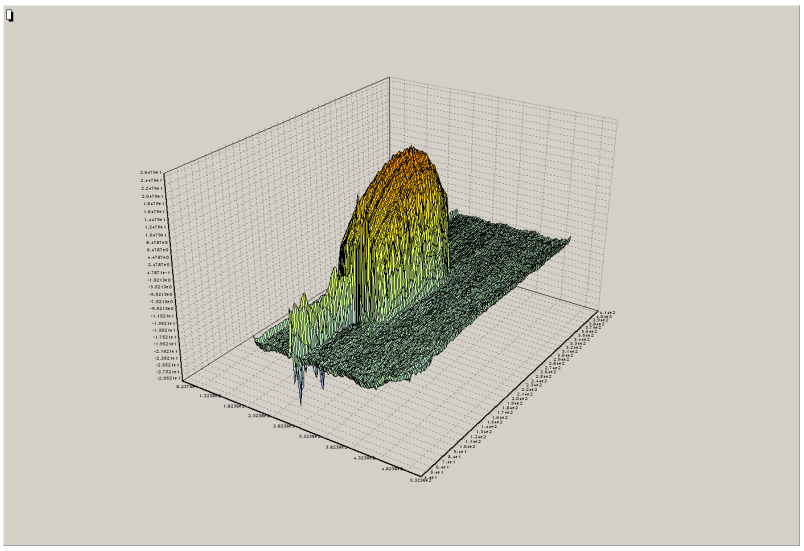

Figure 57. The resulting measurement of the above computer mouse.

The measurement system presented here is only expected to be capable of covering one to two square meters of the object surface, depending on the measurement accuracy needed and the experimental conditions. However, both the projector and the camera, which constitute the hardware needed for the measurement set-up, are now relatively inexpensive components. Therefore, the measurement principle described here can be

used for setting up several systems along the turbine blade without increasing the measurements' costs.
It is also appropriate for destructive blade-tests where a high probability of hardware damage occurs.

Measurements performed with the fringe projection system

In the following section, the results from using the fringe projection system (FPS) in the full-scale wind turbine blade spar test are presented. The spar for a 34m wind turbine blade was tested to failure under flapwise loading. Its geometry is depicted in Figure 58.

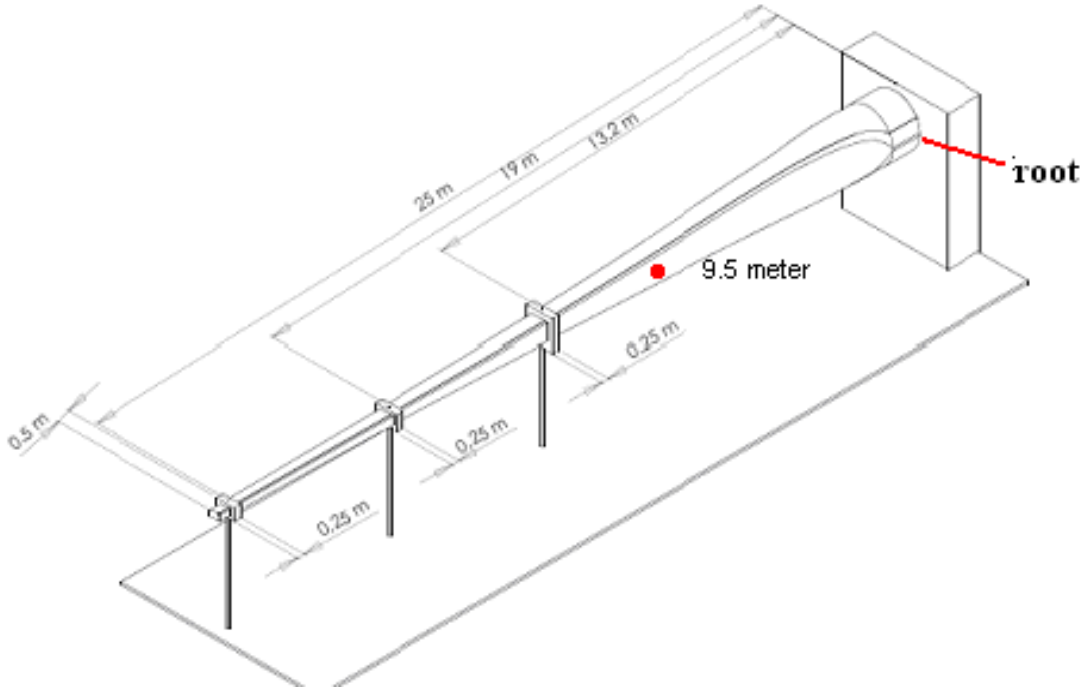

Figure 58. The spar under test. The measurement area under consideration is marked at distance of 9.5 meters from the spar root

From the FE simulations model, a large local displacement is expected to occur at a distance of 9 to 10 meter from the root of the spar. Therefore, the area at the 9.5 meter segment was measured in this experiment. Two sets of measurements have been performed: A compressive cap and a trailing ledge web deflection. The two measurements are discussed further.

A fixture for the projector-camera arrangement has been made where both the angle of illumination and the camera angle can be adjusted. The angle of illumination is chosen to be normal to the surface of interest (α=0), and the camera is the looking at the surface from a skew angle, β, see Figure 59.

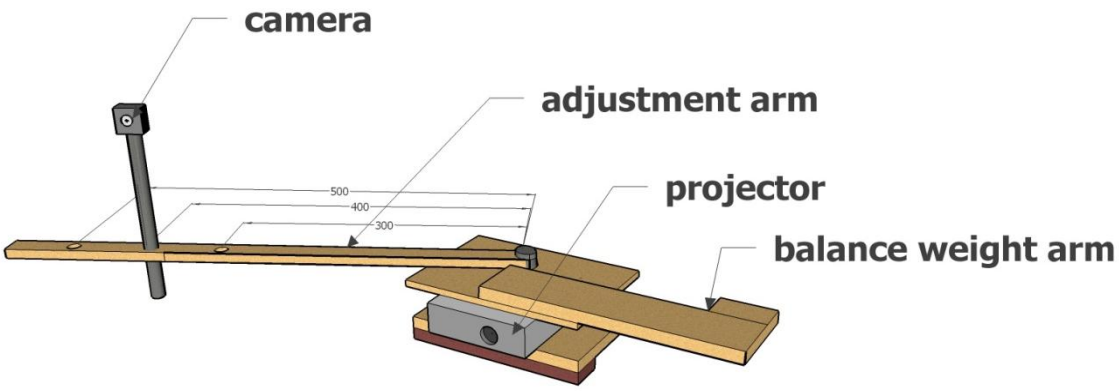

Figure 59. The fixture for the projector and the camera.

The cap deflection measurement

The compressive cap deflection test was performed inside the spar. The fringe projection system was fixed at the corner of spar and illuminates the surface of interest, see Figure 60. There are two advantages of using the corner as a fixed point for FPS:
(a) It is necessary to place the FPS as far from the measured surface as possible to obtain a large measuring area. The corner position of the FPS system proposed maximizes the measured surface, which is otherwise limited by maximum size of the image the projector is able to create. Obviously, the size of the spar is constant.
(b) During the test, the corner is the most stable part of the spar and thus it obtains the smallest local deflections during the bending. Hence, measuring at the corner is considered the most reliable and effective position inside the spar. In the suggested setup, the effective measuring area on the local compressive cap surface is approximately 500mm x 400mm.

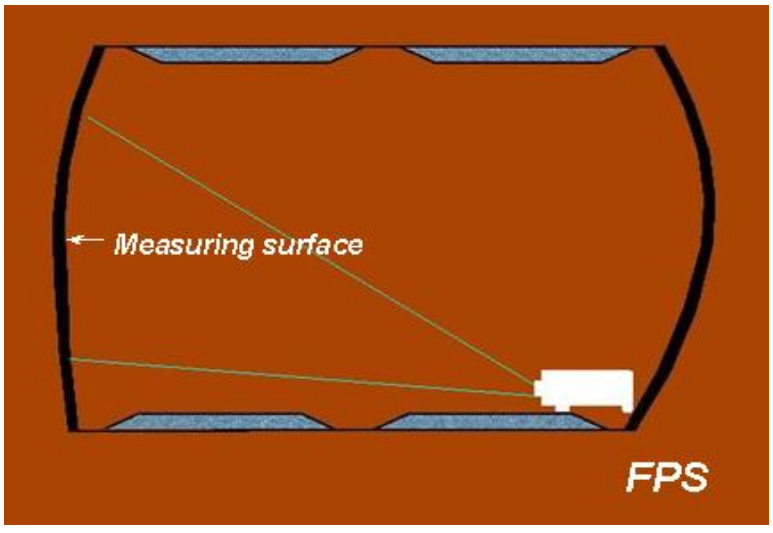

Figure 60. The position of the FPS at the corner inside the spar.

The reference-phase image of the observed surface is presented in Figure 61.

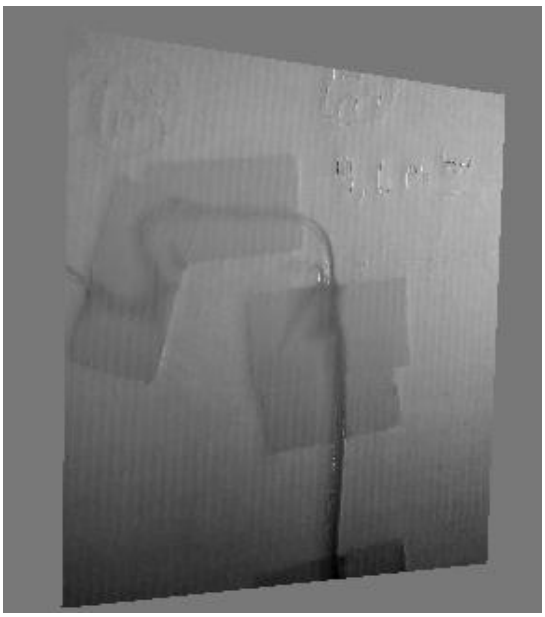

Figure 61. The reference phase image of the observed spar surface. The wire and adhesive tape fixture of a strain-gauge set-up is seen as variations of the surface height.

Cap deflection test result

At various loads of the spar, the entire displacement pattern of the measured surface was recorded with the FPS system. One of the performed measurements is presented in Figure 62a. All local displacements of the surface are shown in a 3D map. In order to compare the result with the displacement values, obtained by using other techniques, the displacements measured at the centre of the image are picked out to form the 2D plot shown in Figure 62b. It can be easily noticed that the displacement of the centre area is a non-linear function of the load (the blue line in the (b)-figure). The measured values of displacements are very close to the FEM simulation results (the red line). It was concluded that the FPS measurements confirm that the FEM model of 34-meter wind turbine blade is accurate enough to be able to obtain the correct non-linear local deflection of the spar surface.

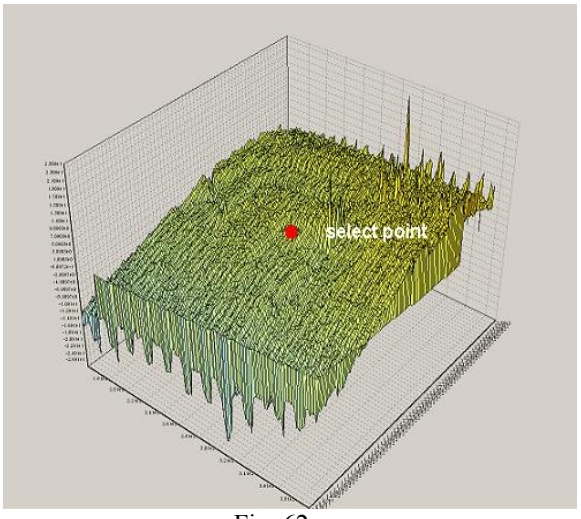

Fig. 62a

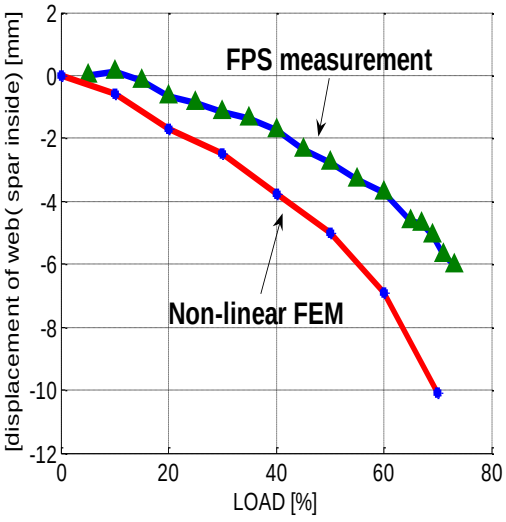

Fig. 62b

Figure 62. (a) The 3D plot displacement of the cap surface at 70% load. (b) the FPS measurements and the FEM result at the centre point of the measurement area.

The local deflection on the cap segment is investigated by observing a plot of the local deflection along the centre line of the spar, i.e. segment from the 9.43 to the 9.71-meter, measured from the root. The line of interest is shown in Figure 63a. The deflection along the line is shown in Figure 63b (the blue line). It can be noticed that there are some deviations from the otherwise smooth deflection. These FPS system measurement deviations are possibly caused by folding of the connection wire and the adhesive tape that constitutes the strain gauge setup.

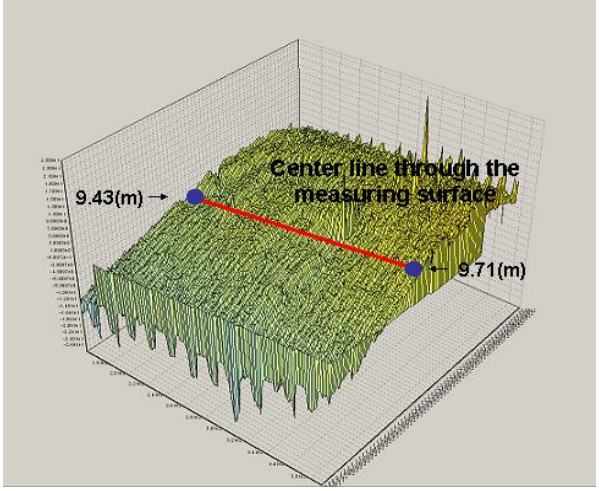

Fig. 63a

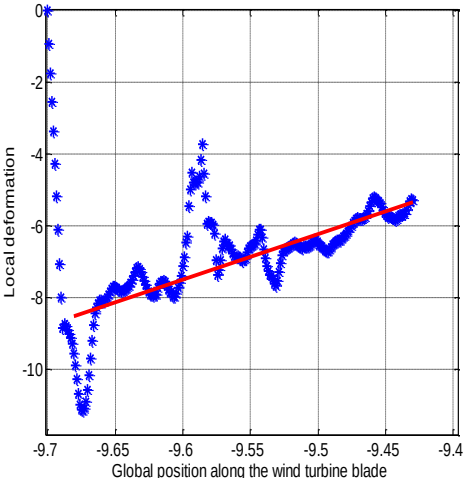

Fig. 63b

Figure 63. (a) The 3D plot of the displacements of the cap surface at 70% load. (b) The measured displacement along the line from 9.43 to 9.71 meters from the root.

Although we have measured the above additional displacements of the strain gauge setup, we are still able to localize the local deflection along the centre line. These measurements confirm that the compressive cap surface has an additional bending. From ARAMIS and non-linear FEM results, we call this oval shape of the localized deflection 'buckling'. We can confirm that the deflection at the 9.65m position is approximately 2 mm higher than for 9.45m.

The trailing edge of web deflection measurement

The local trailing edge web deflection is an interesting item in the full-scale spar test. Comparing with the cap deflection test, where the space for the set-up was limited inside the spar, an outside measurement of the trailing web allows for a larger measurement area. The measurement set-up is shown in Figure 64. A long steel bracket was constructed to support the FPS above the spar. The whole system was supported in two spar corners. In that manner, the FPS may follow the large overall movements of the whole spar during load and is able to measure only the local deflection of the upper spar surface.

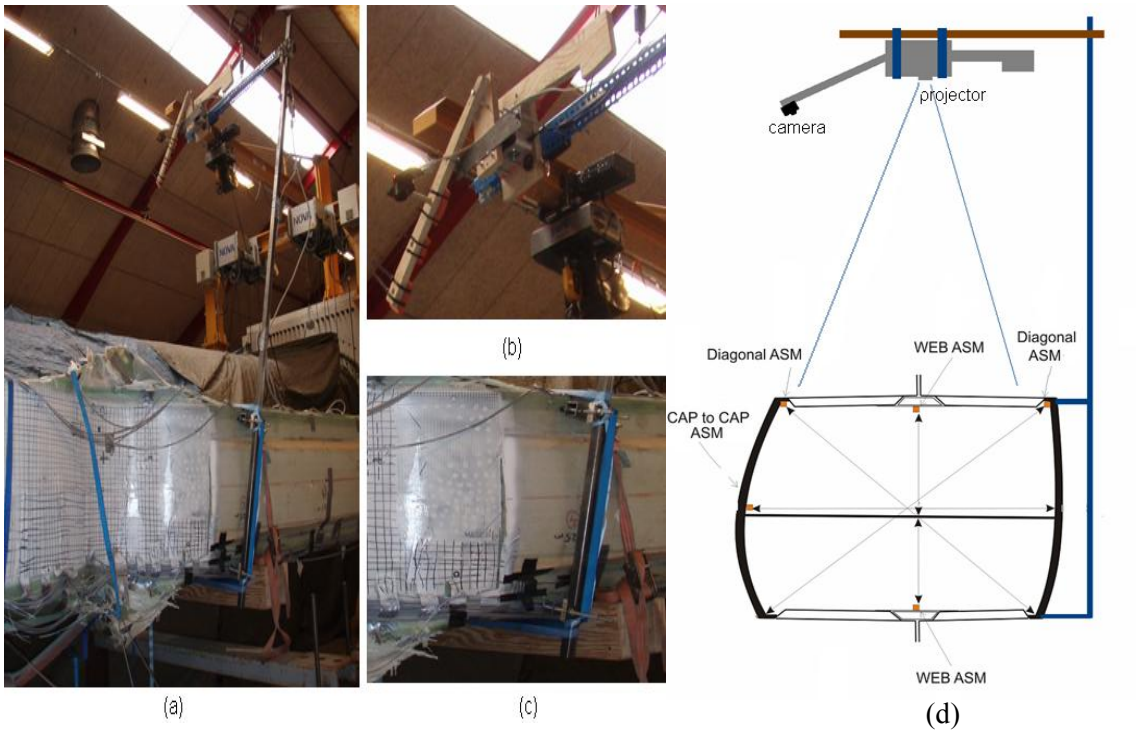

Figure 64. Photo of test setup: Fig. a: The setup for the trailing edge web deflection measurement. Fig. b: The FPS before the trailing web. Fig. c: The holder was supported at the two spar corners. Fig. d: Sketch of measuring setup

The surface image captured by the camera is seen in Figure 65.

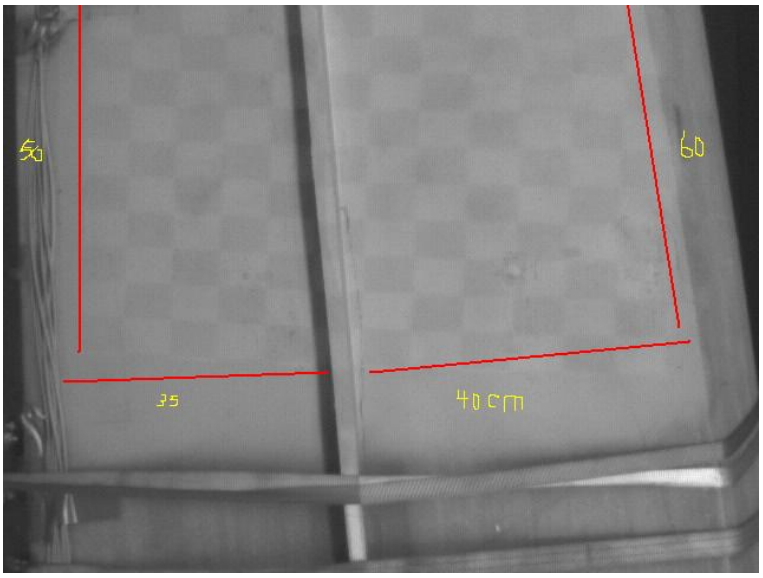

Figure 65. The surface of the web seen by the camera.

The measurement results obtained from the trailing web deflection was not as accurate as the results obtained from the cap deflection test. In Figure 66 it is seen that the measured displacements have large variations. However, we are still able to reconstruct the deflection of the trailing web centreline of the at the 9.6-meter segment to be 2 or 3-millimeter by means of geometrical estimation.

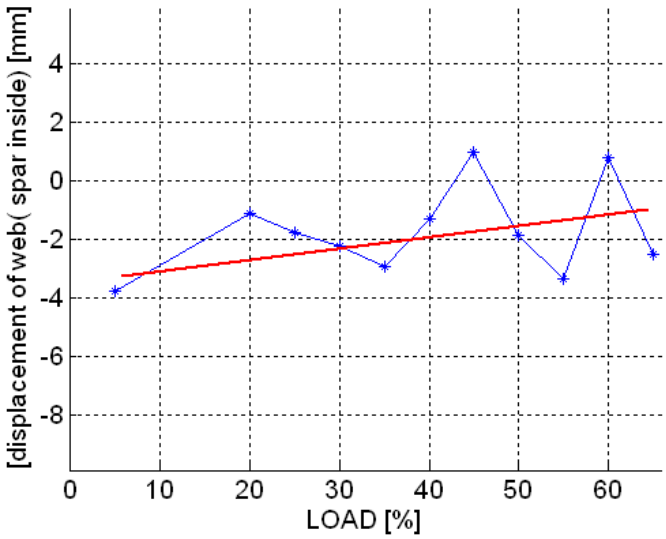

Figure 66. The deflection of the centreline of the 9.6-meter segment as a function of the spar load.

The disturbed results are believed to be caused by setup problems. The major problem is the light in the workshop which could interfere with the weak light from the small projector employed. Therefore, the camera cannot capture a clear fringe image from the web surface. The secondary problem is that the steel bracket supporting FPS was not stiff enough. Thereby, the whole set-up suffered from small vibrations and deflections, which disturb the measurements seriously.

Appendix D: Acoustic Emission measurement

Background to AE monitoring on Wind turbine blades

Introduction

When certain dynamic processes occur in or on the surface of a material some of the energy that is released generates elastic stress waves; we might say vibrations. These stress waves propagate from the source and can be detected by sensitive transducers. The signal from these transducers (once amplified) is then available for analysis. Information about the location, severity and nature of the event causing the stress wave emission can be deduced from the received signals.

When loaded, structural polymer composite material emits a huge number of these transient stress waves as a result of non-reversible (plastic) micro-damage events such as matrix cracking, tribology at delaminations, fibre breaks, etc. This multitude of small-scale events is detectable long before a reduction in structure stiffness and/or the appearance of visible (macro-scale) cracking.

When a composite structure is loaded to an “extreme” degree, a significant increase in general stress wave activity can be expected. And in cases where a structure is loaded “normally” any area which has already sustained local damage (as the result of an impact, static overload, or severe fatigue for example) will also return an increase in local stress wave emission activity relative to the surrounding "good" material.

The potential exists, therefore, to locate defects and damaged areas in composite structures, before they become threatening to the structure integrity, by monitoring these transient stress waves. It is also possible to chart the progression of structural response to loading towards ultimate failure in this way.

As the signal frequency generally does not fall in the human audible range, the term acoustic emission (AE) is a misnomer and the alternative term stress wave emission (SWE) would be a more accurate description of the phenomenon, both are used but acoustic emission is the expression in more widespread use.

Application

The Acoustic Monitoring systems used by Risø National Laboratory within the Wind Energy Industry have provided:-

- Blade monitoring during testing
    1. Standard (industry approved) testing
    2. Speciality (one-off) testing
    3. Static testing
    4. Fatigue testing
- In-service blade monitoring
    1. Applied blade test loading while on the turbine
    2. During normal operation over an extended period (12 months +)

Some of this work has been within funded research projects, but most has been through direct commercial contracts with the blade manufacturers. In this way, a great deal of practical know-how and experience in this area has been gathered.

Application during structural testing

Feedback from the sensors gives the test controller more confidence when applying loads because he has an improved feeling for how the blade is responding and how close it may be to failure. The probability of an invalid test due to unwanted damage, for example crush damage at loading yokes, is greatly reduced. The occurrence of unexpected damage is more likely to be detected and conducting structure inspections between loadings is made simpler and more focused. Various structure specific damage types can be identified as loading takes place. This all has the effect of increasing the "working" time / "resting" time ratio of the blade whilst it lies in the test rig, thus saving money. [1]

Application in service

The large offshore wind farms planed for the near future will require a level of sensor technology sufficient to monitor general condition from on-shore stations. The continuous monitoring (operational condition and structural response) of all rotating components in the farm will give a higher level of safety and reduce the overall requirement for manual inspection. [2]

The turbine blades of a modern wind farm are incredibly large rotating components subjected to cyclic load variations (both the aerodynamic loading and the constant variation in gravitational loading during rotation) which can lead to fatigue damage or failure in the structural materials.

The greatest uncertainty concerning the lifetime of a wind turbine blade is related to the uncertainties concerning that particular structures material properties, and not in the wind loading it will be subjected to during service. This means that the development of fatigue damage can never be accurately predicted purely from modelled (or even measured) loading profiles, and that such profiles are insufficient to determine where, when, and which blades will produce damage. The philosophy must therefore be to monitor all blades and only inspect the few that show signs of developing critical damage under operation, the opposite of what is currently done.

The vision is of future blades containing sensors that give very early indications of any damage that is classed as critical or that is developing unacceptably rapidly. This early indication allows the option of changing operating conditions, and of a timely inspection, repair or replacement.

Test system set up

8-channel SIMPAL AE system [3] consisting of:

- one controller module
- one (8 channel) measurement node
- 8 AE-SS1 low profile sensors and sufficient co-axial cabling
- A laptop running SIMPAL-Vu controller software version 6.4E

Notes on the set-up

- Very little set up time is necessary. For short to medium duration tests it is only necessary to attach cabling and sensors with tape. This also makes it possible to relocate sensors midway through tests in response to the blade structural response.
- The co-axial cabling was attached to the eight channels of the measurement node and the cabling run out in pairs along the length of the blade to 3m, 6m, 9m and 12m. Tape was used to hold the cabling in position. Enough slack was allowed to permit the deflection of the blade without pulling on the sensors or system.
- Once all other preparations were complete, and the AE sensor locations confirmed, the sensors were attached to the blade with tape. Some surface preparation was required to ensure a good bond, i.e. that the surface was dry, matt and free of grease/oil.
- A thin layer of couplant gel under each sensor was used to ensure good signal detection
- A sensor location schematic shown in the figure
- A detection level of 40dB was used throughout the testing.
- All activity detected by the sensors is recorded and allocated within the time "bin" period in which it occurred. A 5 second bin length ensures uninterrupted data collection for 1 hour without the need for manual data download. This was sufficient time monitor each complete load/unload sequence.
- The blade was also monitored overnight by using a 1 minute data bin. And during the one month period in which the blade test was reconfigured and loaded in torsion, the unattended SIMPAL AE system remained operational with a bin period of 2 hours.

Sensor distribution

After each test the schematic shown was annotated to display the general AE activity profile within the box-beam associated with that loading; see section 11.8 for examples.

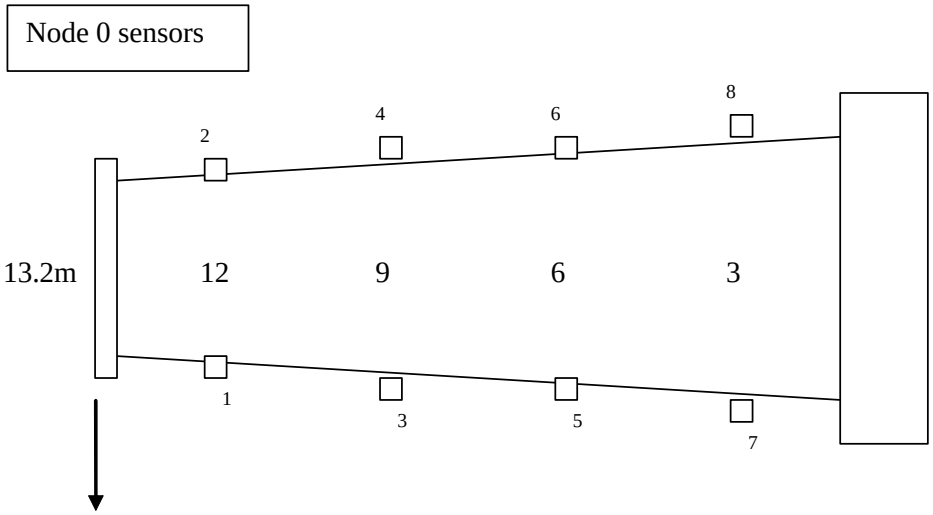

Figure 67. Scheme showing sensor distribution

Serial number	Node	Channel	Radius (m)	Side
05031	0	1	12	SS
05273	0	2	12	PS
05239	0	3	9 (*)	SS
05277	0	4	9	PS
05241	0	5	6	SS
05280	0	6	6	PS
05285	0	7	3	SS
05283	0	8	3	PS

Table 1. This table presents Node 0 sensor information

(*) This sensor is close to the end of Top Hat stiffener on the Suction side, a critical area.

Time line for the AE monitoring

Highlights of the testing showing recorded AE data available

Monday 10th July 2006

0900	Arrive at Sparkær
1000	Sparkær SIMPAL system set up
1100	Tape up eight cables along the length of the blade and wire up to SIMPAL (final sensor attachment to be approved)
1400	Sensors on
1600	Sensor check (tap) all ok
1750	TAP TEST

Tuesday 11th July 2006

0900	System set to monitor as other test preparations take place Output reflects the area where work is being done TEST SETUP
1400	Test download and system re-set
1745 - 1810	**System check 11 July (loading up to 50%)**
1815 - 1900	**Test one (loading up to 60%)**

Wednesday 12th July 2006

0900 - 0920	**System check 12 July (loading up to 60%)**
1030 - 1050	**Test two (loading to 69%)**
1220 - 1250	**Test three (loading to 75%)**
1430 - 1500	**Test four (loading to 77%)**

13th July – 21st August 2006

During this time the SIMPAL system was unattended, but left to record AE activity. Work on the beam over this time included an alteration of the loading arrangement and then an applied torsion load.

There is activity on the following dates which suggest activity on or near the beam.
24th, 25th, 27th (July), 02nd, 03rd, 04th, 11th and 14th (August)
There is significant activity on the following dates which suggest an applied torsional load: 08th, 15th, 16th, 18th and 21st (August)

Tuesday 22nd August 2006

1030	Arrive at Sparkær
1100	Check SIMPAL system (all functions ok)
1130	Download data from July - August
1530 - 1630	**System check 22 August (loading to 60%)**
1830 - 1900	**Test five (loading to 70%)**

Wednesday 23rd August 2006

0830 - 0930	**Test six (loading to 60%)**
1030 - 1115	**Test seven (loading to 79%)**
1130 - 1220	**Test eight (load to fail at 77%)**

Burst rating

Date	Test	Maximum Load %	"Burst rating"
11th July	System check 11 July	50%	2.98
11th July	Test one	60%	20.4
12th July	System check 12 July	60%	26.0
12th July	Test two	69%	256
12th July	Test three	75%	319
12th July	Test four	77%	265
13th July – 21st August	Torsion testing	?	31.81
22nd August	System check 22 August	60%	3.6
22nd August	Test five	70%	81
23rd August	Test six	65%	13
23rd August	Test seven	79%	1130
23rd August	Test eight	77% (and FAIL)	7800

Table 2. The table presents burst rating for all system checks and tests

This table shows the entire test sequence, and the maximum load applied for each test. For each test a "burst rating" value has been calculated, being the maximum recorded activity corrected for "bin" length, in order that relative maximum activity for each loading can be compared.

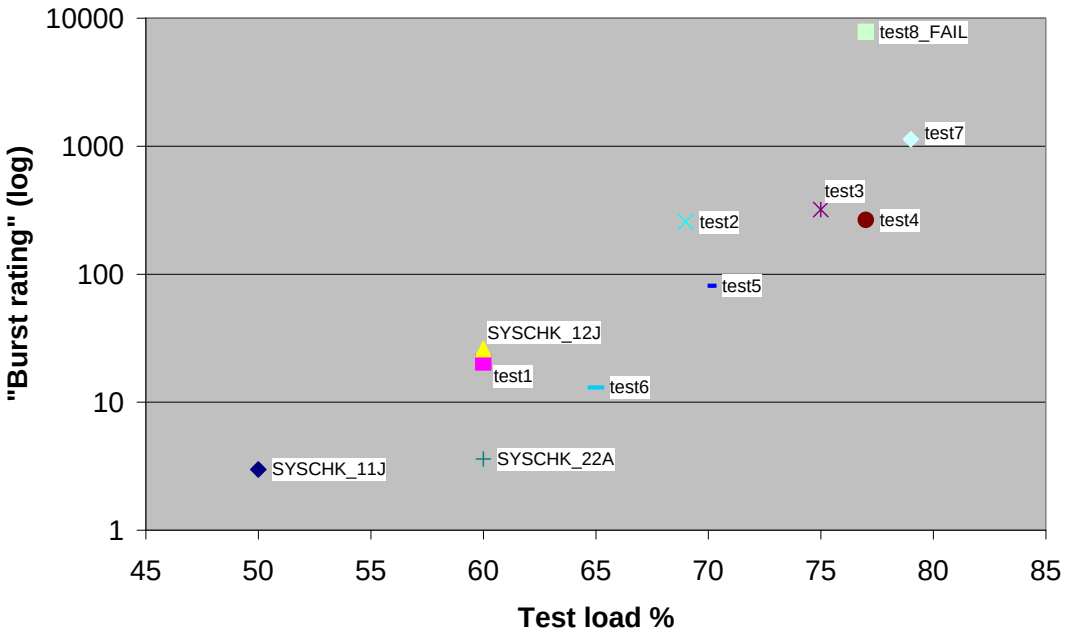

Figure 68. Burst rating for all system checks and tests

Discussion

The AE monitoring provided a quick, adaptable, and effective way to support this one-off structure test. The combined output from all the test loads gives a useful visual summary of the entire test history (see the graphs in section 13.8). The channel activity for each loading gives an unambiguous indication of which structural sections are generating acoustic response under load.

The output and "burst rating" calculations help control the load application, ensures the activity profile is as expected for the test, and avoids premature failure. This permits the load to approach ultimate failure load with a greater confidence of not destroying the structure.

It can be seen from test load three and four in July that the blade was loaded to 75% and 77% respectively. In August it was possible to load up to 79% during test seven, before achieving 77% and ultimate failure in test eight. This indicates that the blade came very close to ultimate failure load several times during testing. In this way a better understanding of the structural response close to failure can be achieved.

References

[1] M.McGugan, T.Bech, B.F.Sørensen, E. Jørgensen and O.J.D.Kristensen, "Improving the Structural Testing of Wind Turbine Blades by Monitoring Acoustic Emission", Proceedings of the 4th International Workshop on Structural Health Monitoring (pages 820-827), Stanford University, Stanford, California, USA. September 15-17, 2003.

[2] B.F.Sørensen, L.Lading, P.Sendrup, M.McGugan, C.P.Debel, O.J.D.Kristensen, G.C.Larsen, A.M.Hansen, J.Rheinländer, J.Rusborg and J.D.Vestergaard, "Fundamentals for remote structural health monitoring of wind turbine blades - a preproject". Risø-R-1336(EN) (2002) 36 p

[3] http://www.holroyd-instruments.com/smproducts.html

AE Graphs

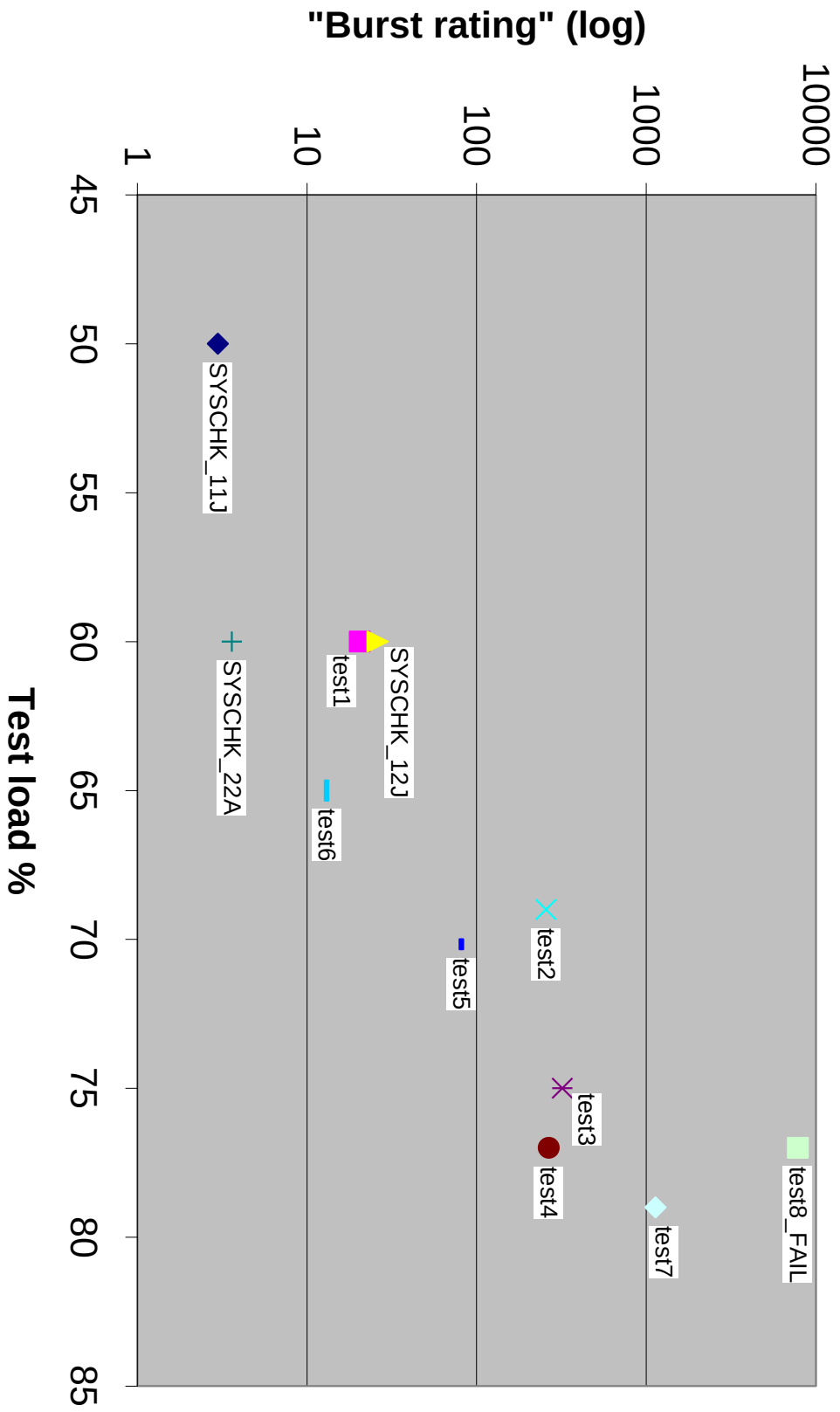

Figure 69. Burst rating (i)

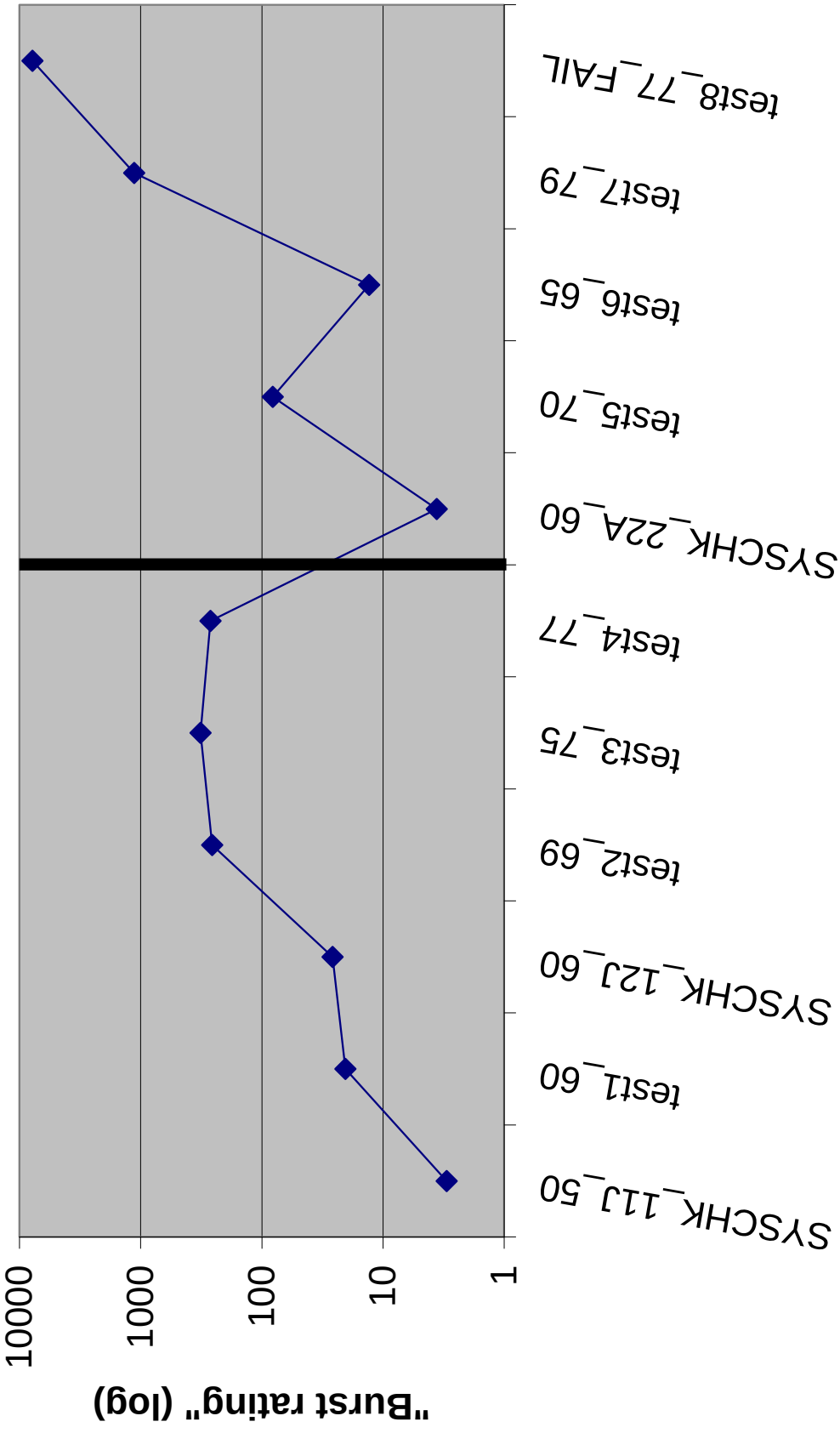

Figure 70. Burst rating (ii)

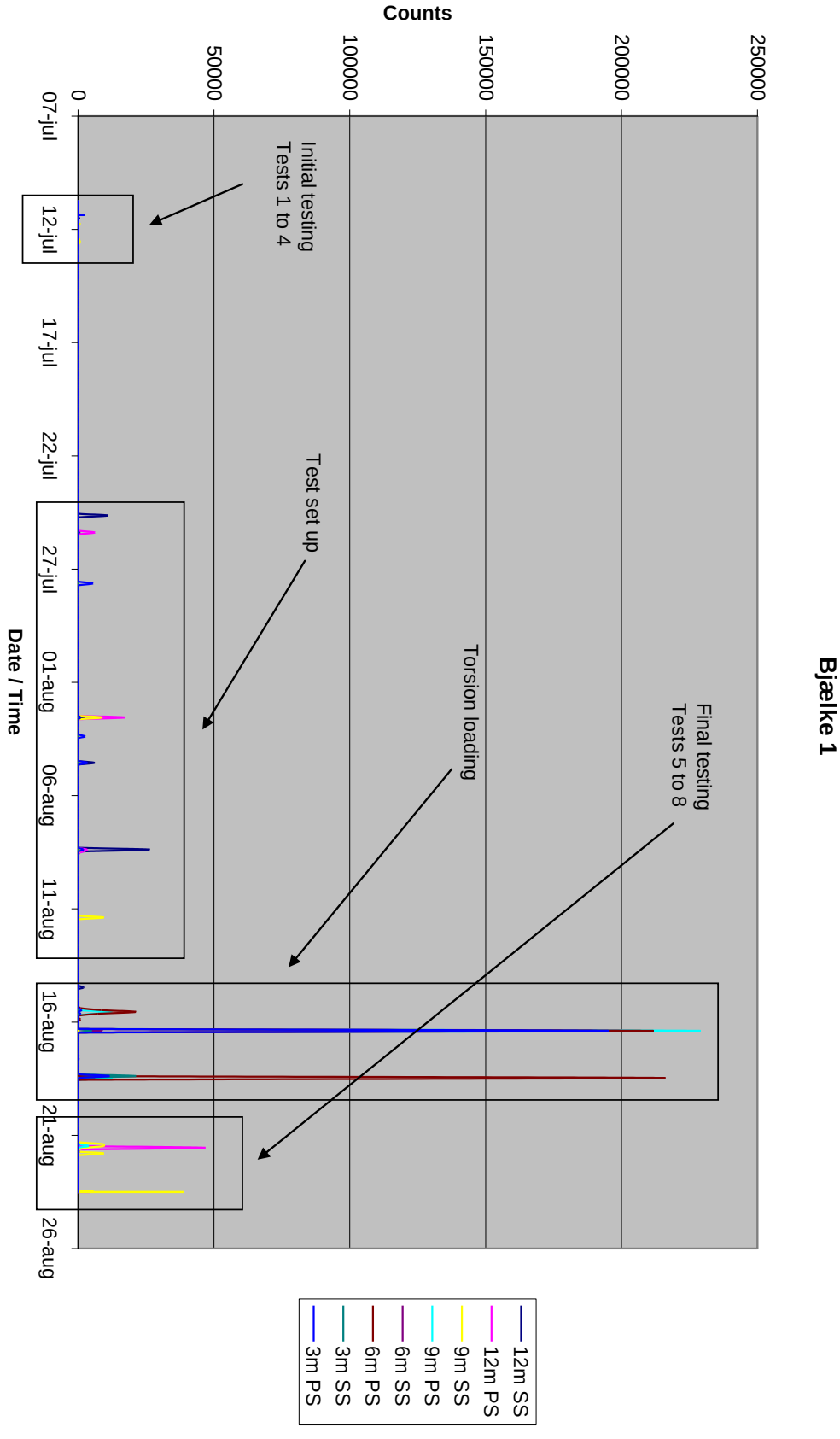

Figure 71. Bjælke 1 AE output 07 July – 26 August (all)

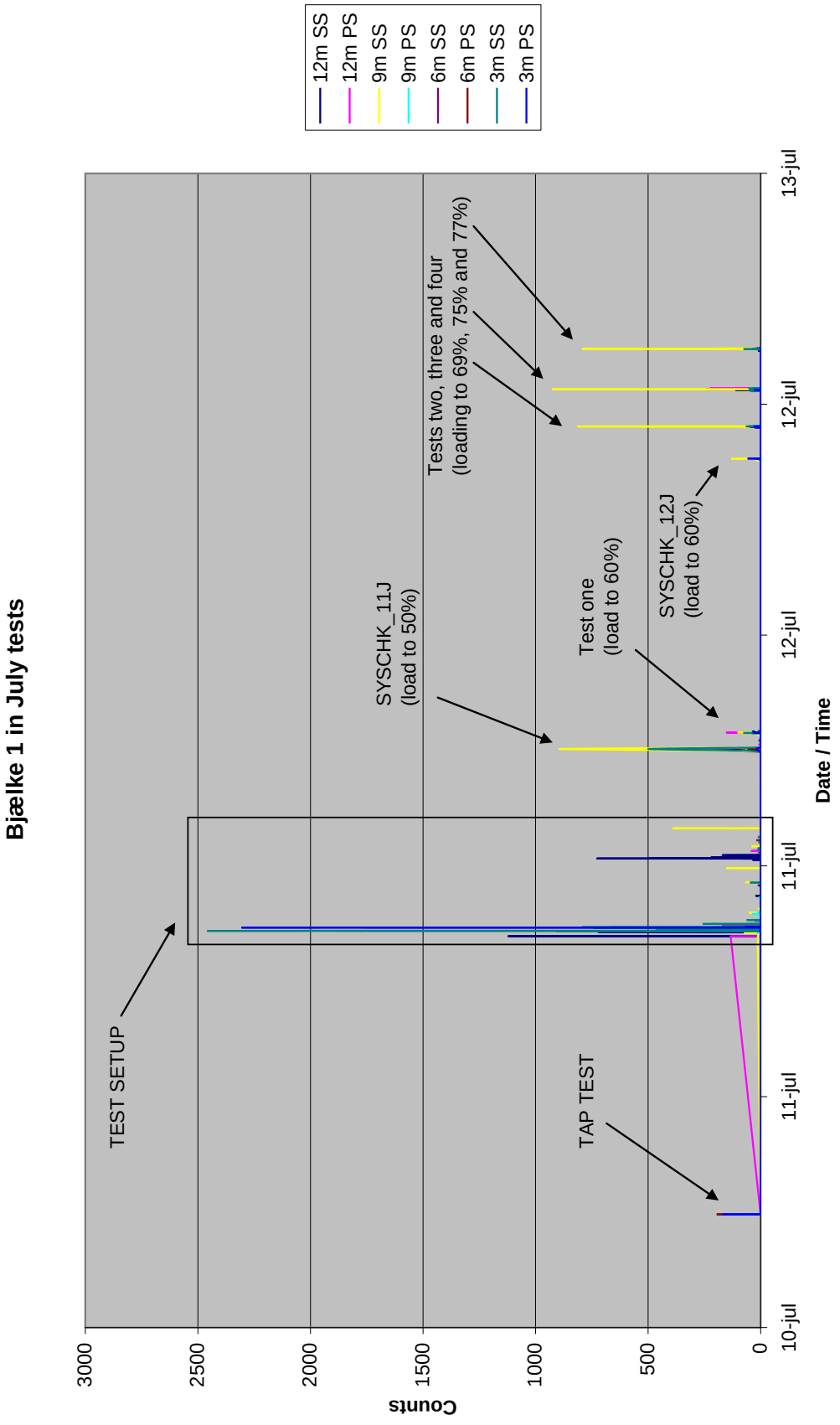

Figure 72. Bjælke 1 AE output 10 July – 13 July (initial flapwise tests)

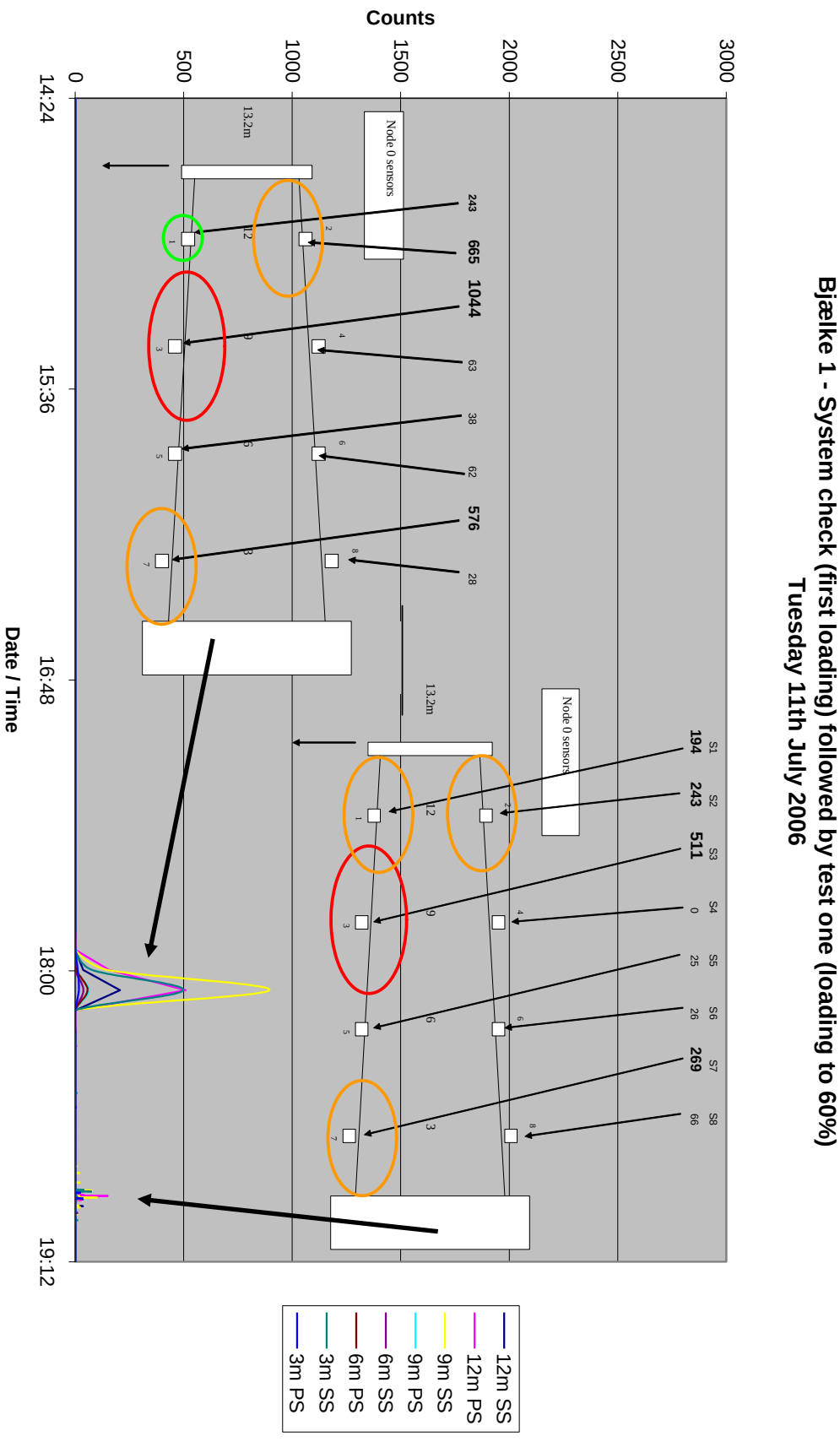

Figure 73. Bjælke 1 AE output 11 July (SYSCHK_11J_50 and test1_60)

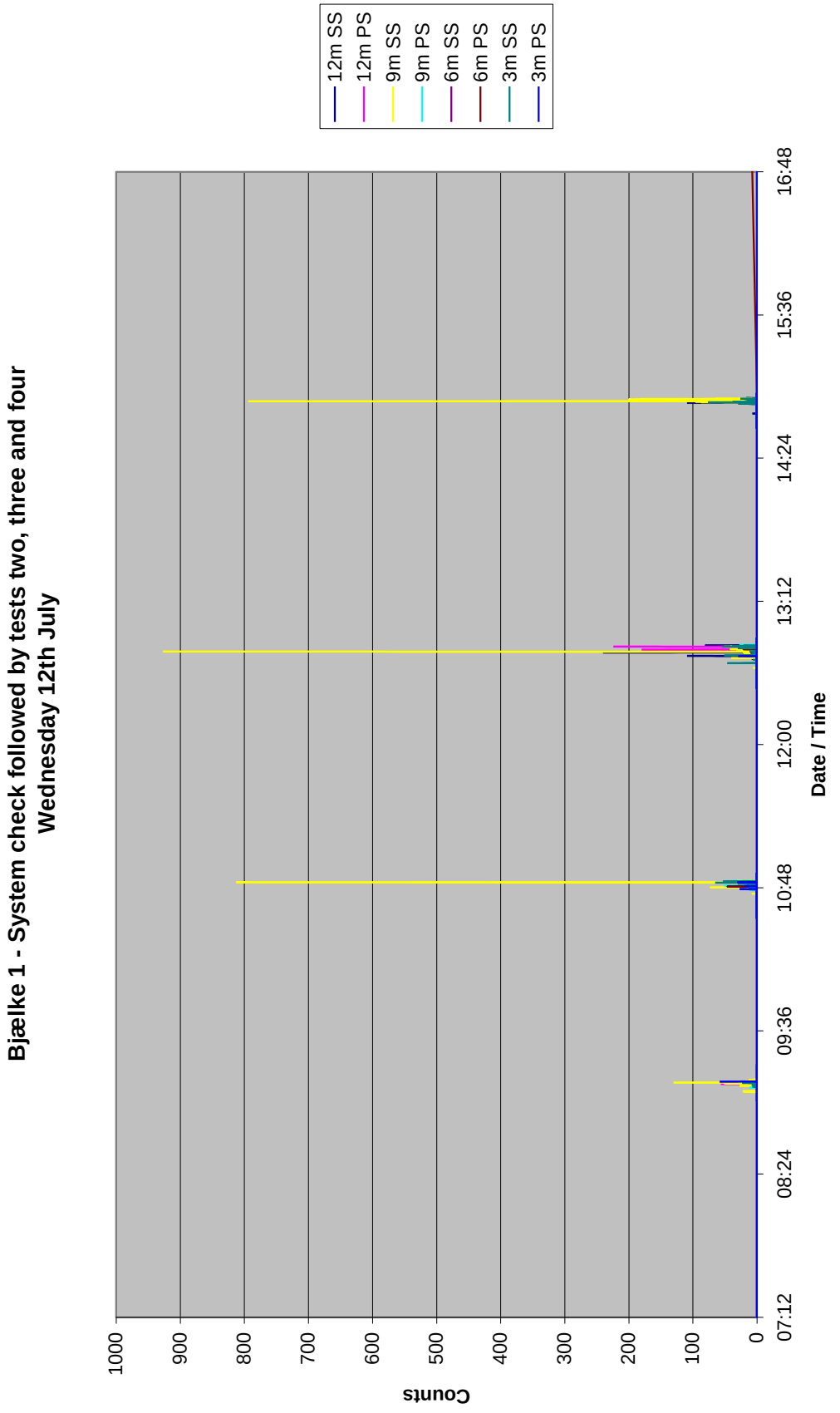

Figure 74. Bjælke 1 AE output 12 July (all)

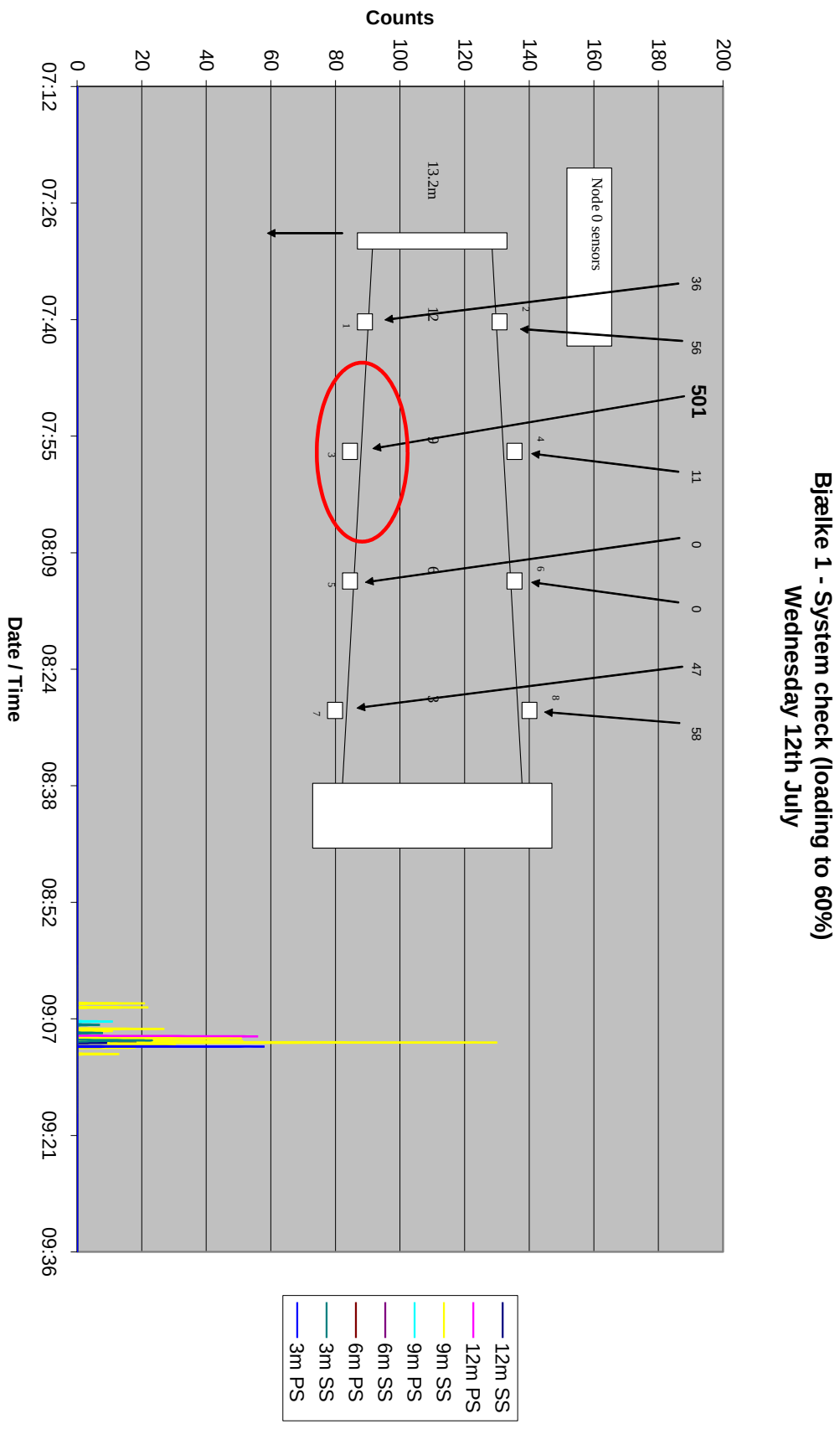

Figure 75. Bjælke 1 AE output 12 July (SYSCHK12J_60)

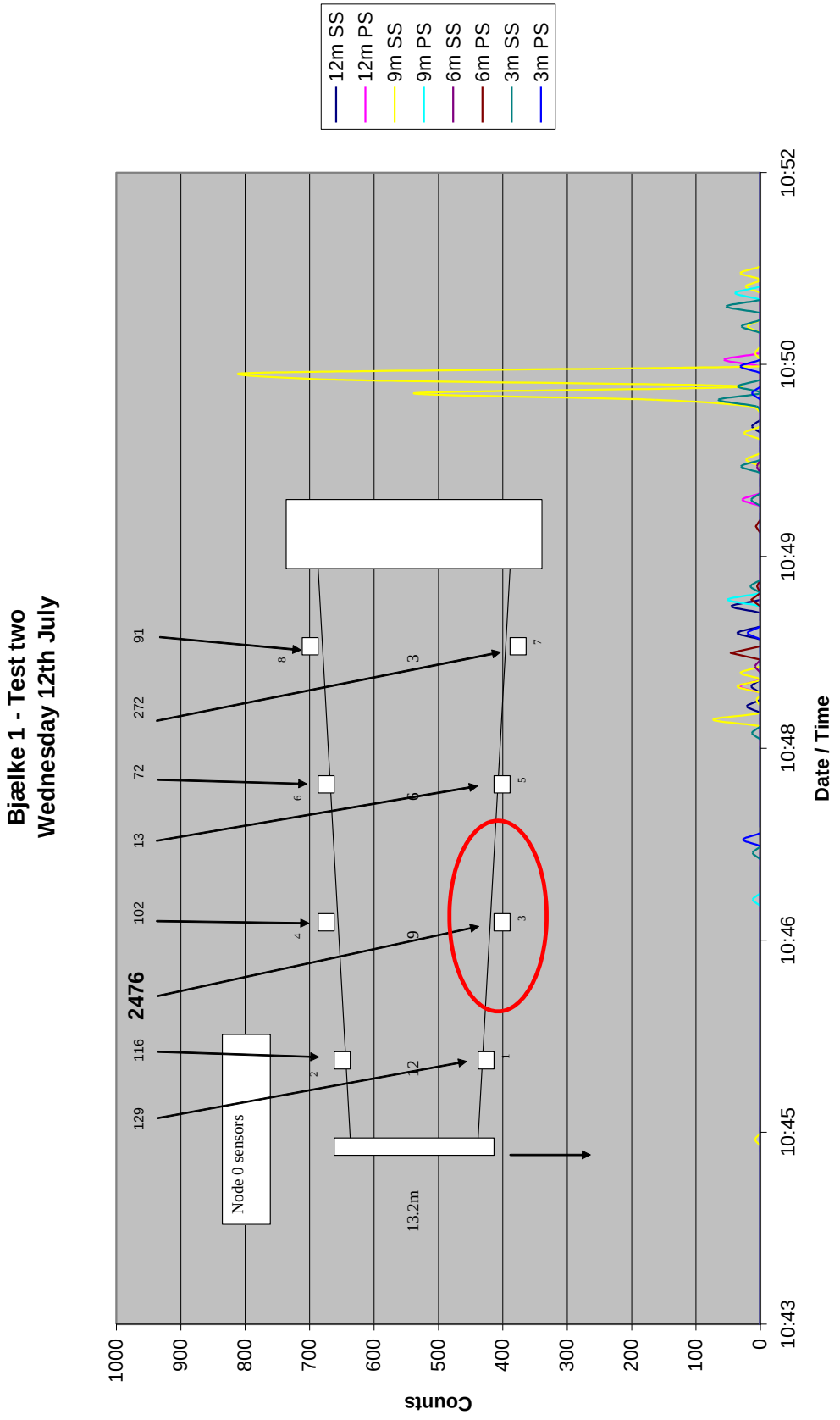

Figure 76. Bjælke 1 AE output 12 July (test2_69)

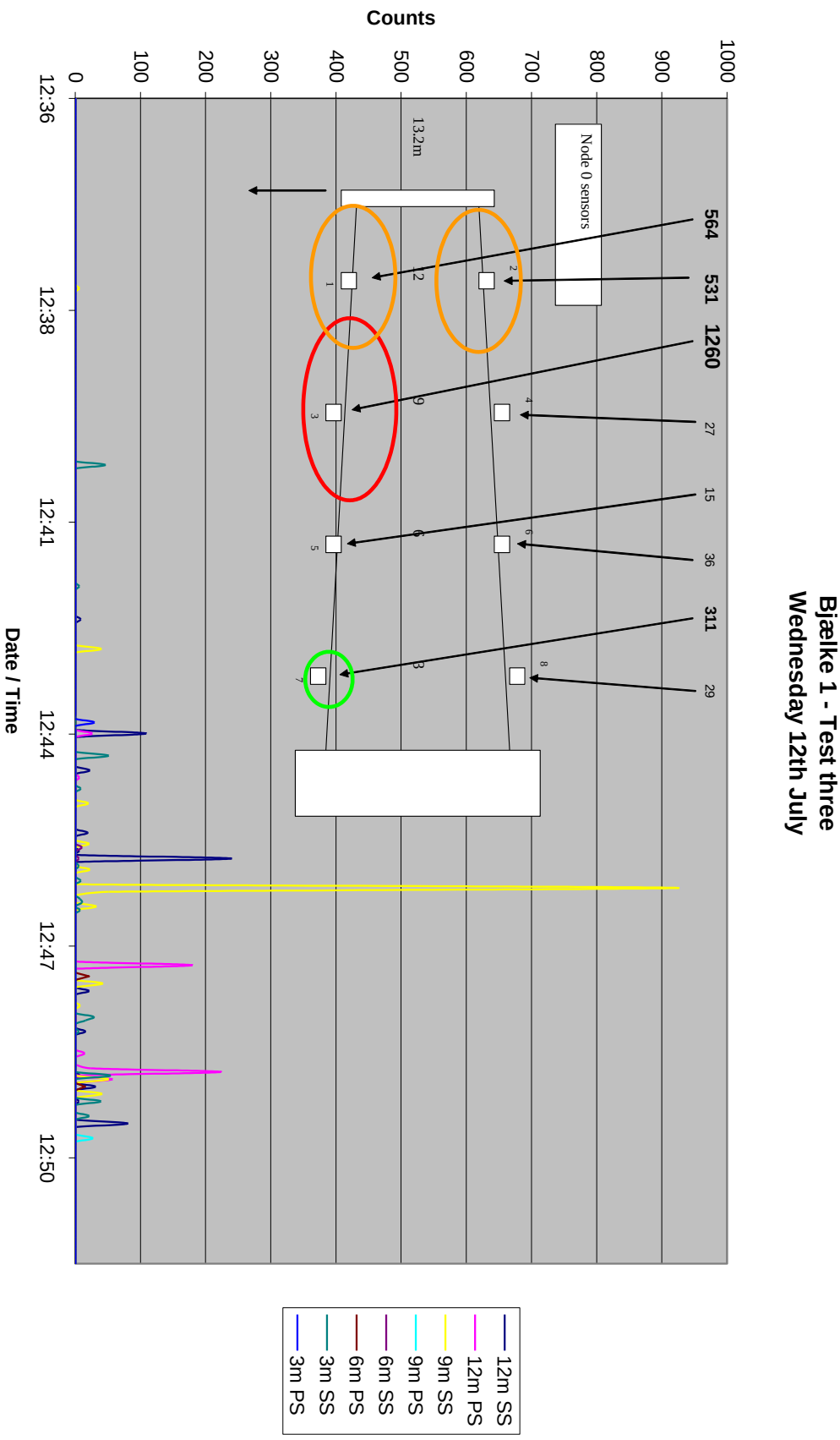

Figure 77. Bjælke 1 AE output 12 July (test3_75)

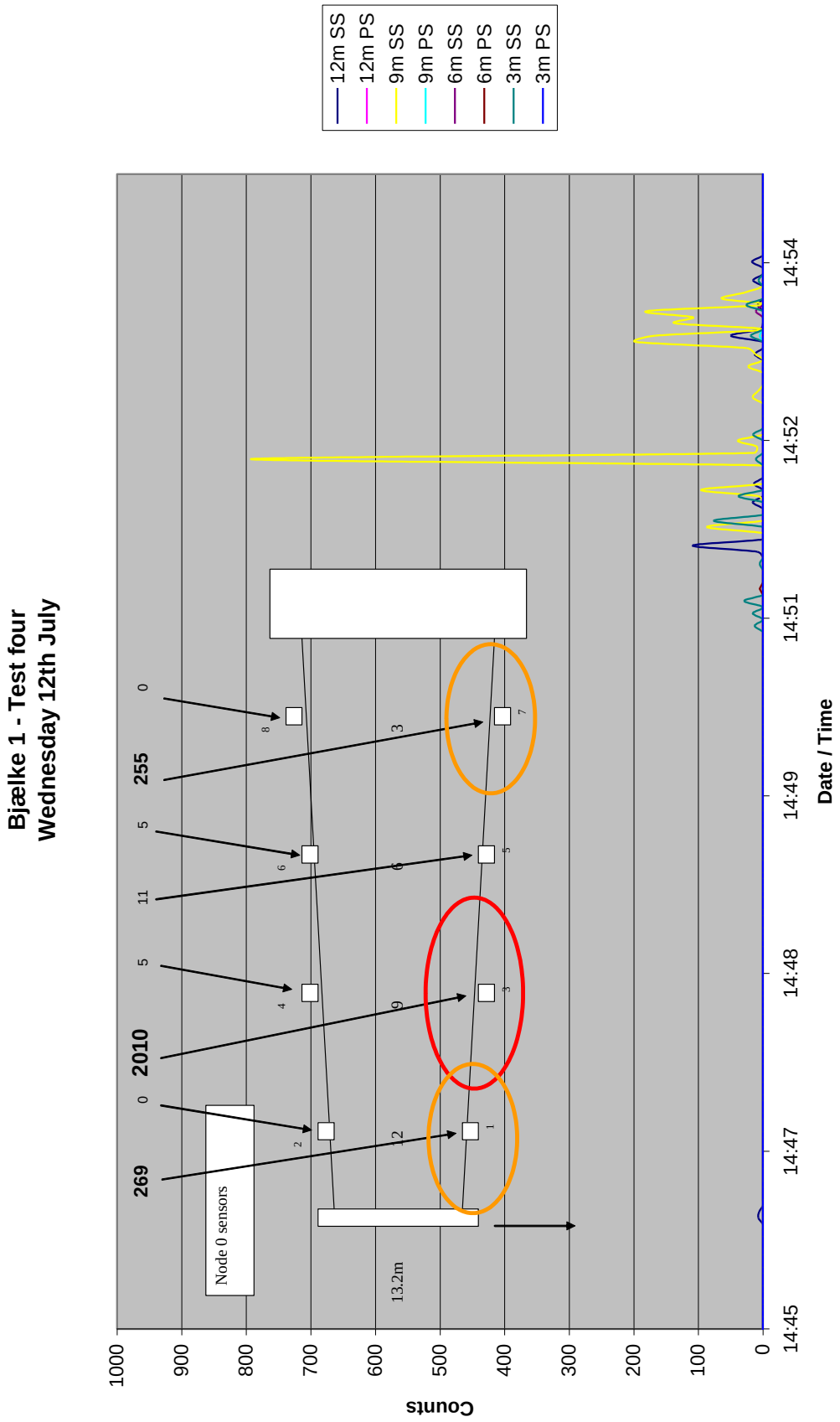

Figure 78. Bjælke 1 AE output 12 July (test4_77)

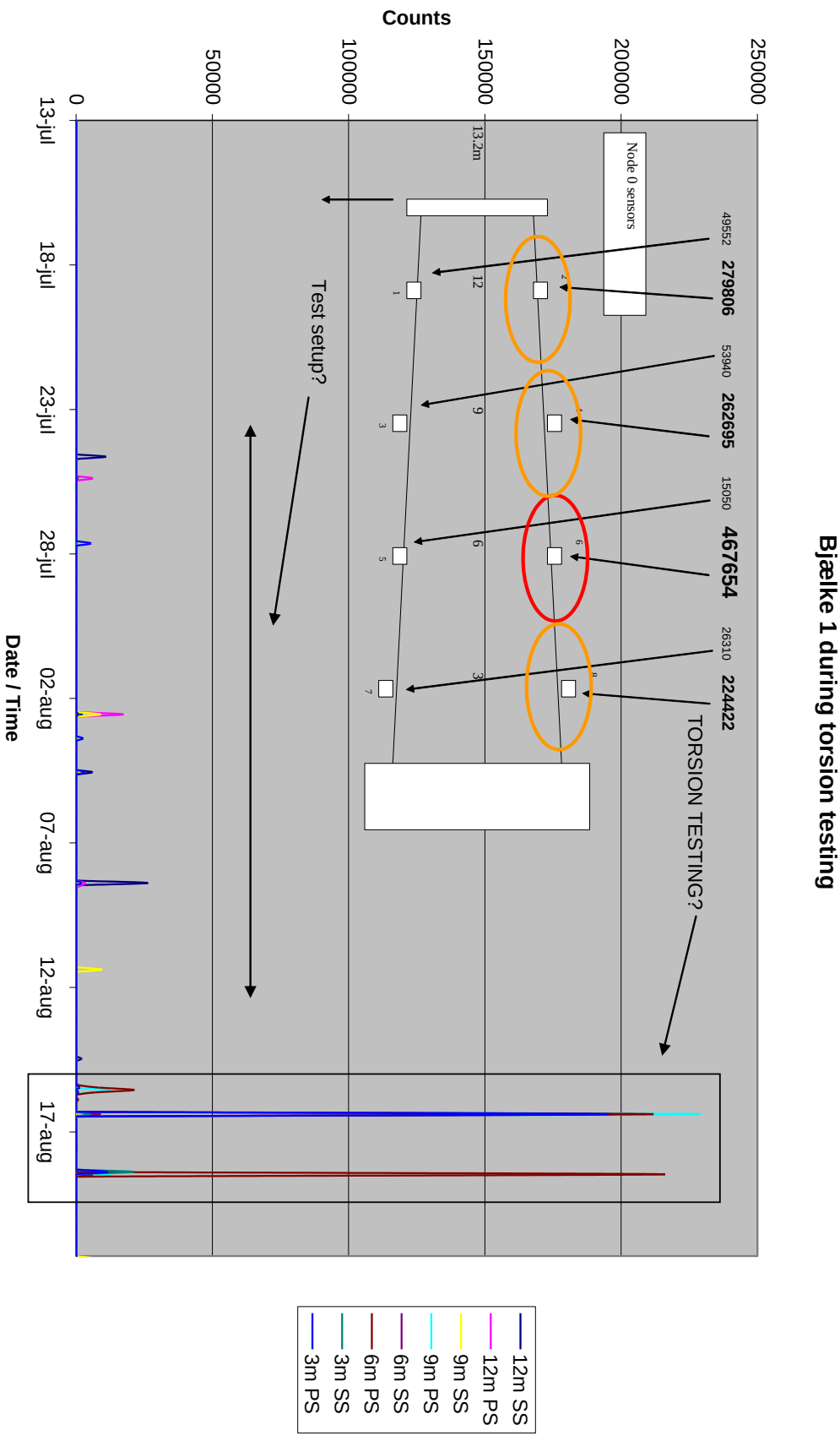

Figure 79. Bjælke 1 AE output 11 July – 22 August (set up + torsion testing)

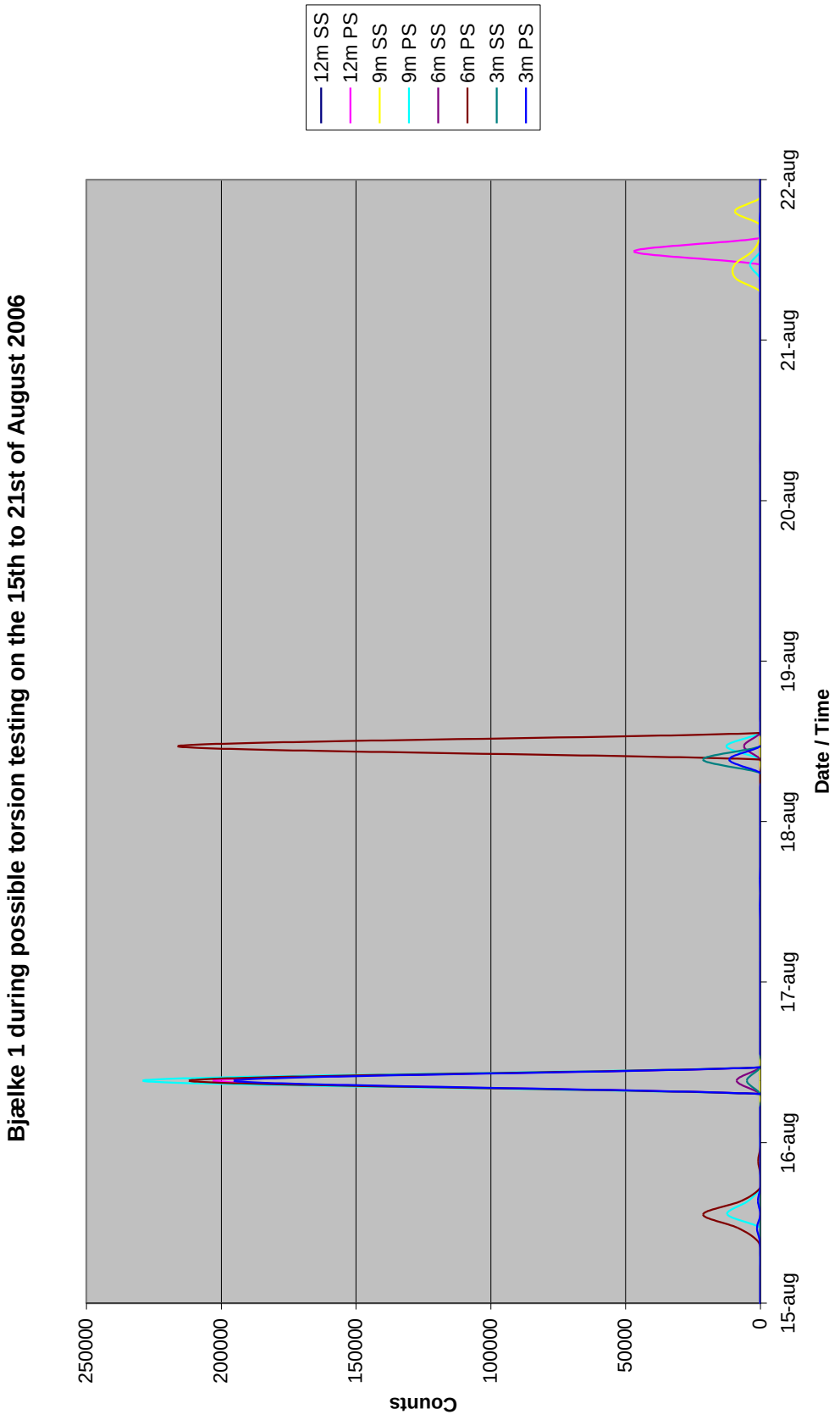

Figure 80. Bjælke 1 AE output 15 August – 22 August (torsion testing)

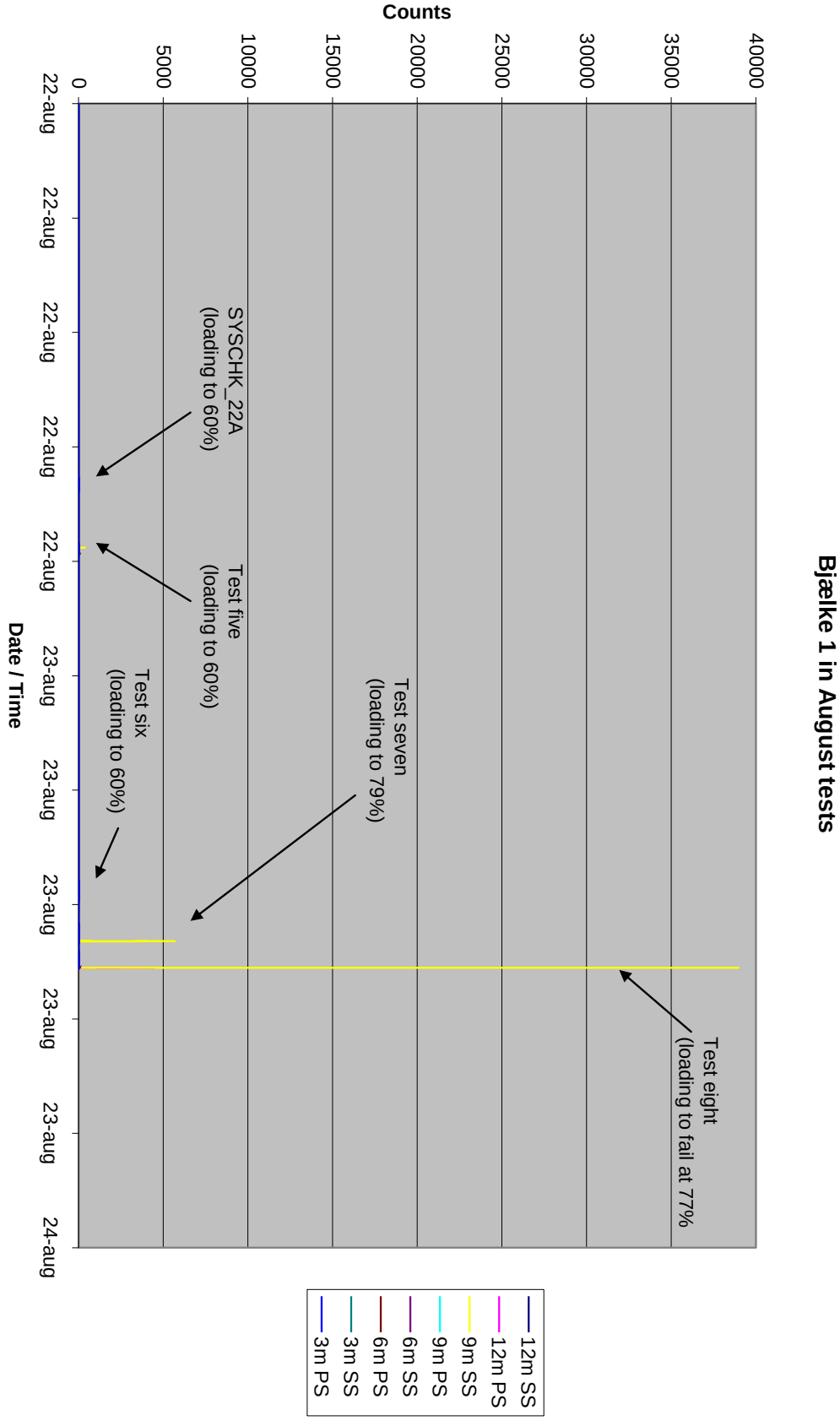

Figure 81. Bjælke 1 AE output 22 August – 24 August (final flapwise tests)

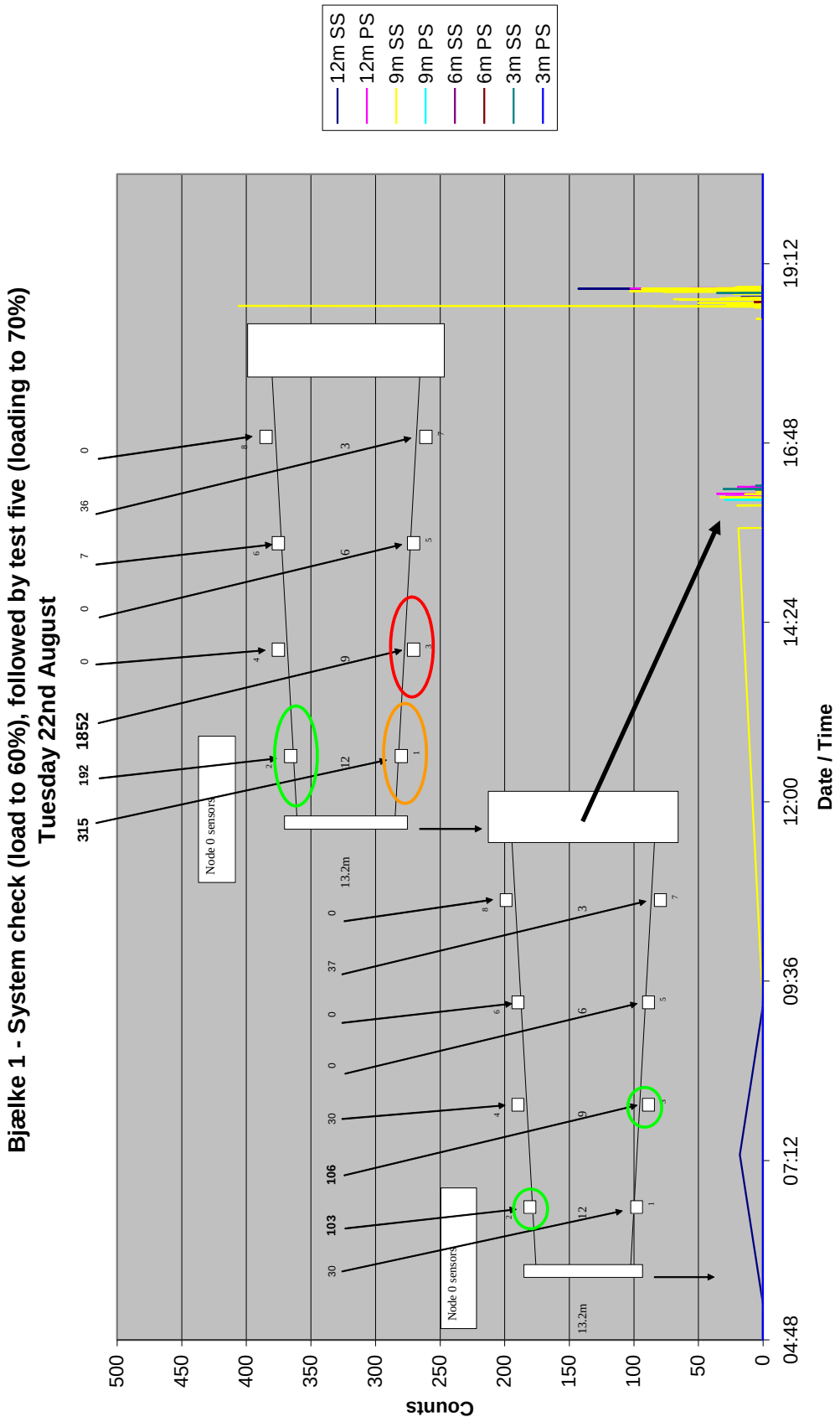

Figure 82. Bjælke 1 AE output 22 August (SYSCHK_22A_60 and test5_70)

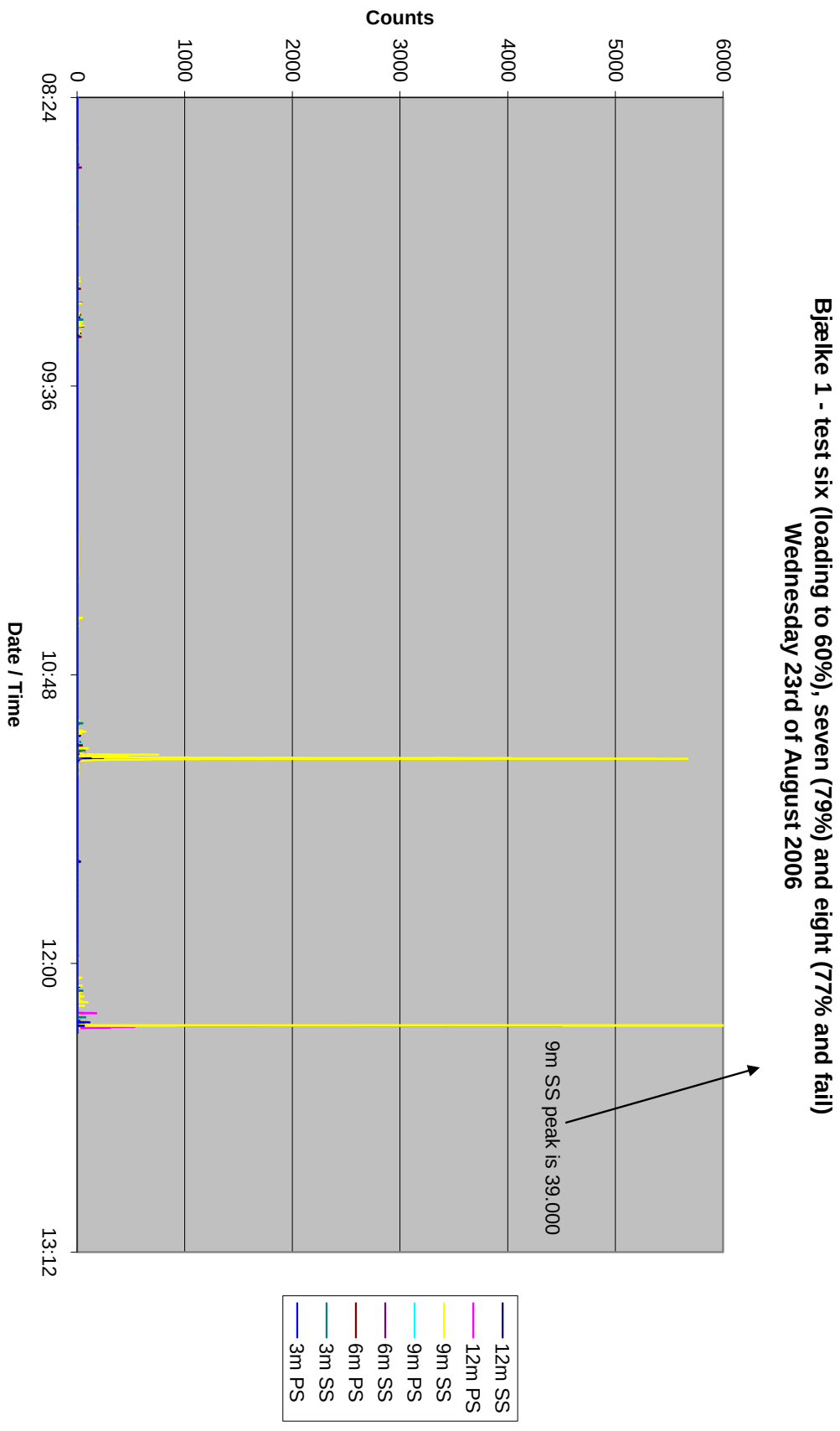

Figure 83. Bjælke 1 AE output 22 August (test6_65, 7_79 and 8_77_fail)

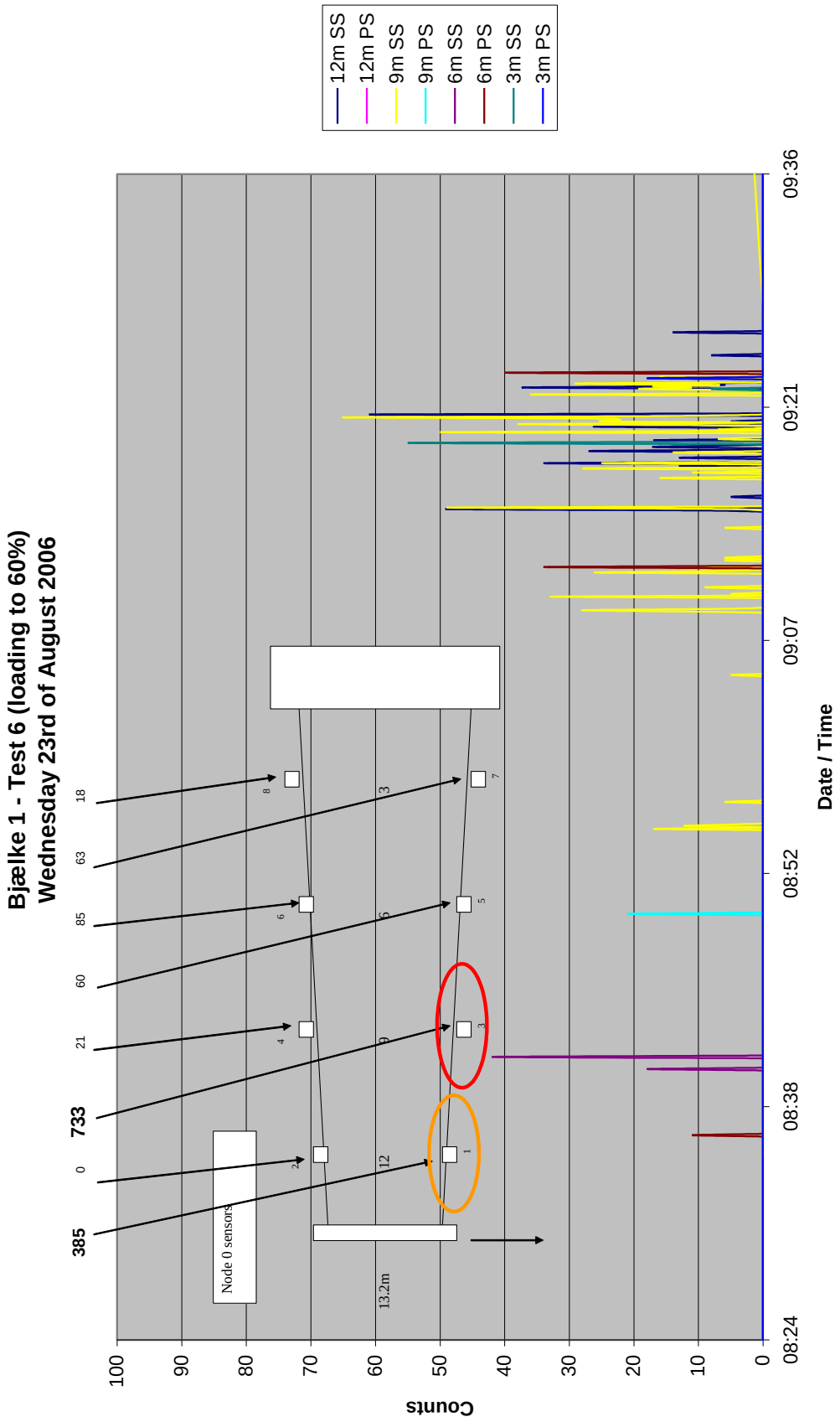

Figure 84. Bjælke 1 AE output 22 August (test6_65)

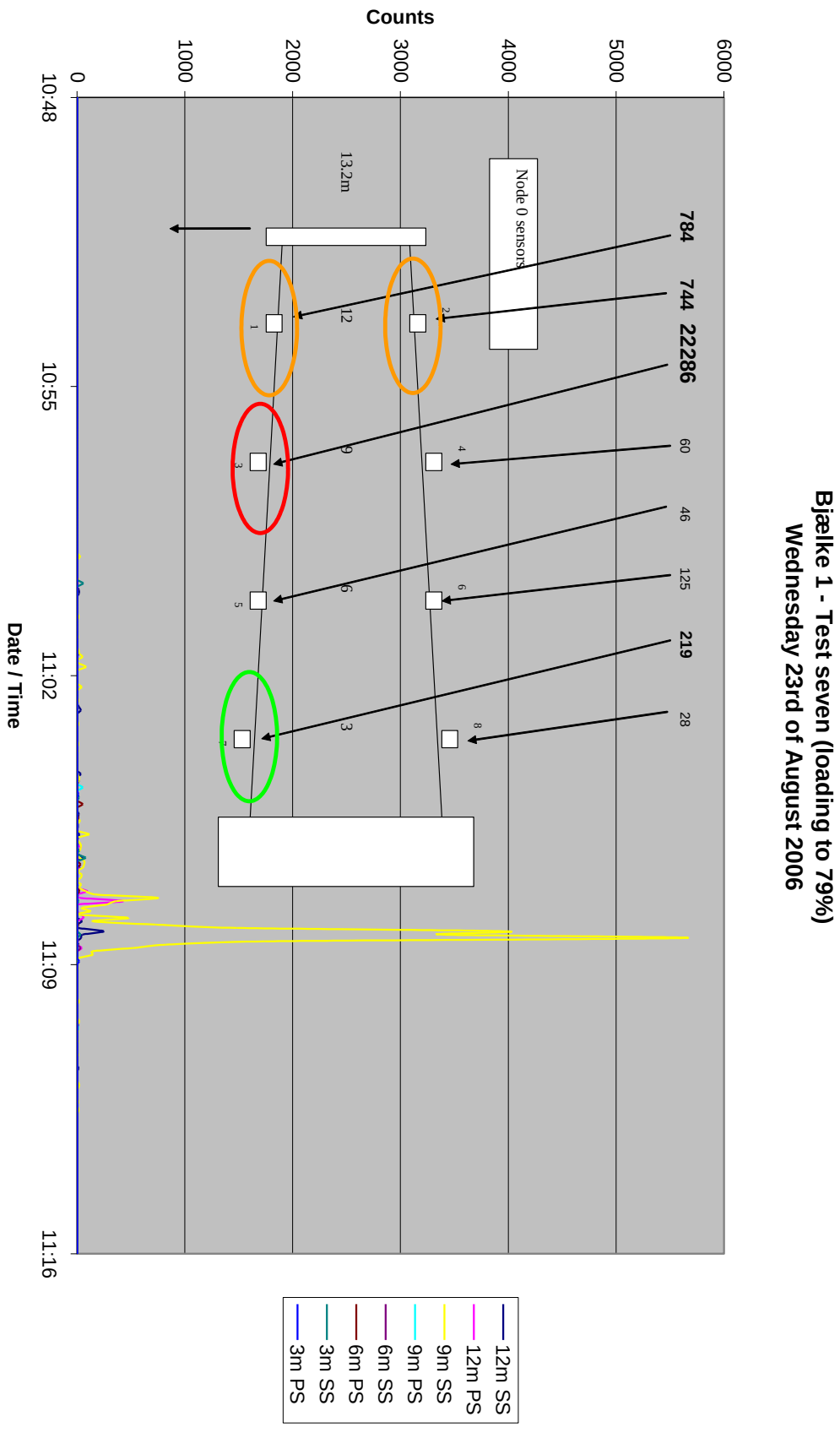

Figure 85. Bjælke 1 AE output 22 August (test7_79)

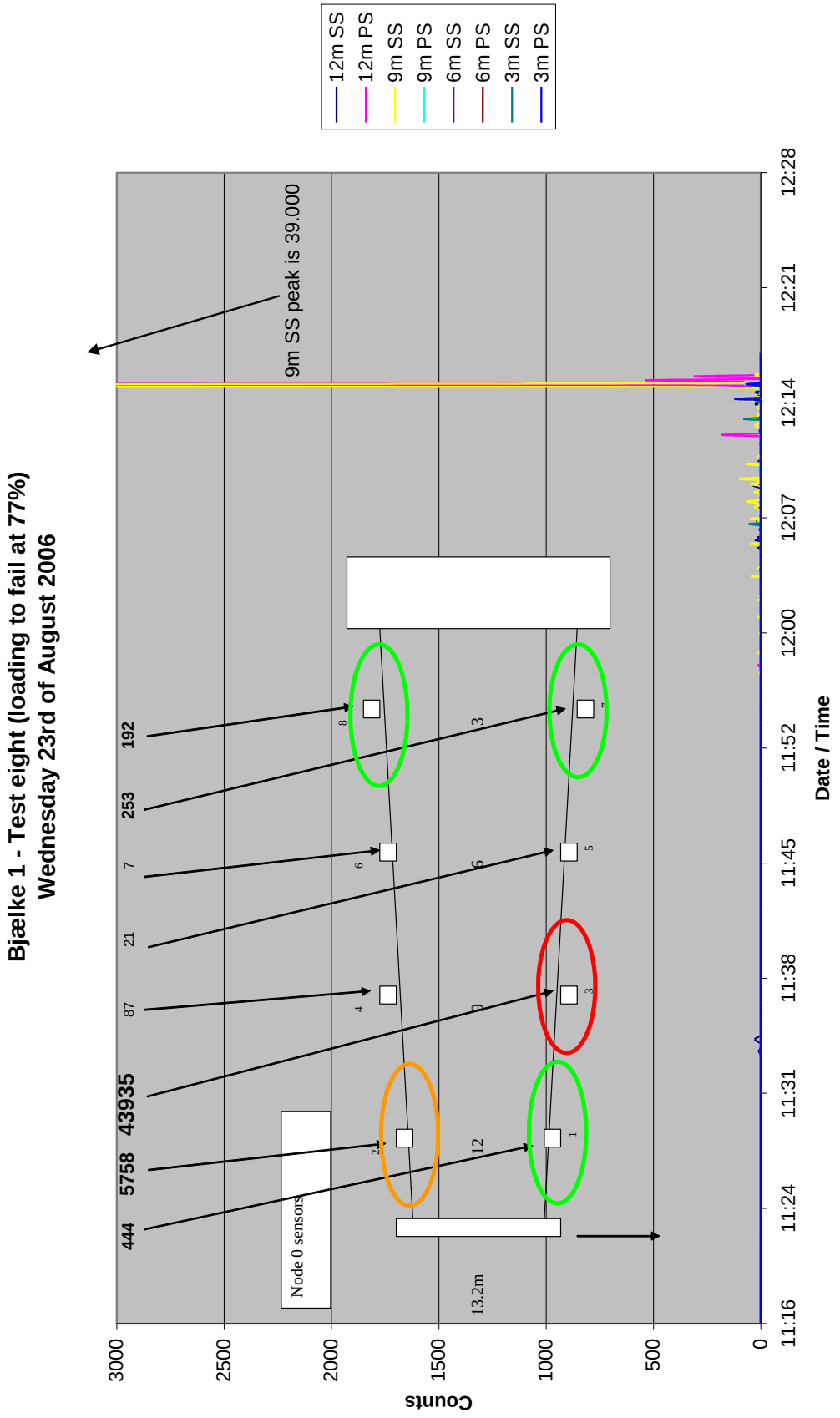

Figure 86. Bjælke 1 AE output 22 August (test8_77_fail)

Appendix E: Measured strain gauge results from the flapwise test

Strain Gauge plan

Numbering of strain Gauge from 8-8-06

Distance from start [m]	Longitudinal compression Outer surface	Inner surface		Longitudinal tension Outer surface	Inner surface
1.9	1	2		Flap test	Valgt fra 19
2.25	3	4		Torsion test	Valgt fra 18
2.6	5	6		Ulitmate flap te	Valgt fra 19
3.00	7	8		85	86
3.5	9	10		87	88
4.00	11	12		89	90
4.5	13	14		91	92
5.00	15	16		93	94
5.5	17	18		95	96
6.00	19	20		97	98
6.5	21	22		99	100
7.00	23	24		101	102
7.5	25	26		103	104
8.00	27	28		105	106
8.5	29	30		107	108
9.25	31	32			
9.6	33	34		109	110
9.75	35	36			
10.00	37	38		111	112
10.25	39	40		113	114
10.5	41	42		115	116
10.75	43	44		117	118
11.00	45	46		119	120
11.25	47	48		121	122
11.5	49	50		123	124
11.75	51	52		125	126
12.00	53	54		127	128
12.25	55	56		129	130
12.5	57	58		131	132
12.75	59	60		133	134
13.00	61	62		135	136
13.5	63	64			
14.00	65	66		137	138
14.5	67	68			
15.00	69	70		139	140
15.5	71	72			
16.00	73	74		141	142
16.5	75	76			
17.00	77	78		143	144
17.5	Annuleres 79	Annuleres 80			
18.00	Annuleres 81	Annuleres 82			
18.5	Annuleres 83	Annuleres 84			
20.00					
21.00	gauge 79 to 84 Annuleres				
22.00	Due to lack of space in beam				
23.00					
24.00					

stk I denne gruppe 78

stk I denne gruppe 61

Distance from start [m]	Transvers Compress. Outer surface	Inner surface	Transvers Tension Outer surface	Inner surface
1.9				
2.25				
2.6				
3.0	145	146	181	182
3.5				
4.0	147	148	183	184
4.5				
5.0	149	150	185	186
5.5				
6.0	151	152	187	188
6.5				
7.0	153	154	189	190
7.5				
8.0	155	156	191	192
8.5				
9.25				
9.6				
9.75				
10.0	157	158	193	194
10.25				
10.5	159	160	195	196
10.75				
11.0	161	162	197	198
11.25				
11.5	163	164	199	200
11.75				
12.0	165	166	201	202
12.25				
12.5	167	168	203	204
12.75				
13.0	169	170	205	206
13.5				
14.0	171	172		
14.5				
15.0	173	174		
15.5				
16.0	175	176		
16.5				
17.0	177	178		
17.5				
18.0	Annuleres 179	Annuleres 180		
18.5				
20.0				
21.0				
22.0				
23.0				
24.0				

[m]	Tralling edge	Leading Edge	
2.98	207	208	
3.00			211
3.50			
4.00			
4.98	209		
5.00			212
5.50			
6.00			
6.98	210		
7.00			213
7.50			
8.00			
8.50			
9.25			

Distance from start [m]	Leg toward Compression Side (SS) (TC)
13.2m	302 303
19m	306 307

Leg toward tension side (PS) (TC)	
304	305
309	308

Bolt in root section
310
311

TC=toward center

45° Strain

Distance from start [m]	SS (Compression)		PS (Tension side)			
	Out. surf.	In. surf.	Out. surf.		In. surf.	
			Center	Close to coner	Center	Close to coner
9.6						
10.0	229	228	239	241	238	240
10.25						
10.5			243		242	
10.75						
11.0	231	230	245		244	
11.25						
11.5			247		246	
11.75						
12.0			249		248	
12.25						
12.5			251		250	
12.75						
13.0	233	232	253		252	
13.5						
14.0	235	234	255		254	
14.5						
15.0	237	236	257	259	256	258
15.5						
16.0			261		260	
16.5						
17.0			227		226	

45° Strain

	Trail. web toward tension side.				**Trail**. web toward com	
Distance from start [m]	Out. surf.		In. surf.		Out. surf.	In. surf.
	Center	Close to coner	Center	Close to coner		
10.0	263	265	262	264	289	288
10.25						
10.5	267		266			
10.75						
11.0	269		268			
11.25						
11.5	271		270			
11.75						
12.0	273		272			
12.25						
12.5	275		274			
12.75						
13.0	277		276			
13.5						
14.0	279		278			
14.5						
15.0	281	283	280	282	291	290
15.5						
16.0	285		284			
16.5						
17.0	287		286			

	Lead. web toward tension side.		**Lead**. web toward compres. side	
Distance from start [m]	Out. surf.	In. surf.	Out. surf.	In. surf.
10.0	293	292	297	296
10.25				
10.5				
10.75				
11.0				
11.25				
11.5				
11.75				
12.0				
12.25				
12.5				
12.75				
13.0				
13.5				
14.0				
14.5				
15.0	295	294	299	298
15.5				
16.0				
16.5				
17.0				

Graphs of Longitudinal Compression

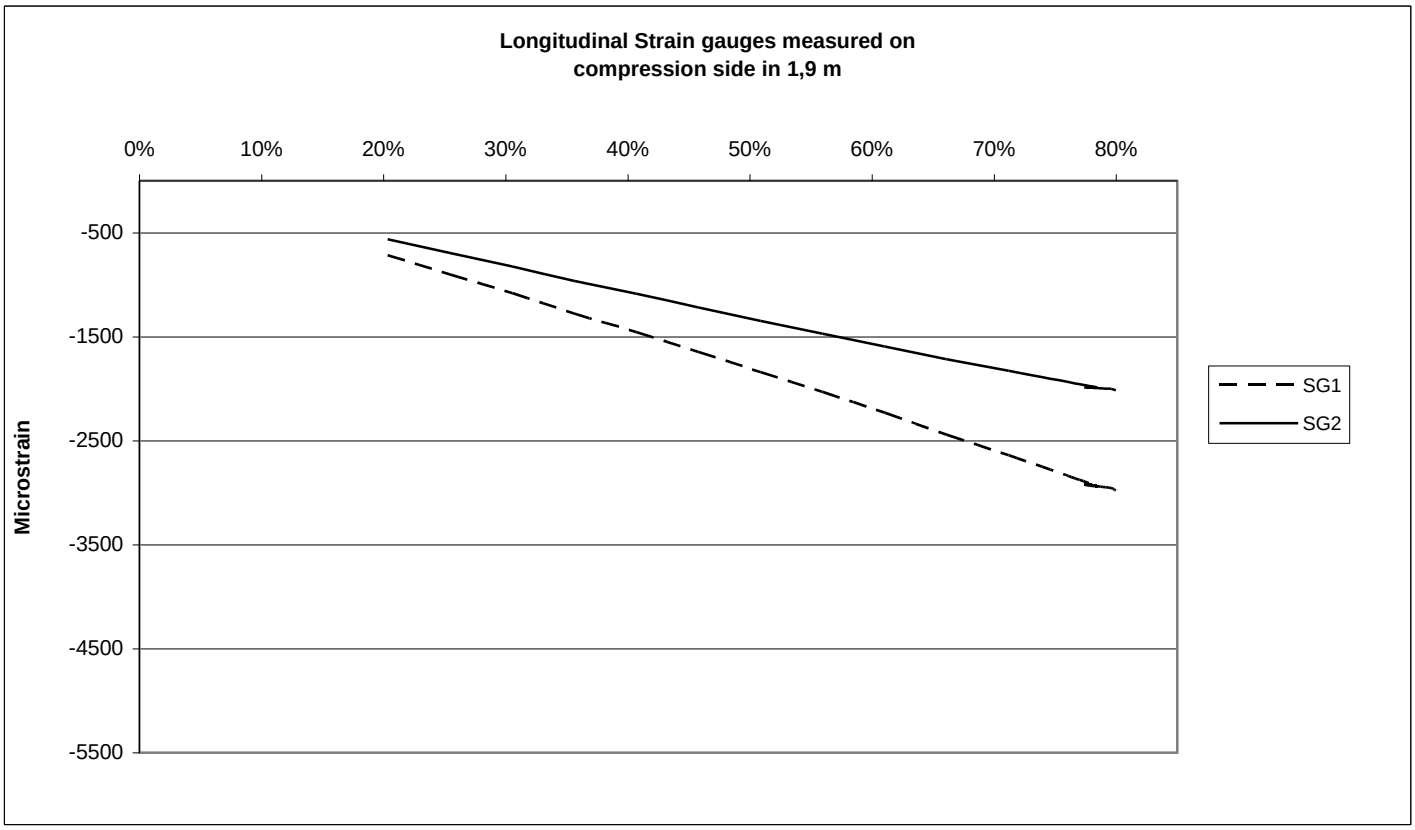

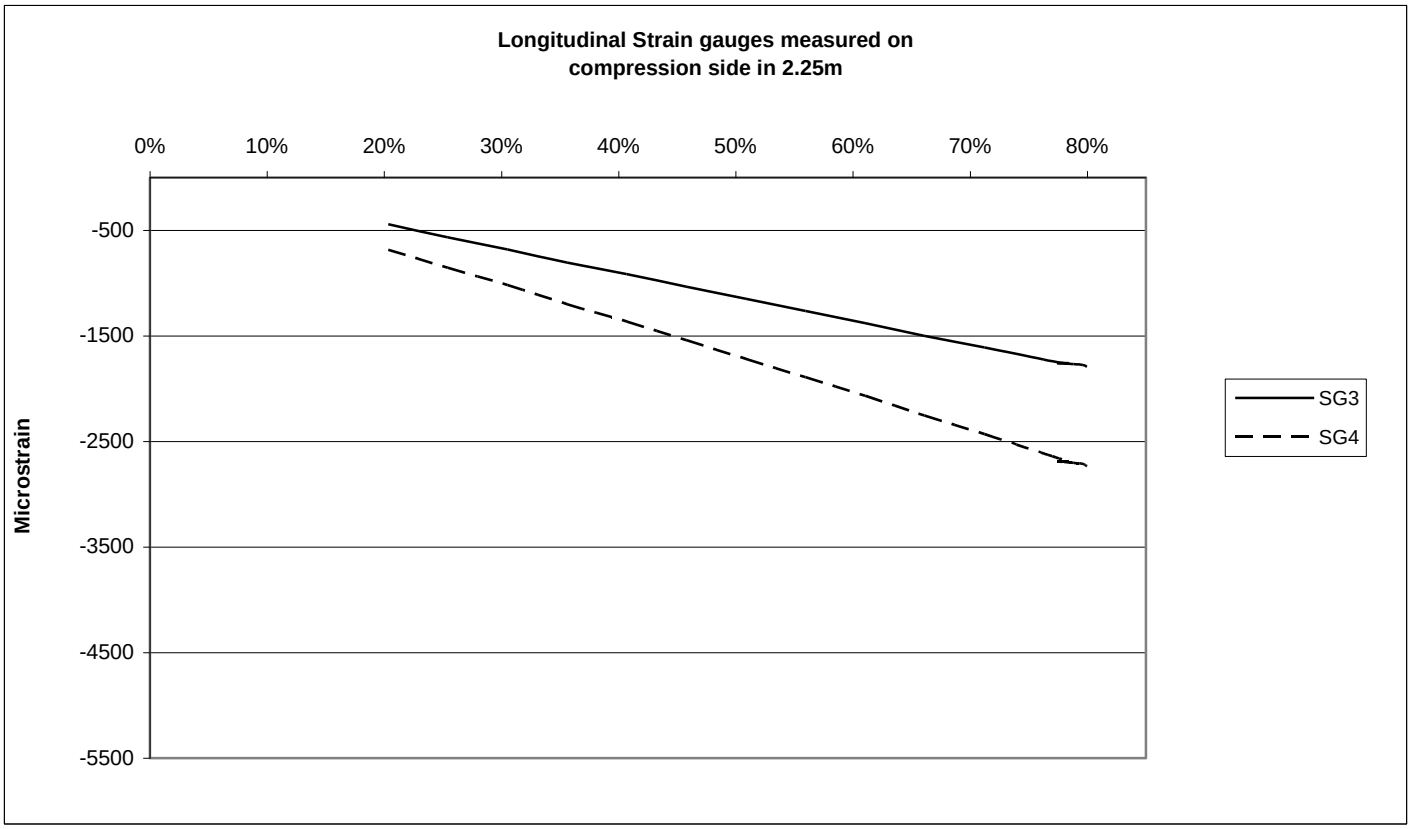

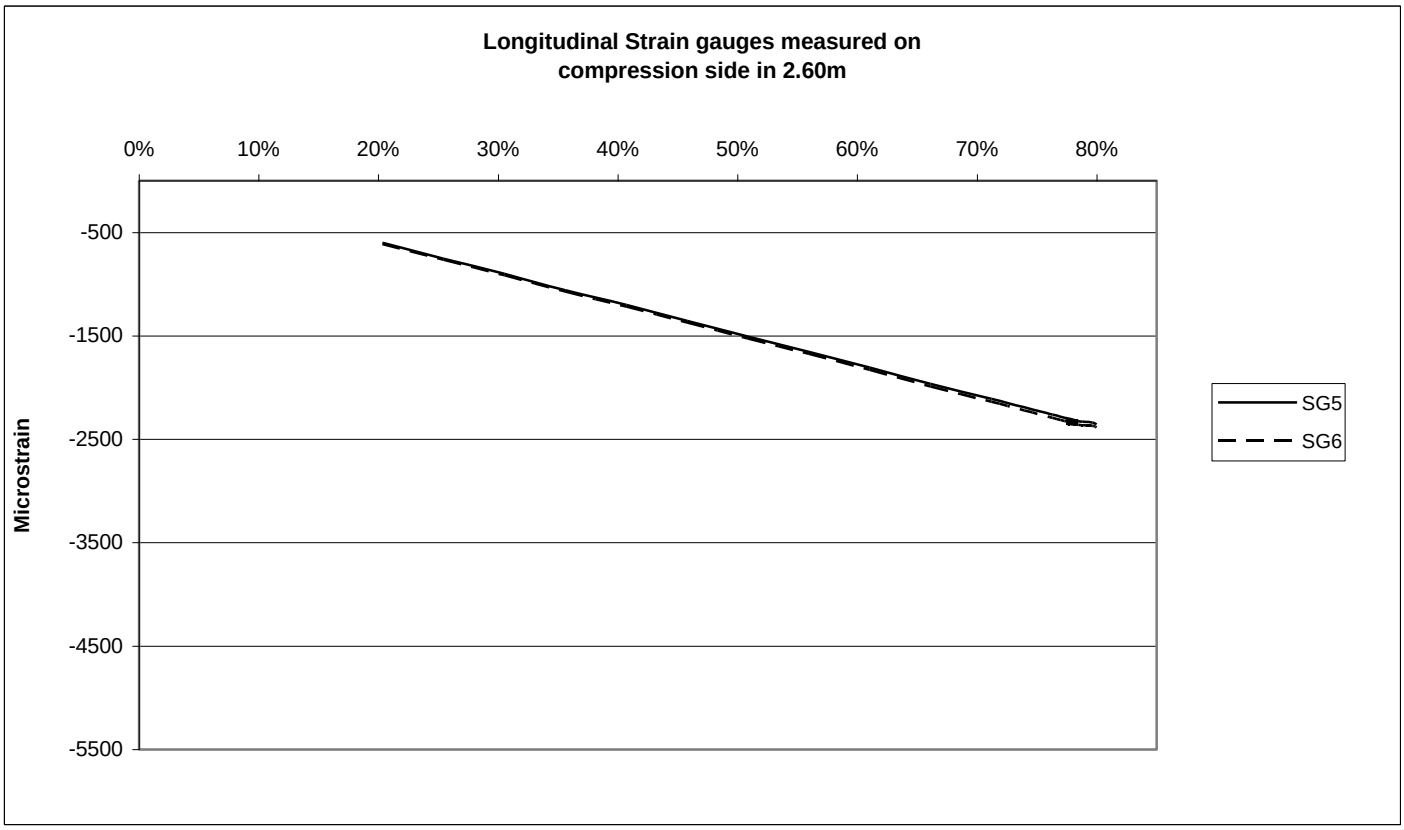
Longitudinal Strain gauges measured on compression side in 2.60m
0%
10%
20%
30%
40%
50%
60%
70%
80%
-500
-1500
-2500
-3500
-4500
-5500
Microstrain
SG5
SG6

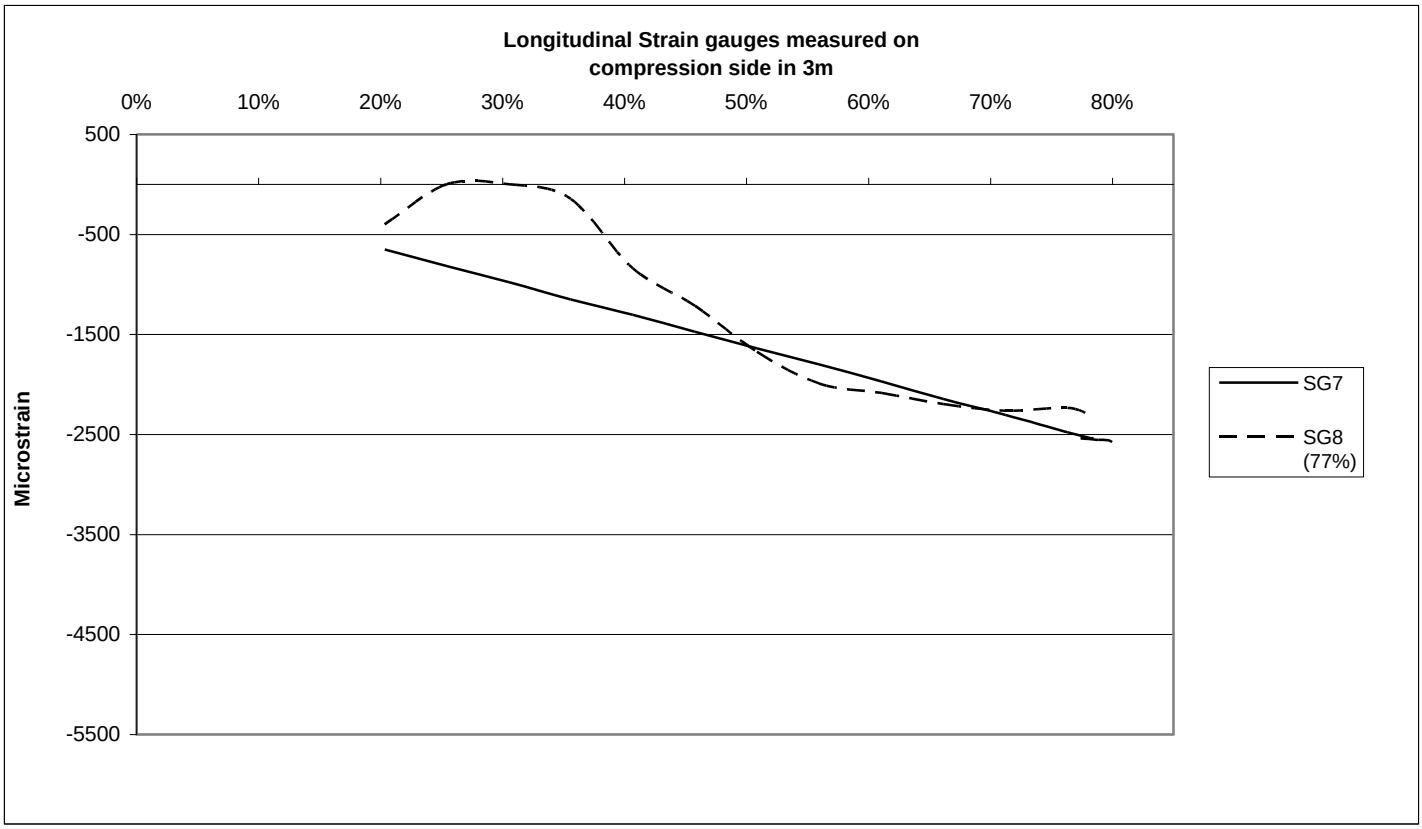
Longitudinal Strain gauges measured on compression side in 3m
0%
10%
20%
30%
40%
50%
60%
70%
80%
500
-500
-1500
-2500
-3500
-4500
-5500
Microstrain
SG7
SG8 (77%)

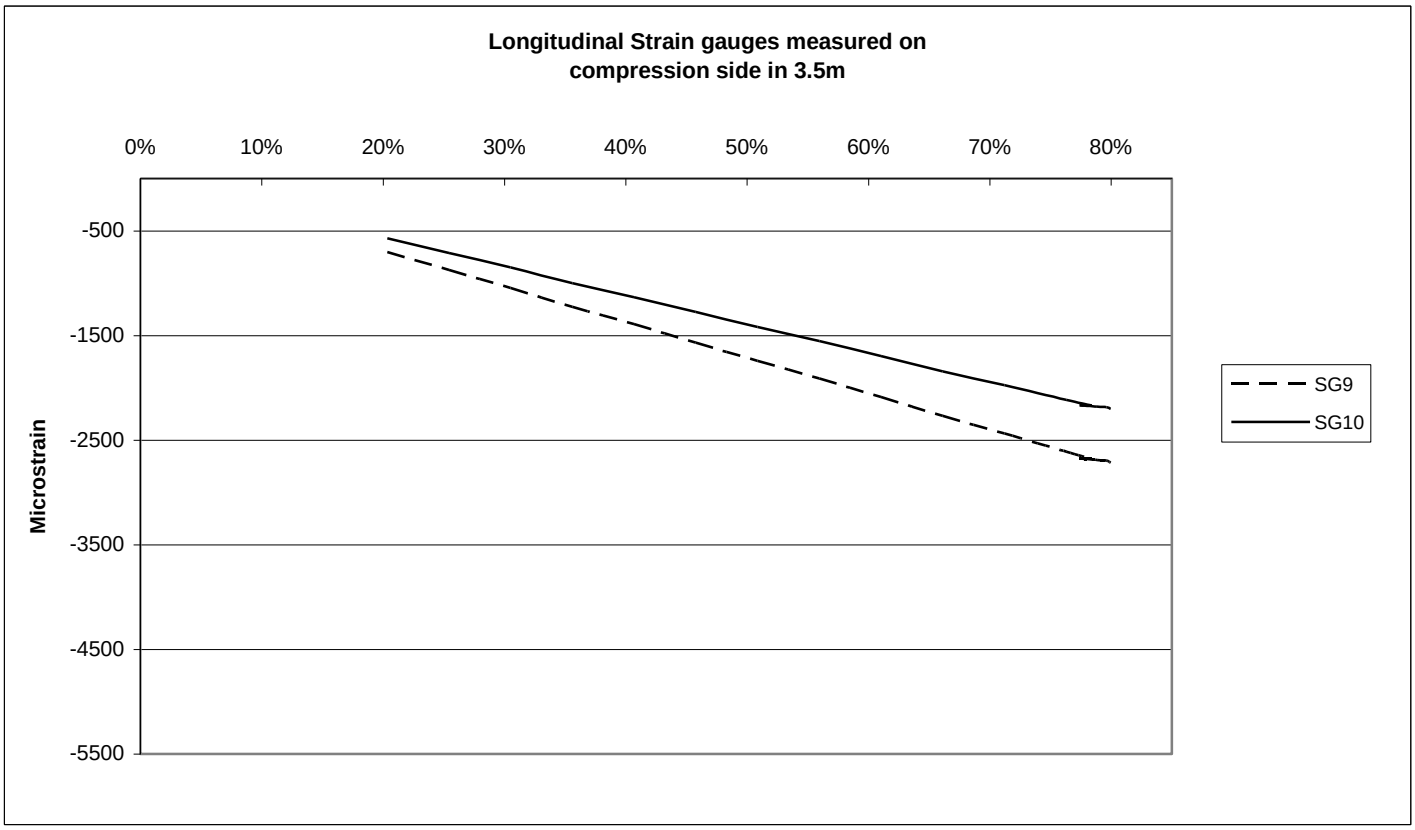
Longitudinal Strain gauges measured on compression side in 3.5m
0%
10%
20%
30%
40%
50%
60%
70%
80%
-500
-1500
-2500
-3500
-4500
-5500
Microstrain
SG9
SG10

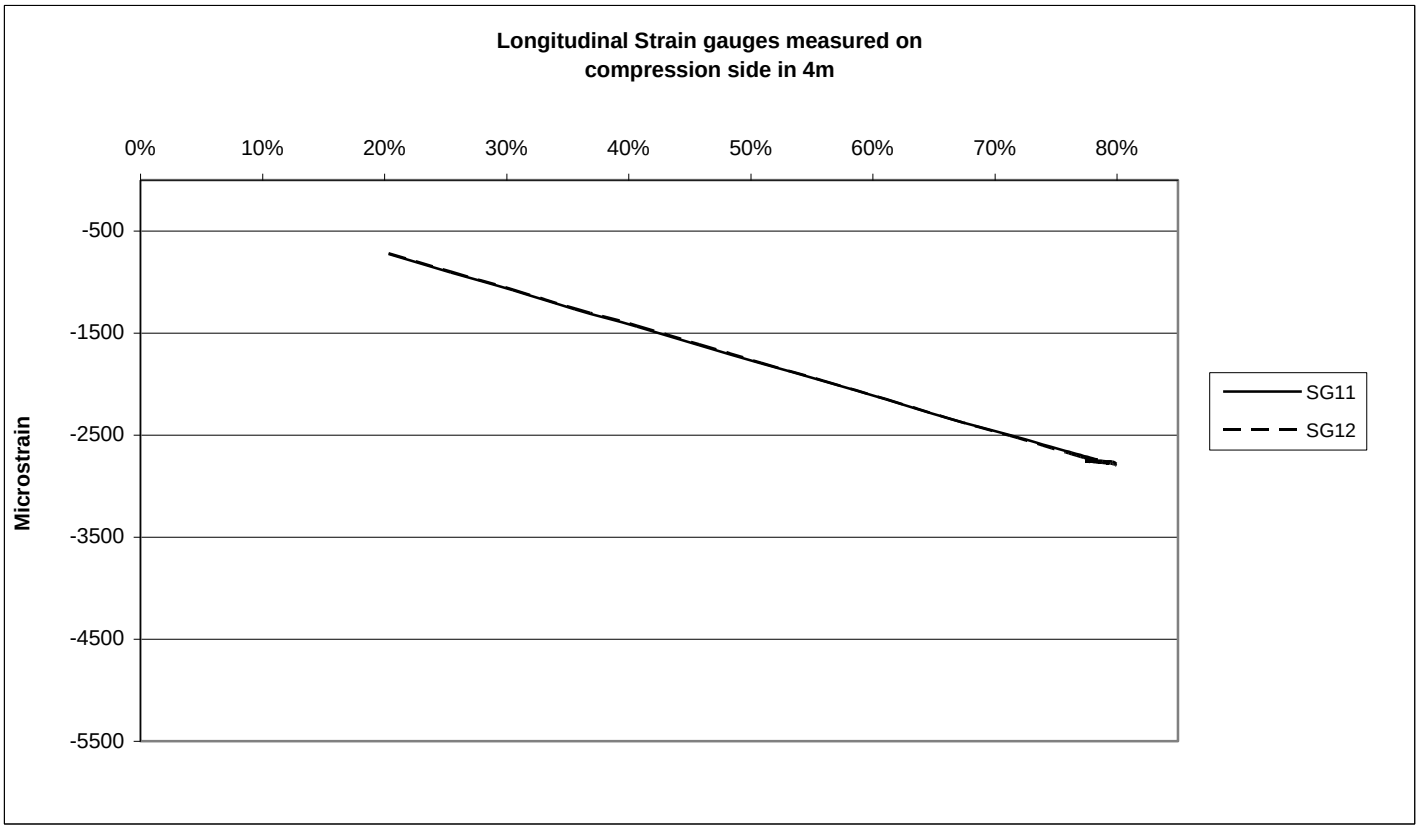
Longitudinal Strain gauges measured on compression side in 4m
0%
10%
20%
30%
40%
50%
60%
70%
80%
-500
-1500
-2500
-3500
-4500
-5500
Microstrain
SG11
SG12

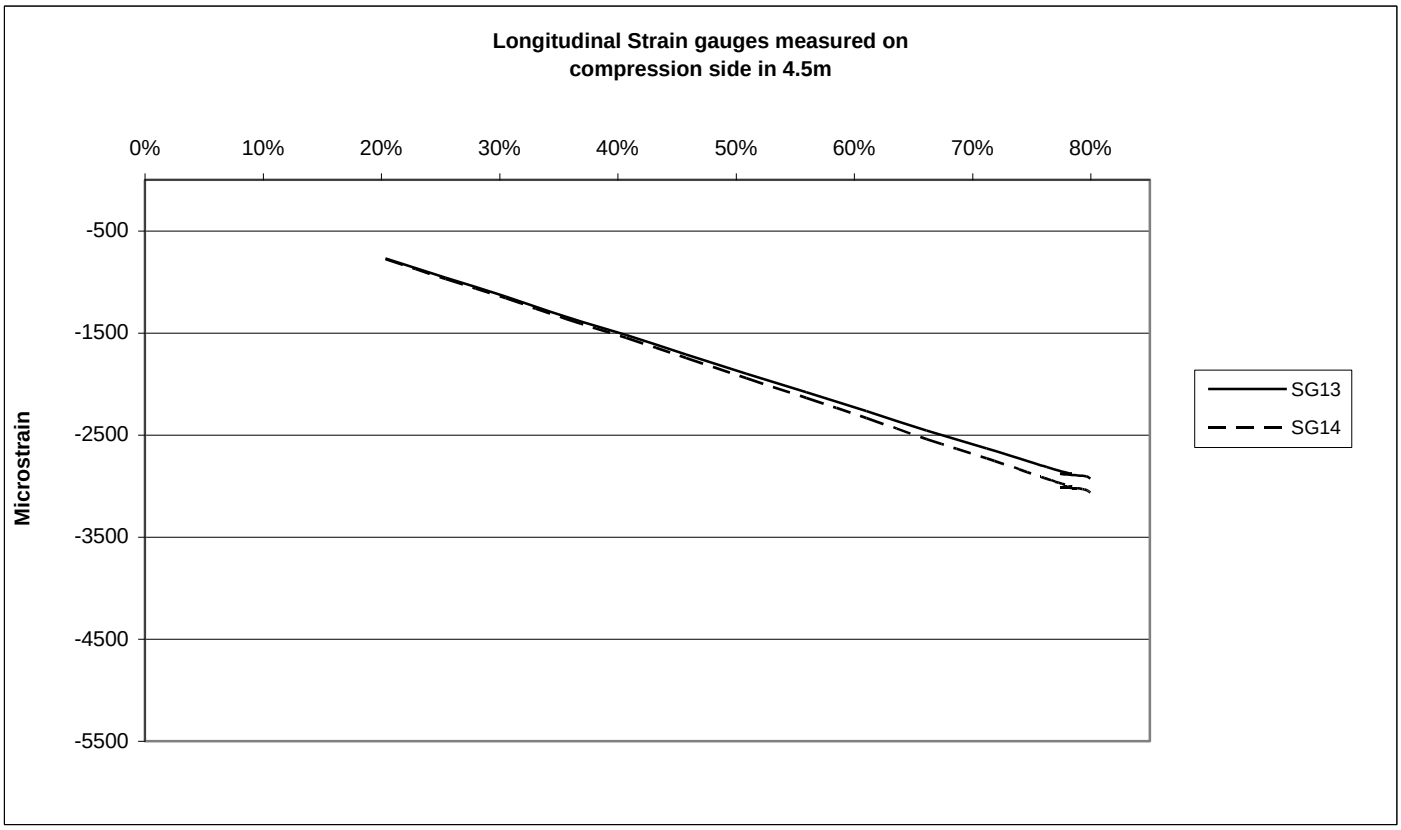
Longitudinal Strain gauges measured on compression side in 4.5m
0%
10%
20%
30%
40%
50%
60%
70%
80%
-500
-1500
-2500
-3500
-4500
-5500
Microstrain
SG13
SG14

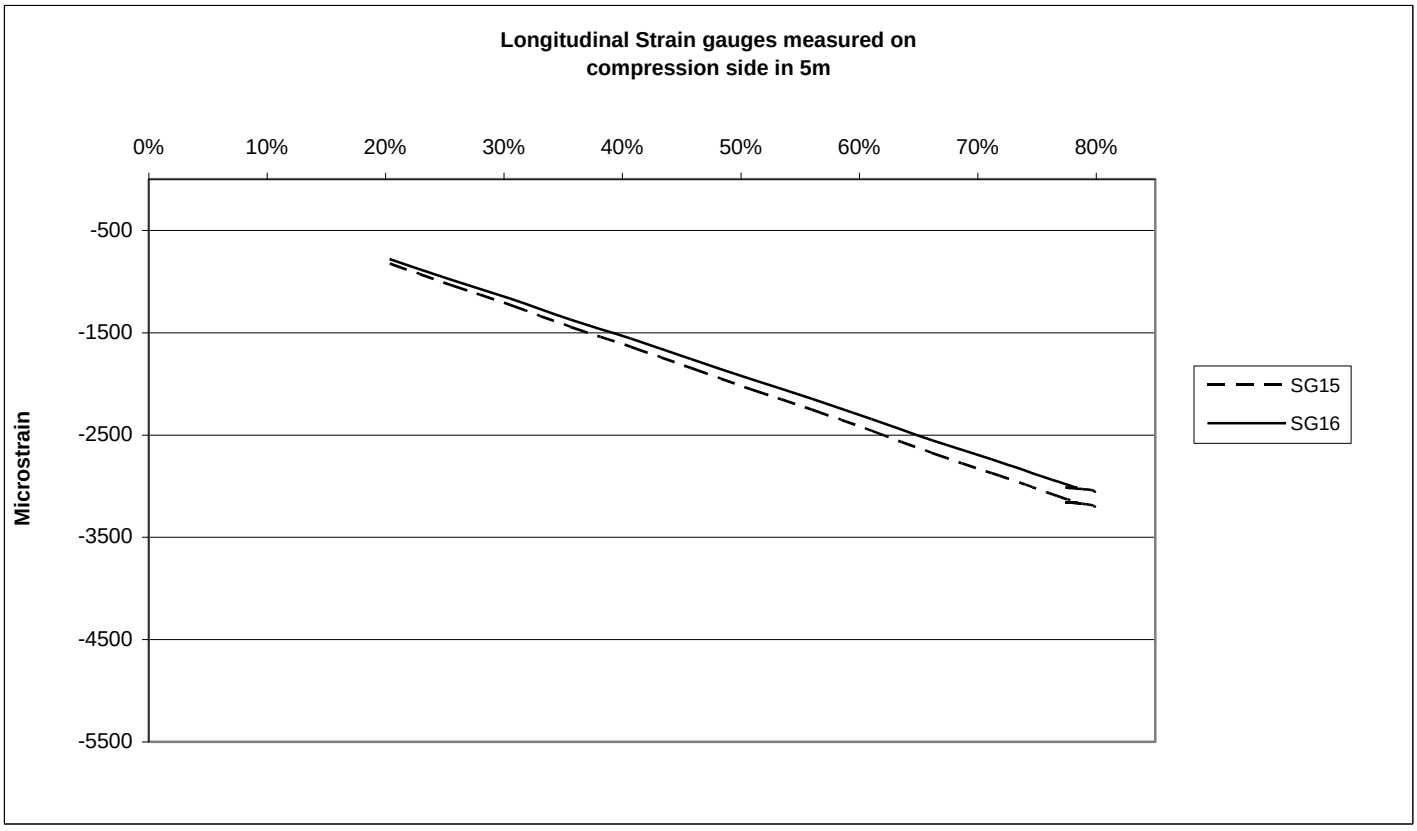
Longitudinal Strain gauges measured on compression side in 5m
0%
10%
20%
30%
40%
50%
60%
70%
80%
-500
-1500
-2500
-3500
-4500
-5500
Microstrain
SG15
SG16

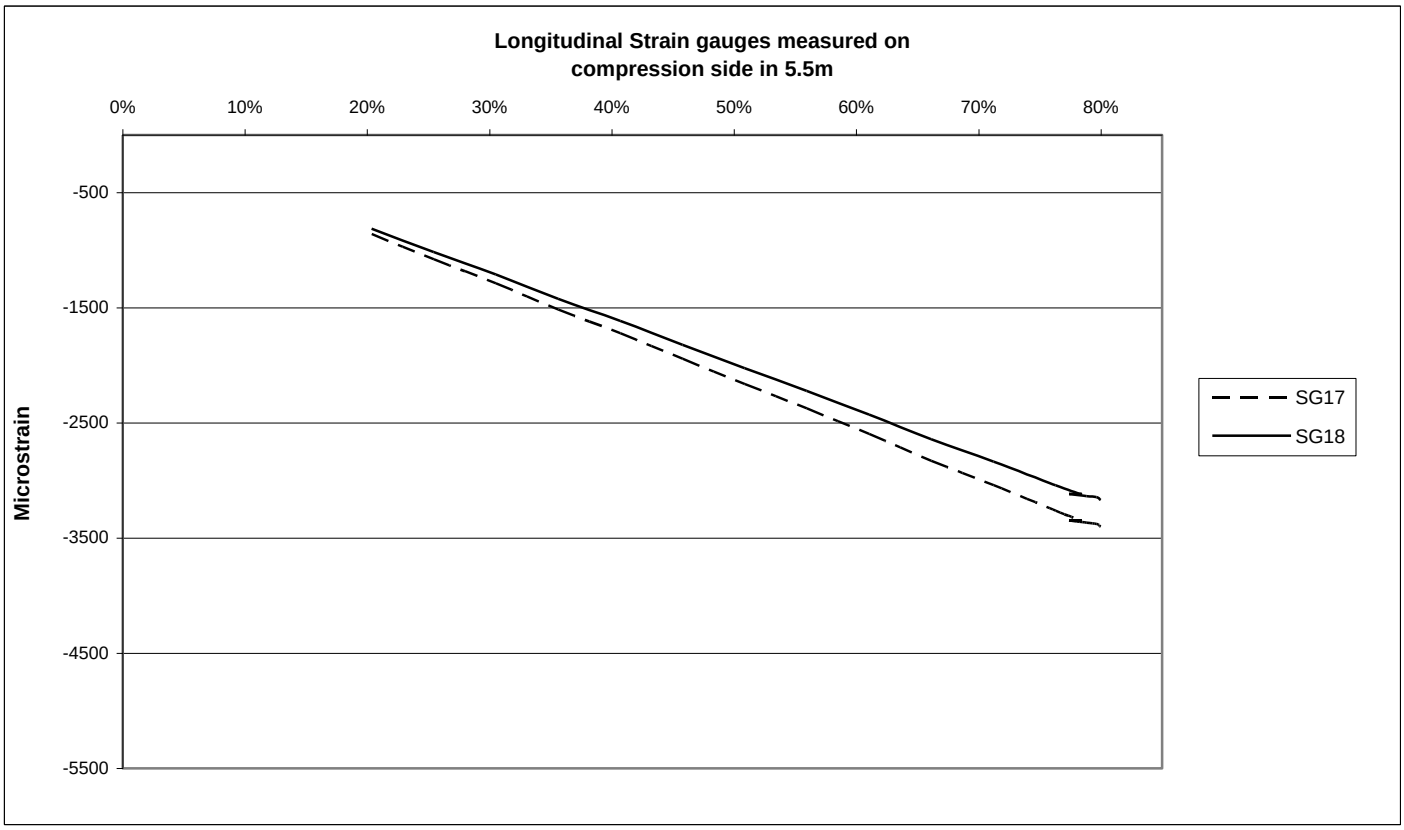
Longitudinal Strain gauges measured on compression side in 5.5m
0%
10%
20%
30%
40%
50%
60%
70%
80%
-500
-1500
-2500
-3500
-4500
-5500
Microstrain
SG17
SG18

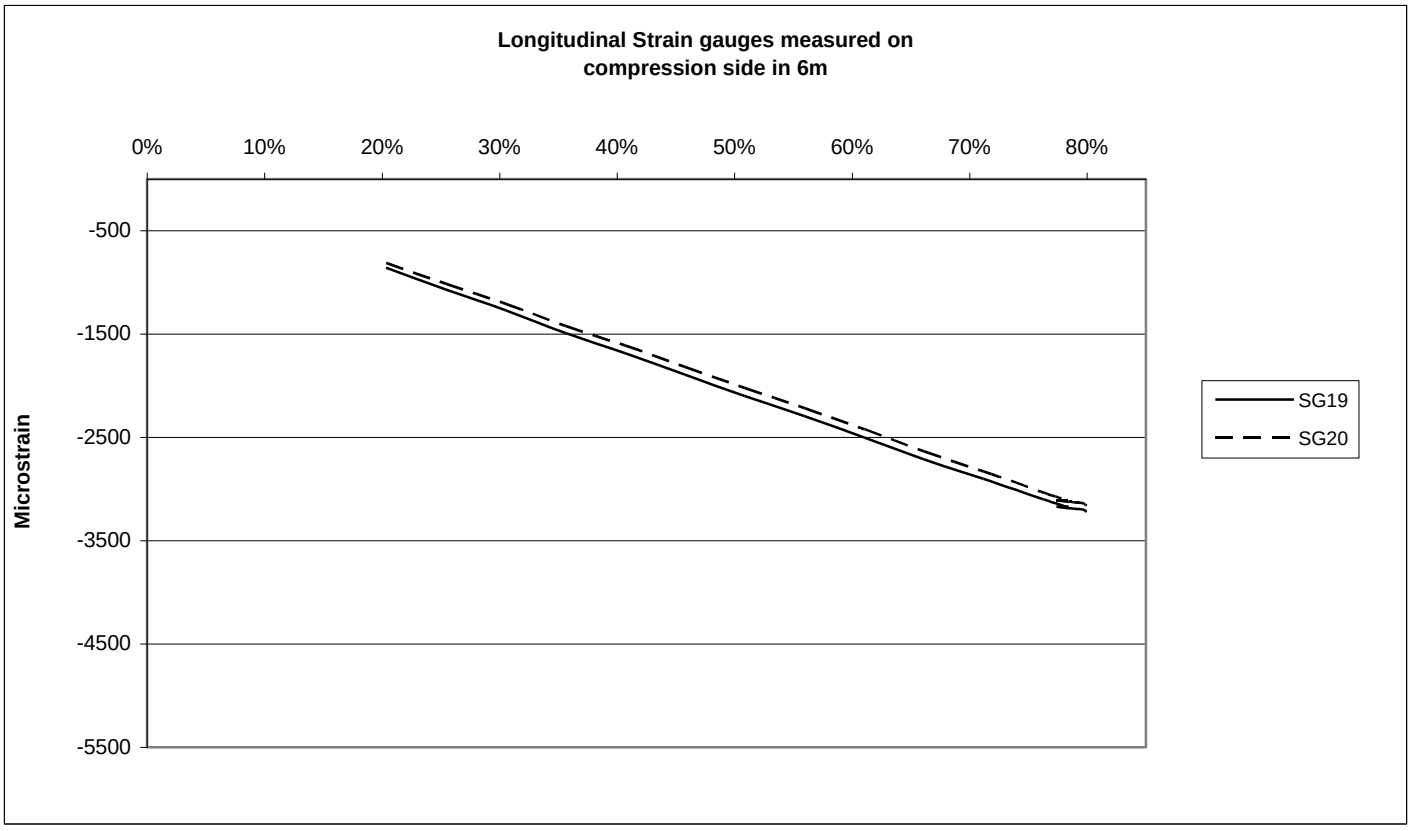
Longitudinal Strain gauges measured on compression side in 6m
0%
10%
20%
30%
40%
50%
60%
70%
80%
-500
-1500
-2500
-3500
-4500
-5500
Microstrain
SG19
SG20

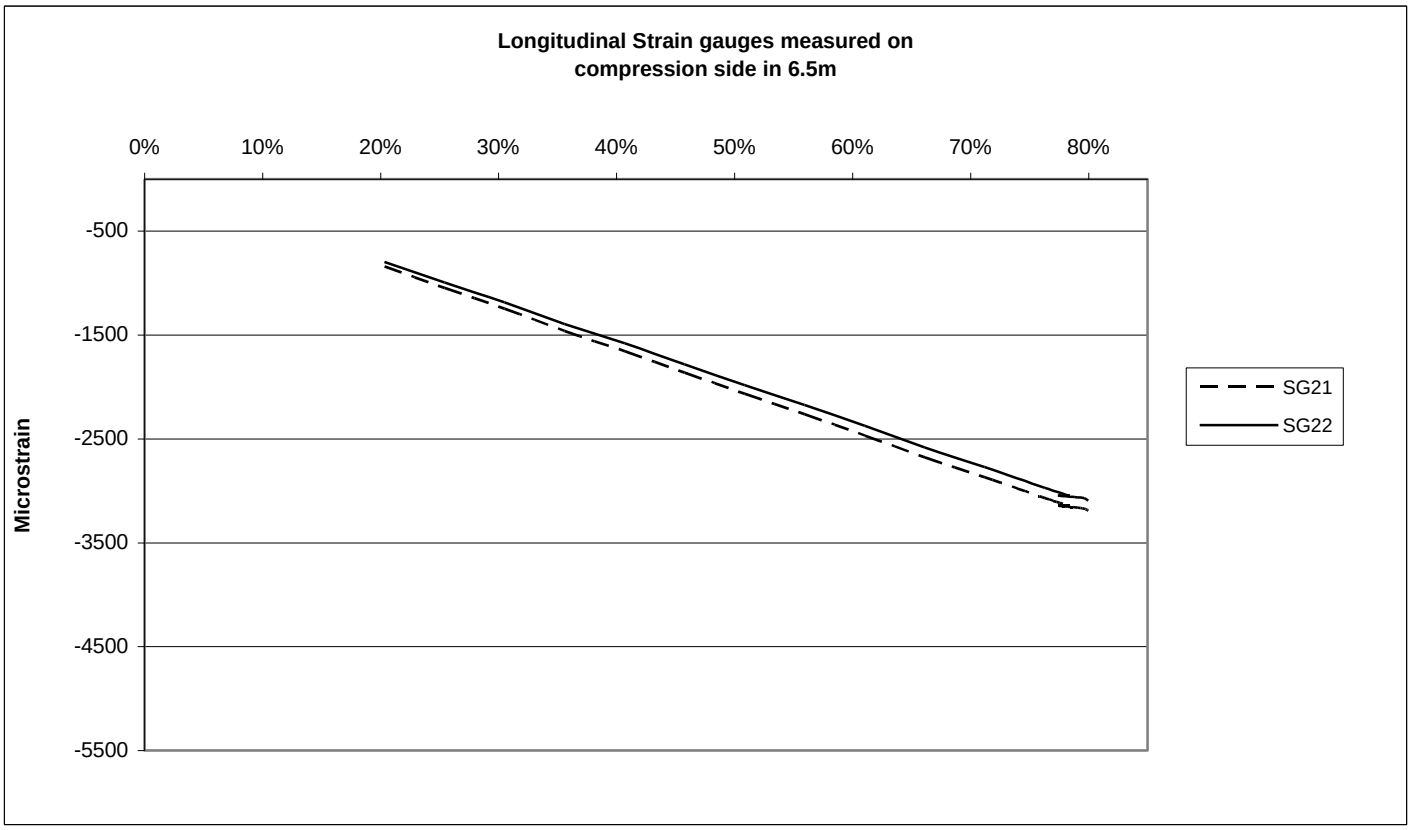
Longitudinal Strain gauges measured on compression side in 6.5m
0%
10%
20%
30%
40%
50%
60%
70%
80%
-500
-1500
-2500
-3500
-4500
-5500
Microstrain
SG21
SG22

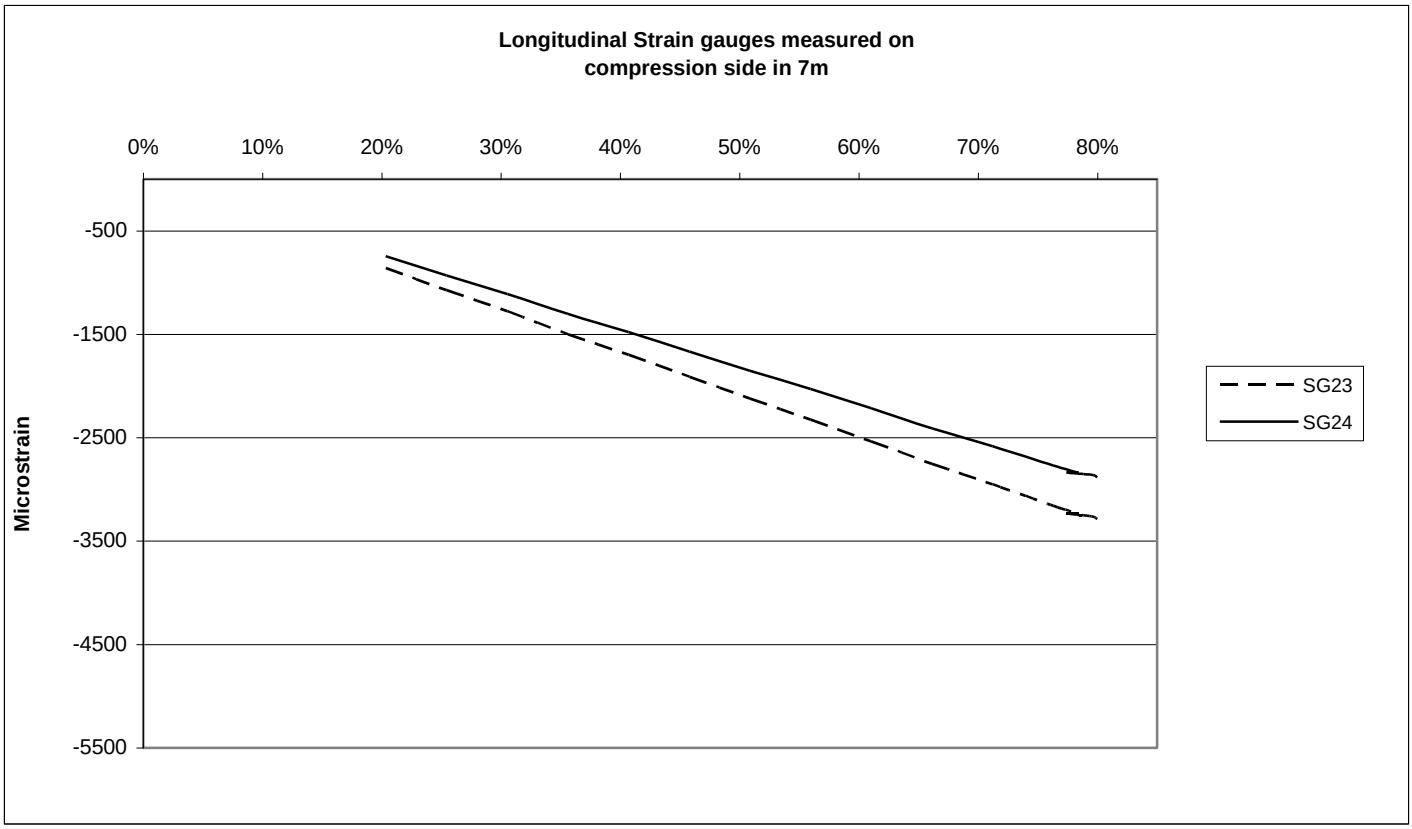
Longitudinal Strain gauges measured on compression side in 7m
0%
10%
20%
30%
40%
50%
60%
70%
80%
-500
-1500
-2500
-3500
-4500
-5500
Microstrain
SG23
SG24

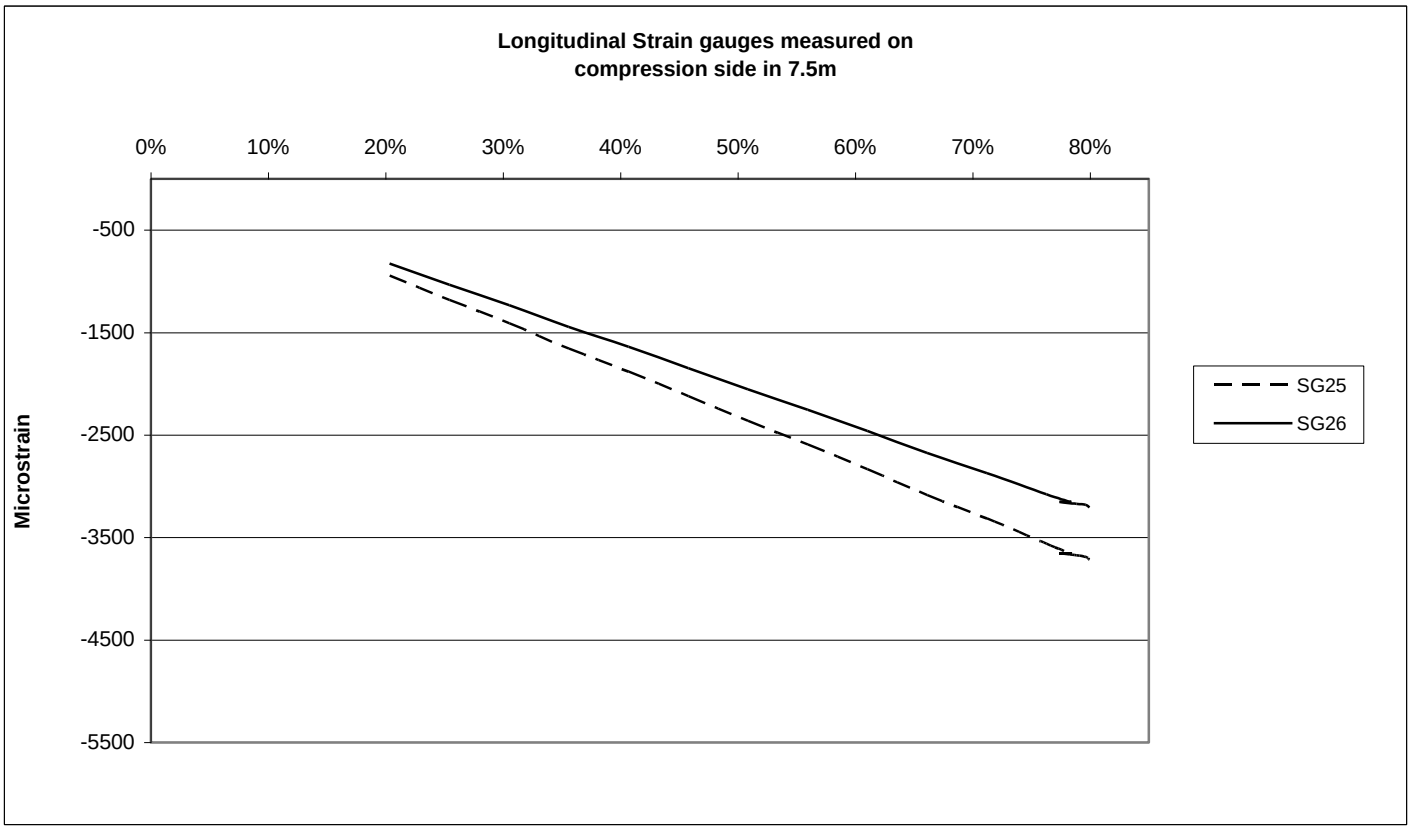
Longitudinal Strain gauges measured on compression side in 7.5m
0%
10%
20%
30%
40%
50%
60%
70%
80%
-500
-1500
-2500
-3500
-4500
-5500
Microstrain
SG25
SG26

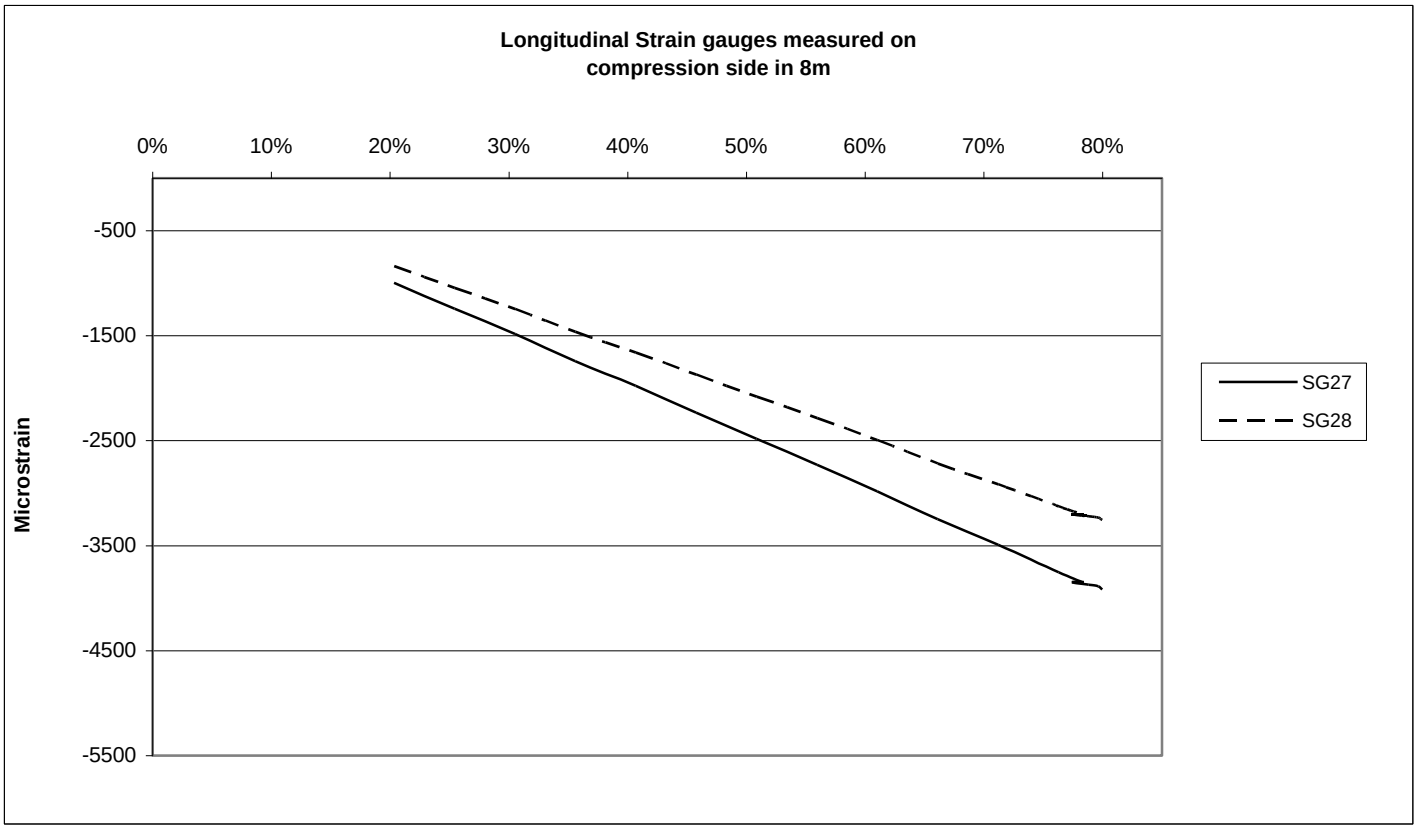
Longitudinal Strain gauges measured on compression side in 8m
0%
10%
20%
30%
40%
50%
60%
70%
80%
-500
-1500
-2500
-3500
-4500
-5500
Microstrain
SG27
SG28

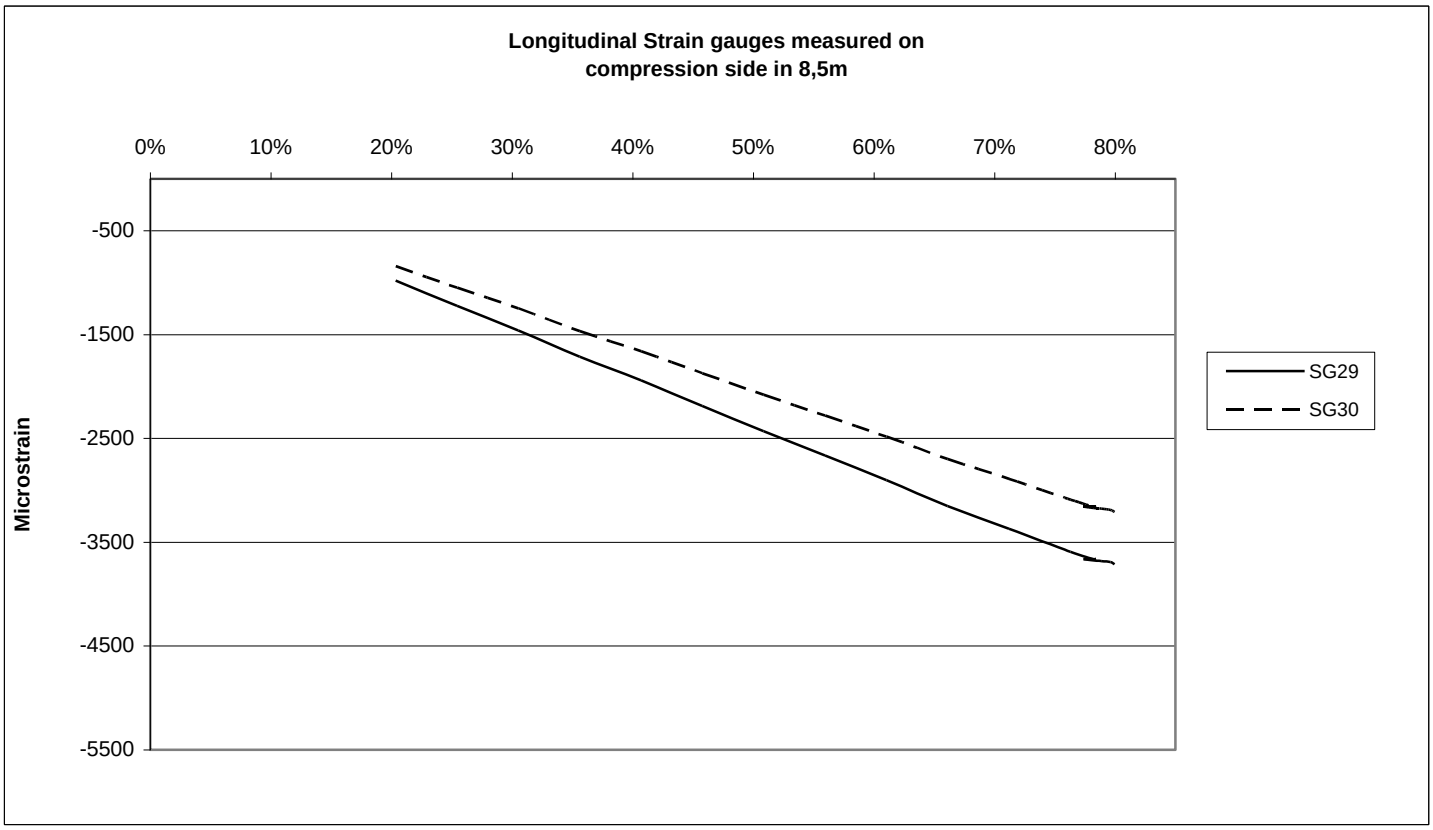
Longitudinal Strain gauges measured on compression side in 8,5m
0%
10%
20%
30%
40%
50%
60%
70%
80%
-500
-1500
-2500
-3500
-4500
-5500
Microstrain
SG29
SG30

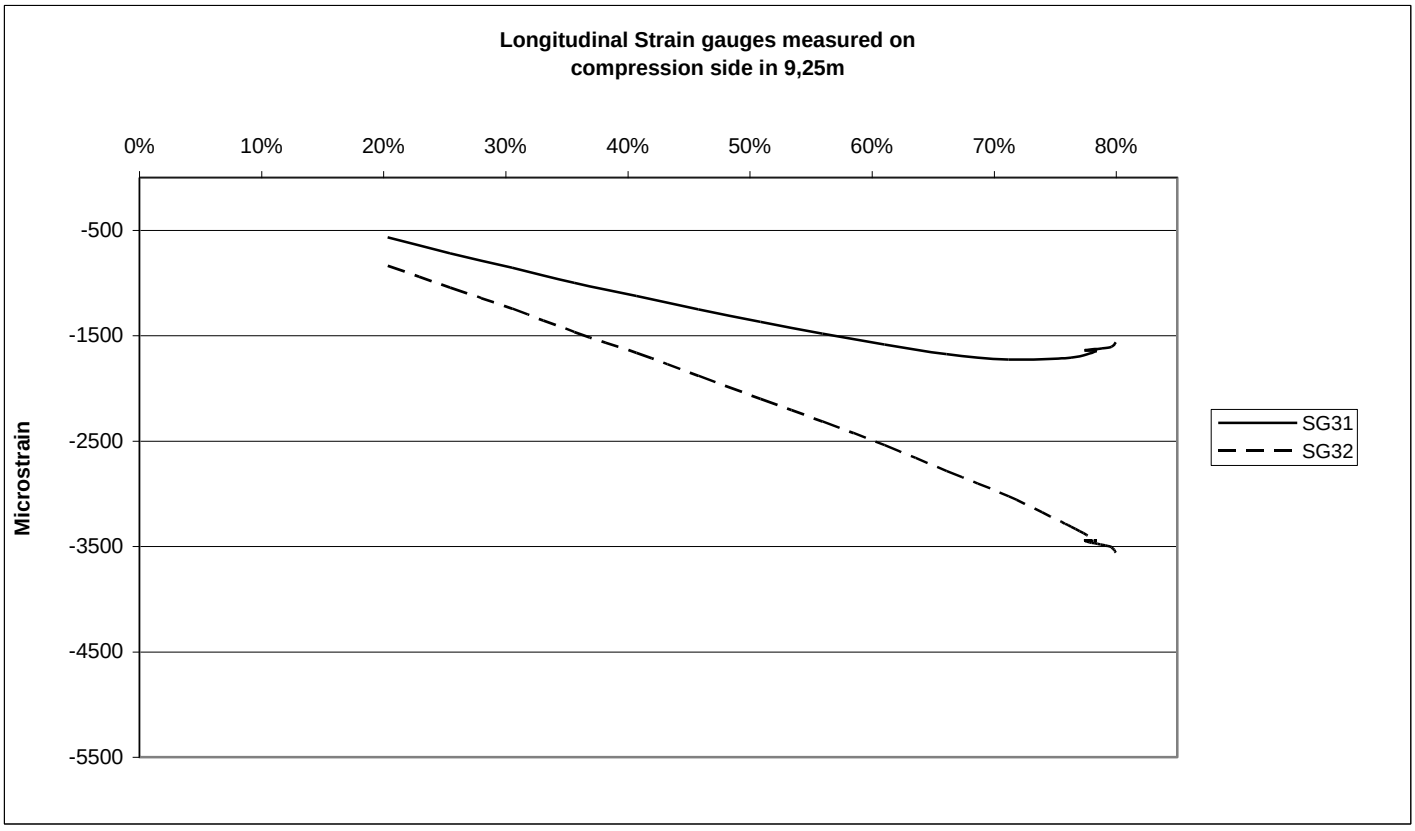
Longitudinal Strain gauges measured on compression side in 9,25m
0%
10%
20%
30%
40%
50%
60%
70%
80%
-500
-1500
-2500
-3500
-4500
-5500
Microstrain
SG31
SG32

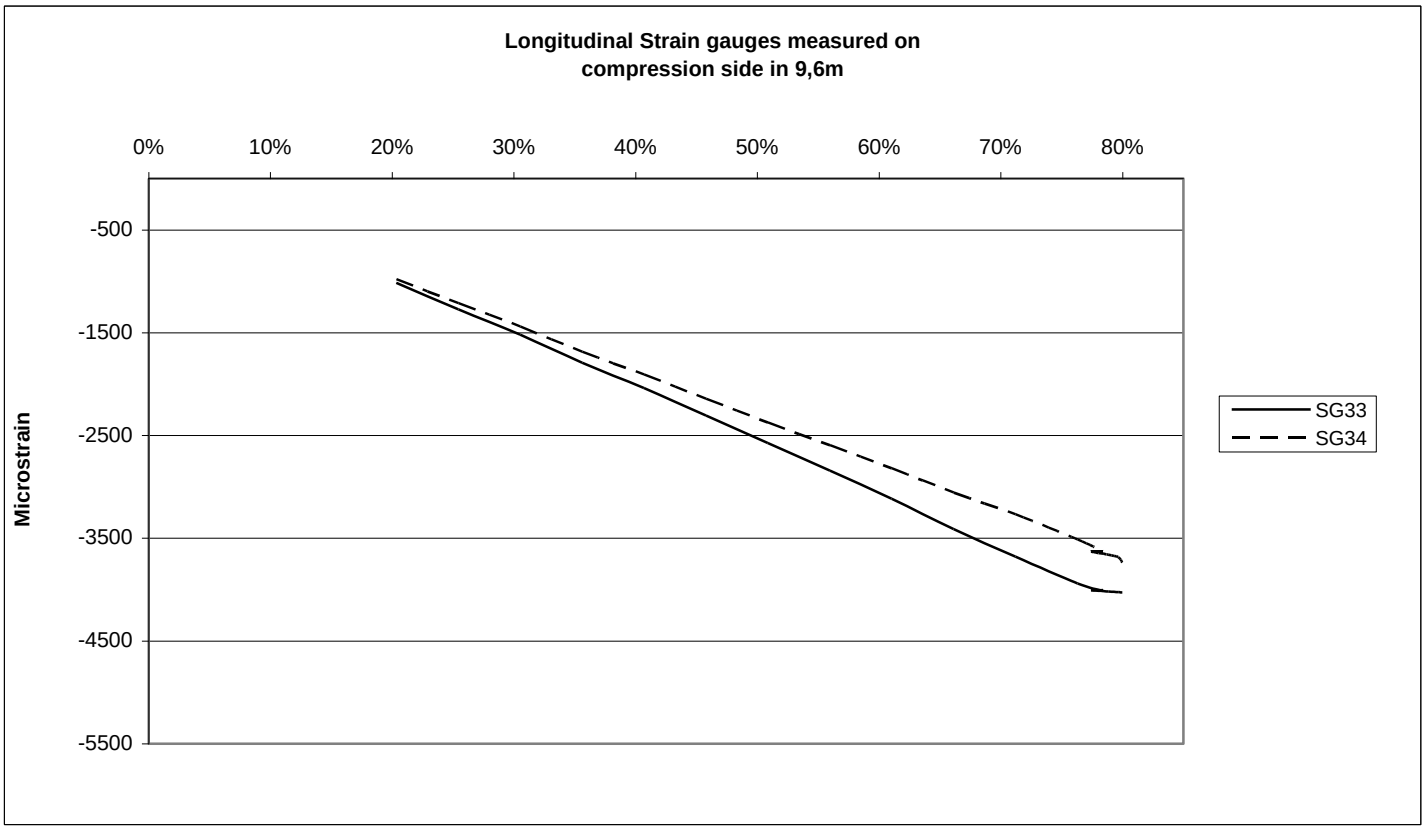
Longitudinal Strain gauges measured on compression side in 9,6m
0%
10%
20%
30%
40%
50%
60%
70%
80%
-500
-1500
-2500
-3500
-4500
-5500
Microstrain
SG33
SG34

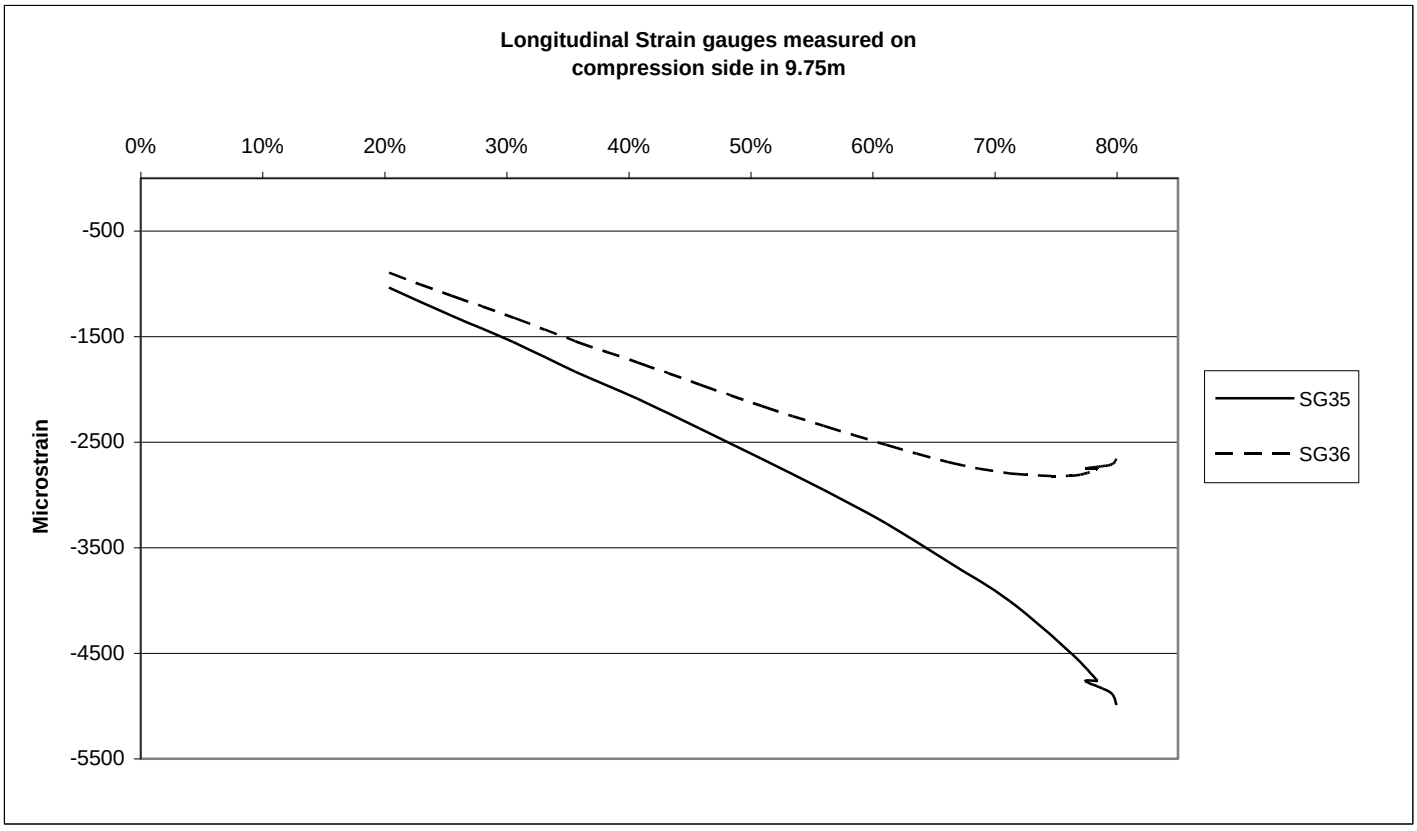
Longitudinal Strain gauges measured on compression side in 9.75m
0%
10%
20%
30%
40%
50%
60%
70%
80%
-500
-1500
-2500
-3500
-4500
-5500
Microstrain
SG35
SG36

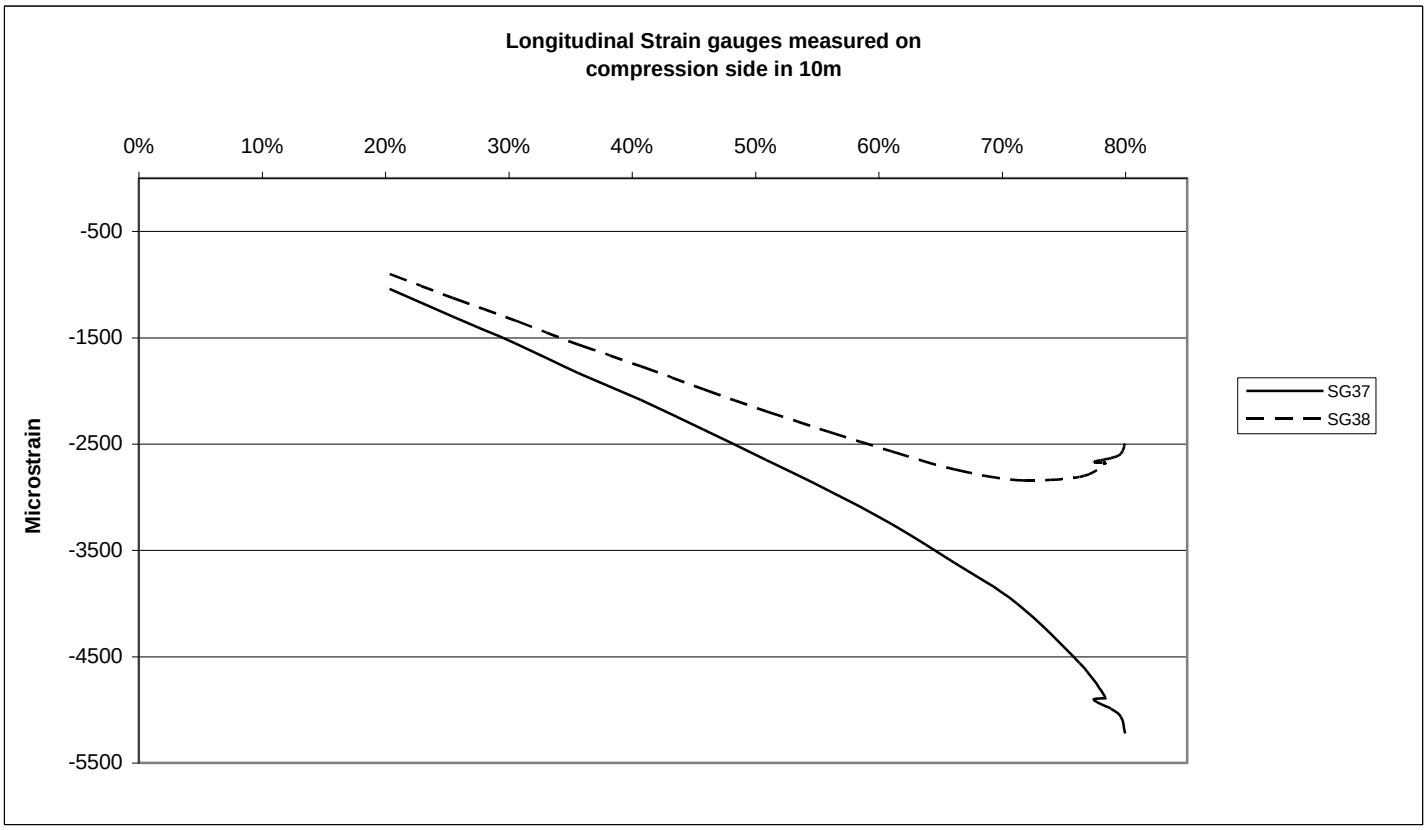
Longitudinal Strain gauges measured on compression side in 10m
0%
10%
20%
30%
40%
50%
60%
70%
80%
-500
-1500
-2500
-3500
-4500
-5500
Microstrain
SG37
SG38

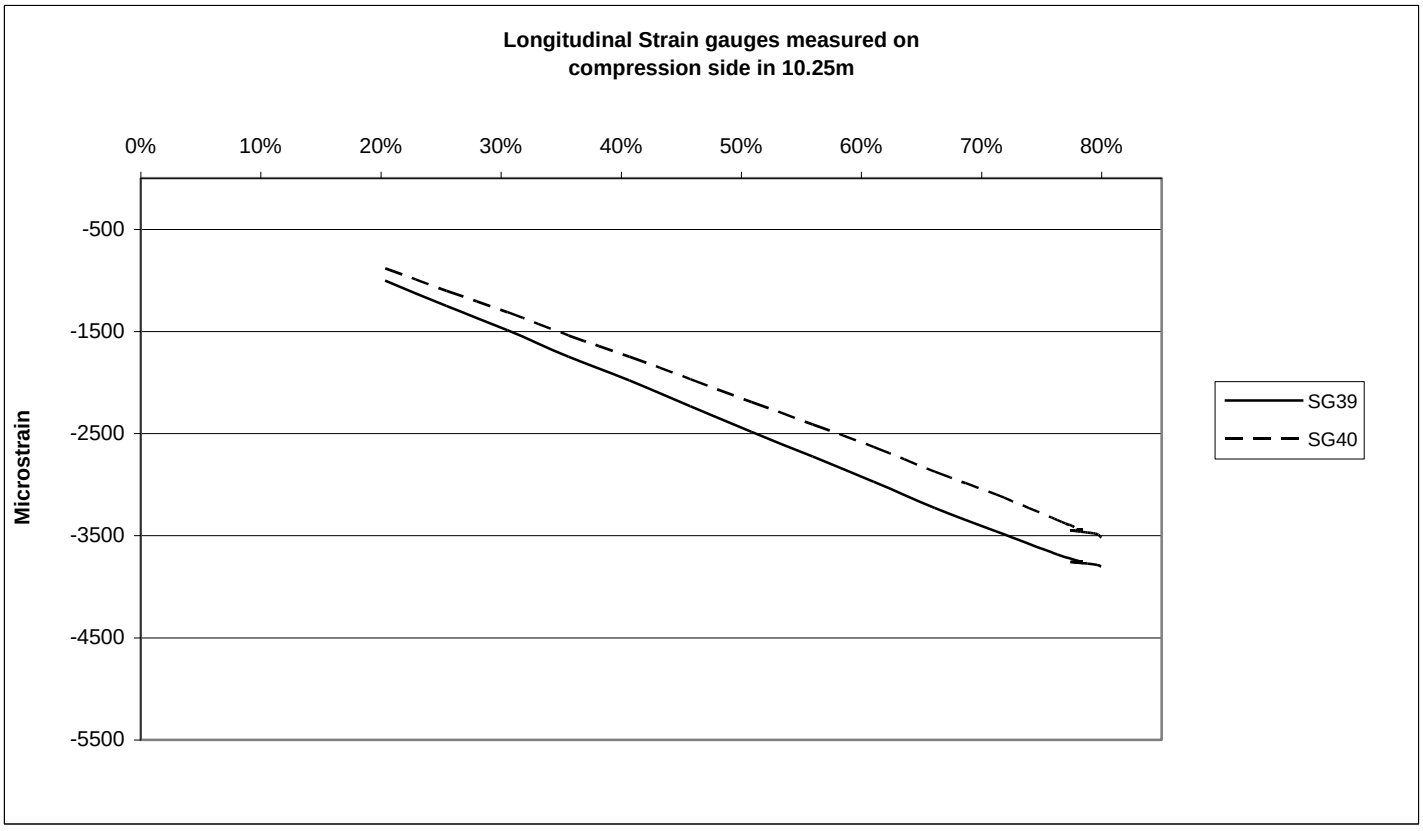
Longitudinal Strain gauges measured on compression side in 10.25m
0%
10%
20%
30%
40%
50%
60%
70%
80%
-500
-1500
-2500
-3500
-4500
-5500
Microstrain
SG39
SG40

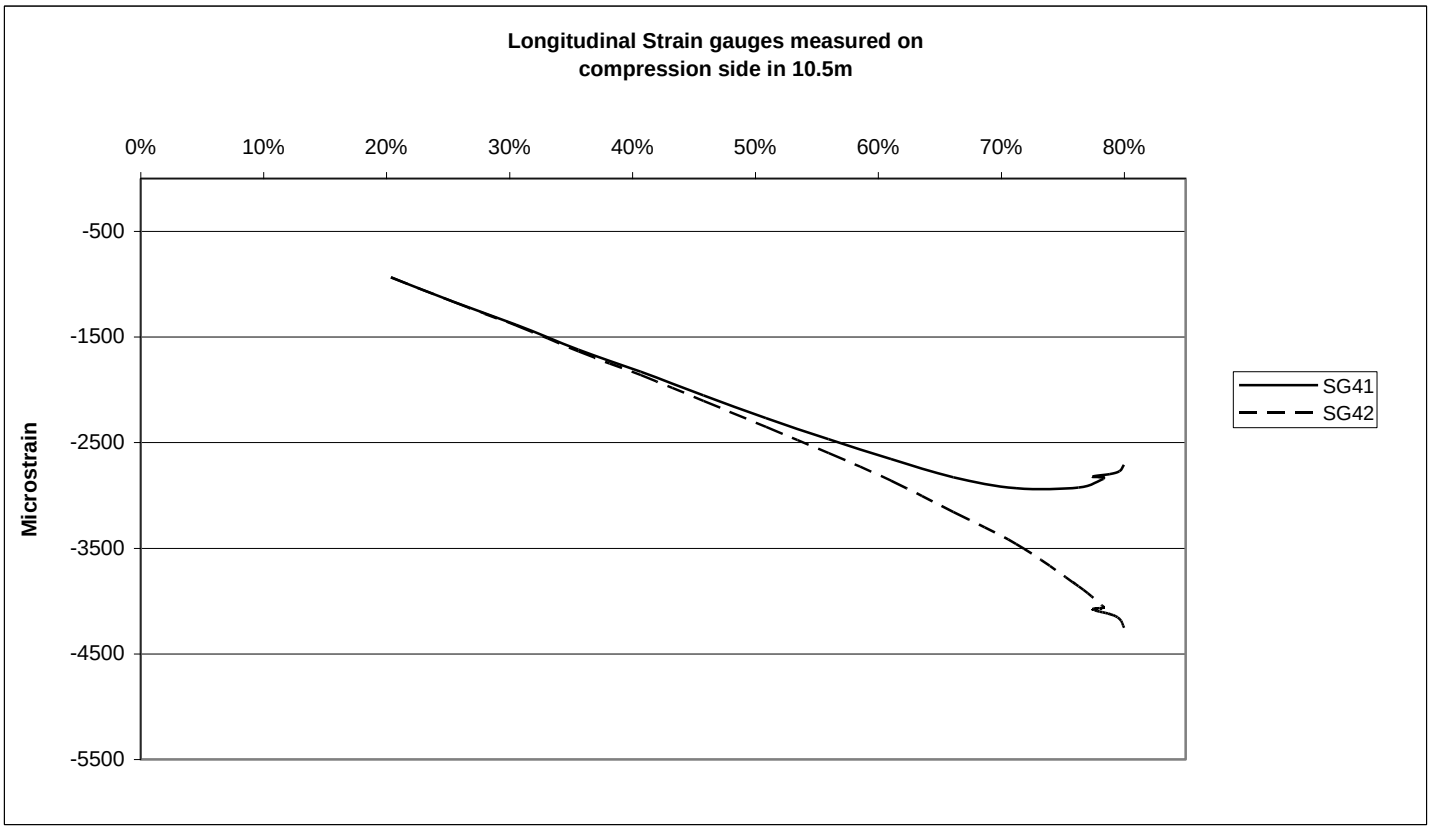
Longitudinal Strain gauges measured on compression side in 10.5m
0%
10%
20%
30%
40%
50%
60%
70%
80%
-500
-1500
-2500
-3500
-4500
-5500
Microstrain
SG41
SG42

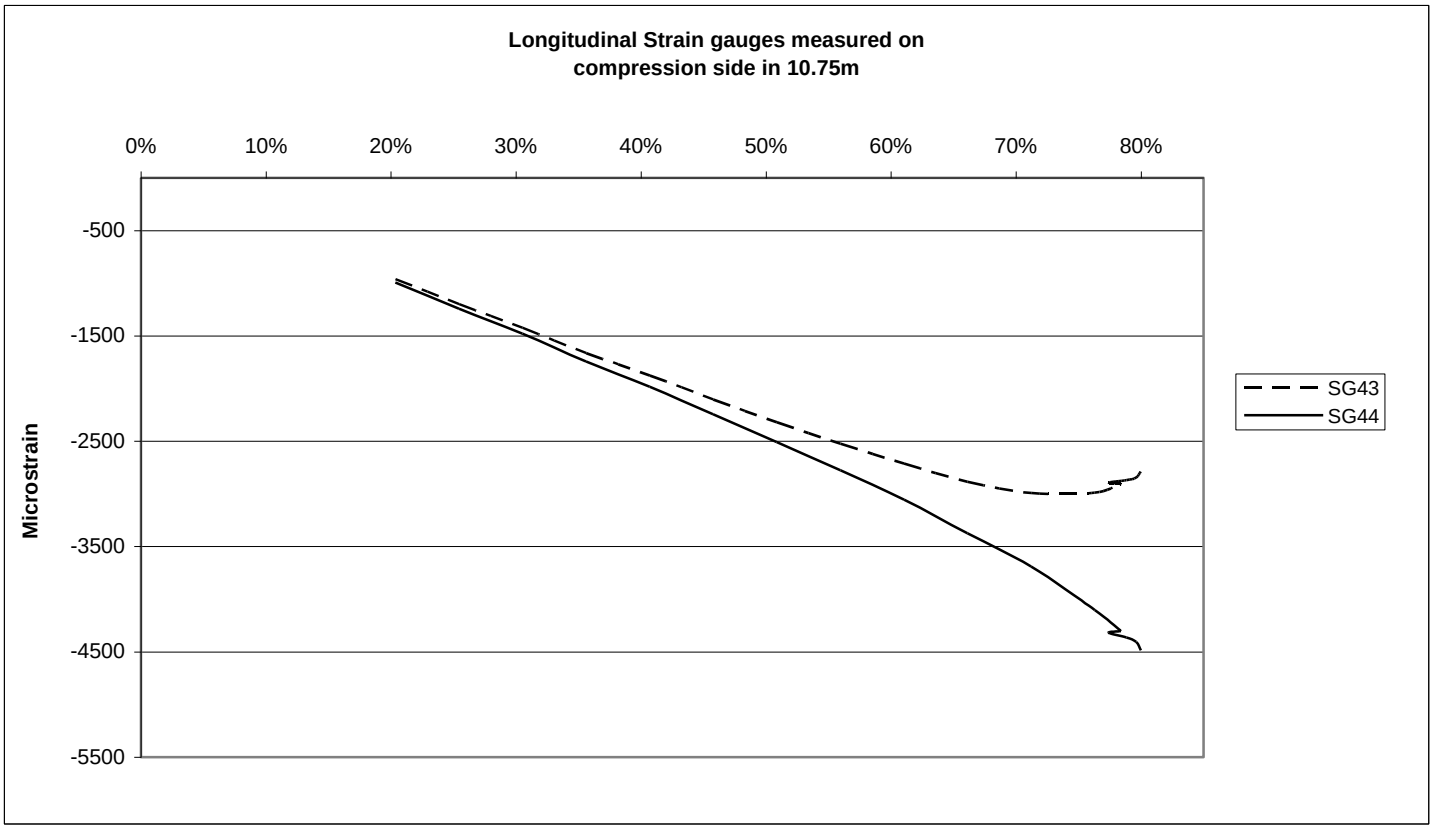
Longitudinal Strain gauges measured on compression side in 10.75m
0%
10%
20%
30%
40%
50%
60%
70%
80%
-500
-1500
-2500
-3500
-4500
-5500
Microstrain
SG43
SG44

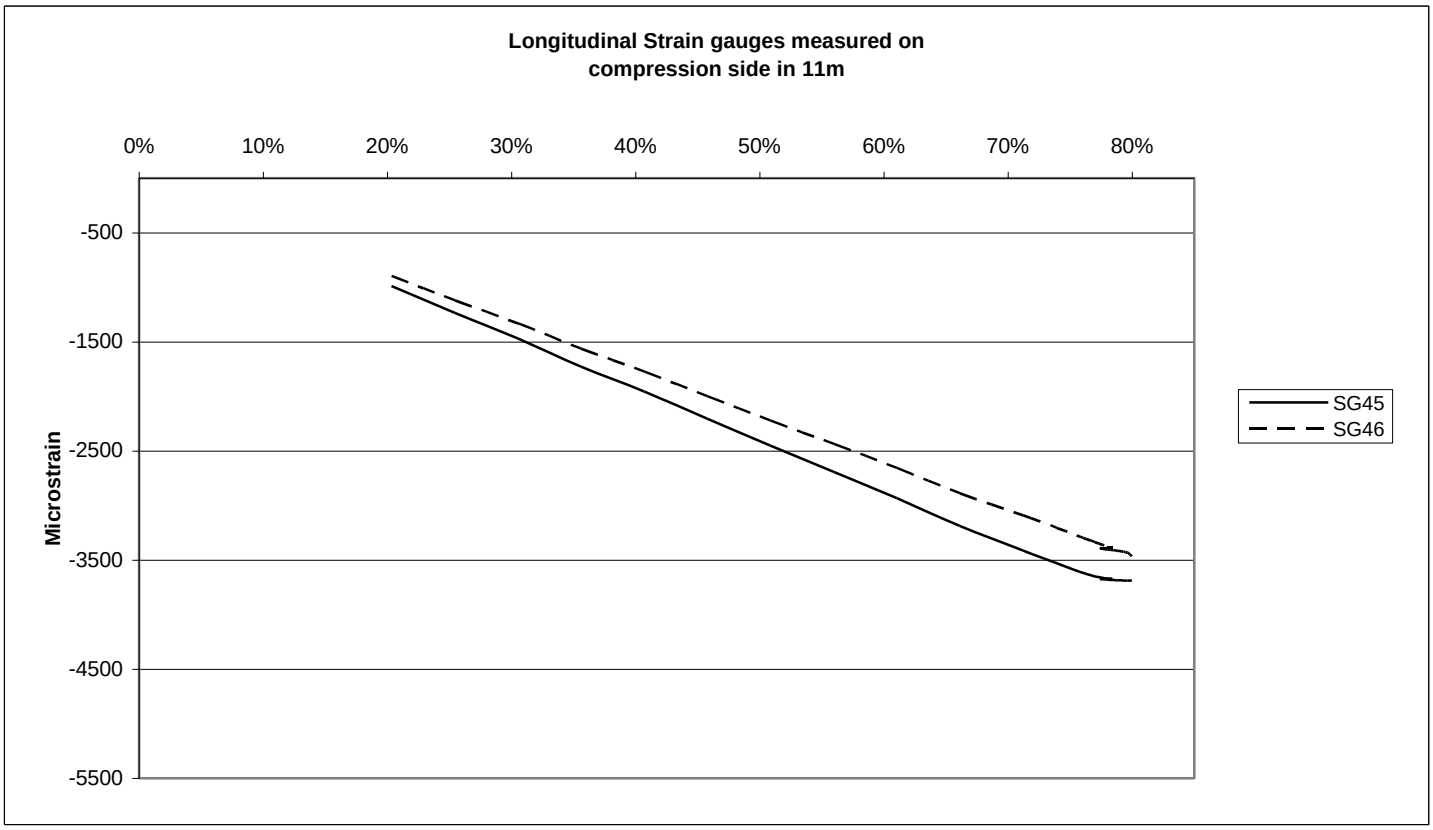
Longitudinal Strain gauges measured on compression side in 11m
0%
10%
20%
30%
40%
50%
60%
70%
80%
-500
-1500
-2500
-3500
-4500
-5500
Microstrain
SG45
SG46

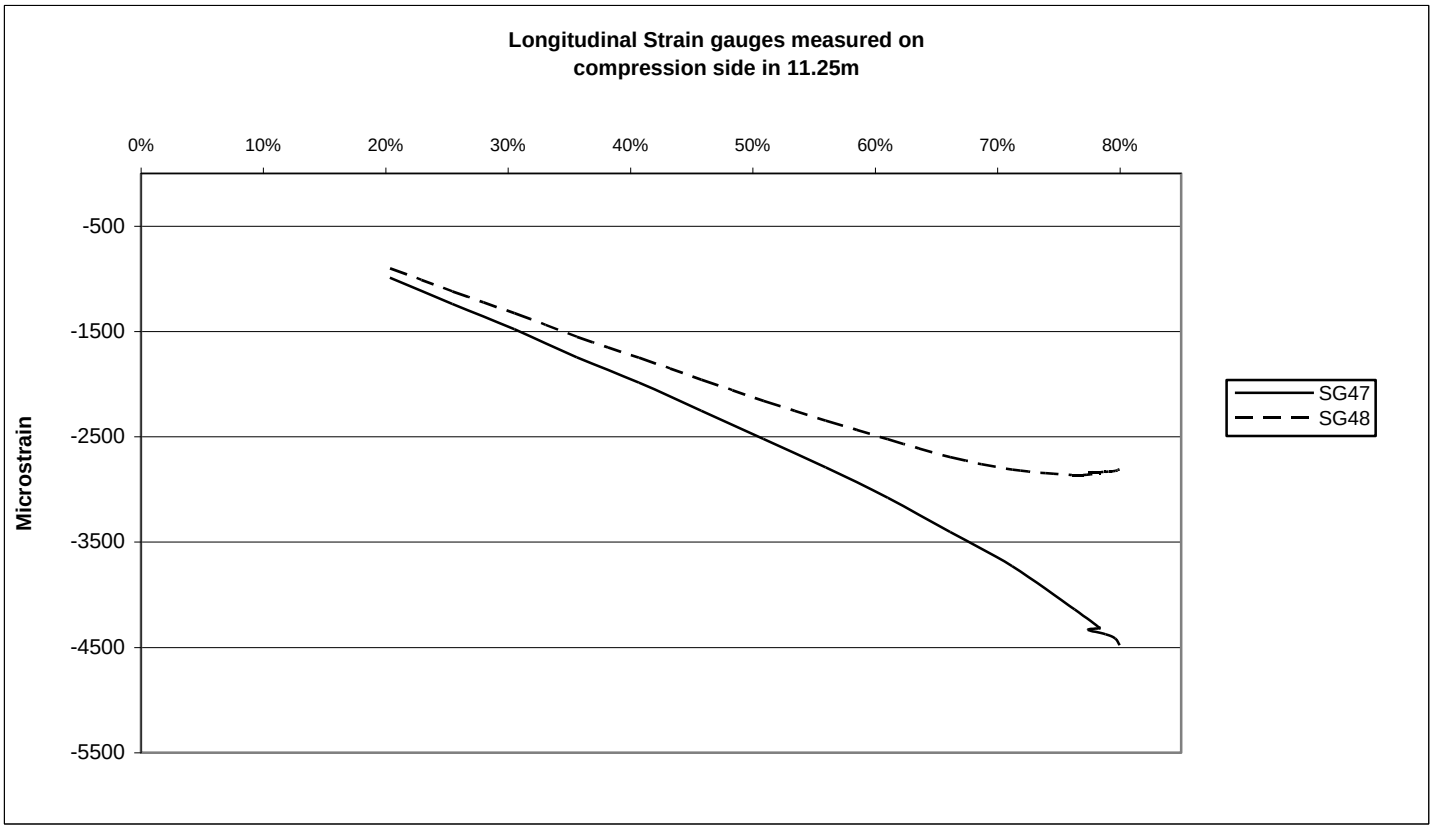
Longitudinal Strain gauges measured on compression side in 11.25m
0%
10%
20%
30%
40%
50%
60%
70%
80%
-500
-1500
-2500
-3500
-4500
-5500
Microstrain
SG47
SG48

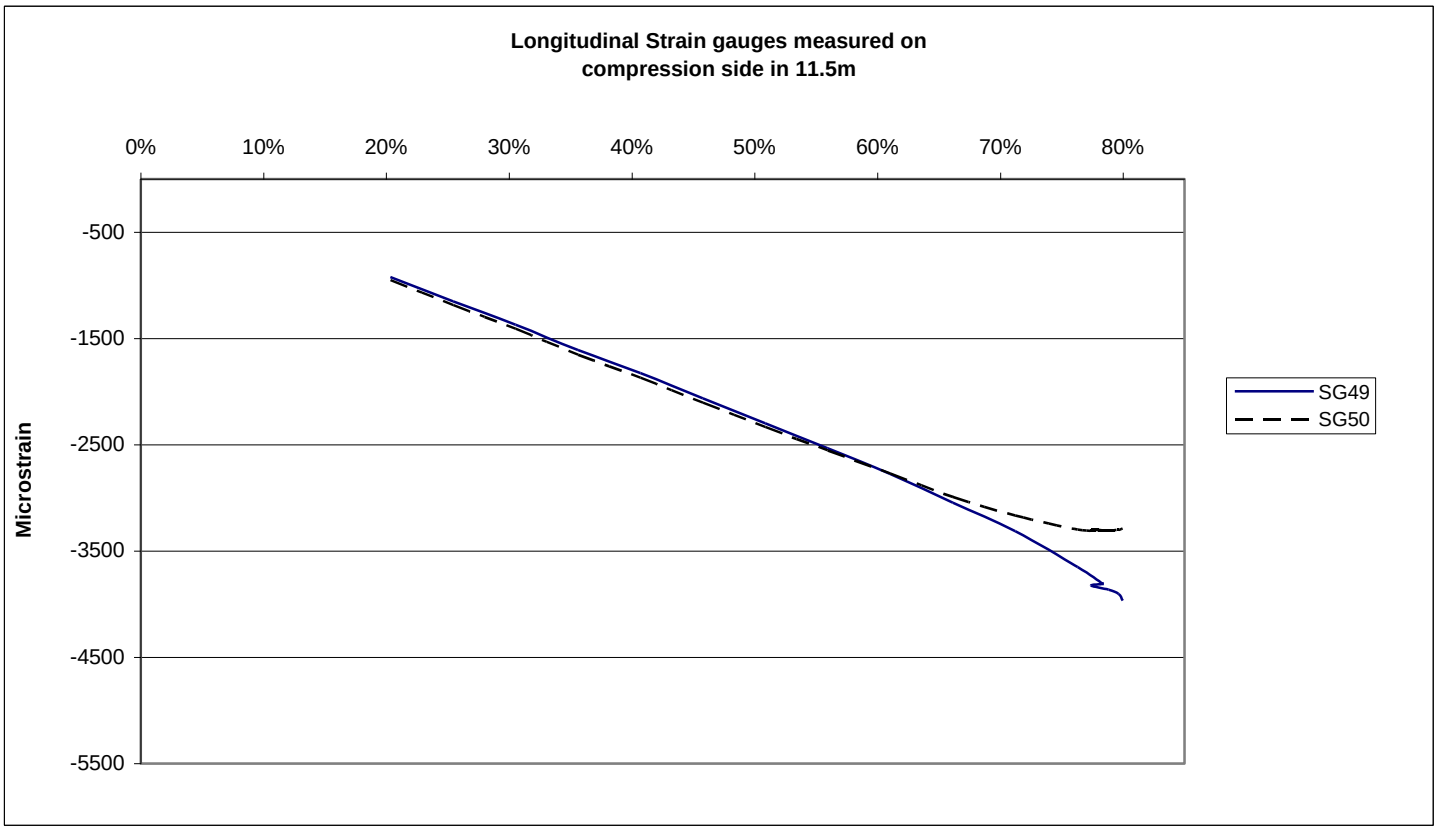
Longitudinal Strain gauges measured on compression side in 11.5m
0%
10%
20%
30%
40%
50%
60%
70%
80%
-500
-1500
-2500
-3500
-4500
-5500
Microstrain
SG49
SG50

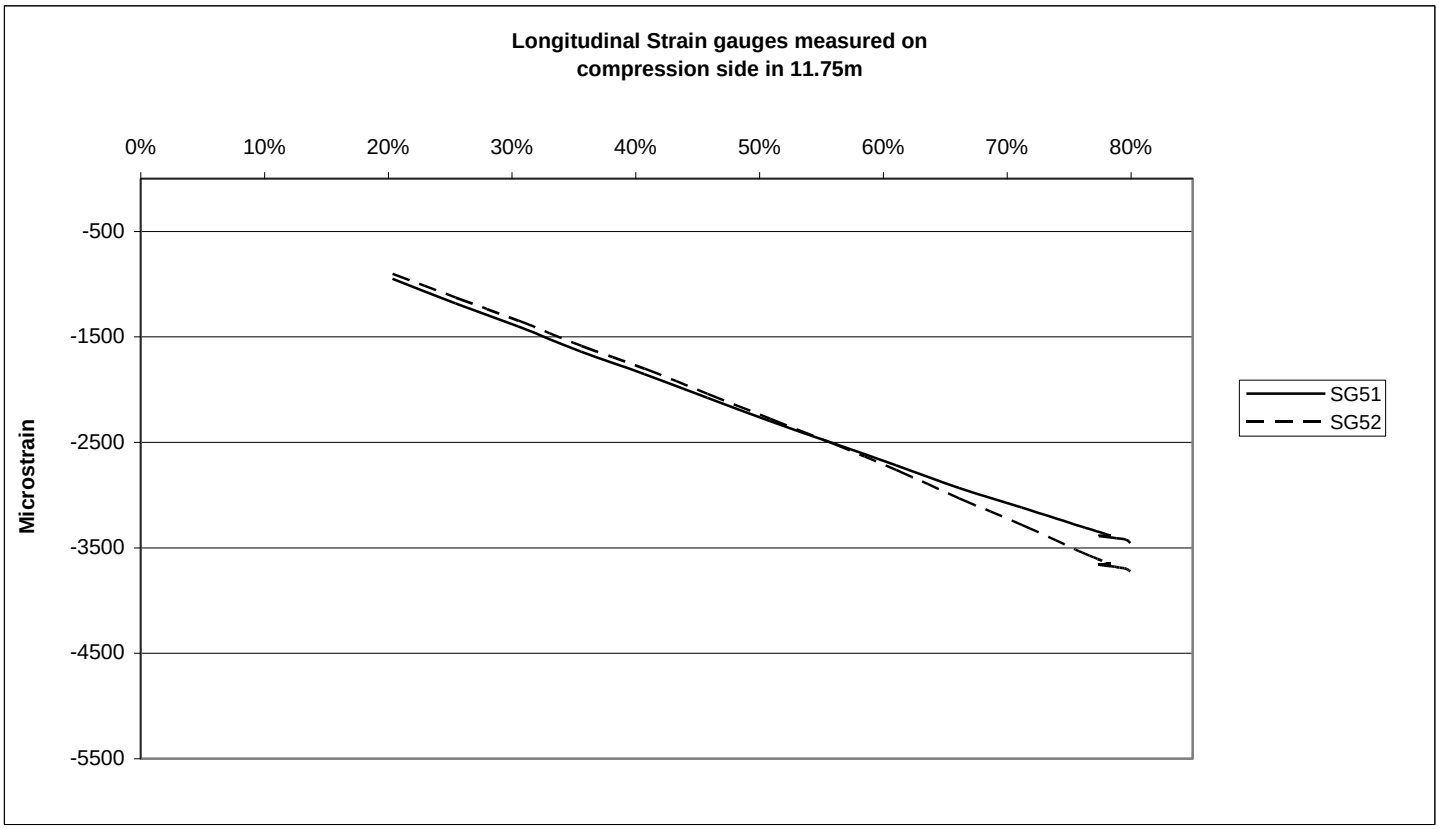
Longitudinal Strain gauges measured on compression side in 11.75m
0%
10%
20%
30%
40%
50%
60%
70%
80%
-500
-1500
-2500
-3500
-4500
-5500
Microstrain
SG51
SG52

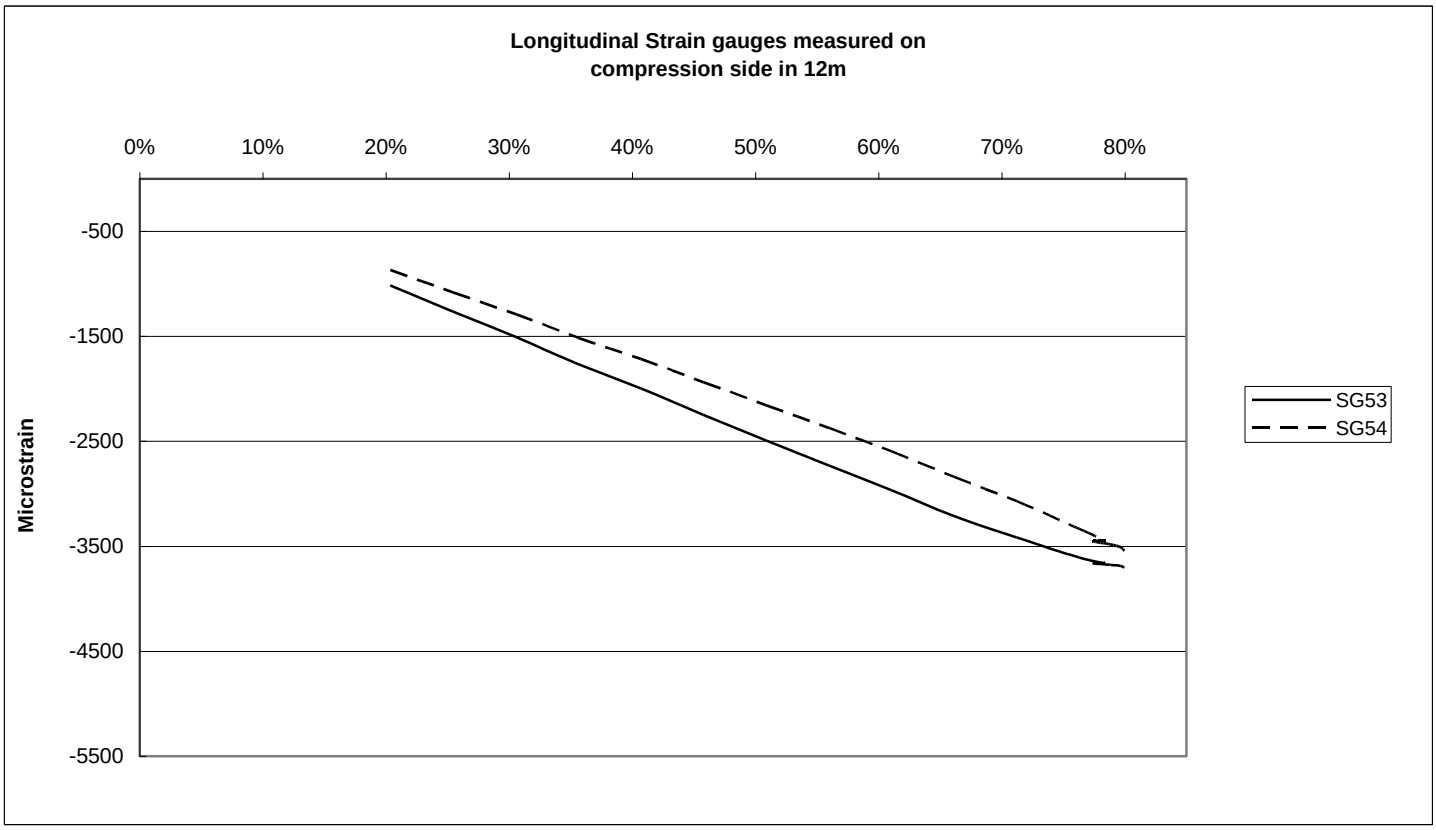
Longitudinal Strain gauges measured on compression side in 12m
0%
10%
20%
30%
40%
50%
60%
70%
80%
-500
-1500
-2500
-3500
-4500
-5500
Microstrain
SG53
SG54

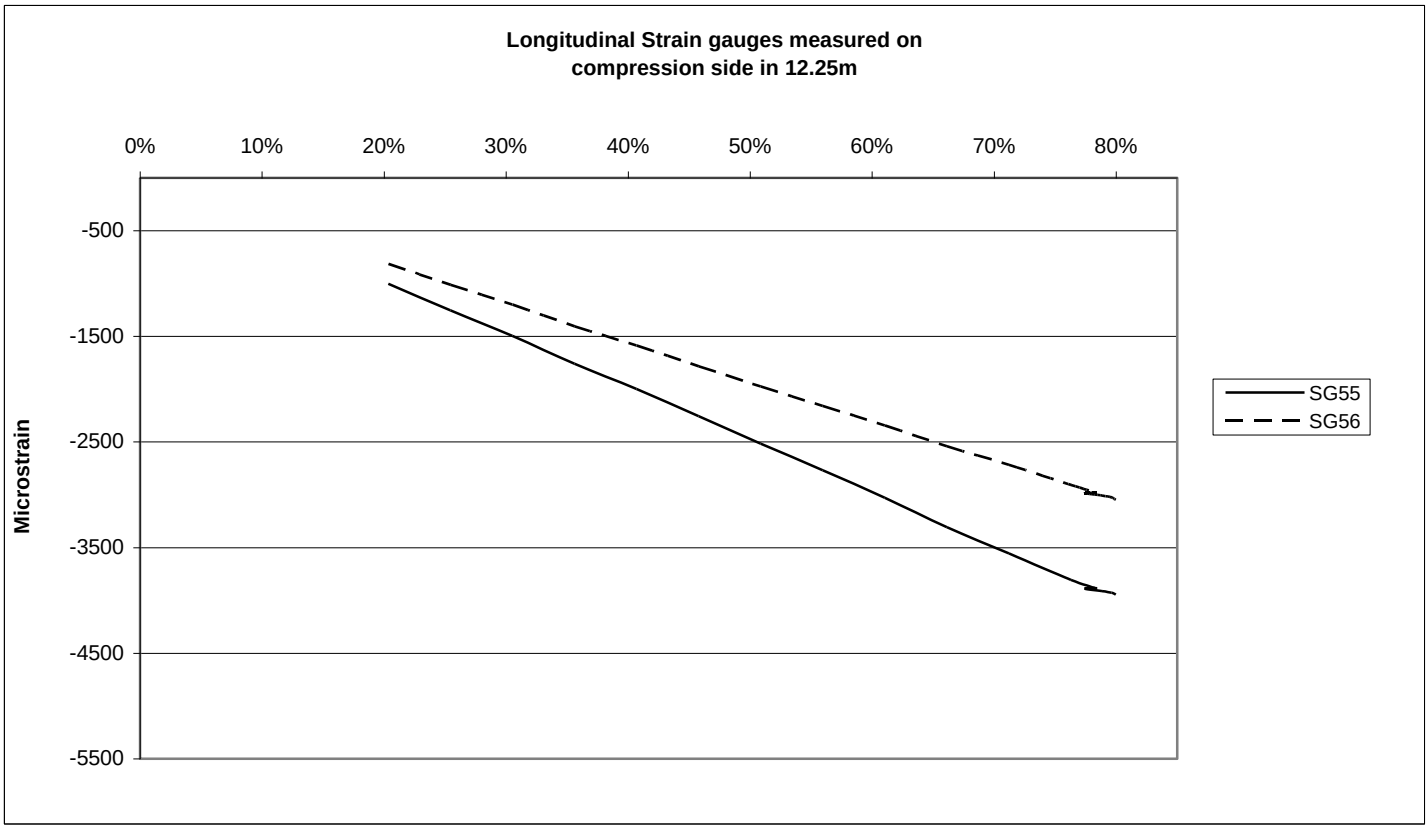
Longitudinal Strain gauges measured on compression side in 12.25m
0%
10%
20%
30%
40%
50%
60%
70%
80%
-500
-1500
-2500
-3500
-4500
-5500
Microstrain
SG55
SG56

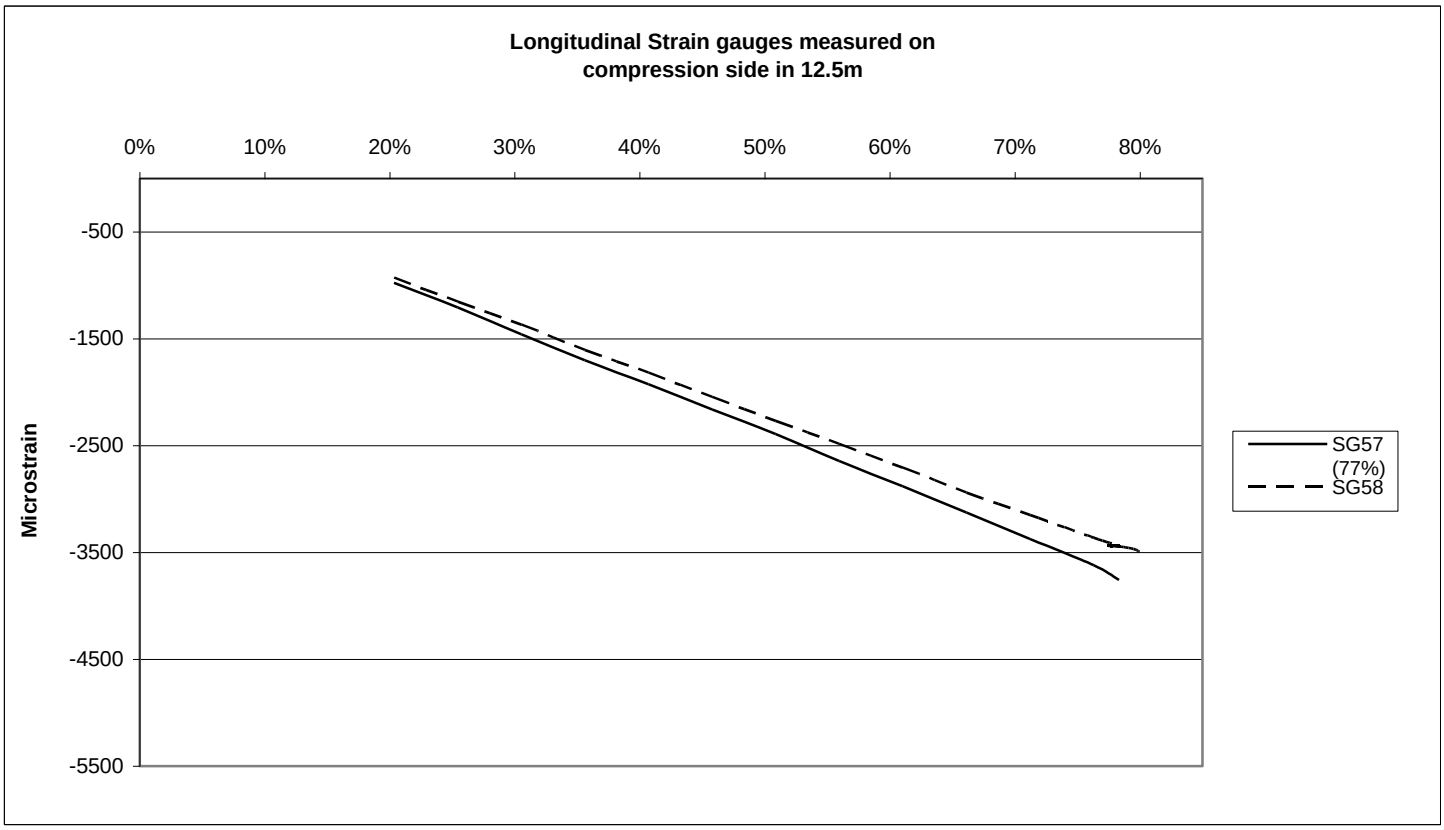
Longitudinal Strain gauges measured on compression side in 12.5m
0%
10%
20%
30%
40%
50%
60%
70%
80%
-500
-1500
-2500
-3500
-4500
-5500
Microstrain
SG57
(77%)
SG58

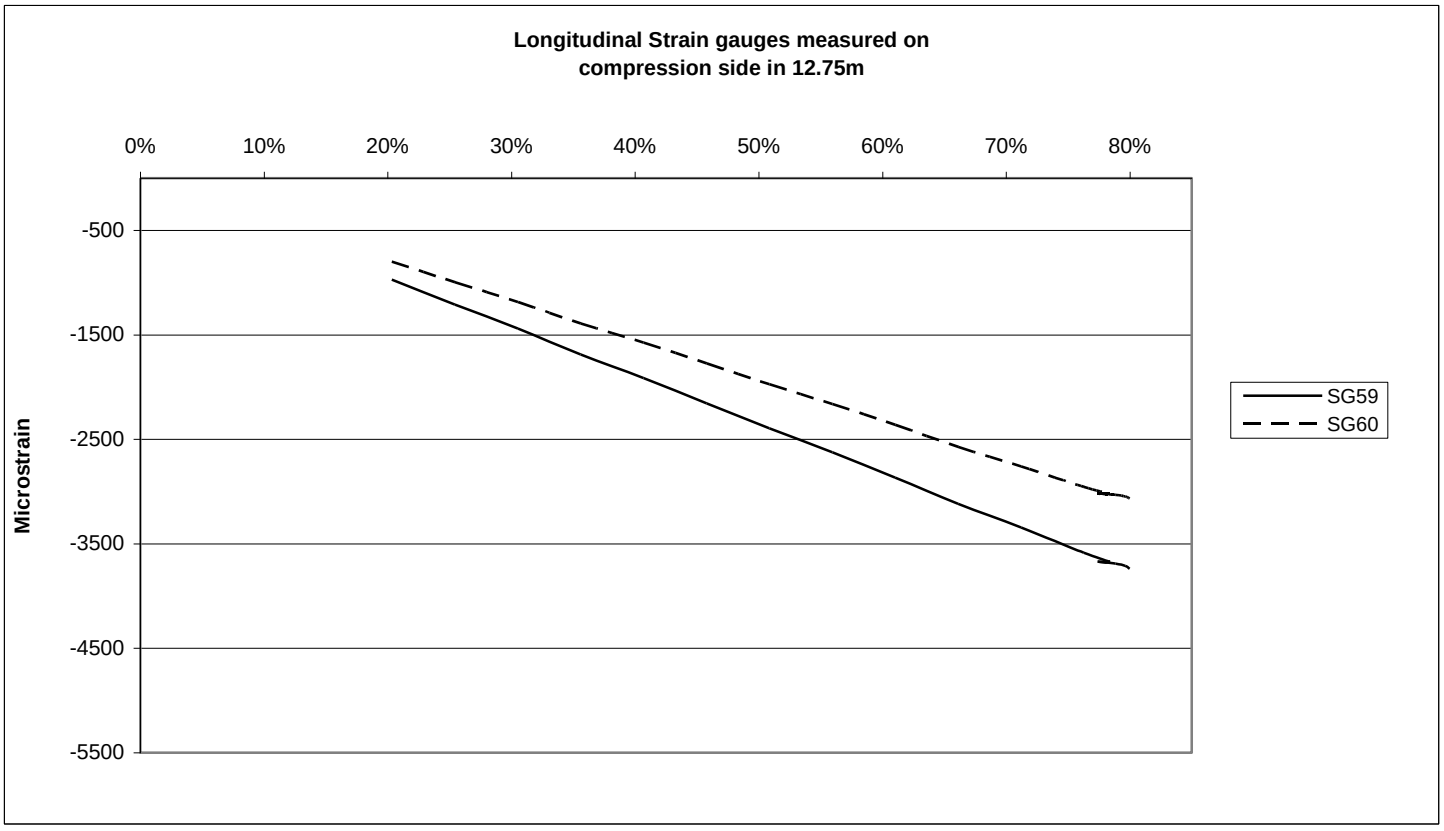
Longitudinal Strain gauges measured on compression side in 12.75m
0%
10%
20%
30%
40%
50%
60%
70%
80%
-500
-1500
-2500
-3500
-4500
-5500
Microstrain
SG59
SG60

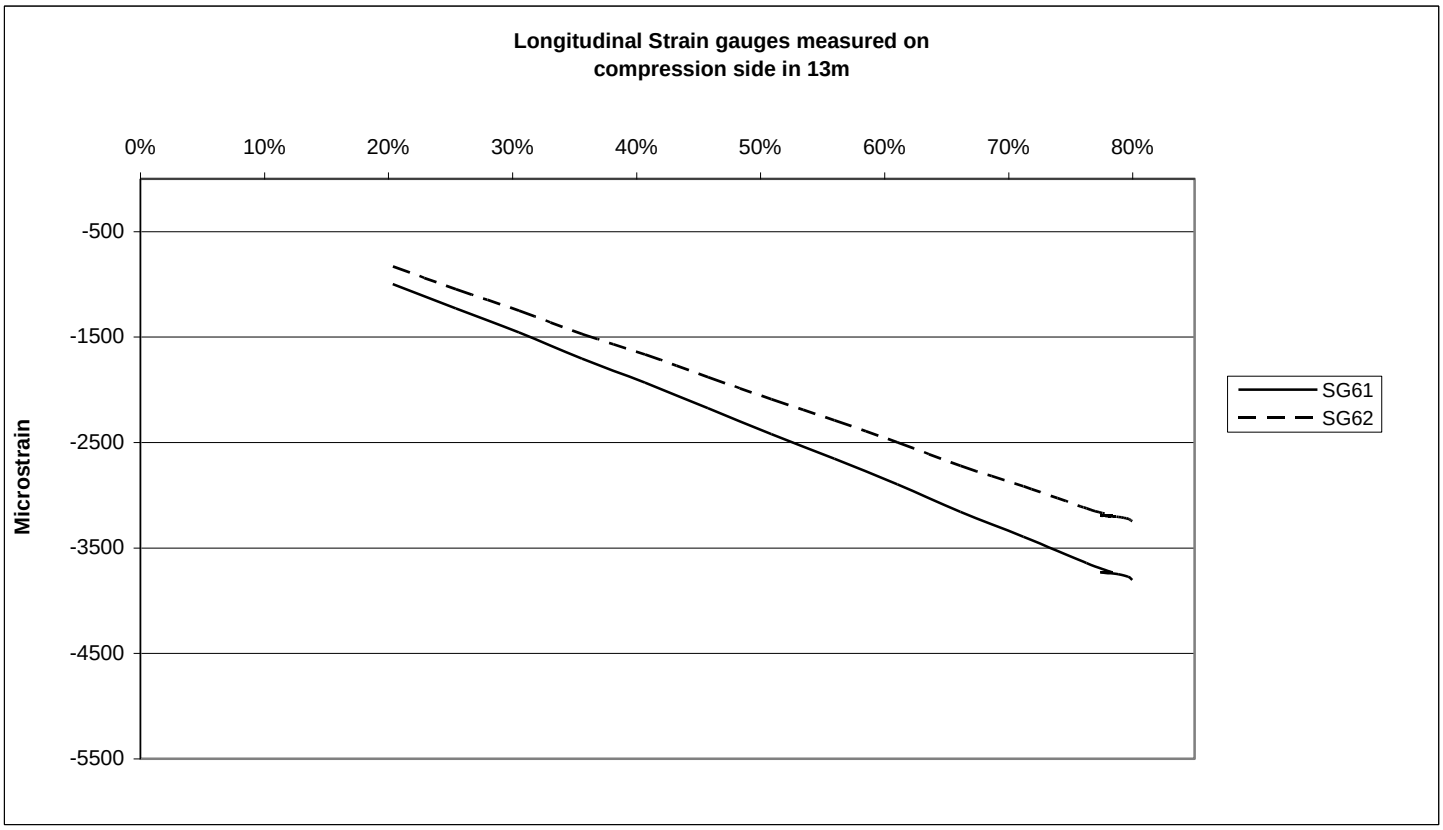
Longitudinal Strain gauges measured on compression side in 13m
0%
10%
20%
30%
40%
50%
60%
70%
80%
-500
-1500
-2500
-3500
-4500
-5500
Microstrain
SG61
SG62

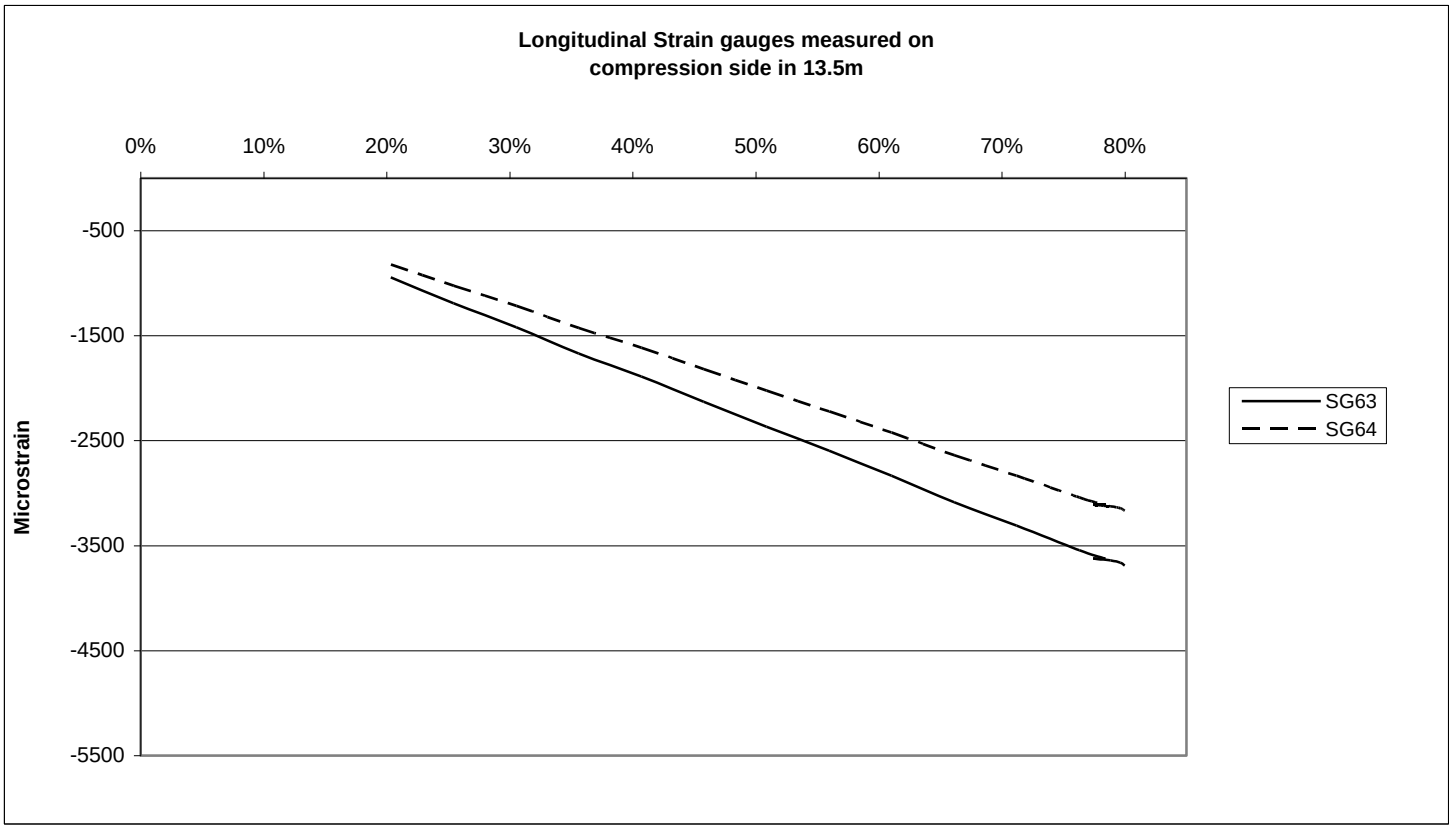
Longitudinal Strain gauges measured on compression side in 13.5m
0%
10%
20%
30%
40%
50%
60%
70%
80%
-500
-1500
-2500
-3500
-4500
-5500
Microstrain
SG63
SG64

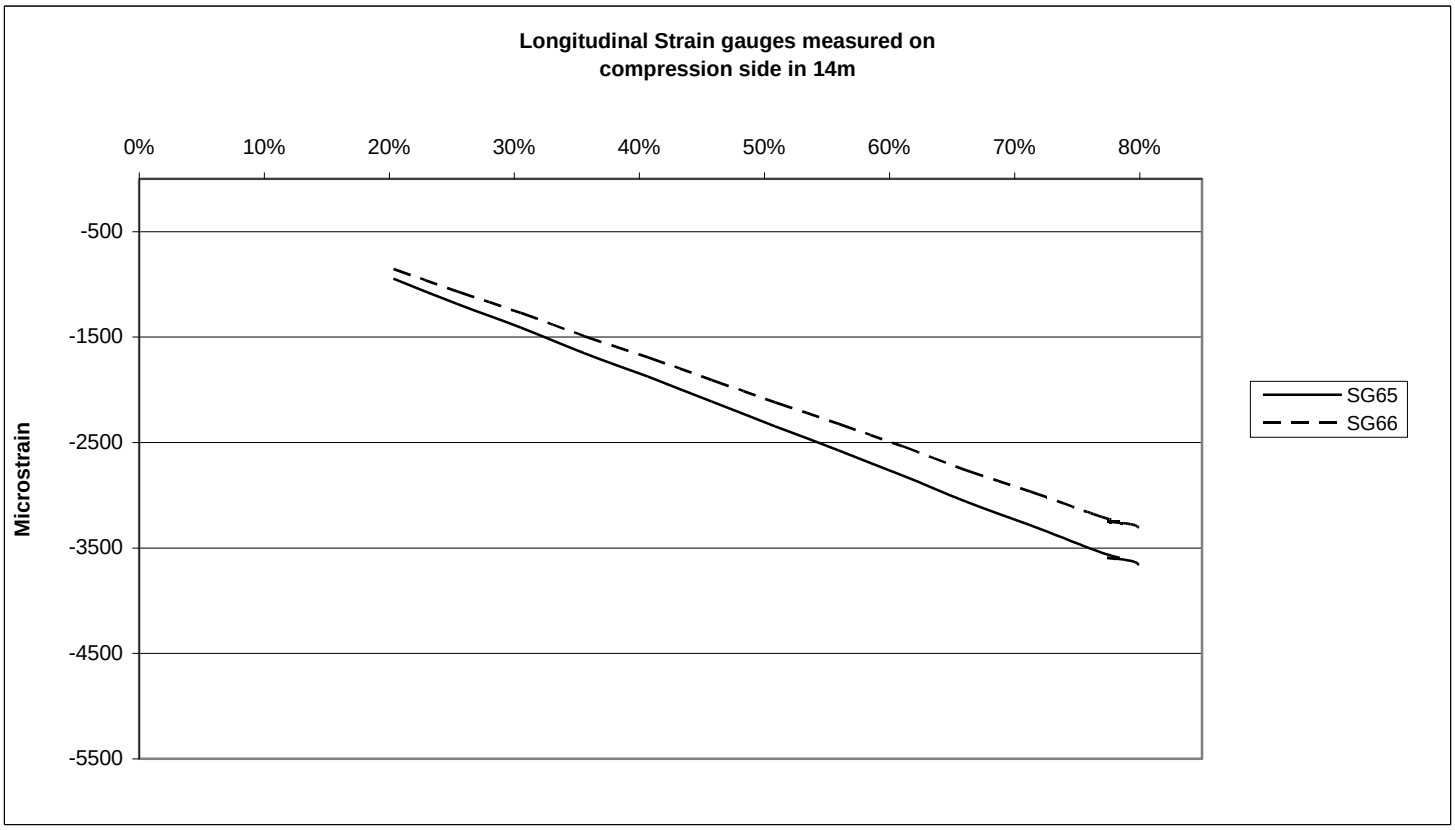
Longitudinal Strain gauges measured on compression side in 14m
0%
10%
20%
30%
40%
50%
60%
70%
80%
-500
-1500
-2500
-3500
-4500
-5500
Microstrain
SG65
SG66

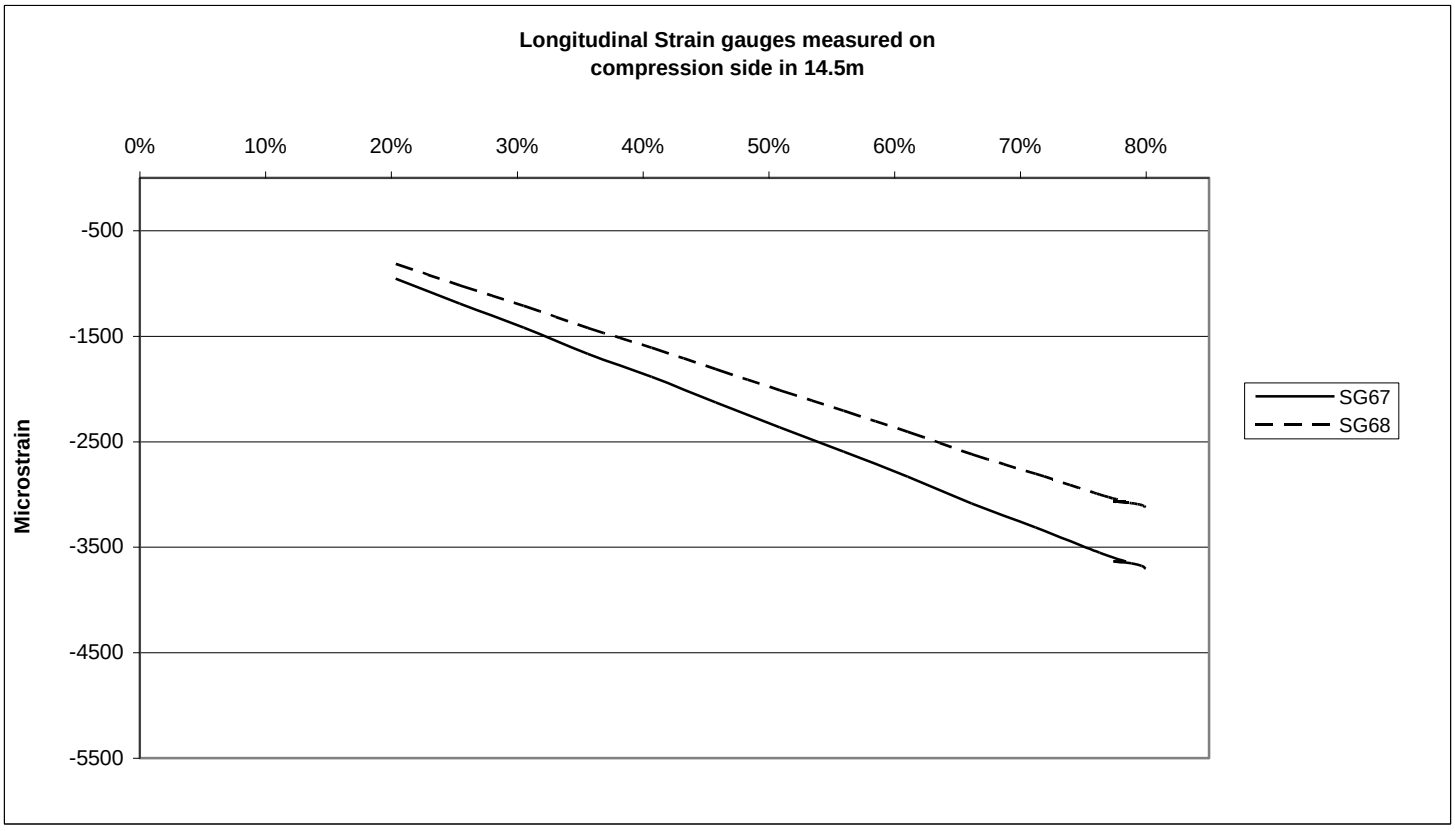
Longitudinal Strain gauges measured on compression side in 14.5m
0%
10%
20%
30%
40%
50%
60%
70%
80%
-500
-1500
-2500
-3500
-4500
-5500
Microstrain
SG67
SG68

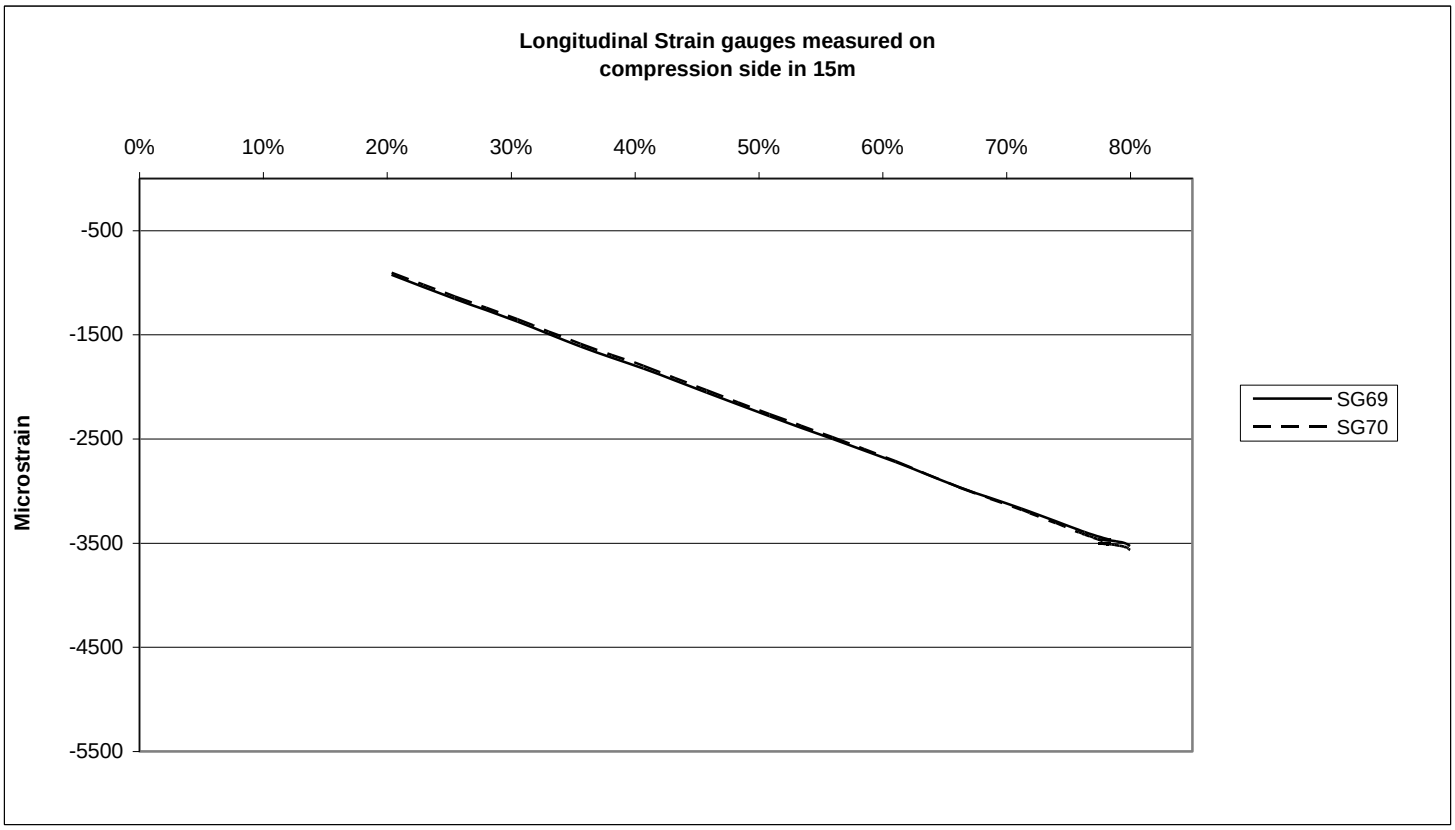
Longitudinal Strain gauges measured on compression side in 15m
0%
10%
20%
30%
40%
50%
60%
70%
80%
-500
-1500
-2500
-3500
-4500
-5500
Microstrain
SG69
SG70

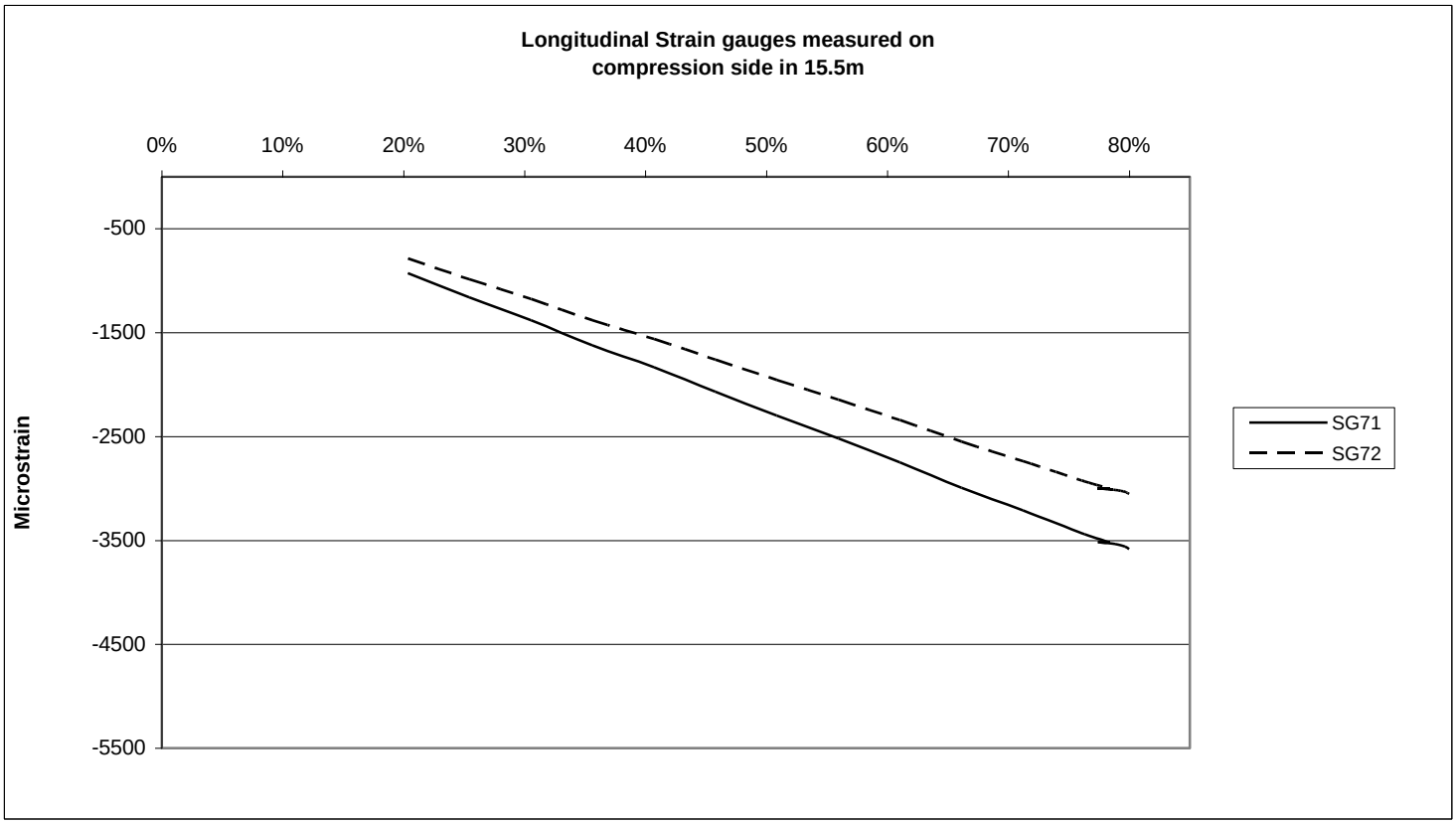
Longitudinal Strain gauges measured on compression side in 15.5m
0%
10%
20%
30%
40%
50%
60%
70%
80%
-500
-1500
-2500
-3500
-4500
-5500
Microstrain
SG71
SG72

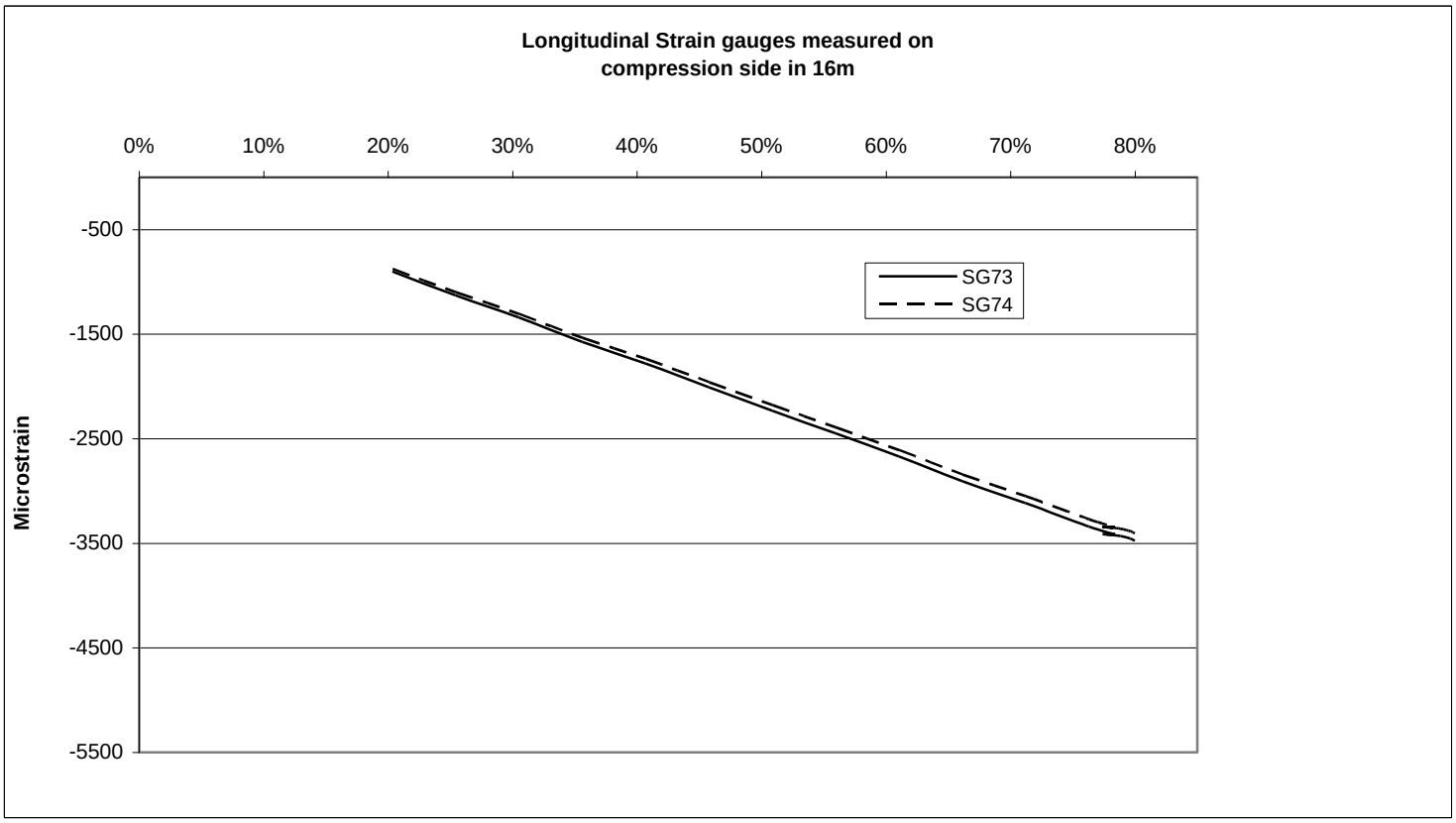
Longitudinal Strain gauges measured on compression side in 16m
0%
10%
20%
30%
40%
50%
60%
70%
80%
-500
-1500
-2500
-3500
-4500
-5500
Microstrain
SG73
SG74

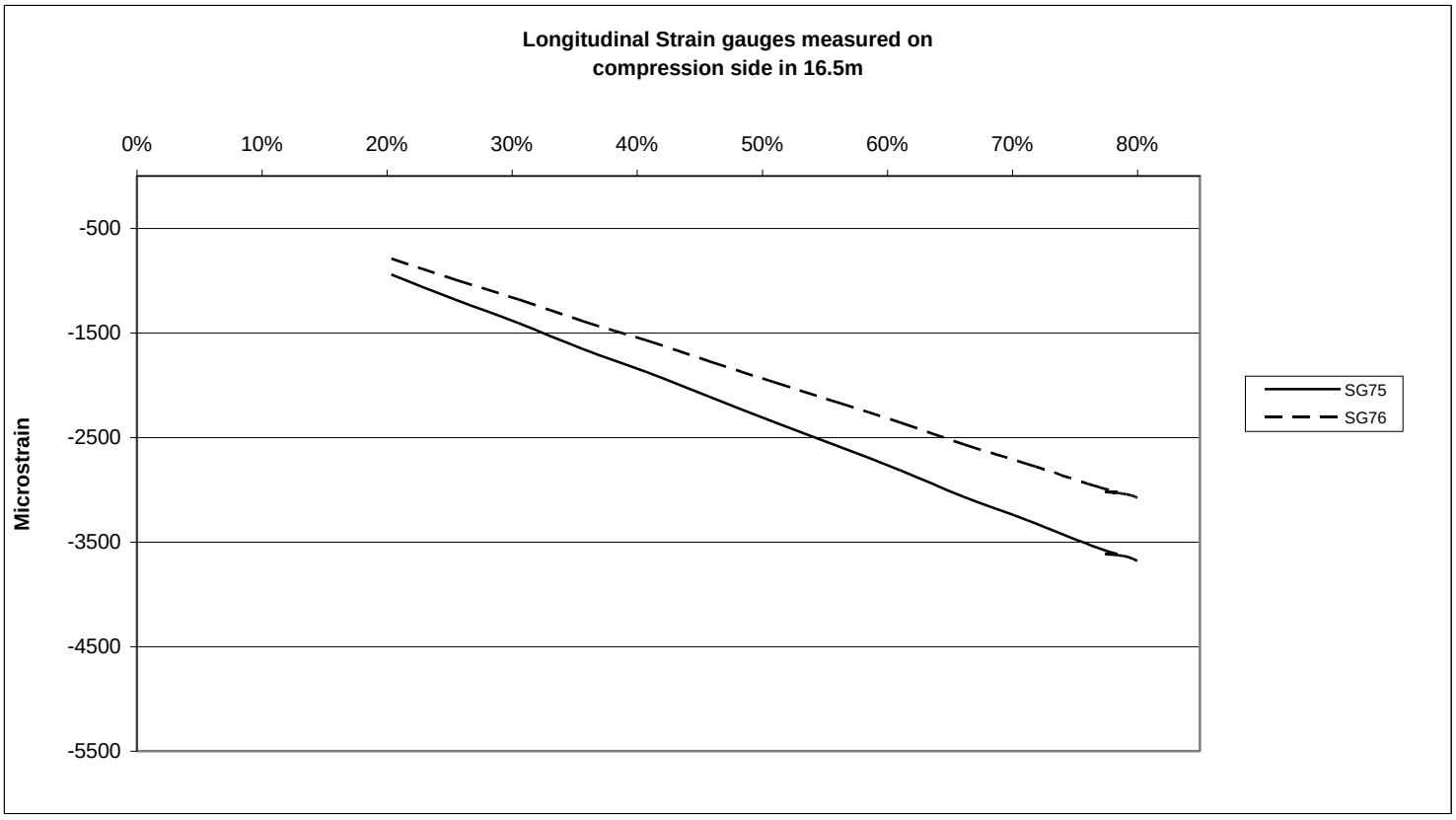
Longitudinal Strain gauges measured on compression side in 16.5m
0%
10%
20%
30%
40%
50%
60%
70%
80%
-500
-1500
-2500
-3500
-4500
-5500
Microstrain
SG75
SG76

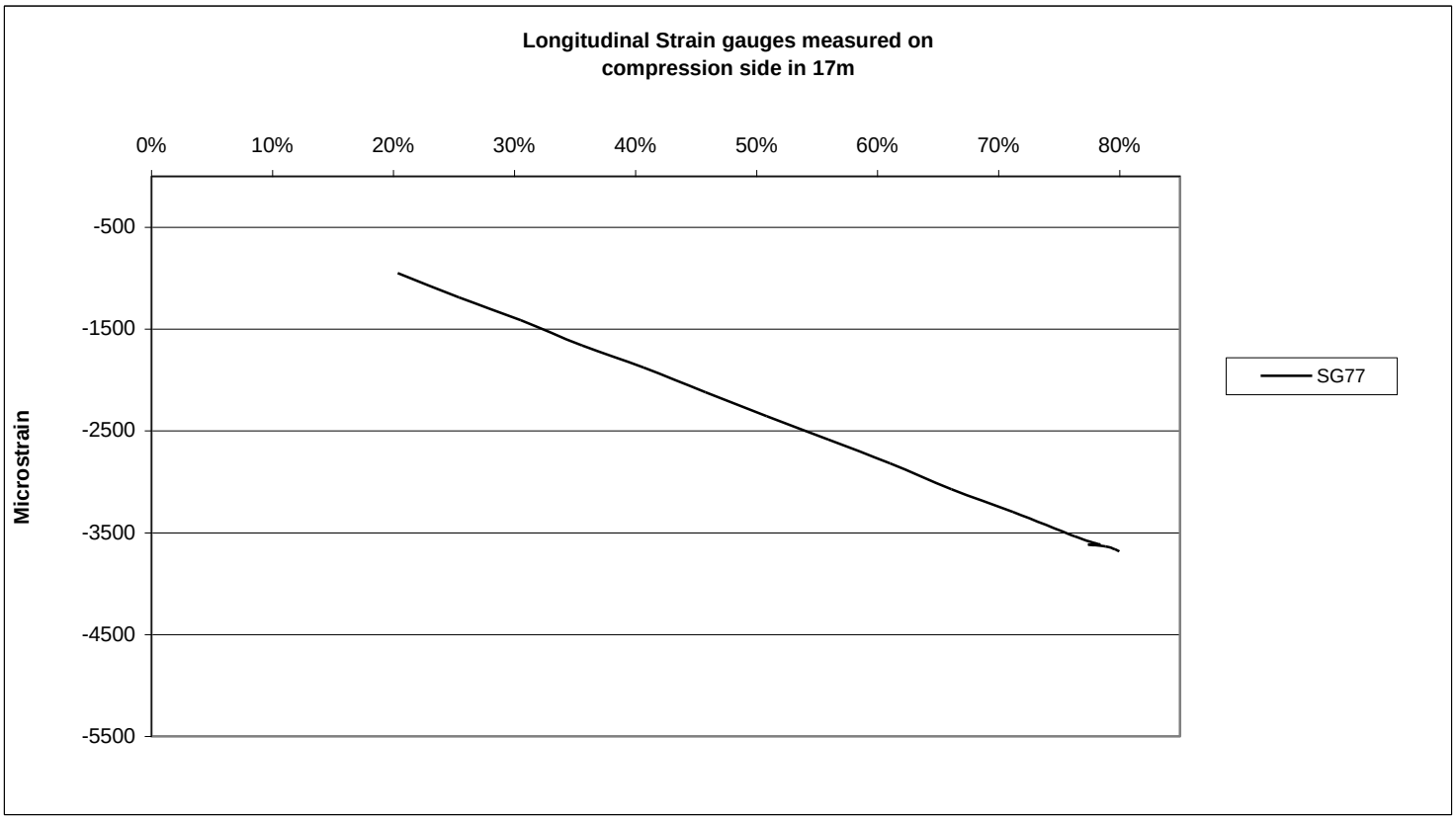
Longitudinal Strain gauges measured on compression side in 17m
0%
10%
20%
30%
40%
50%
60%
70%
80%
-500
-1500
-2500
-3500
-4500
-5500
Microstrain
SG77

Graphs of Longitudinal Tension

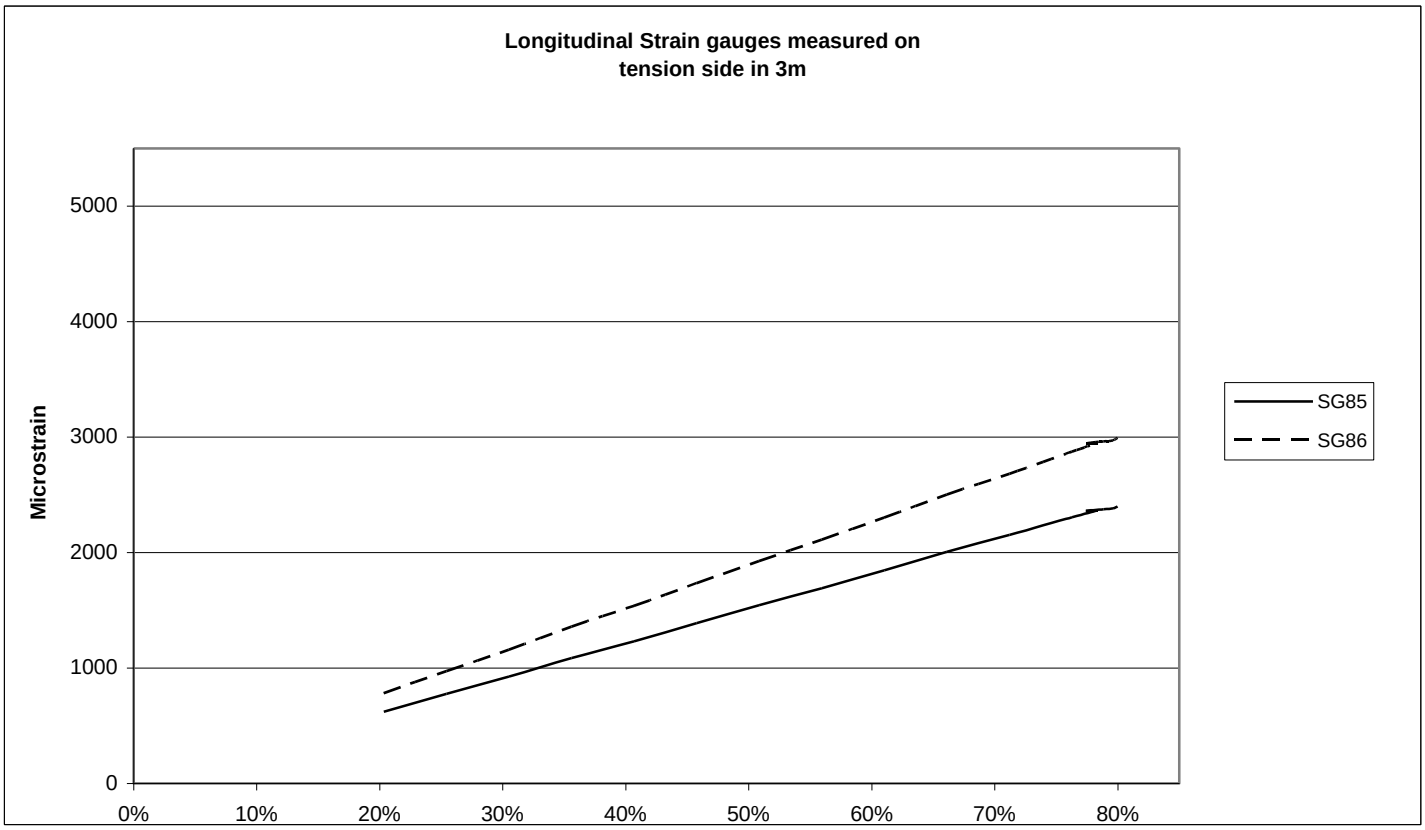

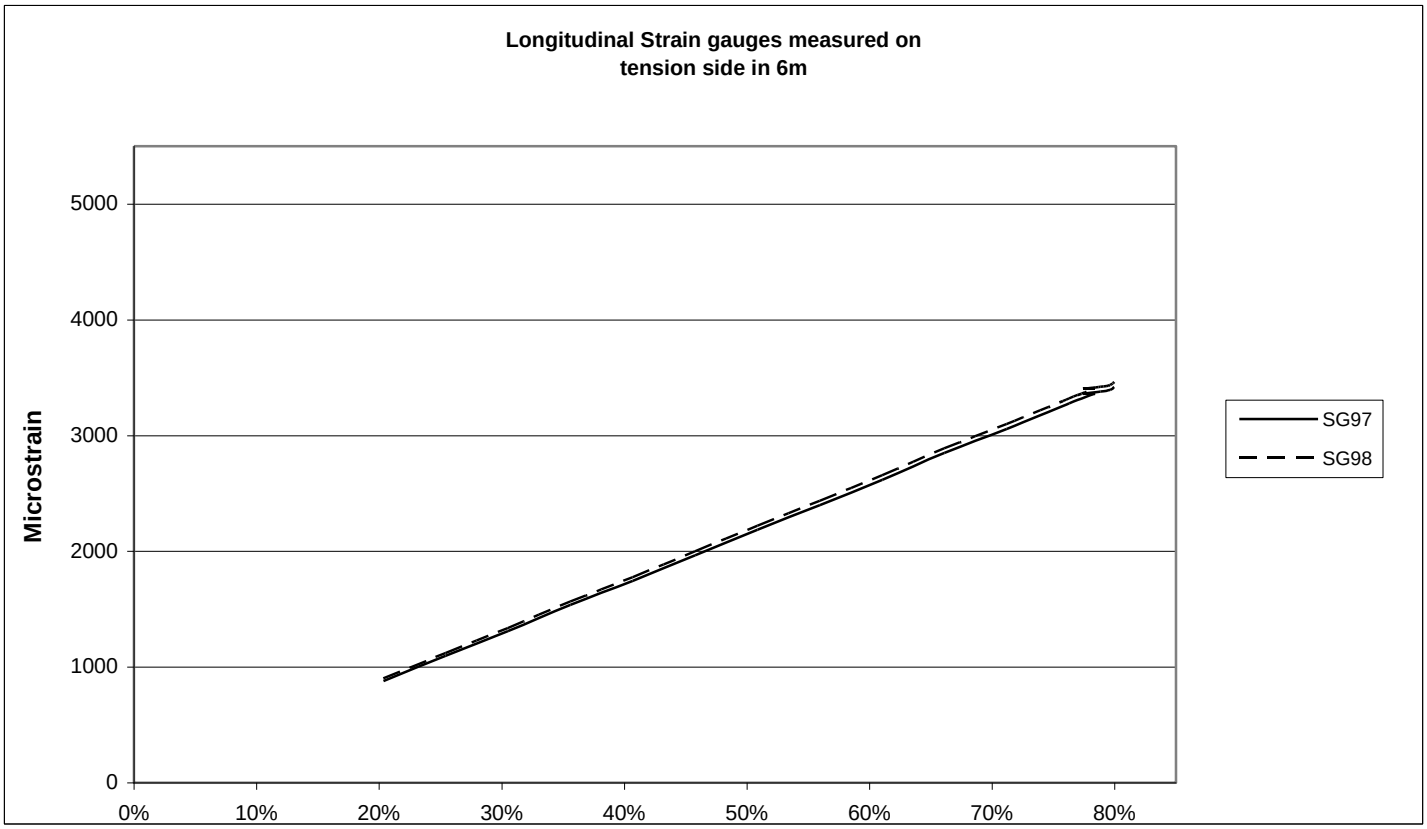

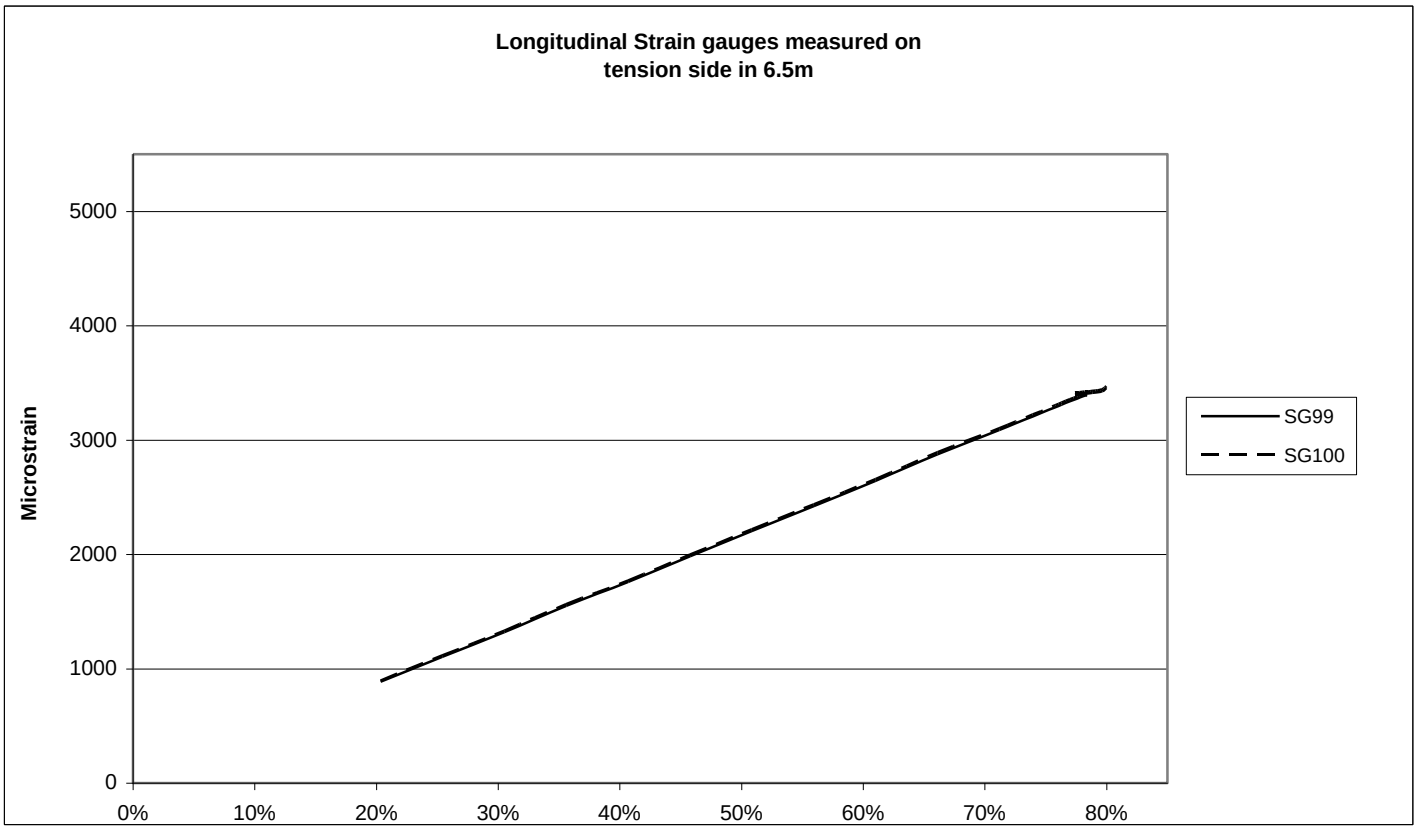
Longitudinal Strain gauges measured on tension side in 6.5m
Microstrain
5000
4000
3000
2000
1000
0
0%
10%
20%
30%
40%
50%
60%
70%
80%
SG99
SG100

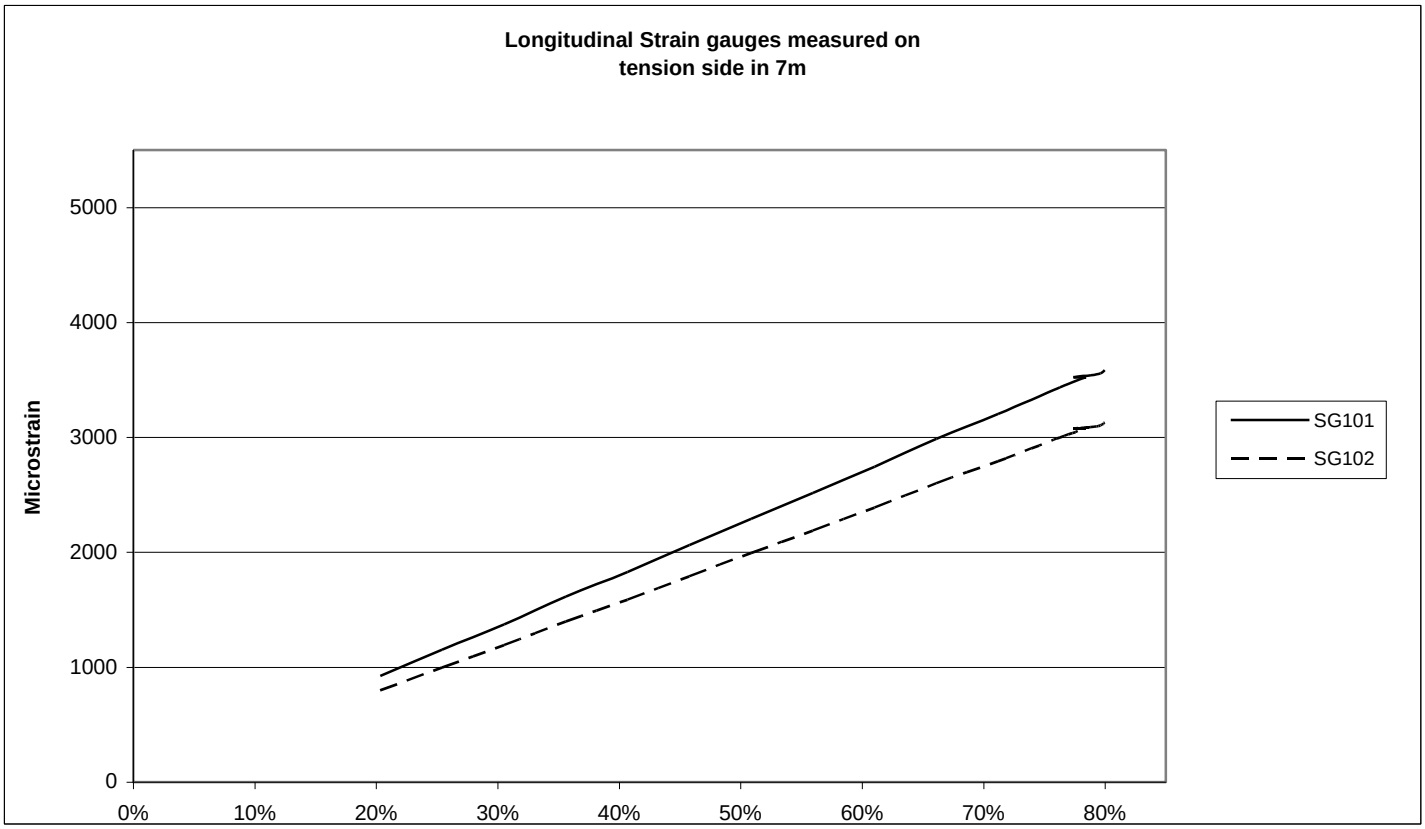
Longitudinal Strain gauges measured on tension side in 7m
Microstrain
5000
4000
3000
2000
1000
0
0%
10%
20%
30%
40%
50%
60%
70%
80%
SG101
SG102

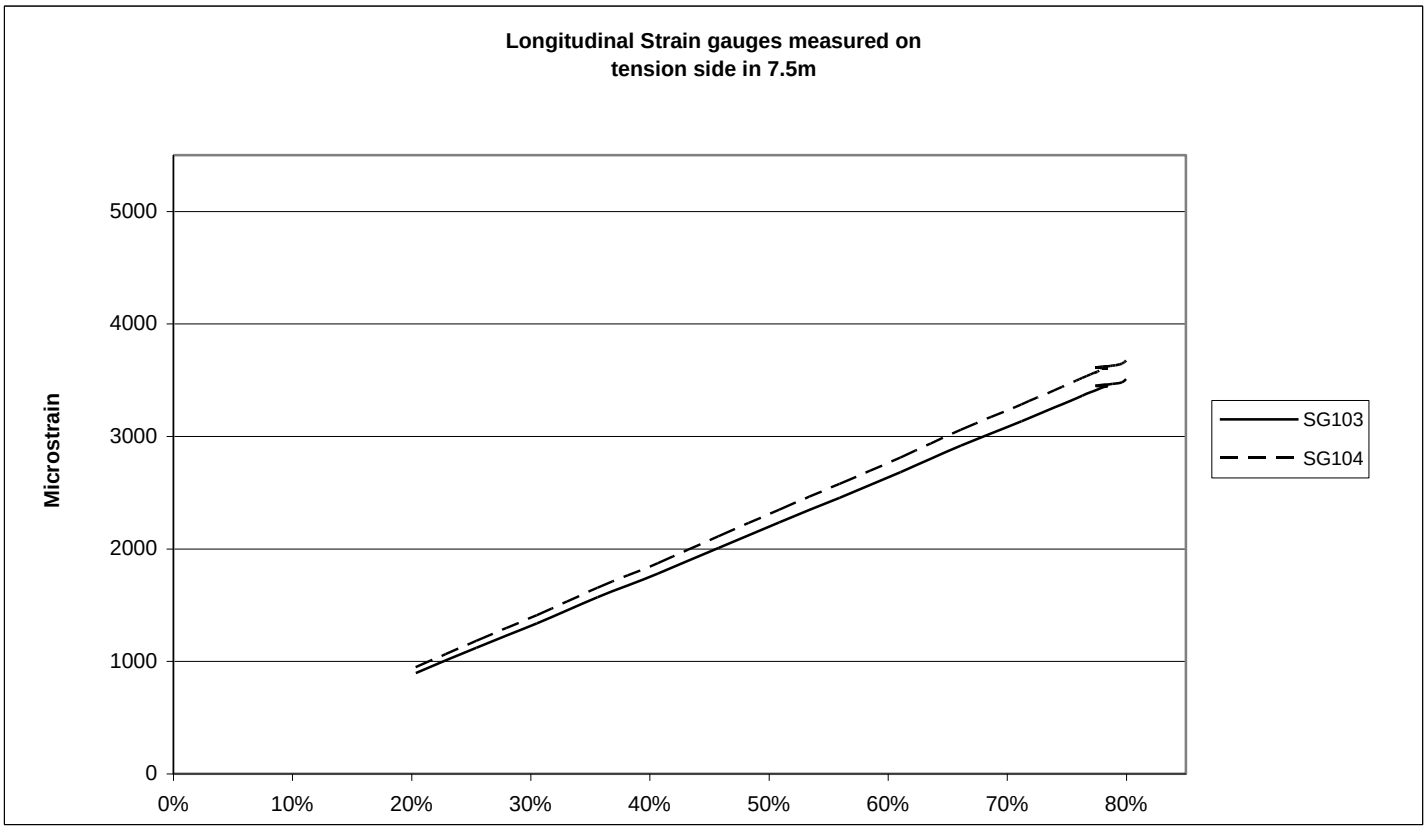
Longitudinal Strain gauges measured on tension side in 7.5m
Microstrain
5000
4000
3000
2000
1000
0
0%
10%
20%
30%
40%
50%
60%
70%
80%
SG103
SG104

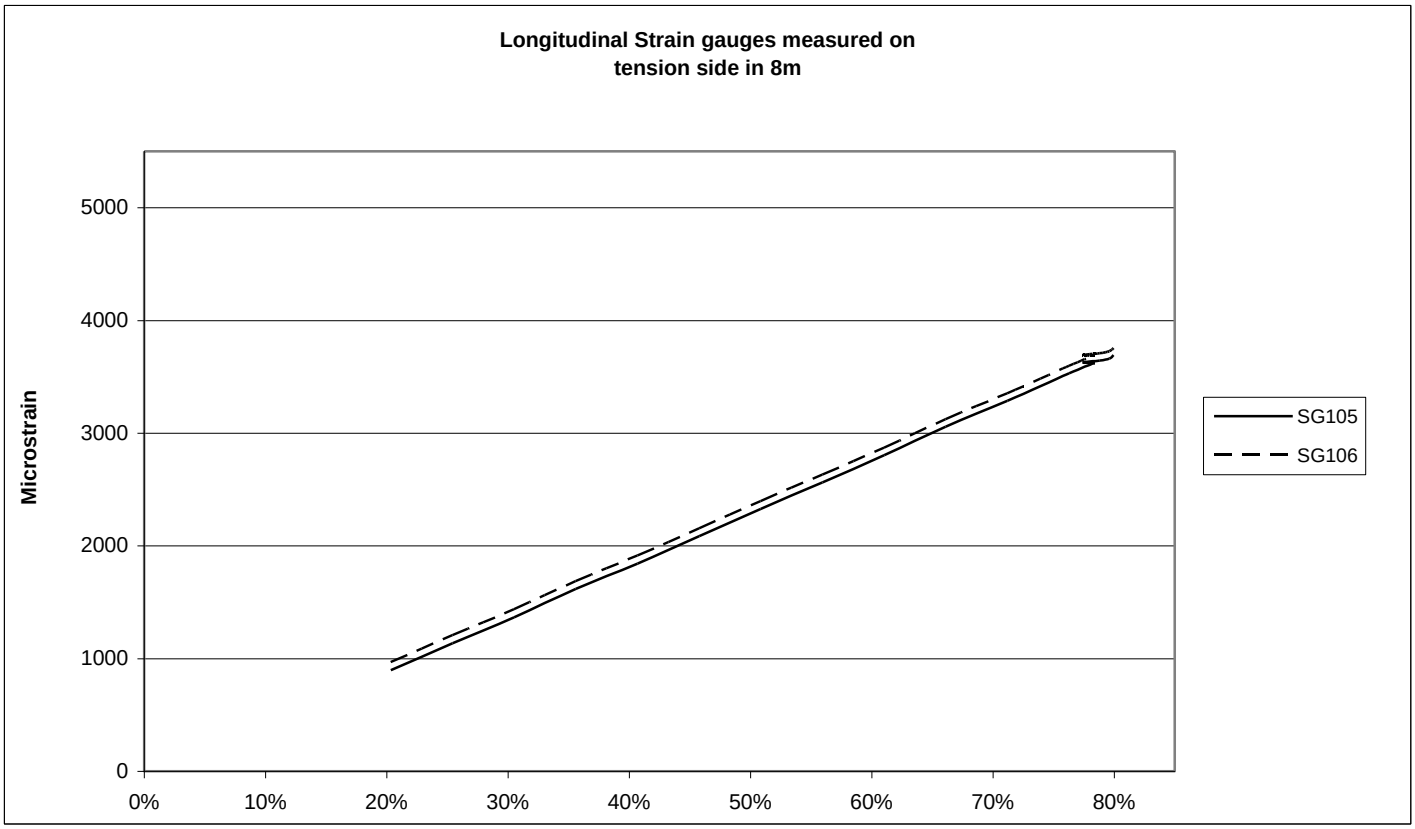
Longitudinal Strain gauges measured on tension side in 8m
Microstrain
5000
4000
3000
2000
1000
0
0%
10%
20%
30%
40%
50%
60%
70%
80%
SG105
SG106

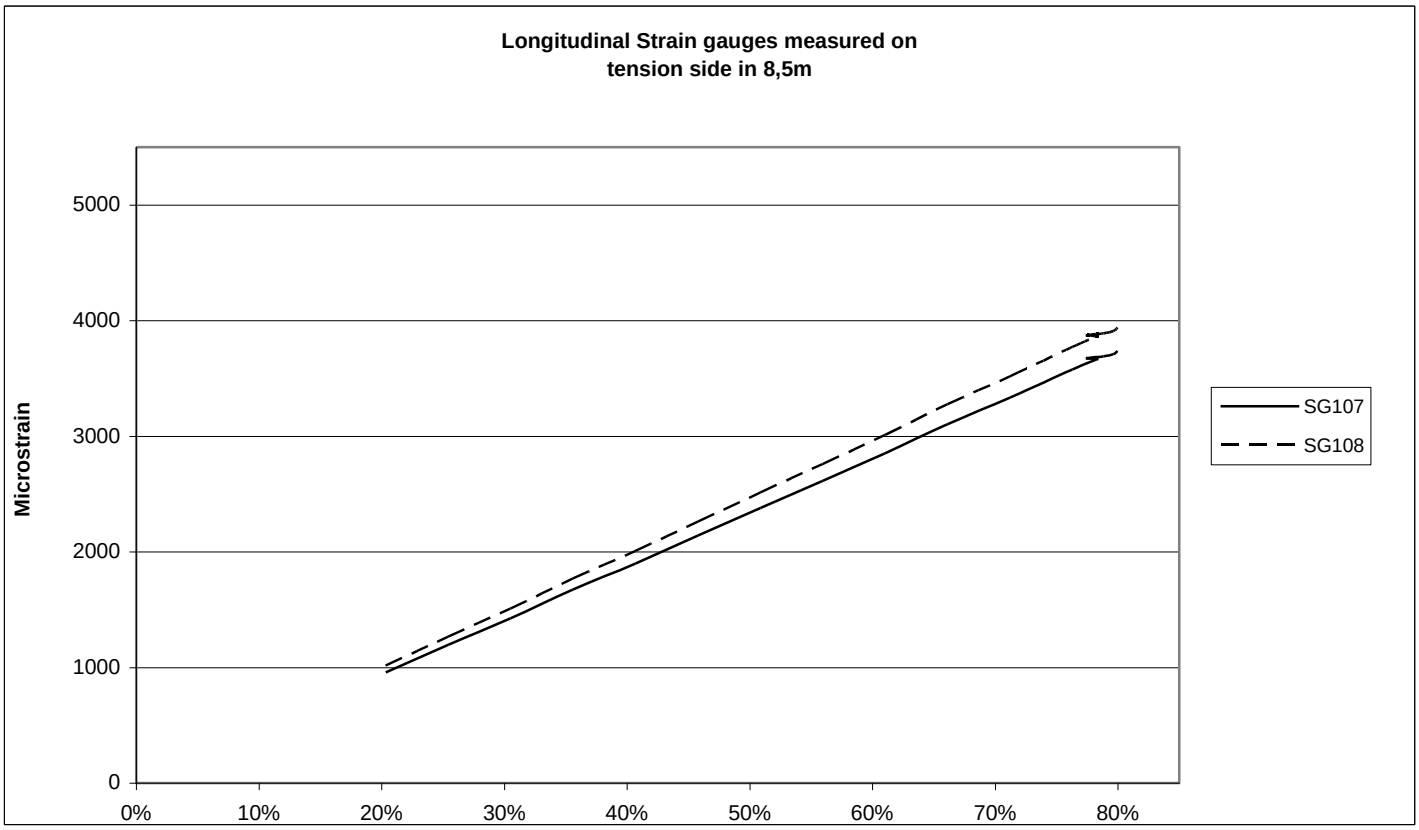
Longitudinal Strain gauges measured on tension side in 8,5m
Microstrain
5000
4000
3000
2000
1000
0
0%
10%
20%
30%
40%
50%
60%
70%
80%
SG107
SG108

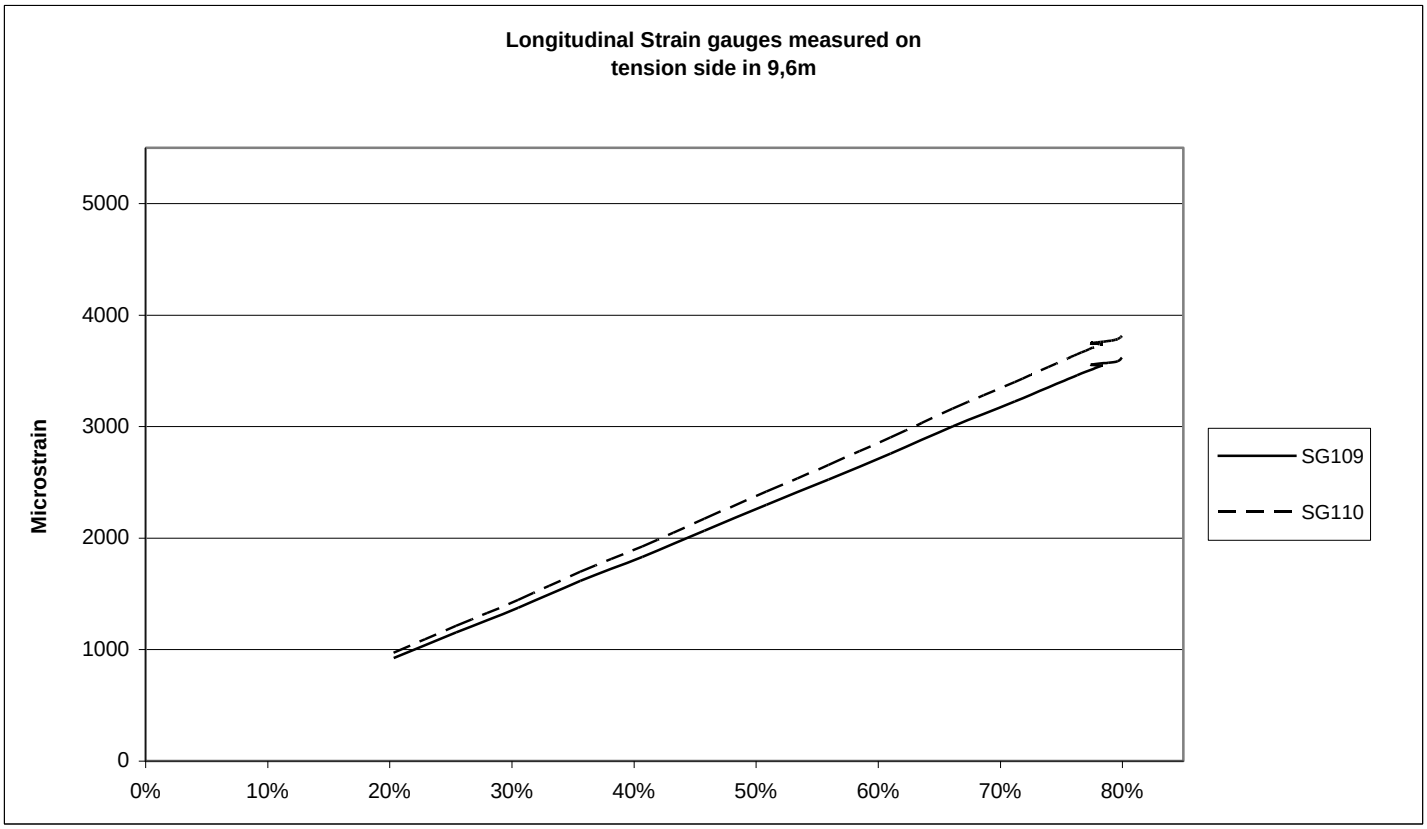
Longitudinal Strain gauges measured on tension side in 9,6m
Microstrain
5000
4000
3000
2000
1000
0
0%
10%
20%
30%
40%
50%
60%
70%
80%
SG109
SG110

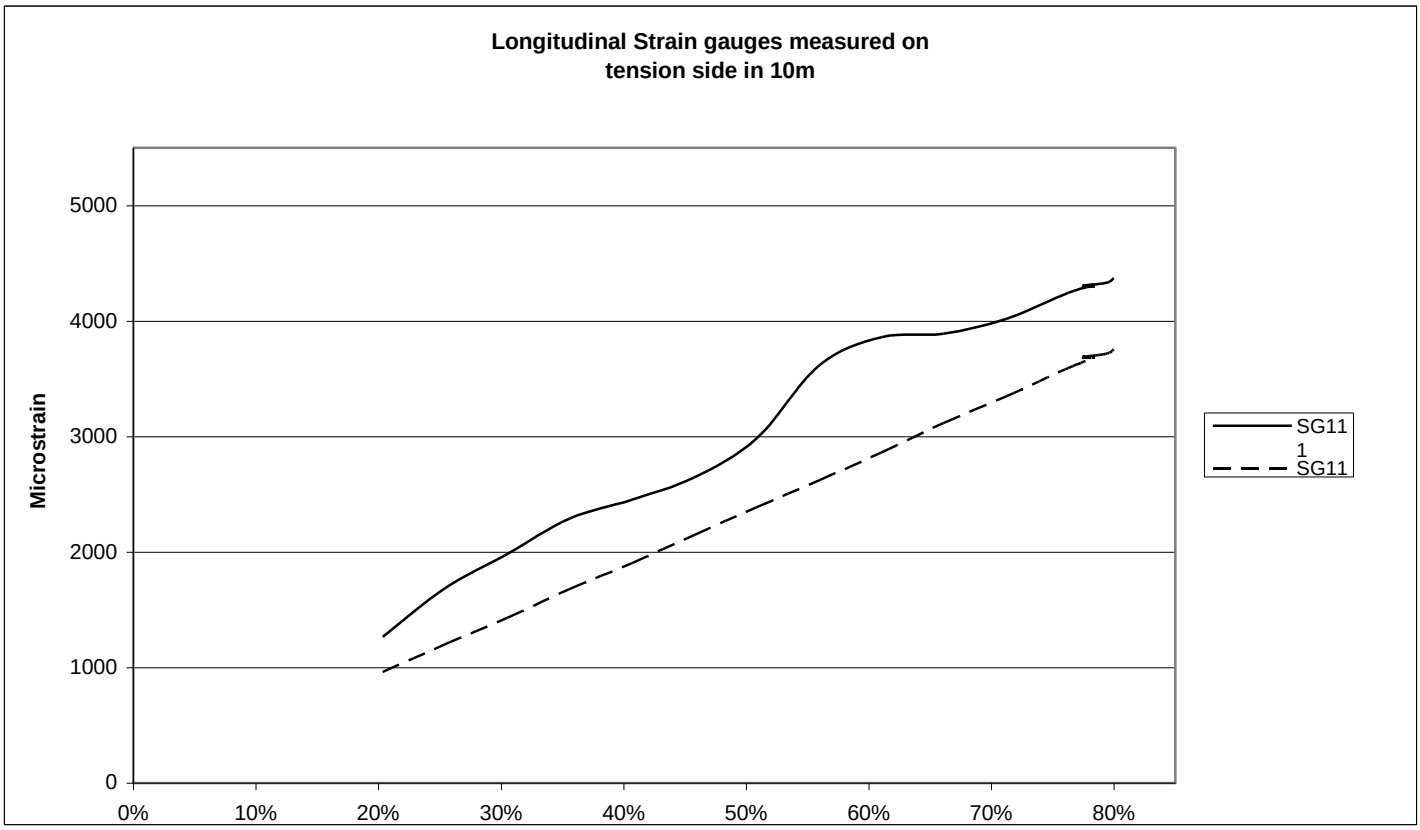
Longitudinal Strain gauges measured on tension side in 10m
Microstrain
5000
4000
3000
2000
1000
0
0%
10%
20%
30%
40%
50%
60%
70%
80%
SG111
SG11

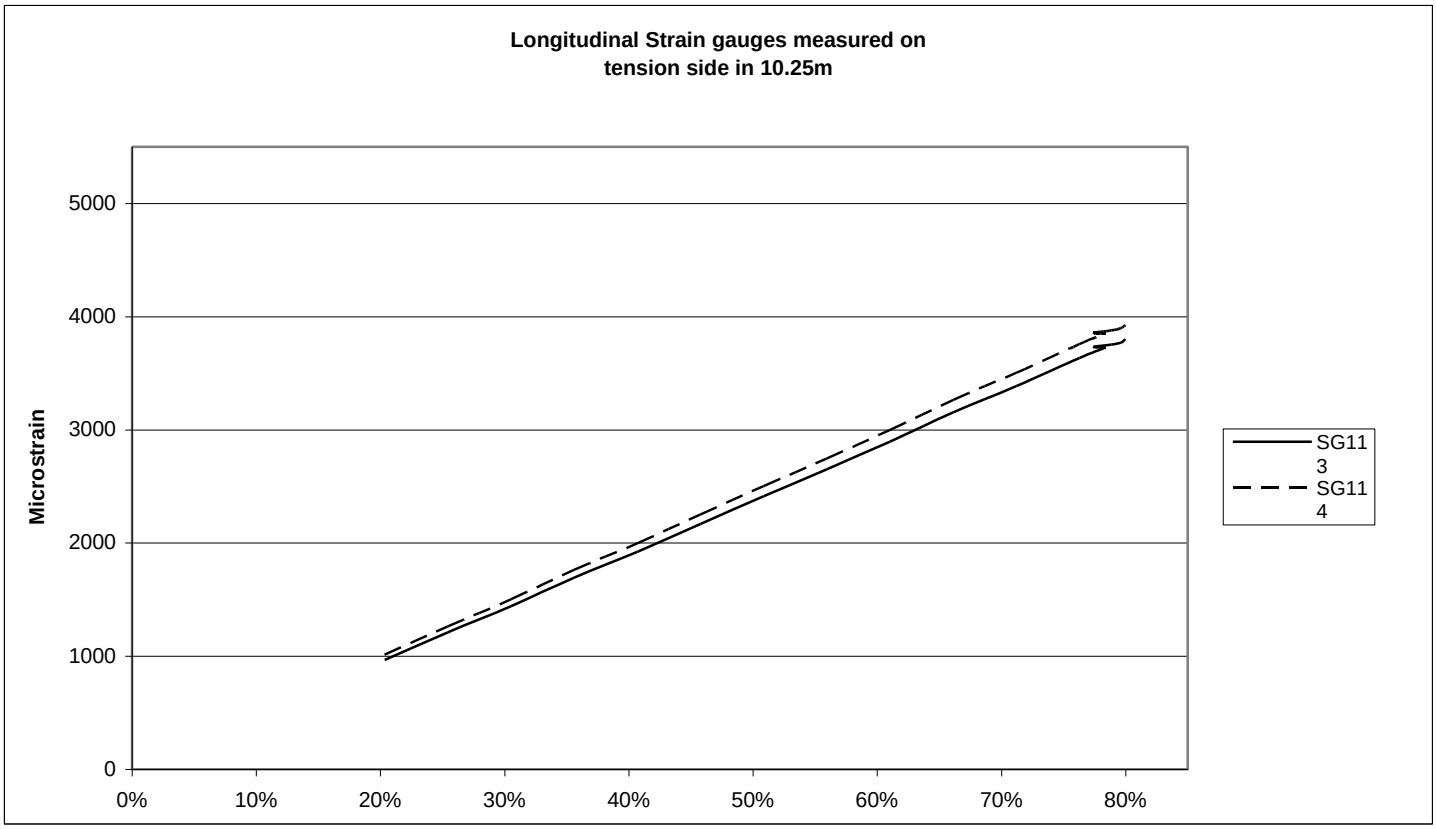
Longitudinal Strain gauges measured on tension side in 10.25m
Microstrain
5000
4000
3000
2000
1000
0
0%
10%
20%
30%
40%
50%
60%
70%
80%
SG113
SG114

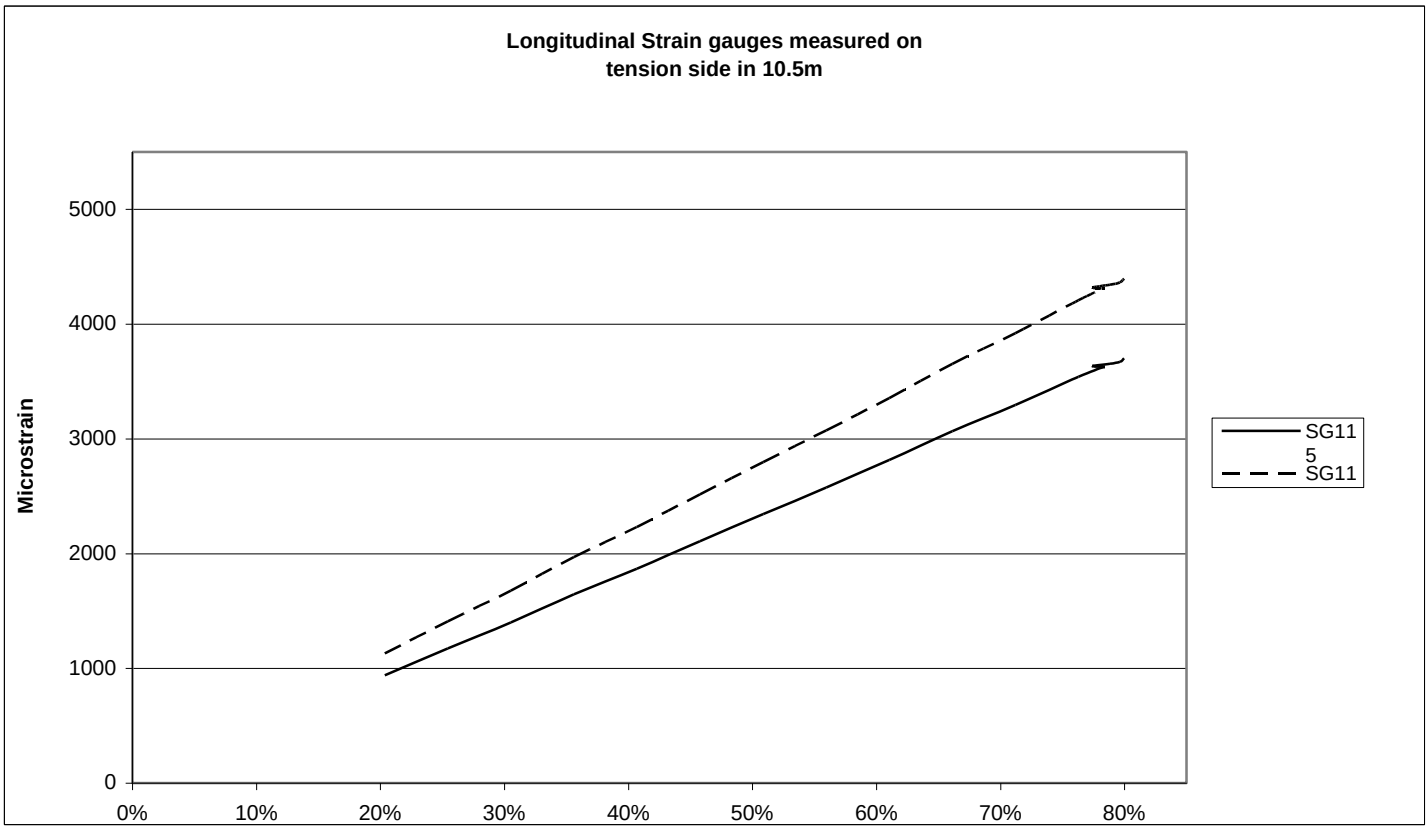
Longitudinal Strain gauges measured on tension side in 10.5m
Microstrain
5000
4000
3000
2000
1000
0
0%
10%
20%
30%
40%
50%
60%
70%
80%
SG115
SG11

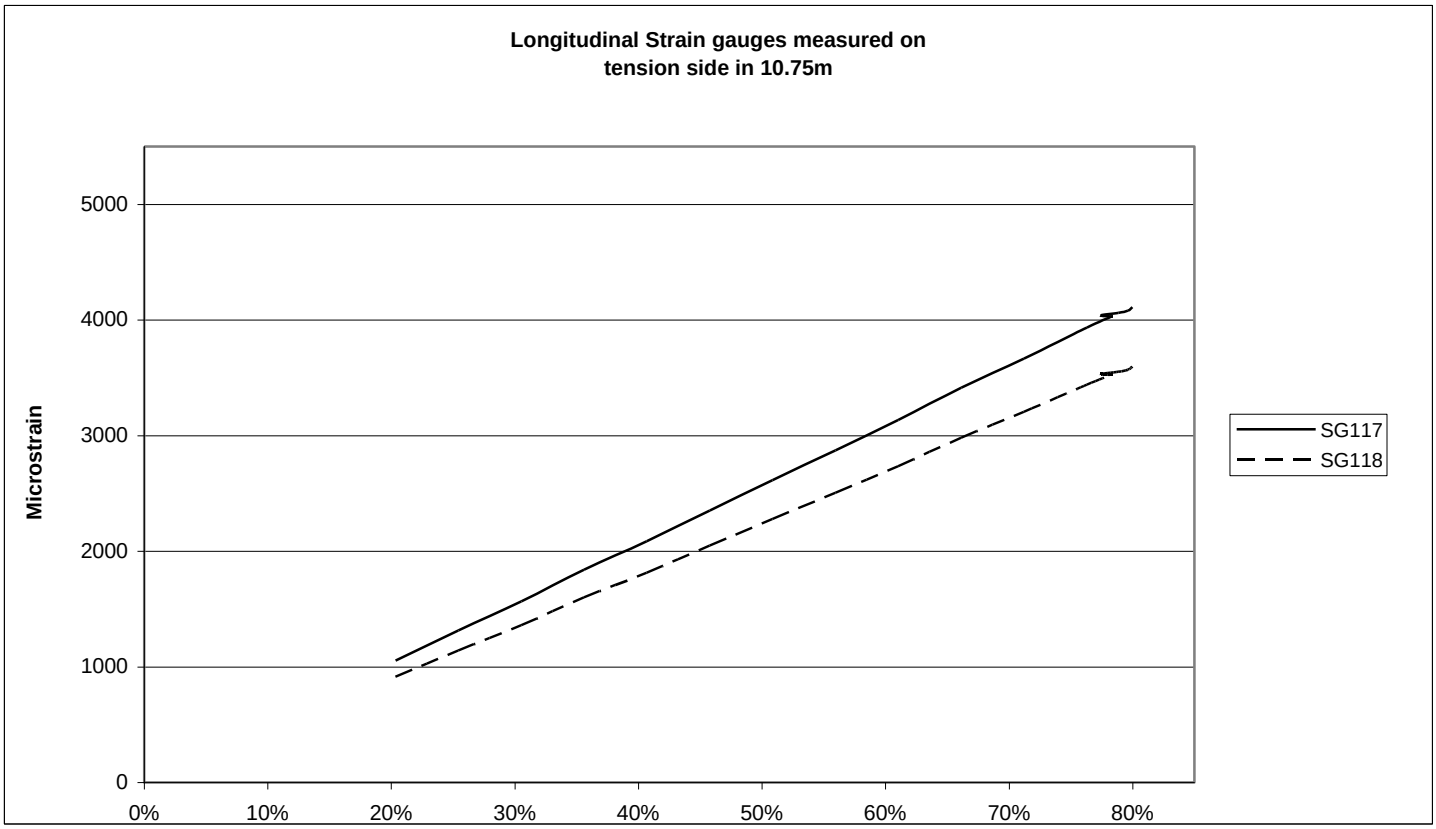
Longitudinal Strain gauges measured on tension side in 10.75m
Microstrain
5000
4000
3000
2000
1000
0
0%
10%
20%
30%
40%
50%
60%
70%
80%
SG117
SG118

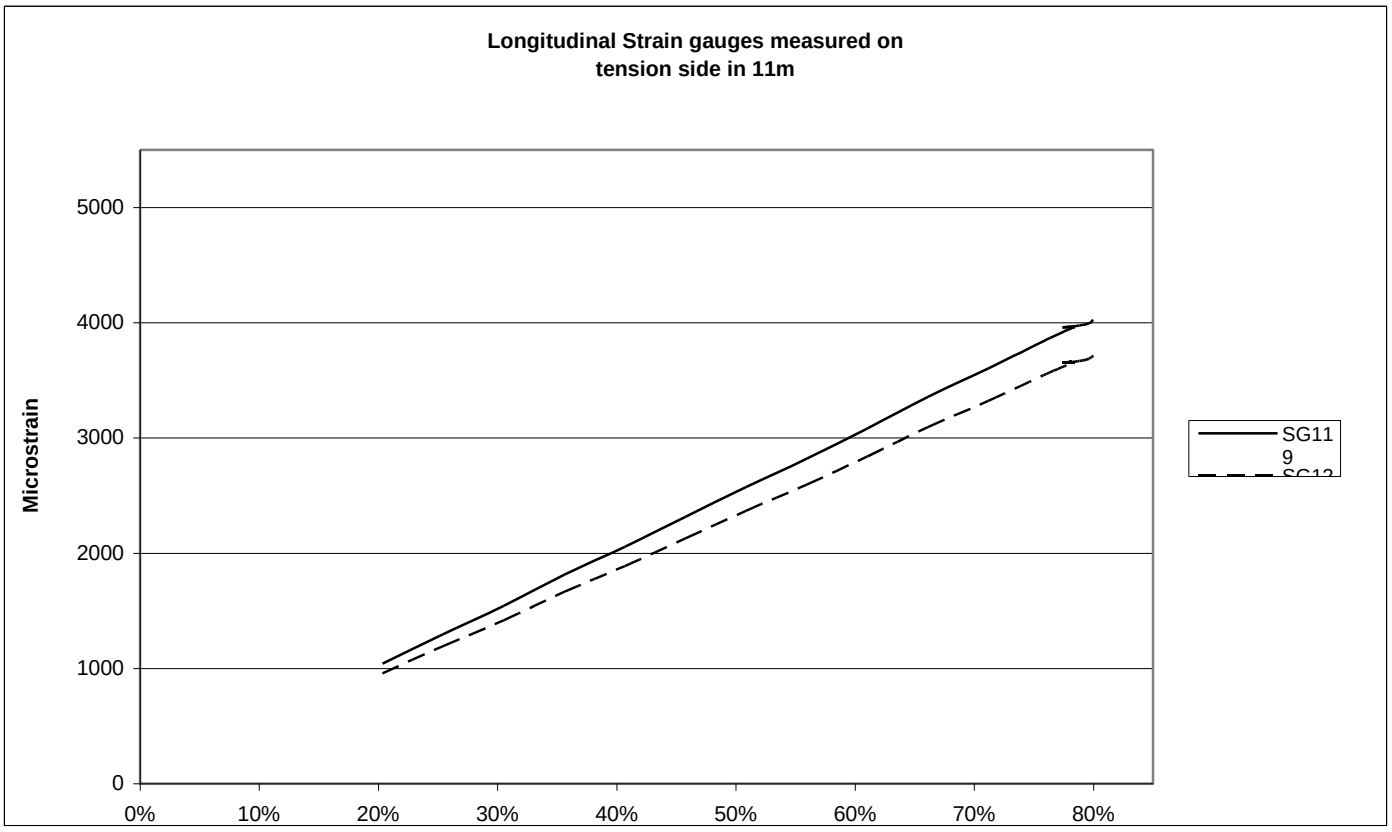
Longitudinal Strain gauges measured on tension side in 11m
Microstrain
5000
4000
3000
2000
1000
0
0%
10%
20%
30%
40%
50%
60%
70%
80%
SG119

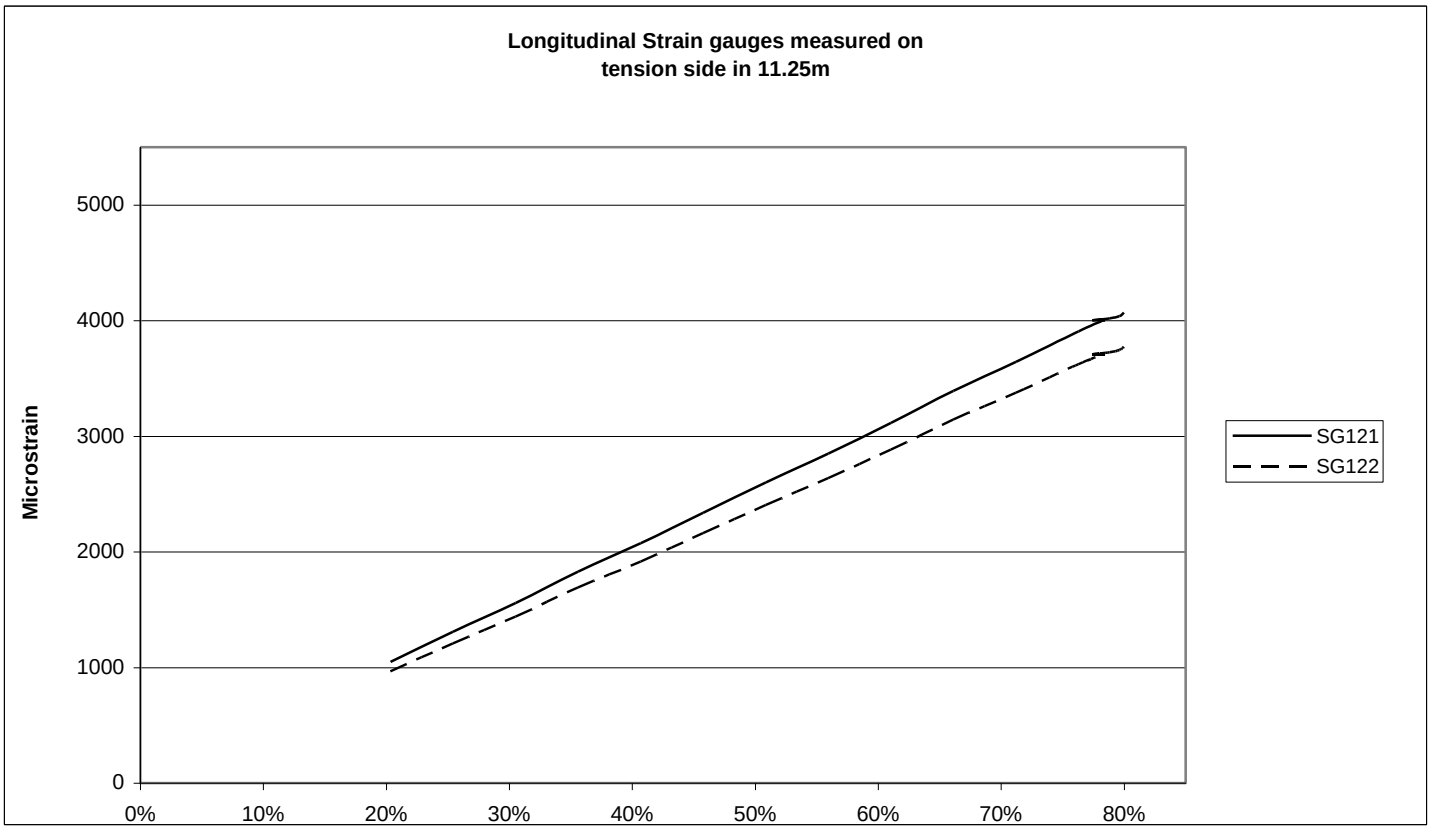
Longitudinal Strain gauges measured on tension side in 11.25m
Microstrain
5000
4000
3000
2000
1000
0
0%
10%
20%
30%
40%
50%
60%
70%
80%
SG121
SG122

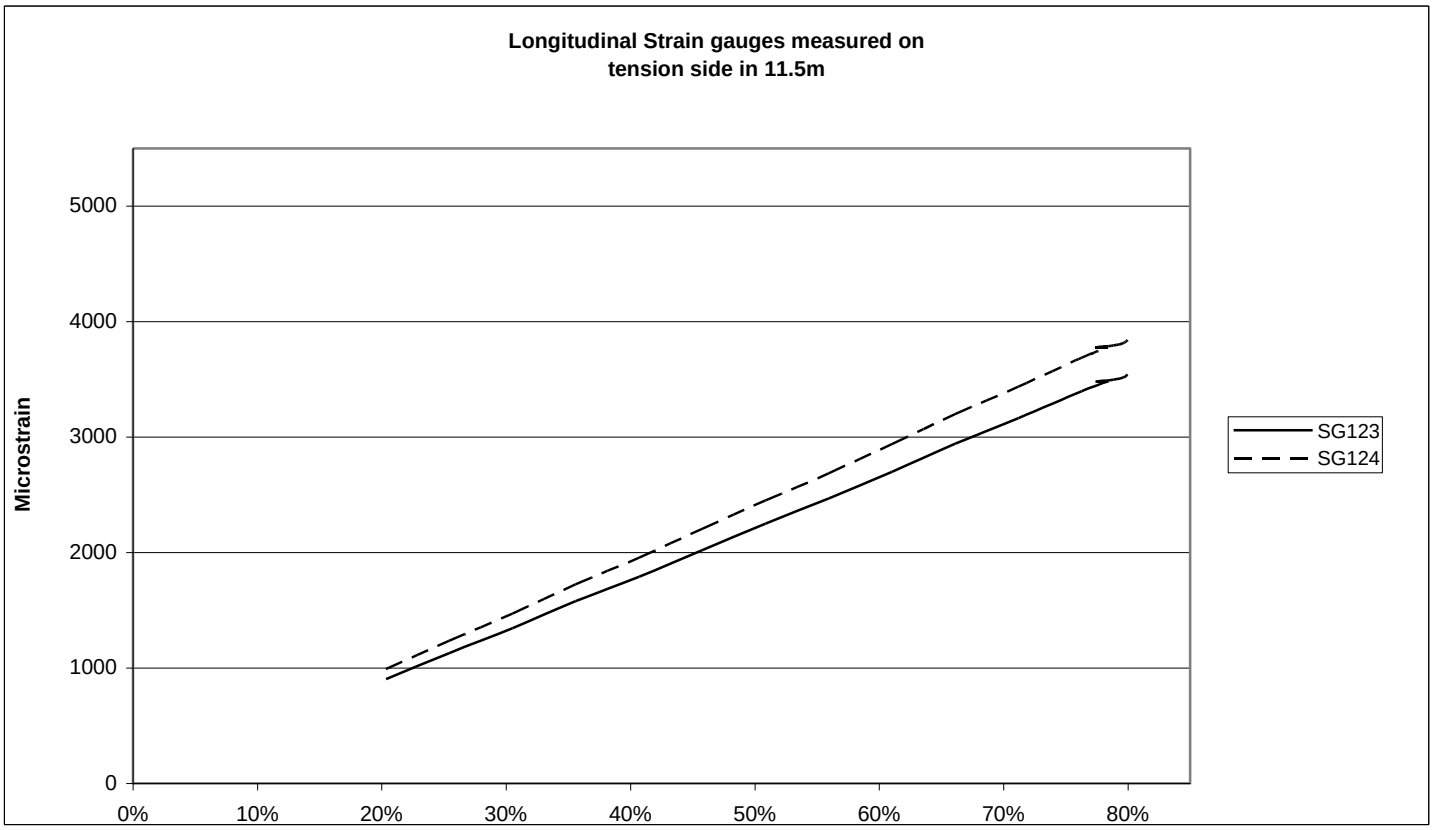
Longitudinal Strain gauges measured on tension side in 11.5m
Microstrain
5000
4000
3000
2000
1000
0
0%
10%
20%
30%
40%
50%
60%
70%
80%
SG123
SG124

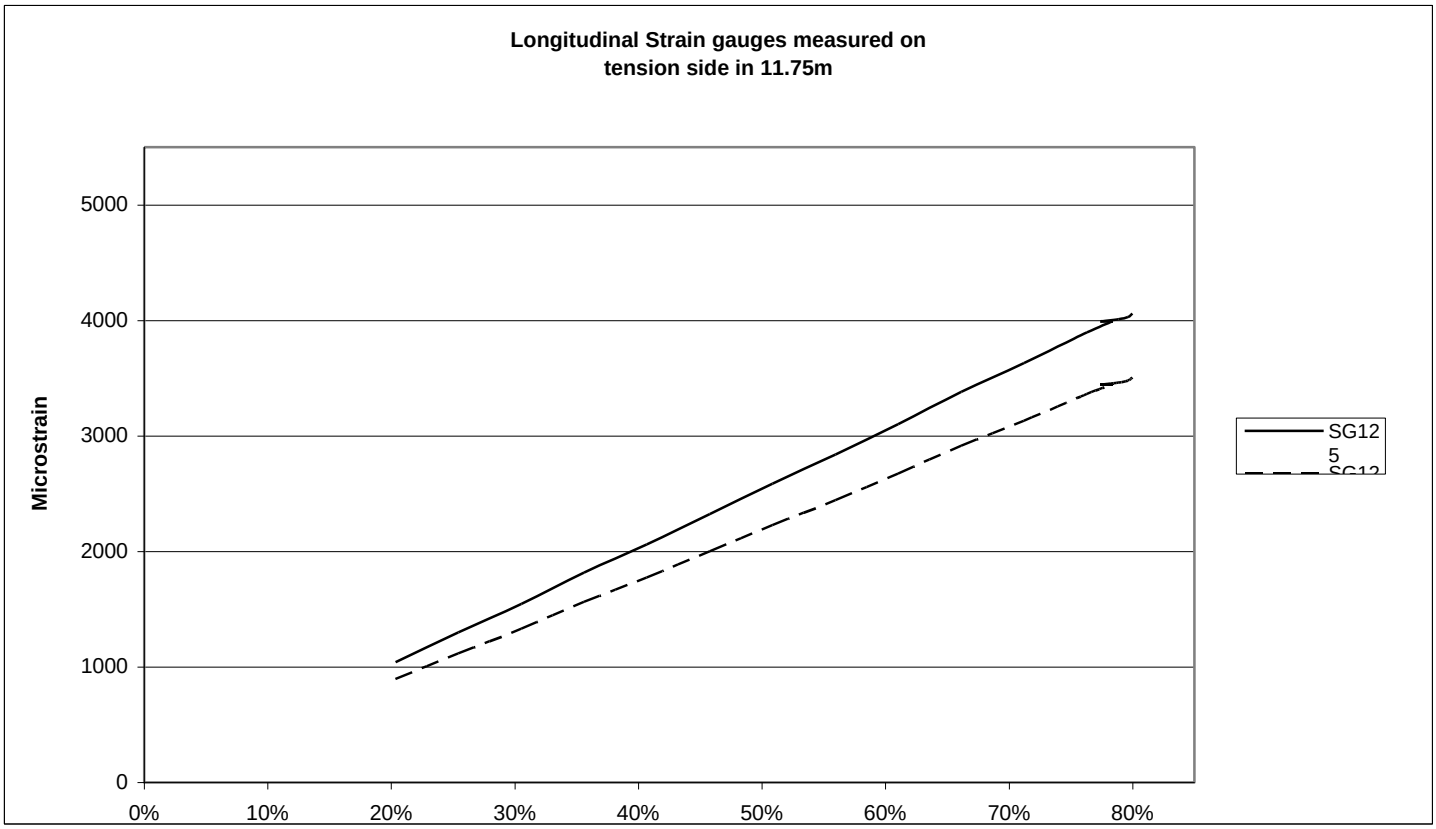
Longitudinal Strain gauges measured on tension side in 11.75m
Microstrain
5000
4000
3000
2000
1000
0
0%
10%
20%
30%
40%
50%
60%
70%
80%
SG125

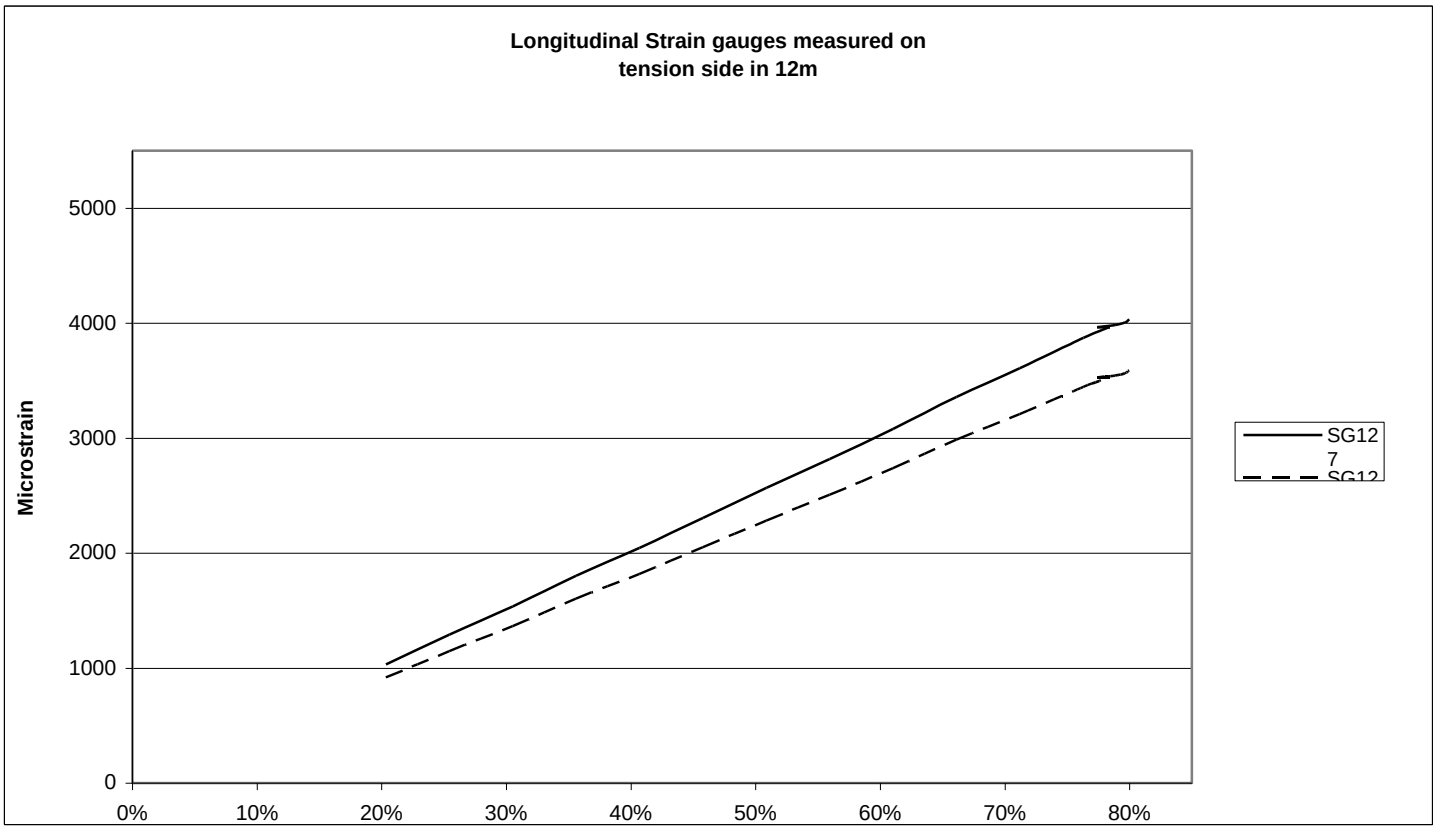
Longitudinal Strain gauges measured on tension side in 12m
Microstrain
5000
4000
3000
2000
1000
0
0%
10%
20%
30%
40%
50%
60%
70%
80%
SG127
SG12

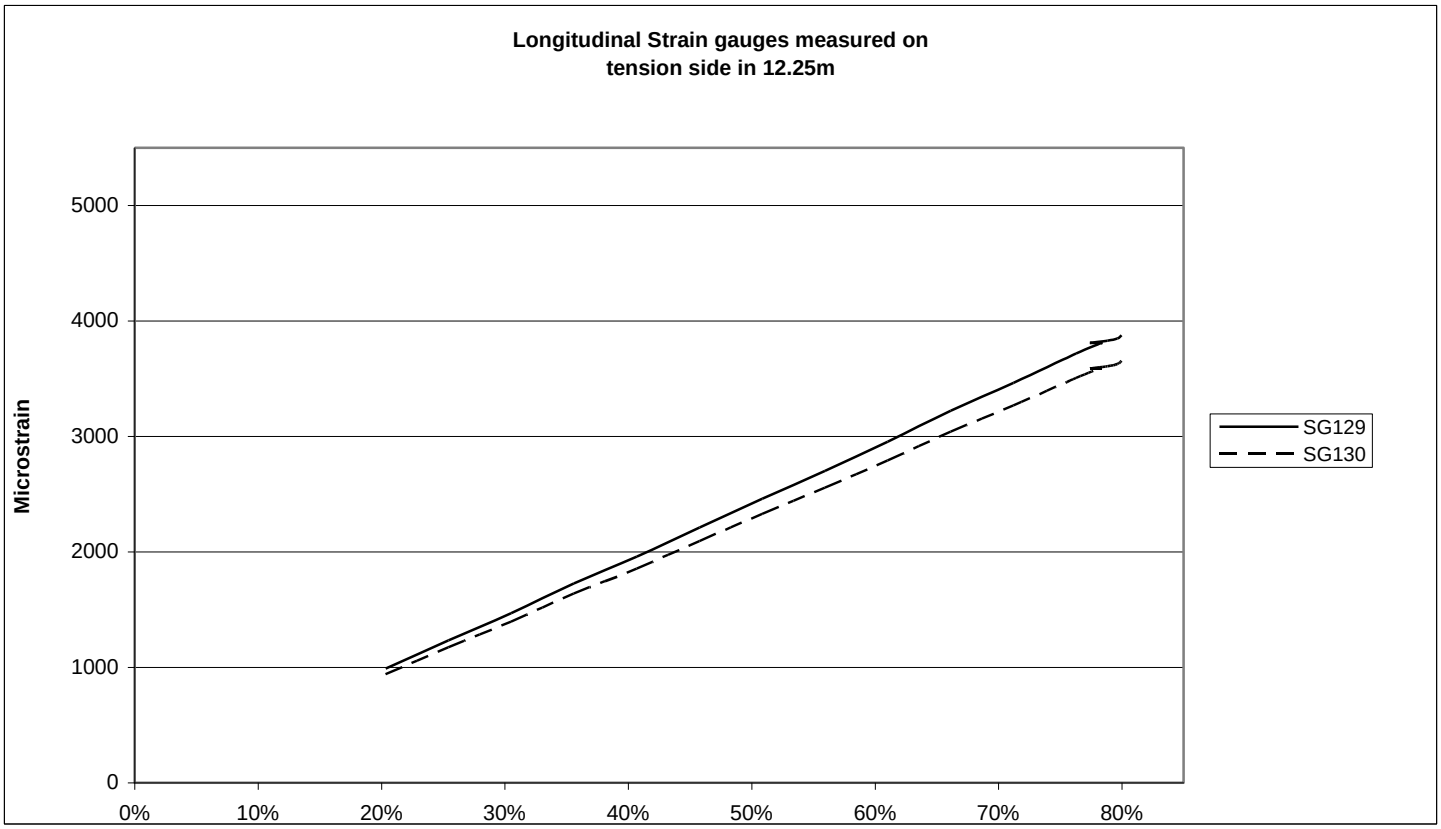
Longitudinal Strain gauges measured on tension side in 12.25m
Microstrain
5000
4000
3000
2000
1000
0
0%
10%
20%
30%
40%
50%
60%
70%
80%
SG129
SG130

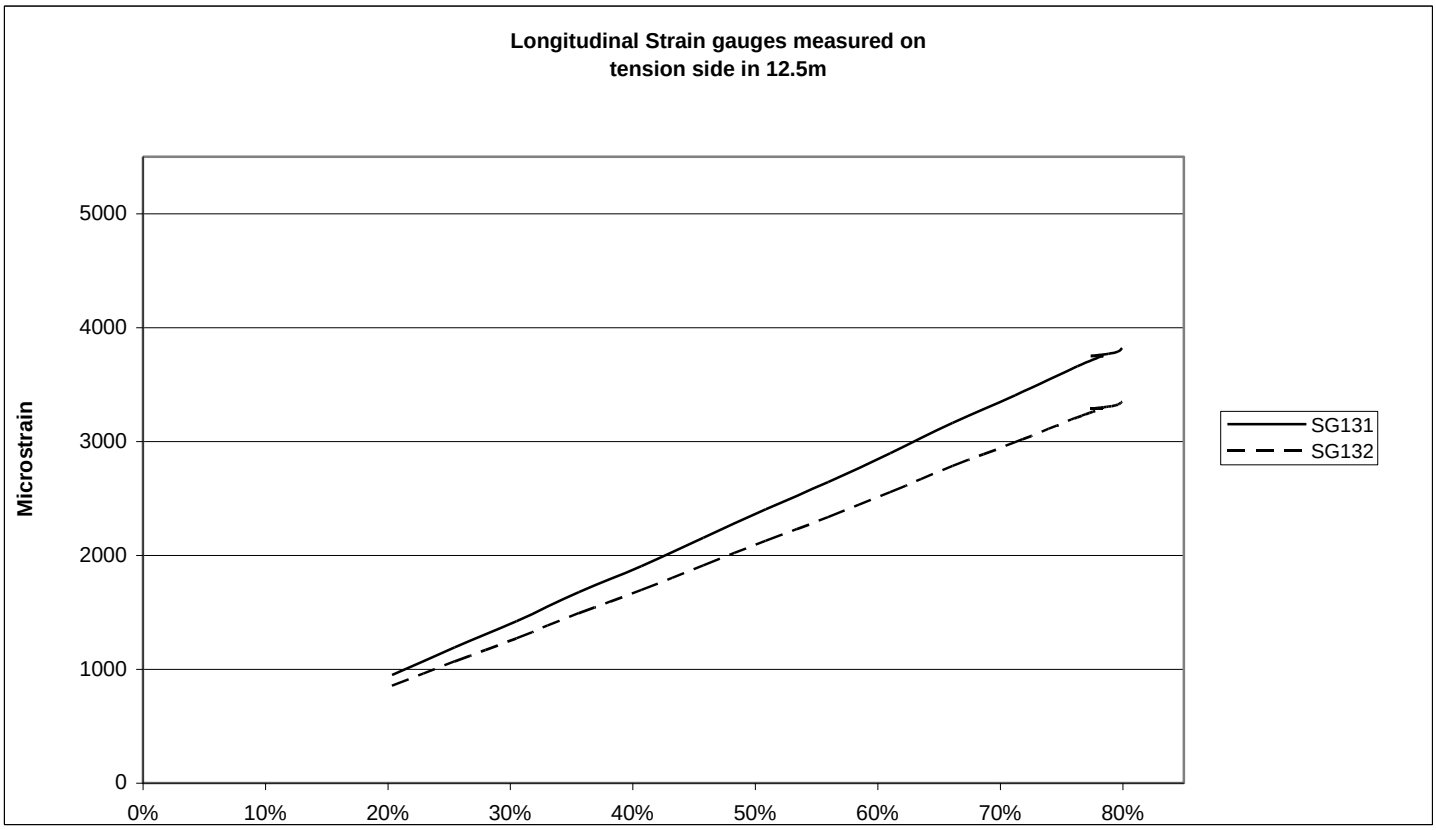
Longitudinal Strain gauges measured on tension side in 12.5m
Microstrain
5000
4000
3000
2000
1000
0
0%
10%
20%
30%
40%
50%
60%
70%
80%
SG131
SG132

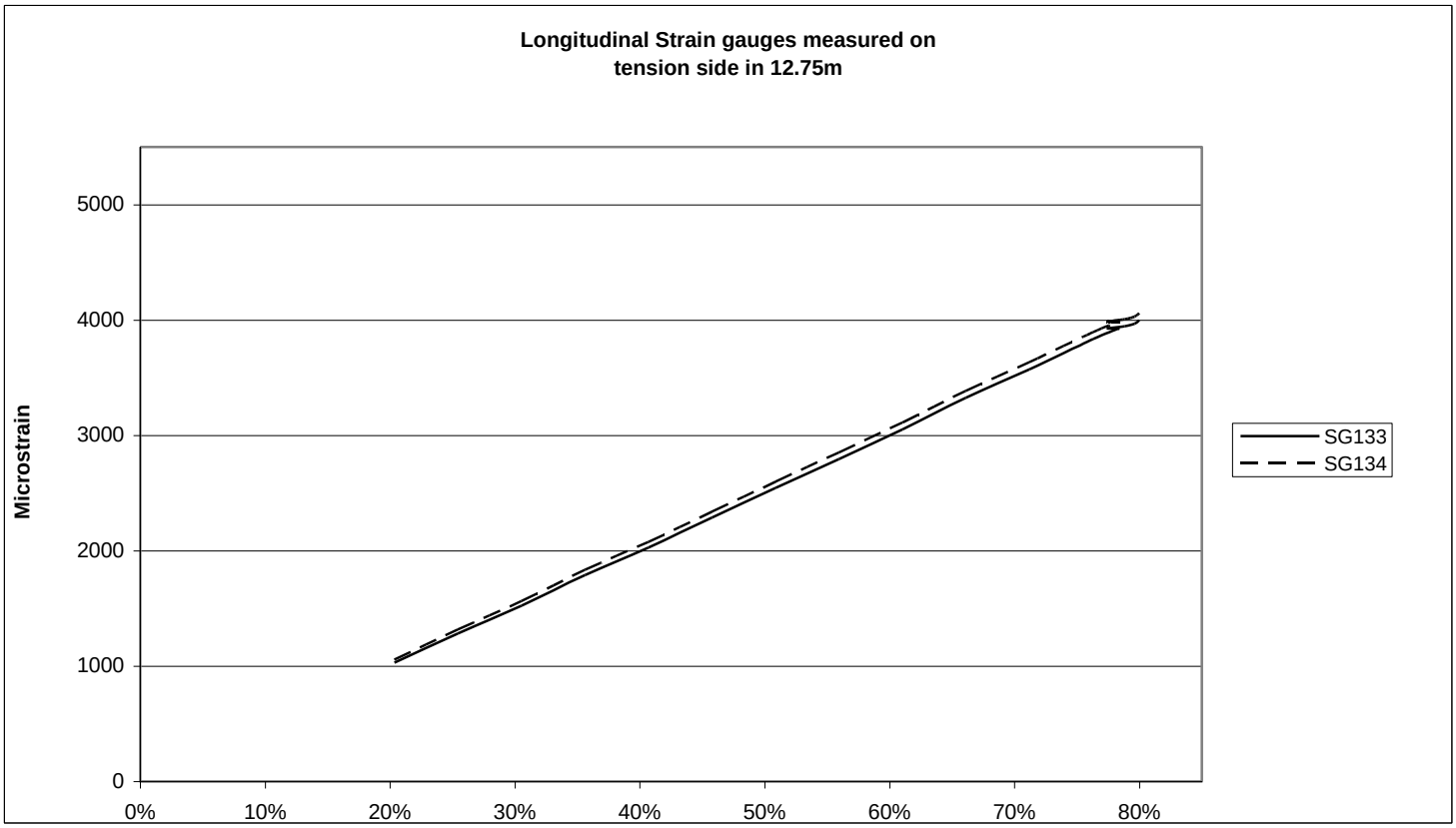
Longitudinal Strain gauges measured on tension side in 12.75m
Microstrain
5000
4000
3000
2000
1000
0
0%
10%
20%
30%
40%
50%
60%
70%
80%
SG133
SG134

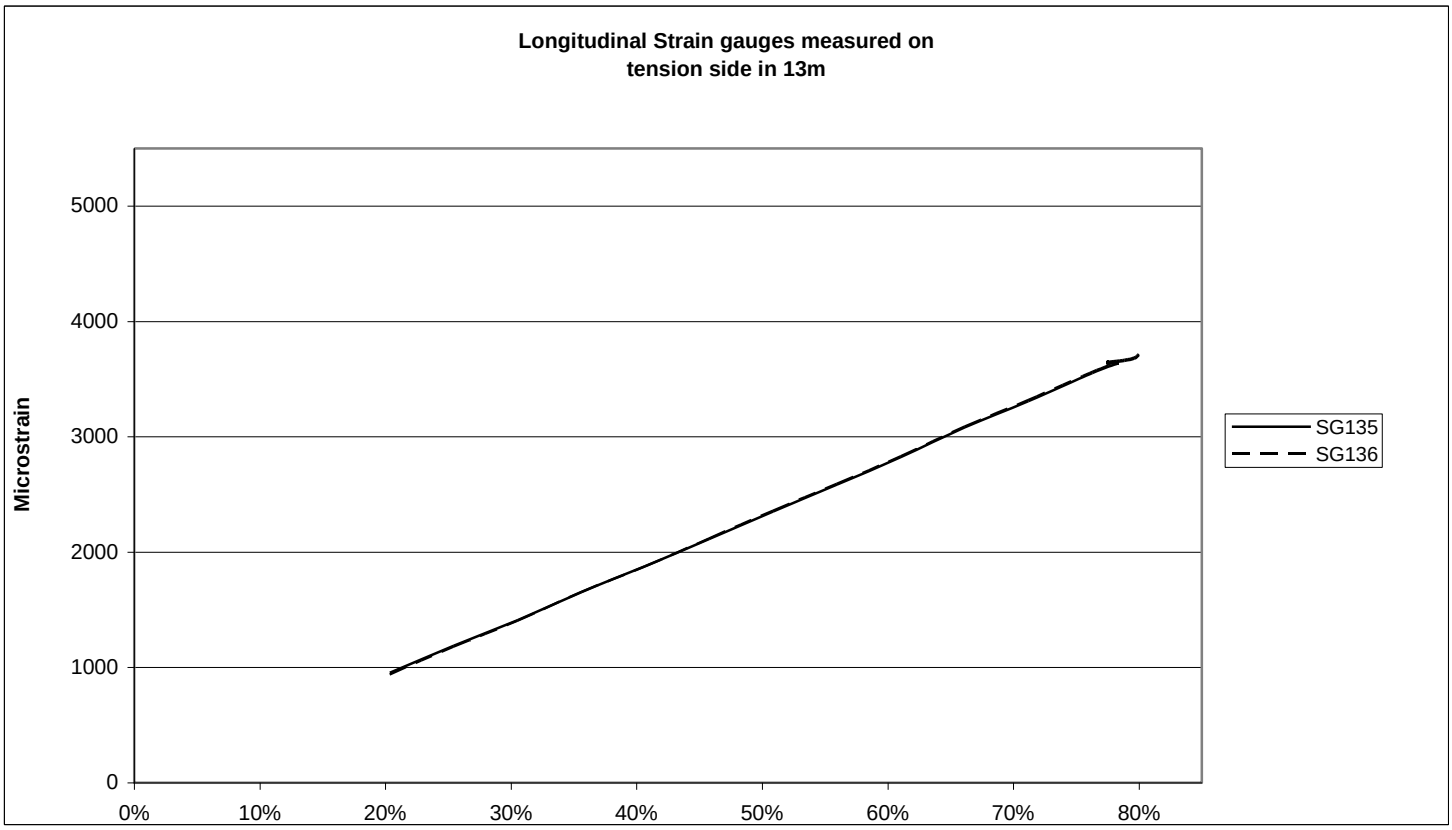
Longitudinal Strain gauges measured on tension side in 13m
Microstrain
5000
4000
3000
2000
1000
0
0%
10%
20%
30%
40%
50%
60%
70%
80%
SG135
SG136

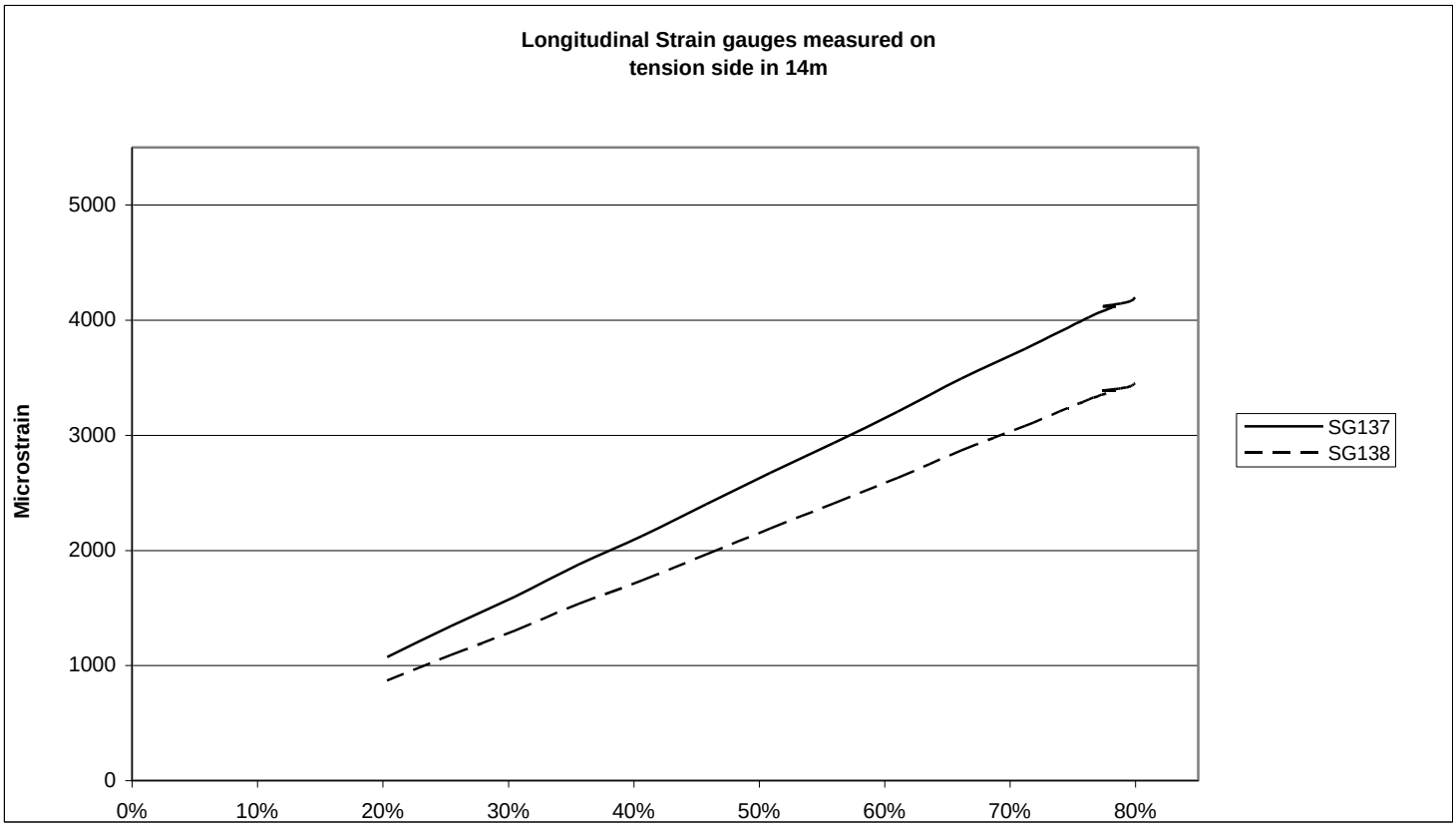
Longitudinal Strain gauges measured on tension side in 14m
Microstrain
5000
4000
3000
2000
1000
0
0%
10%
20%
30%
40%
50%
60%
70%
80%
SG137
SG138

Graphs of Transverse Compression and Tension Strain

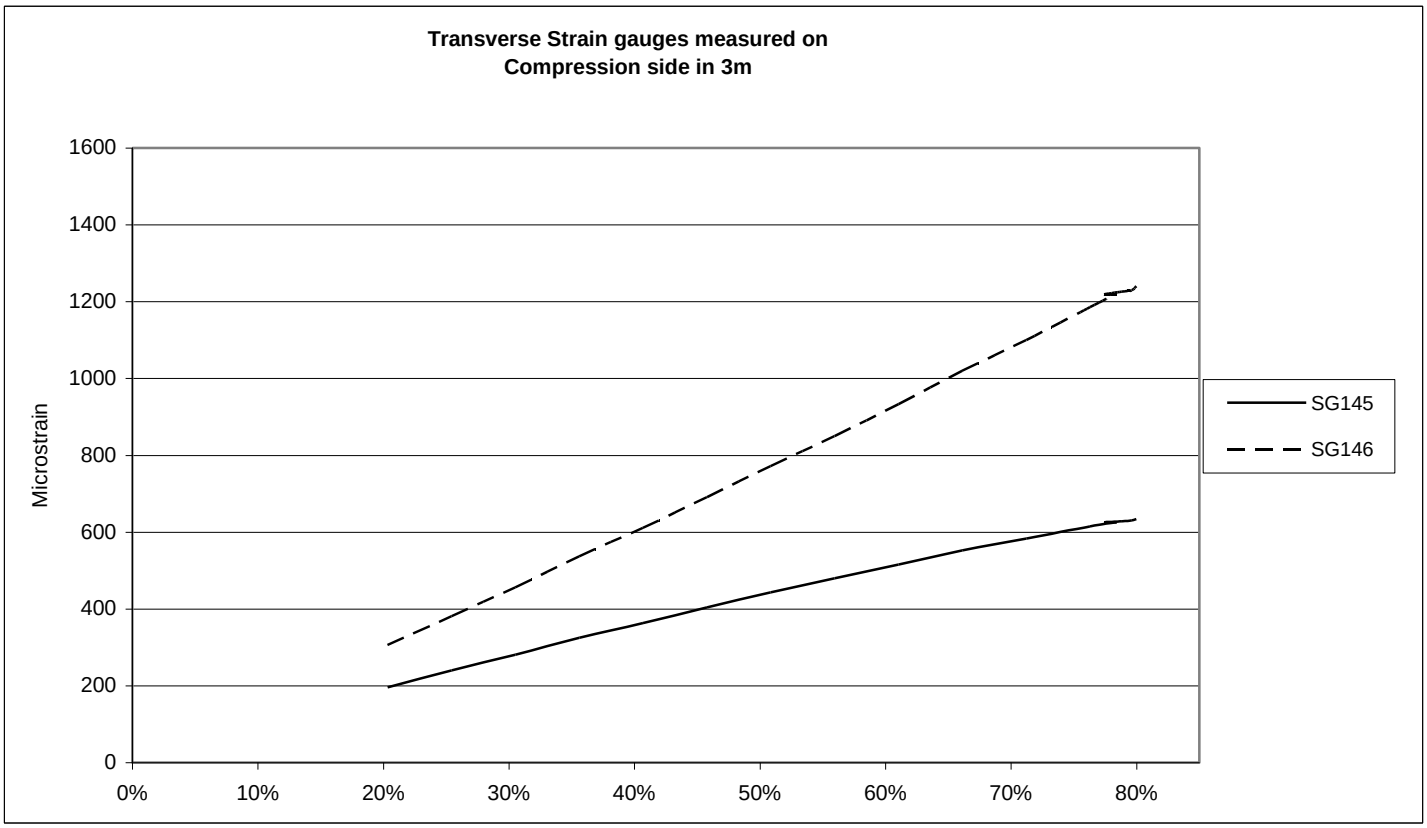

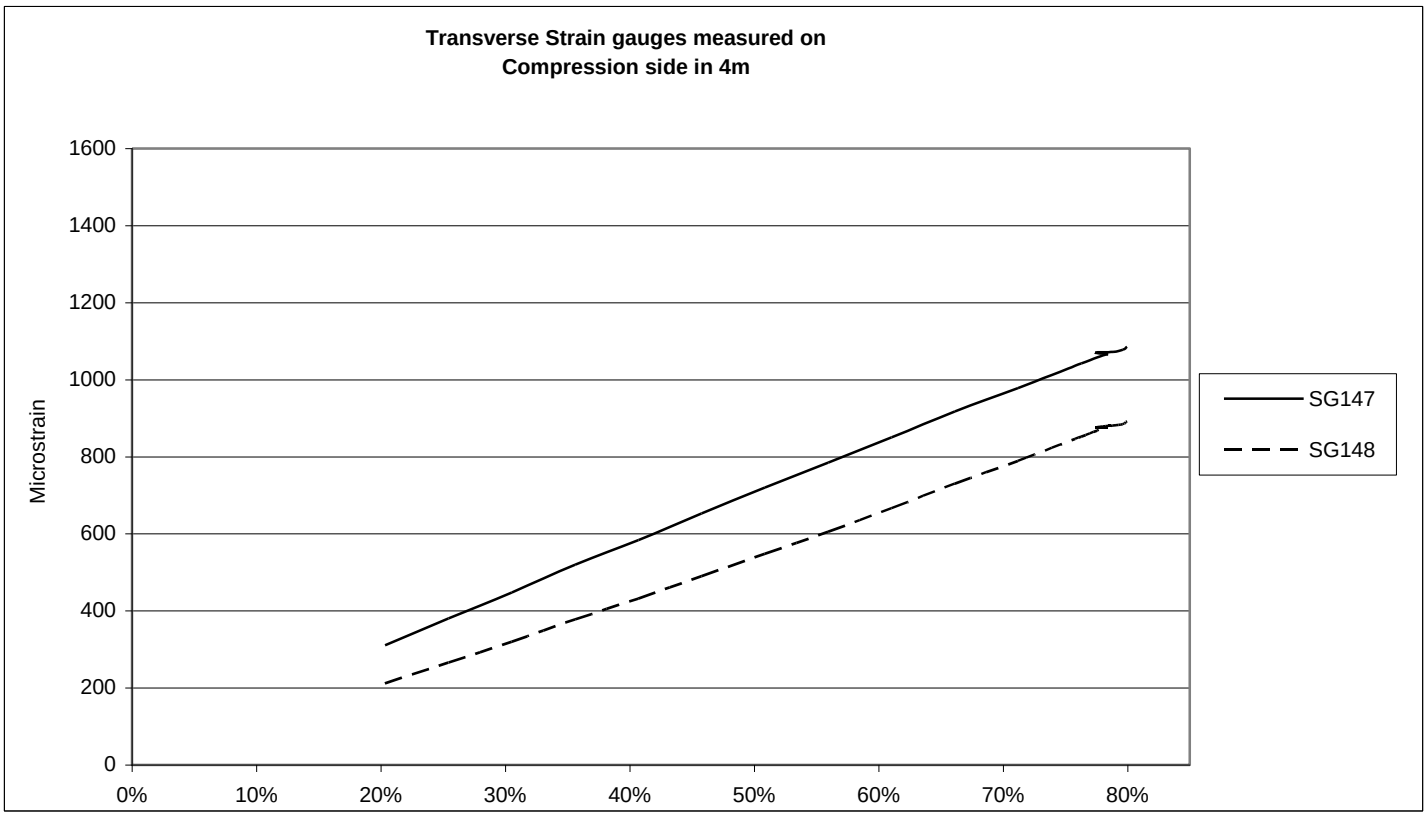

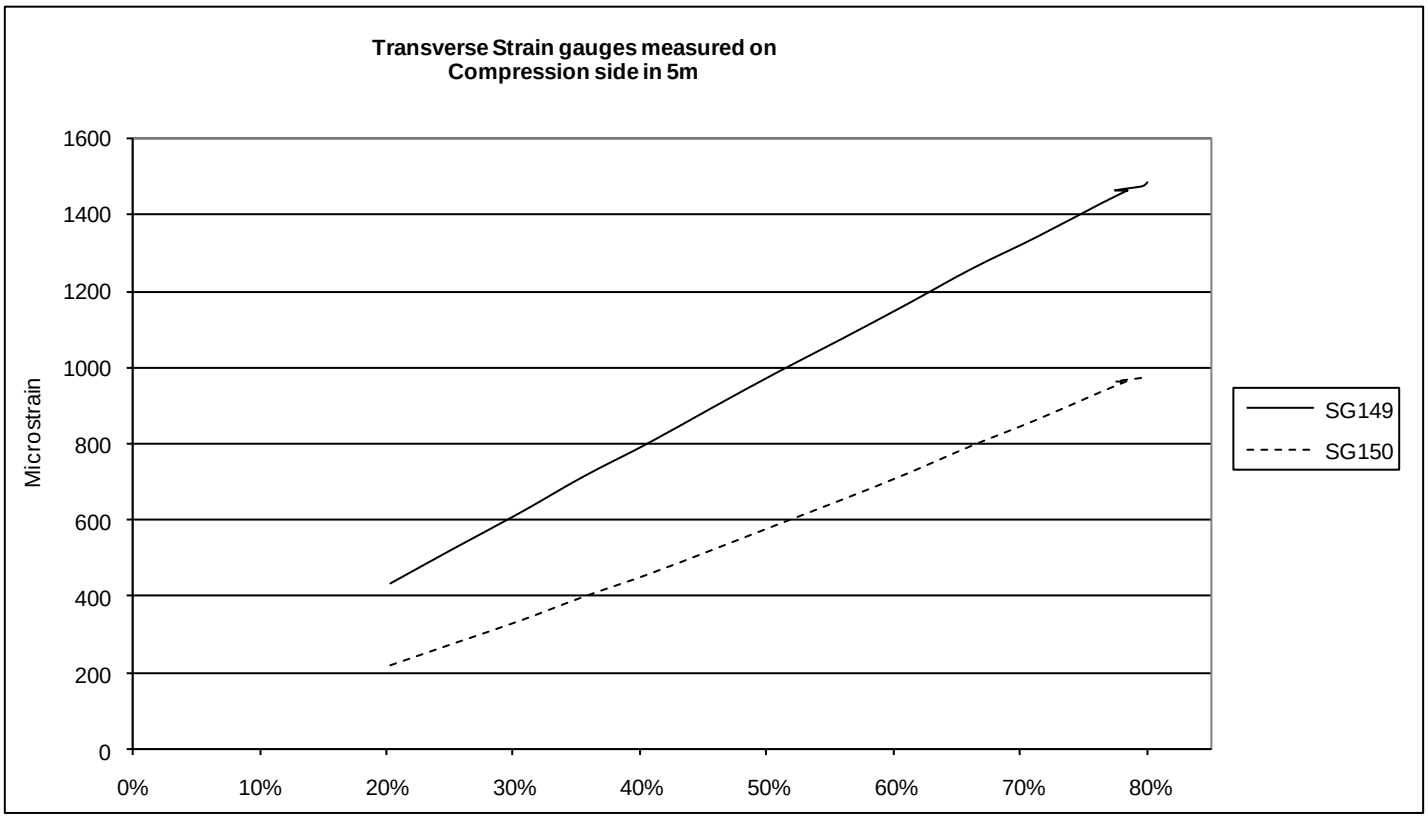
Transverse Strain gauges measured on
Compression side in 5m
Microstrain
1600
1400
1200
1000
800
600
400
200
0
0%
10%
20%
30%
40%
50%
60%
70%
80%
SG149
SG150

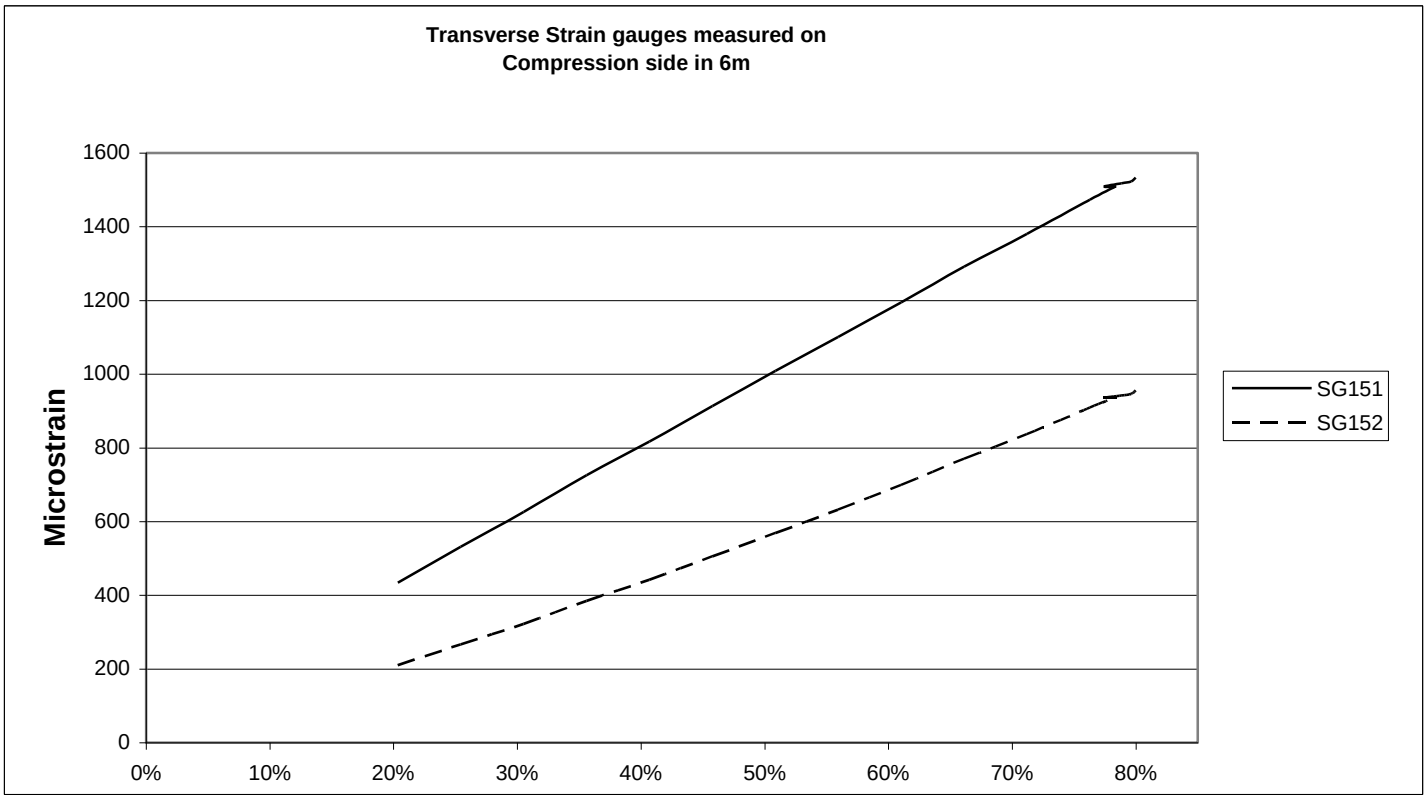
Transverse Strain gauges measured on
Compression side in 6m
Microstrain
1600
1400
1200
1000
800
600
400
200
0
0%
10%
20%
30%
40%
50%
60%
70%
80%
SG151
SG152

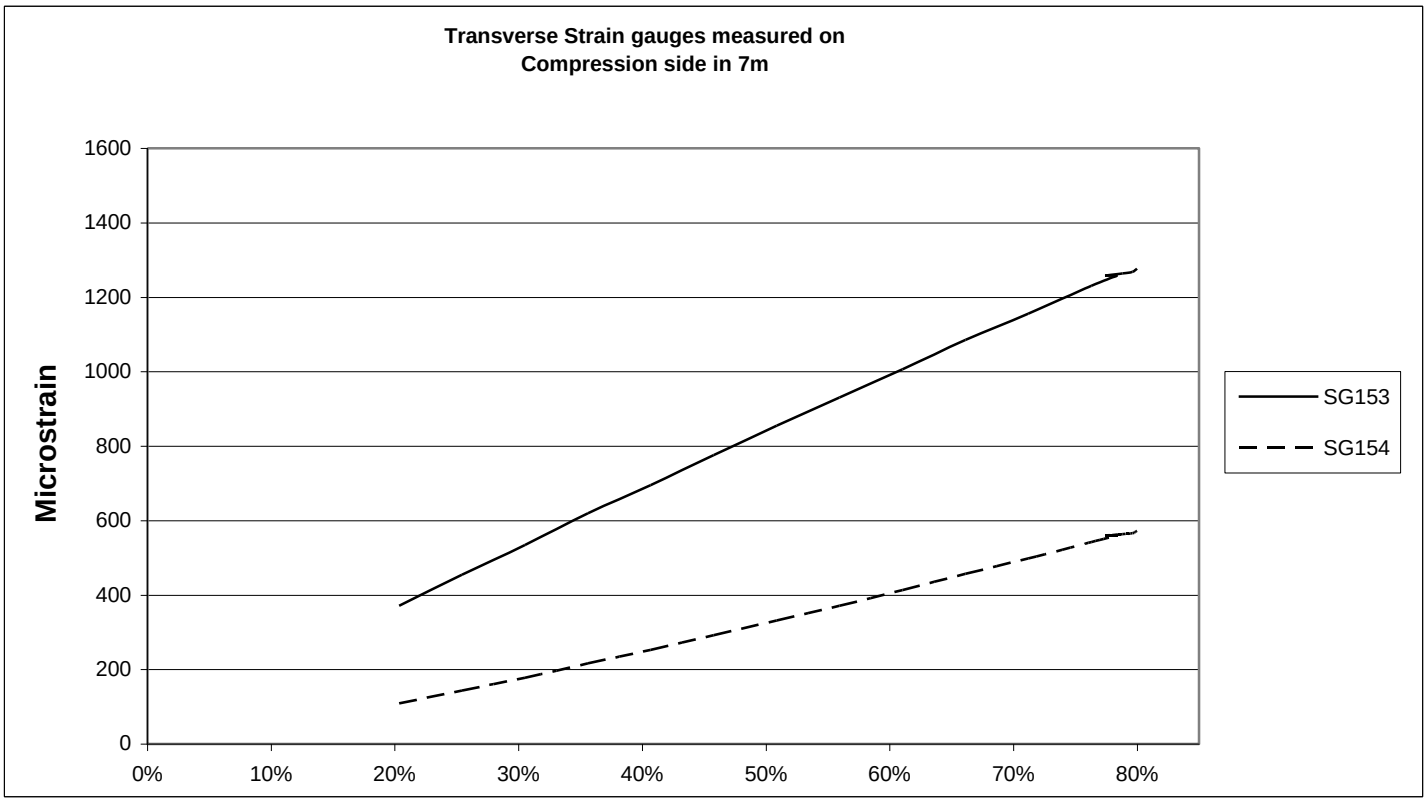
Transverse Strain gauges measured on
Compression side in 7m
Microstrain
1600
1400
1200
1000
800
600
400
200
0
0%
10%
20%
30%
40%
50%
60%
70%
80%
SG153
SG154

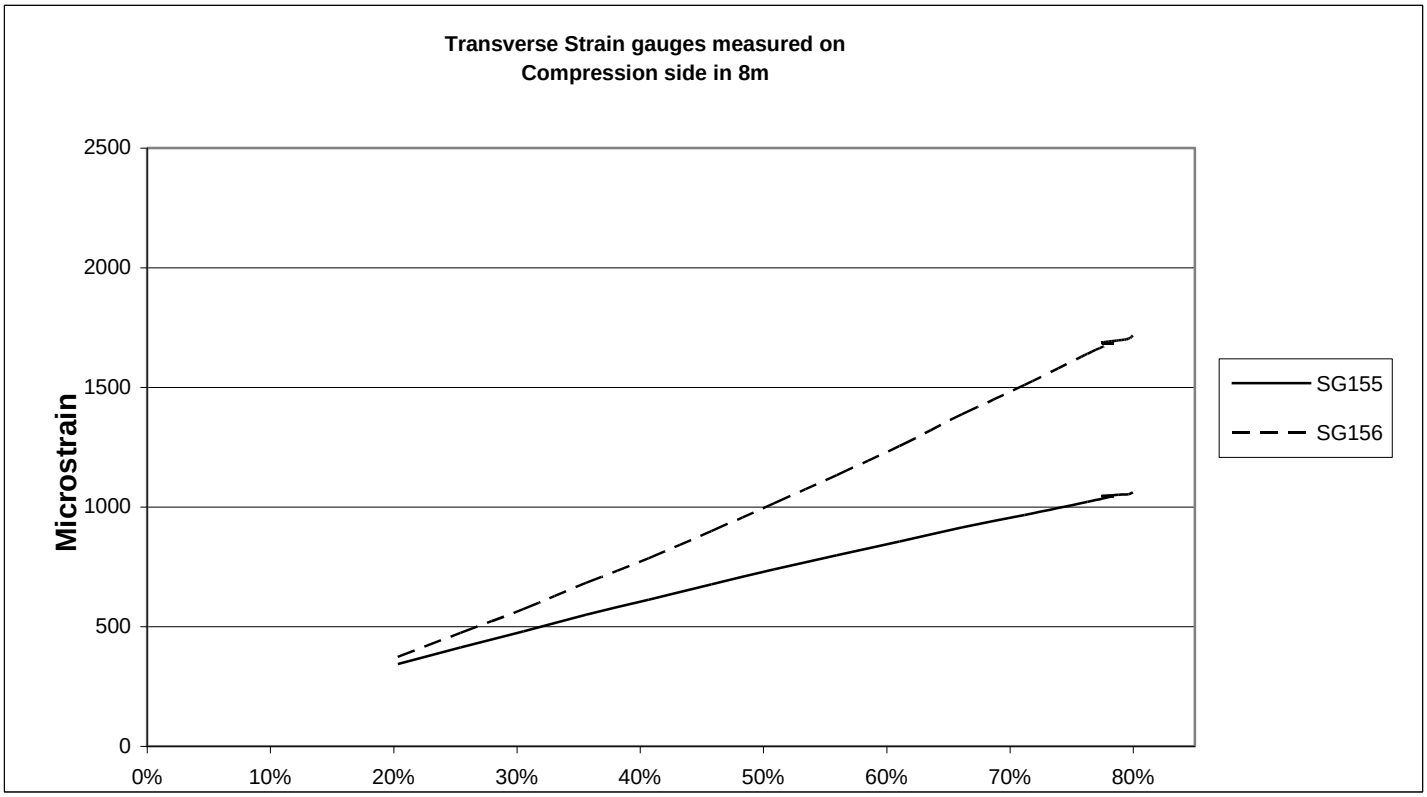
Transverse Strain gauges measured on
Compression side in 8m
Microstrain
2500
2000
1500
1000
500
0
0%
10%
20%
30%
40%
50%
60%
70%
80%
SG155
SG156

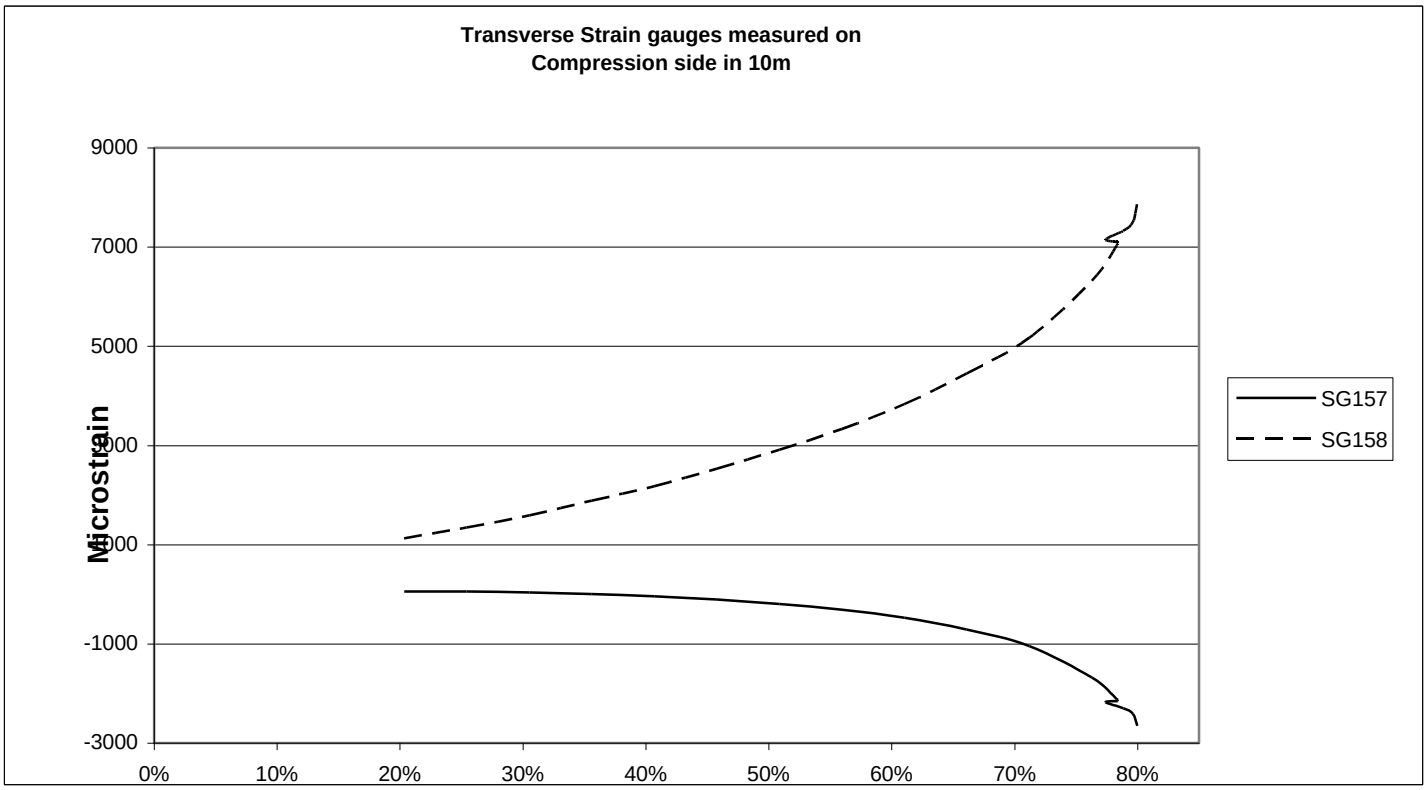
Transverse Strain gauges measured on
Compression side in 10m
9000
7000
5000
-1000
-3000
Microstrain
0%
10%
20%
30%
40%
50%
60%
70%
80%
SG157
SG158

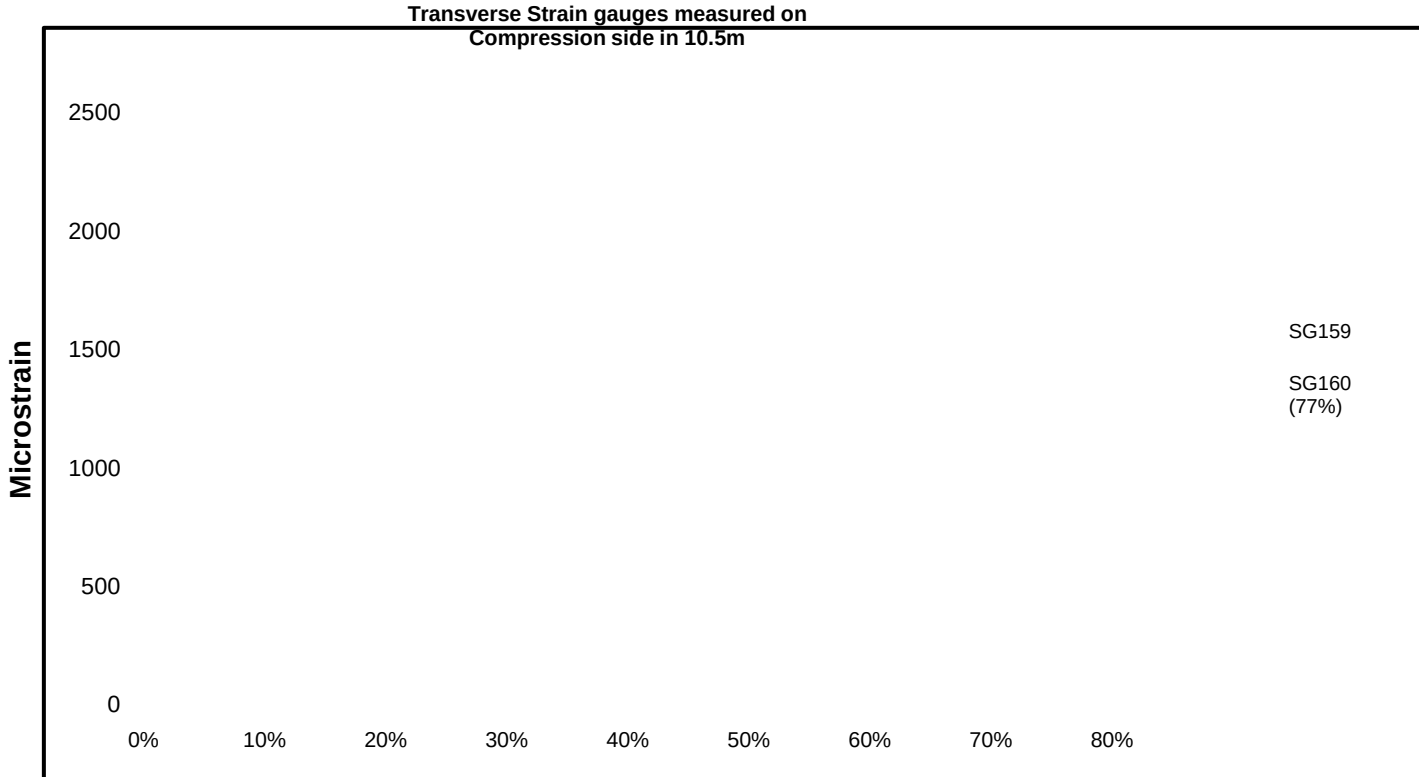
Transverse Strain gauges measured on
Compression side in 10.5m
2500
2000
1500
1000
500
0
Microstrain
0%
10%
20%
30%
40%
50%
60%
70%
80%
SG159
SG160
(77%)

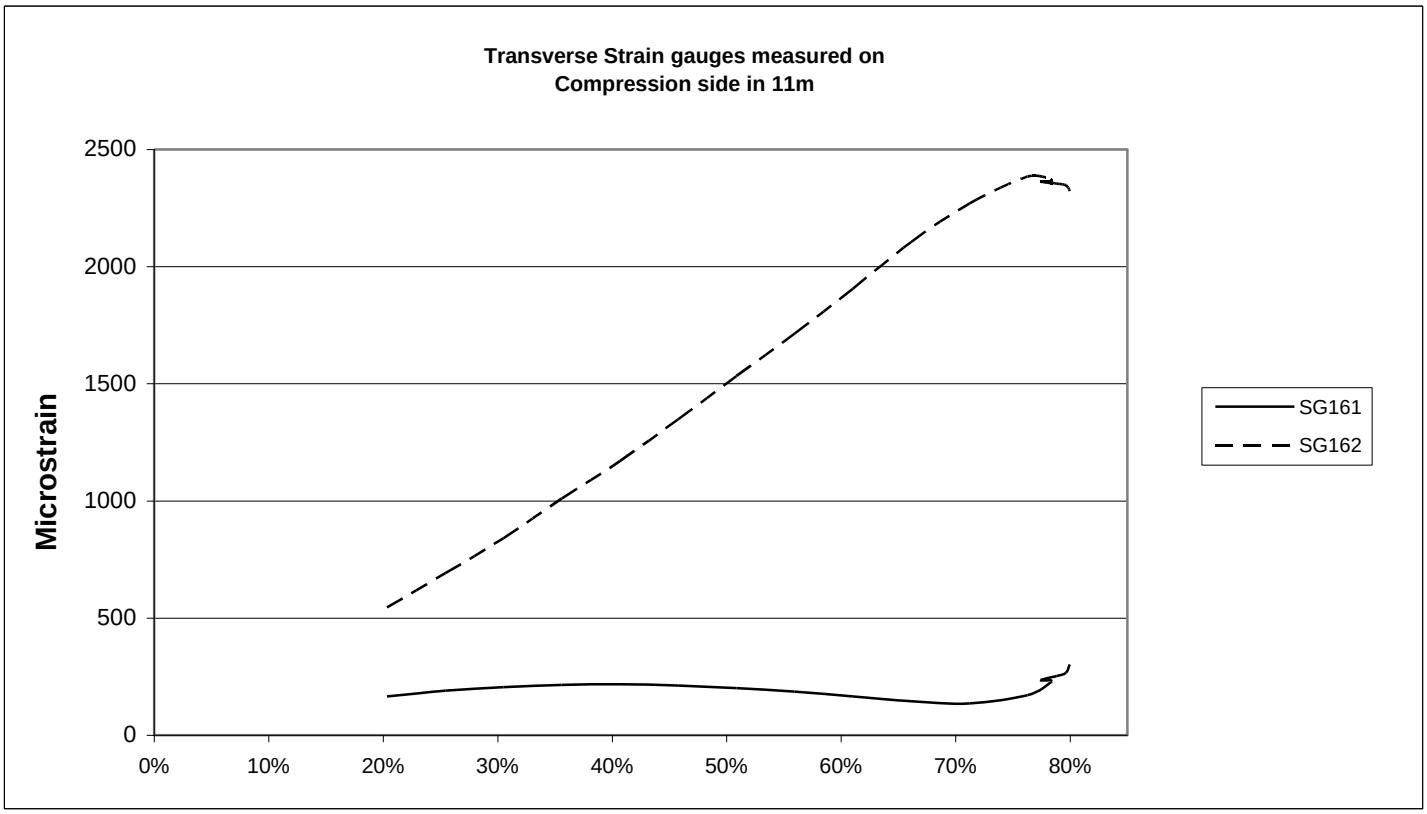
Transverse Strain gauges measured on
Compression side in 11m
Microstrain
2500
2000
1500
1000
500
0
0%
10%
20%
30%
40%
50%
60%
70%
80%
SG161
SG162

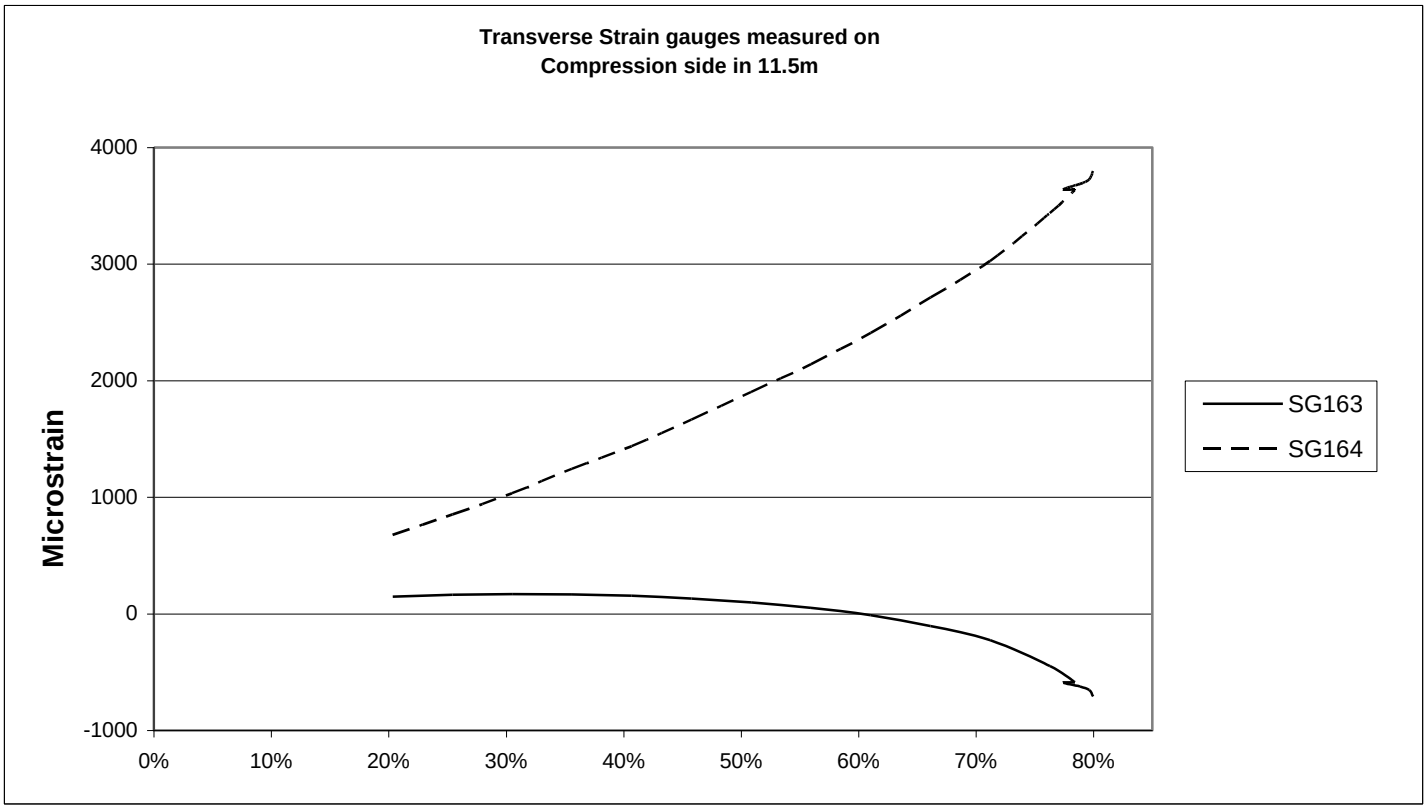
Transverse Strain gauges measured on
Compression side in 11.5m
Microstrain
4000
3000
2000
1000
0
-1000
0%
10%
20%
30%
40%
50%
60%
70%
80%
SG163
SG164

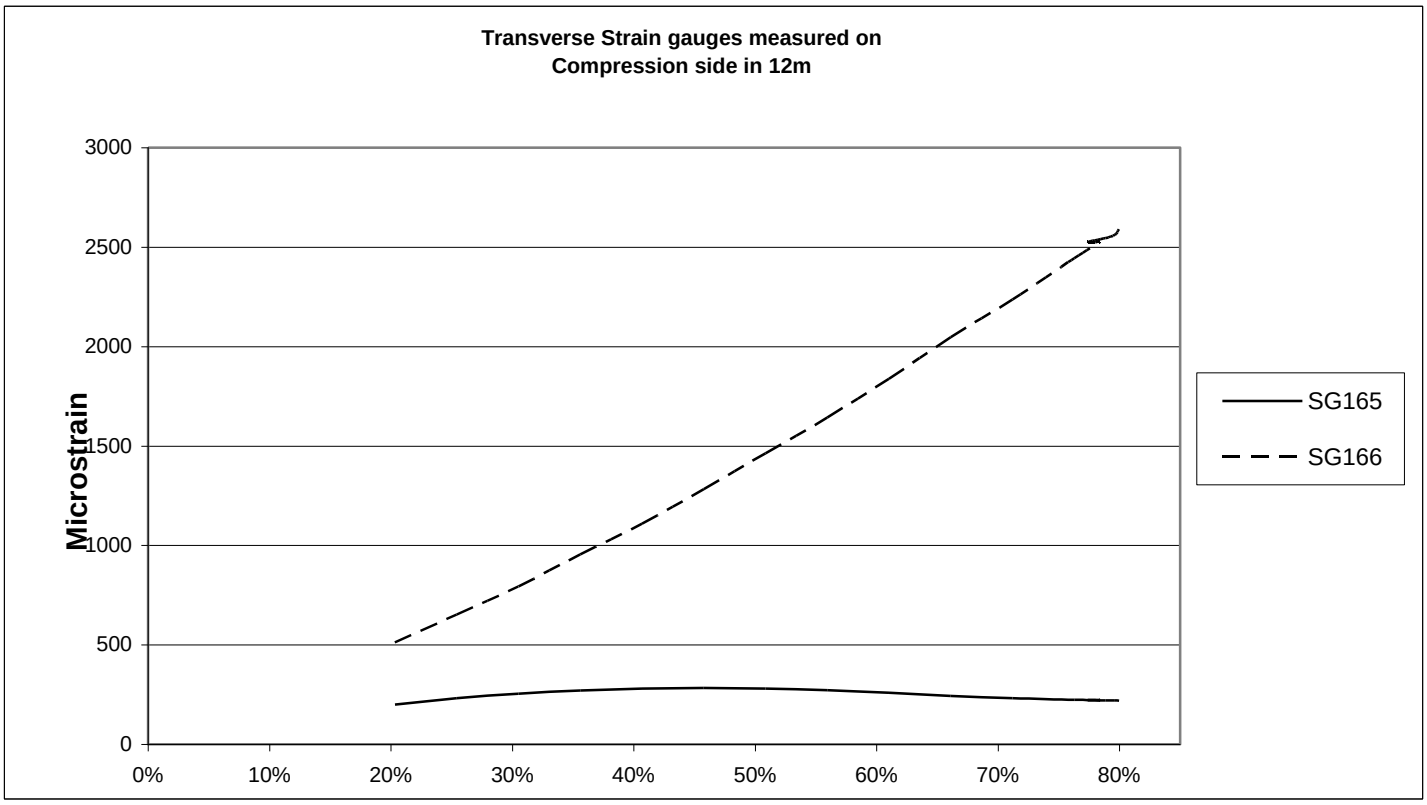
Transverse Strain gauges measured on
Compression side in 12m
Microstrain
3000
2500
2000
1500
1000
500
0
0%
10%
20%
30%
40%
50%
60%
70%
80%
SG165
SG166

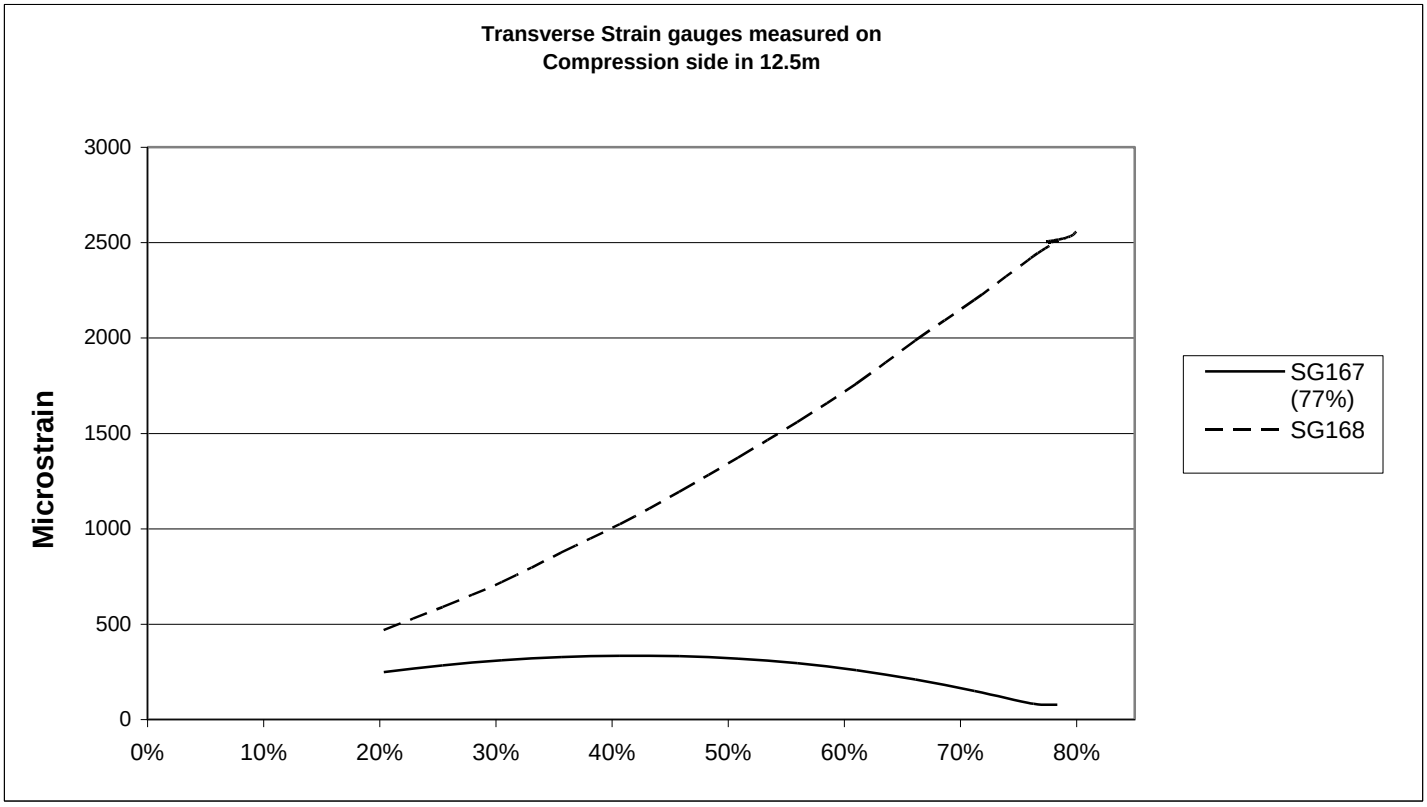
Transverse Strain gauges measured on
Compression side in 12.5m
Microstrain
3000
2500
2000
1500
1000
500
0
0%
10%
20%
30%
40%
50%
60%
70%
80%
SG167
(77%)
SG168

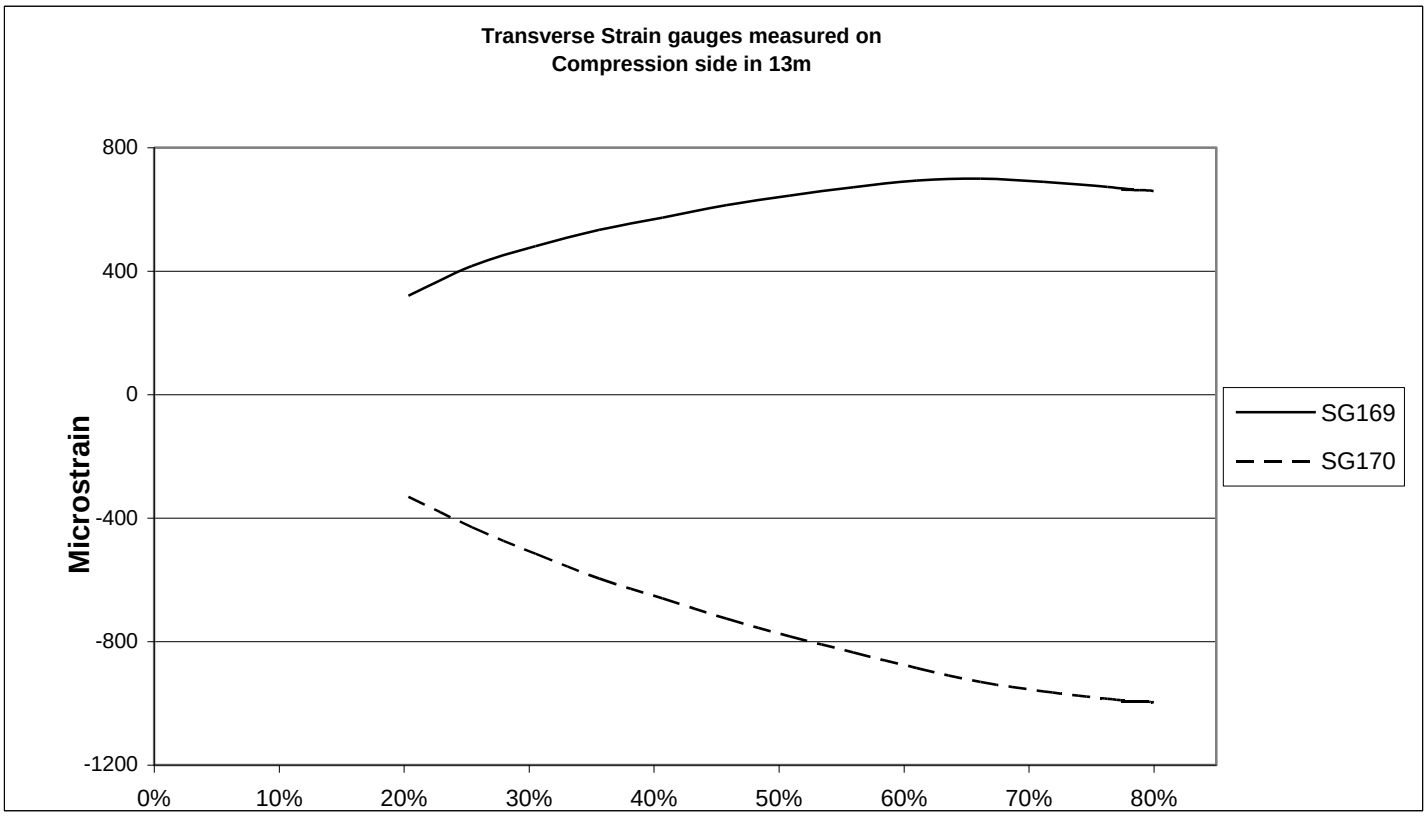
Transverse Strain gauges measured on
Compression side in 13m
800
400
0
-400
-800
-1200
Microstrain
0%
10%
20%
30%
40%
50%
60%
70%
80%
SG169
SG170

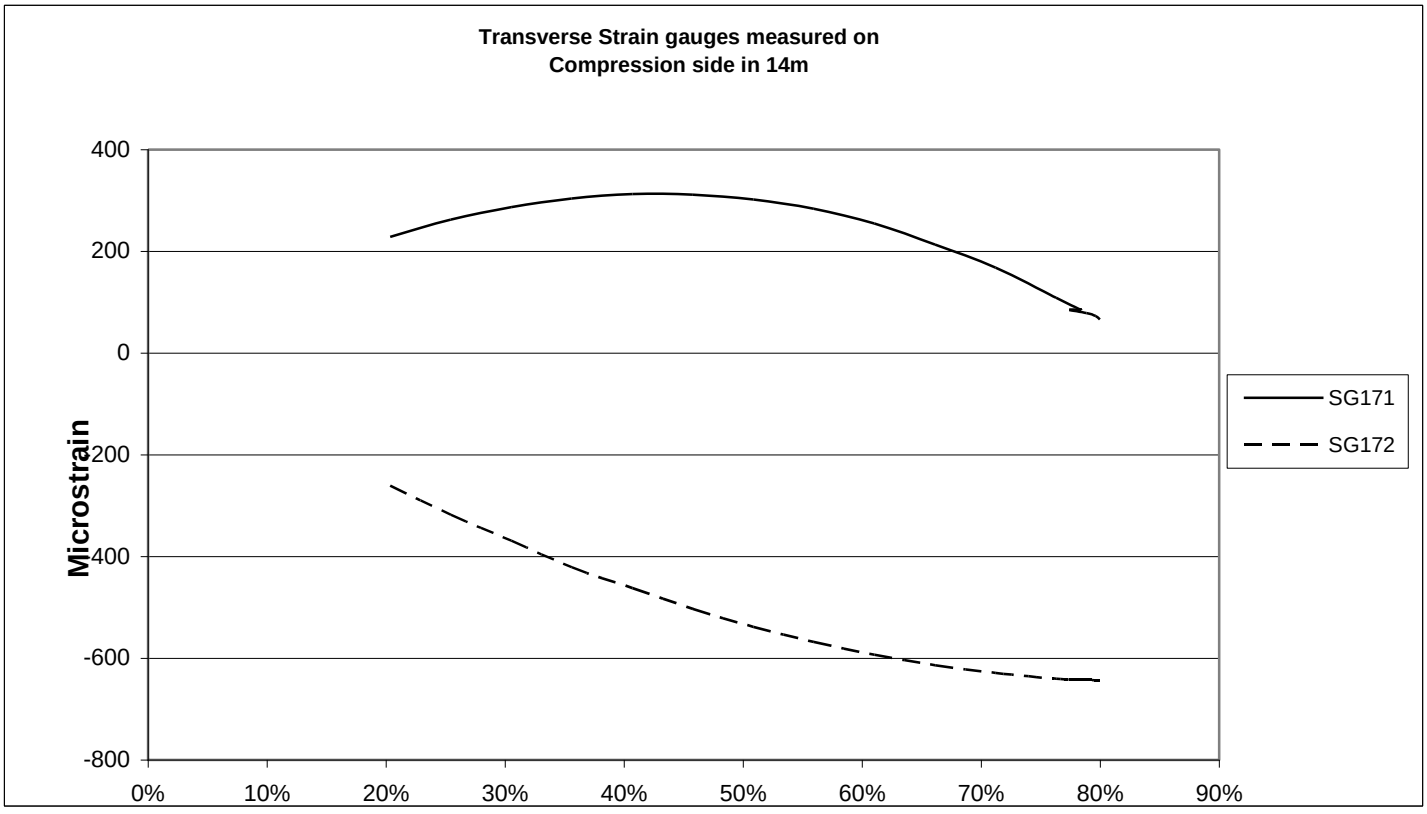
Transverse Strain gauges measured on
Compression side in 14m
400
200
0
-200
-400
-600
-800
Microstrain
0%
10%
20%
30%
40%
50%
60%
70%
80%
90%
SG171
SG172

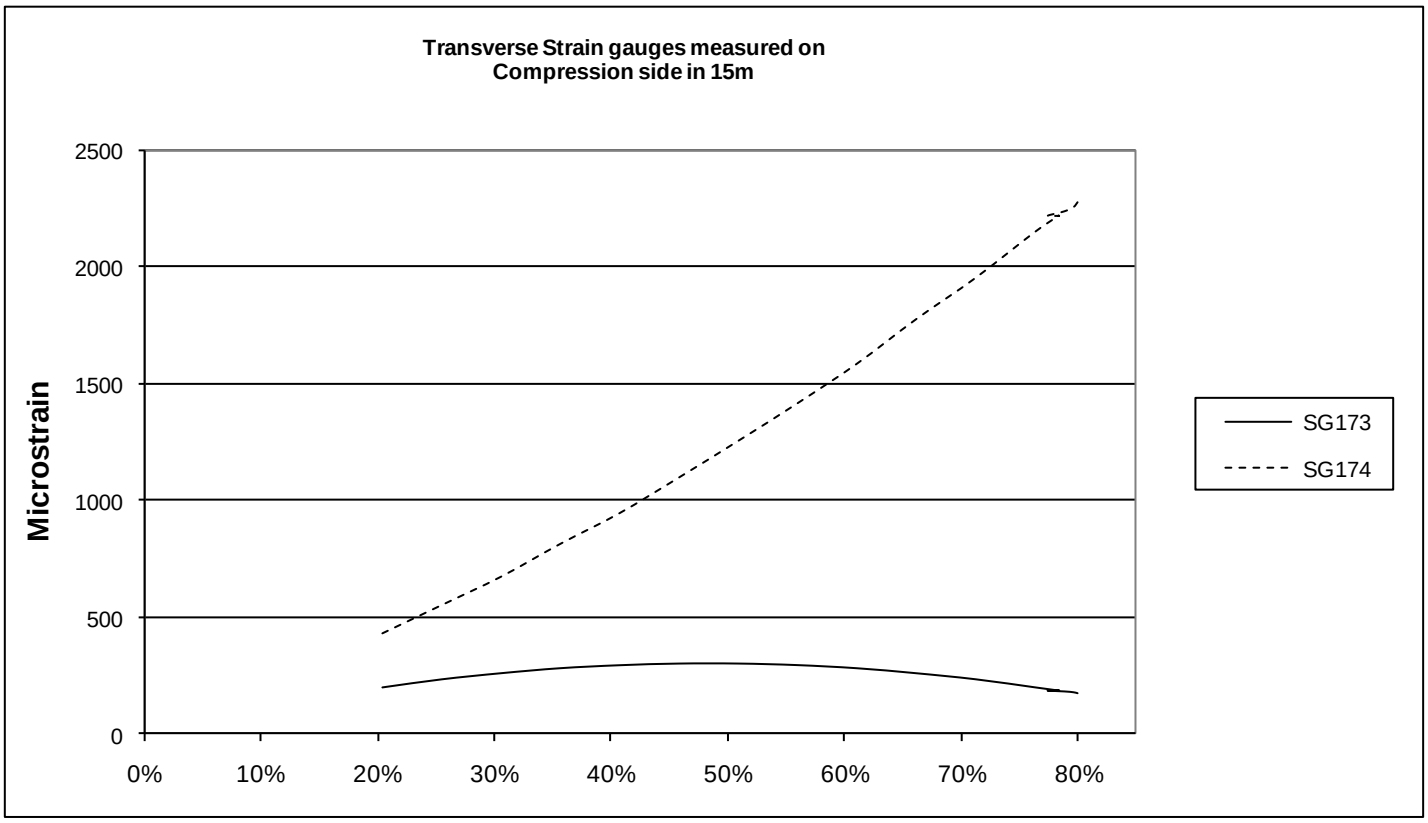
Transverse Strain gauges measured on
Compression side in 15m
Microstrain
2500
2000
1500
1000
500
0
0%
10%
20%
30%
40%
50%
60%
70%
80%
SG173
SG174

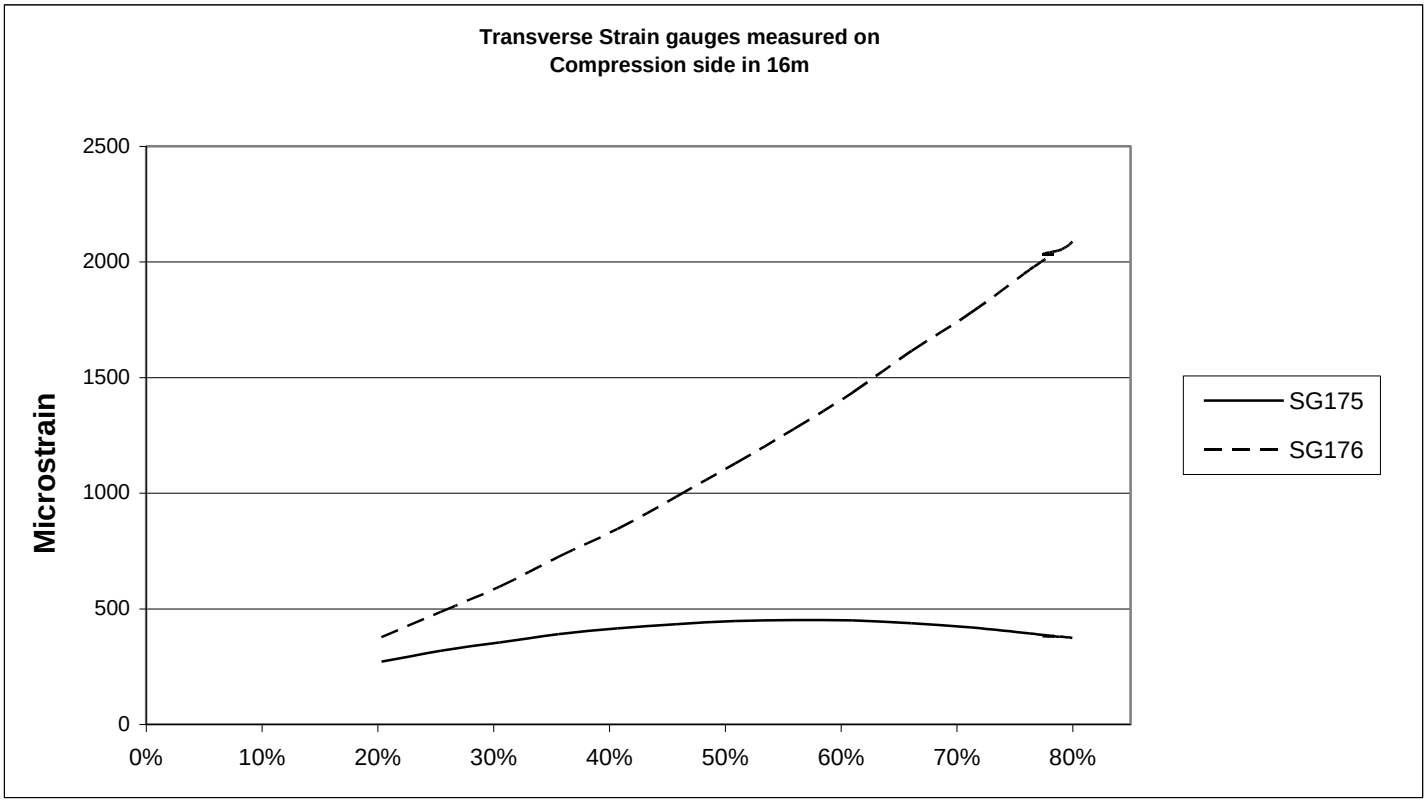
Transverse Strain gauges measured on
Compression side in 16m
Microstrain
2500
2000
1500
1000
500
0
0%
10%
20%
30%
40%
50%
60%
70%
80%
SG175
SG176

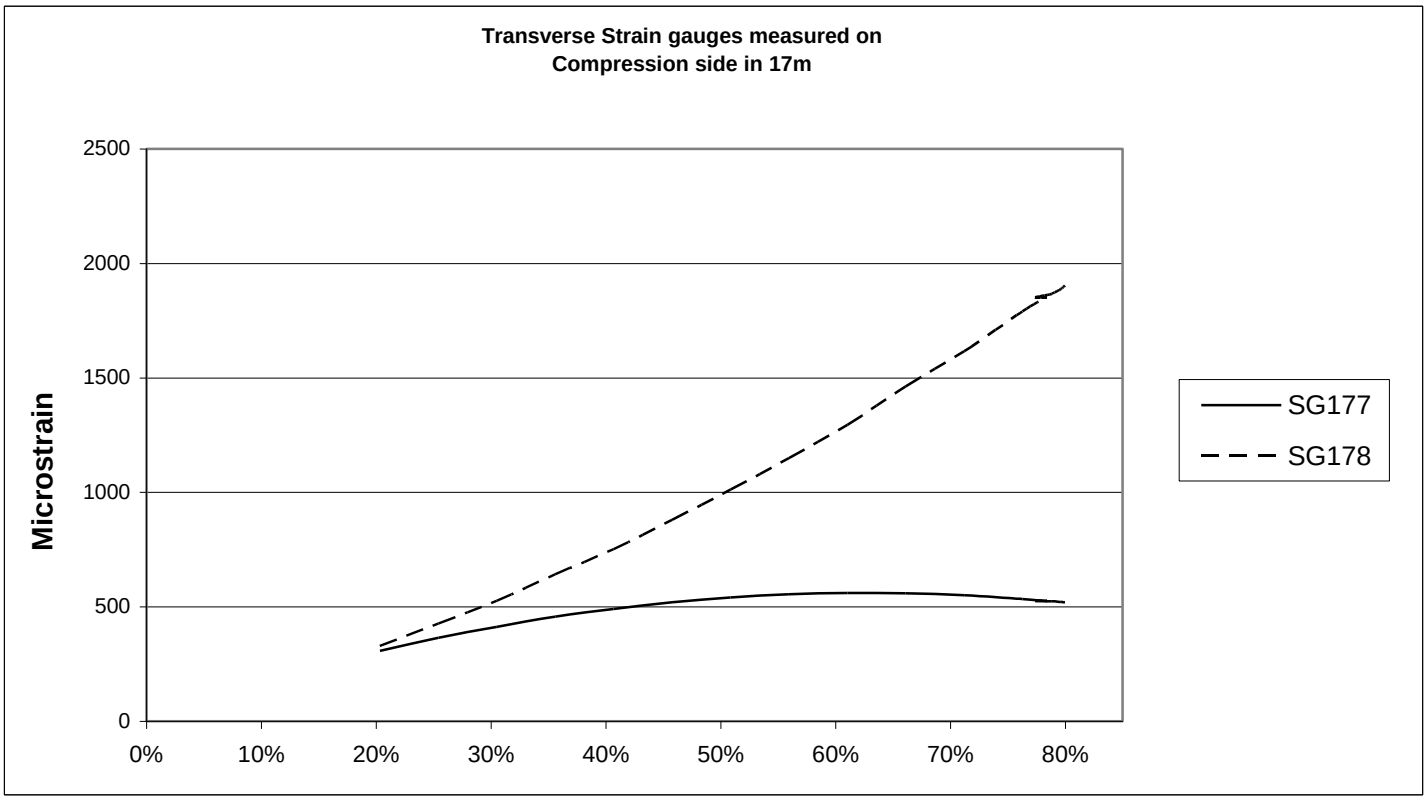
Transverse Strain gauges measured on
Compression side in 17m
Microstrain
2500
2000
1500
1000
500
0
0%
10%
20%
30%
40%
50%
60%
70%
80%
SG177
SG178

Graphs of Transverse Tension

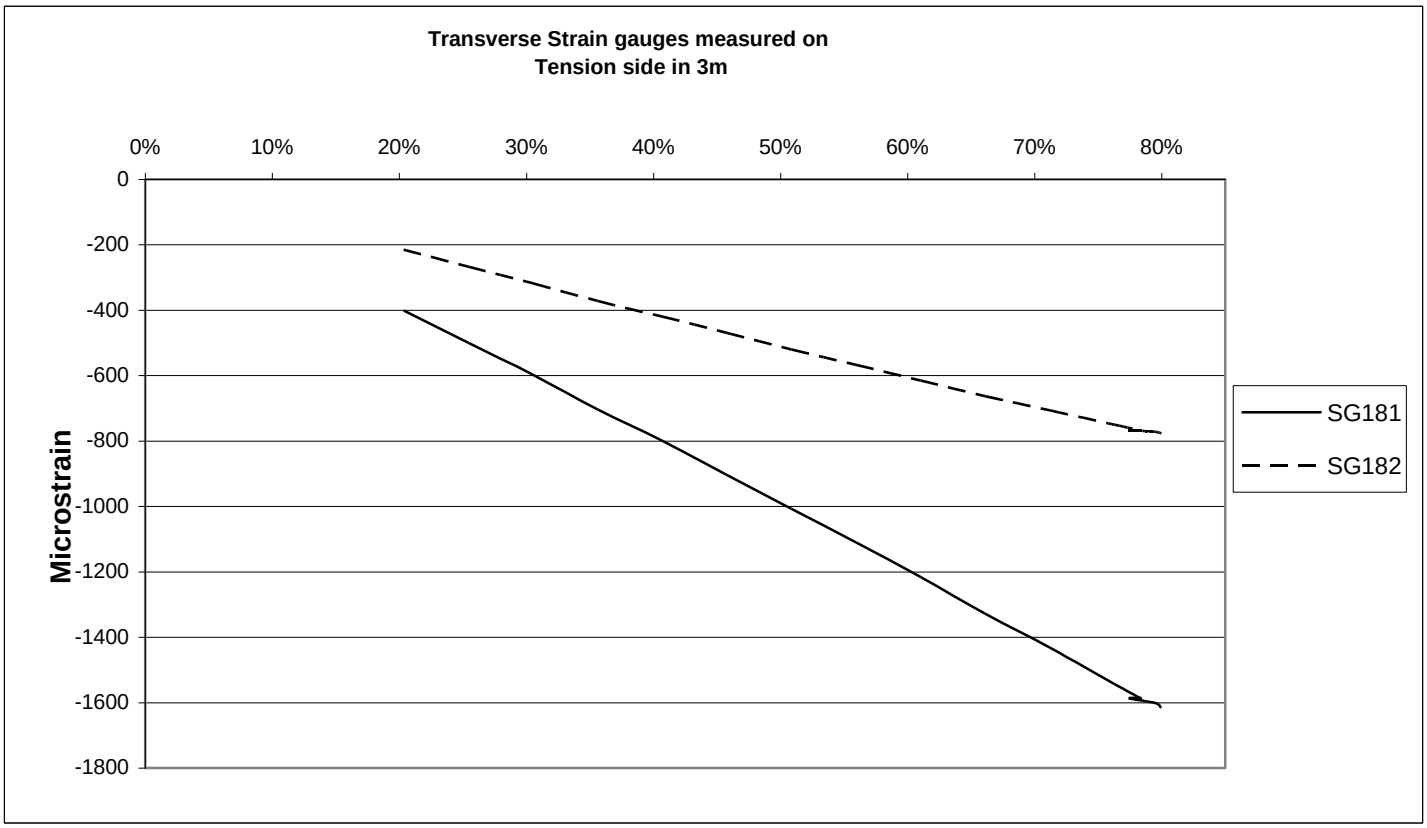

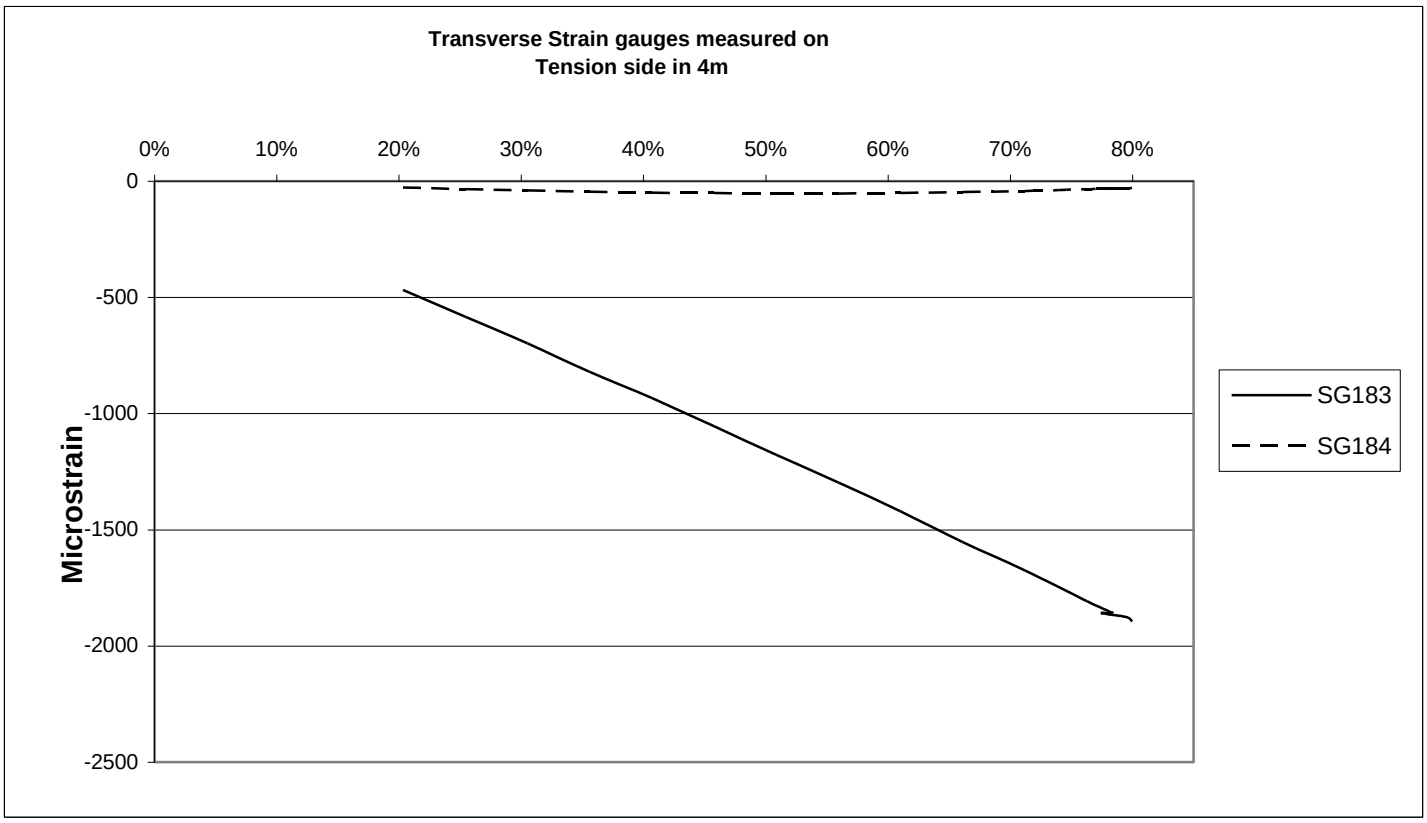

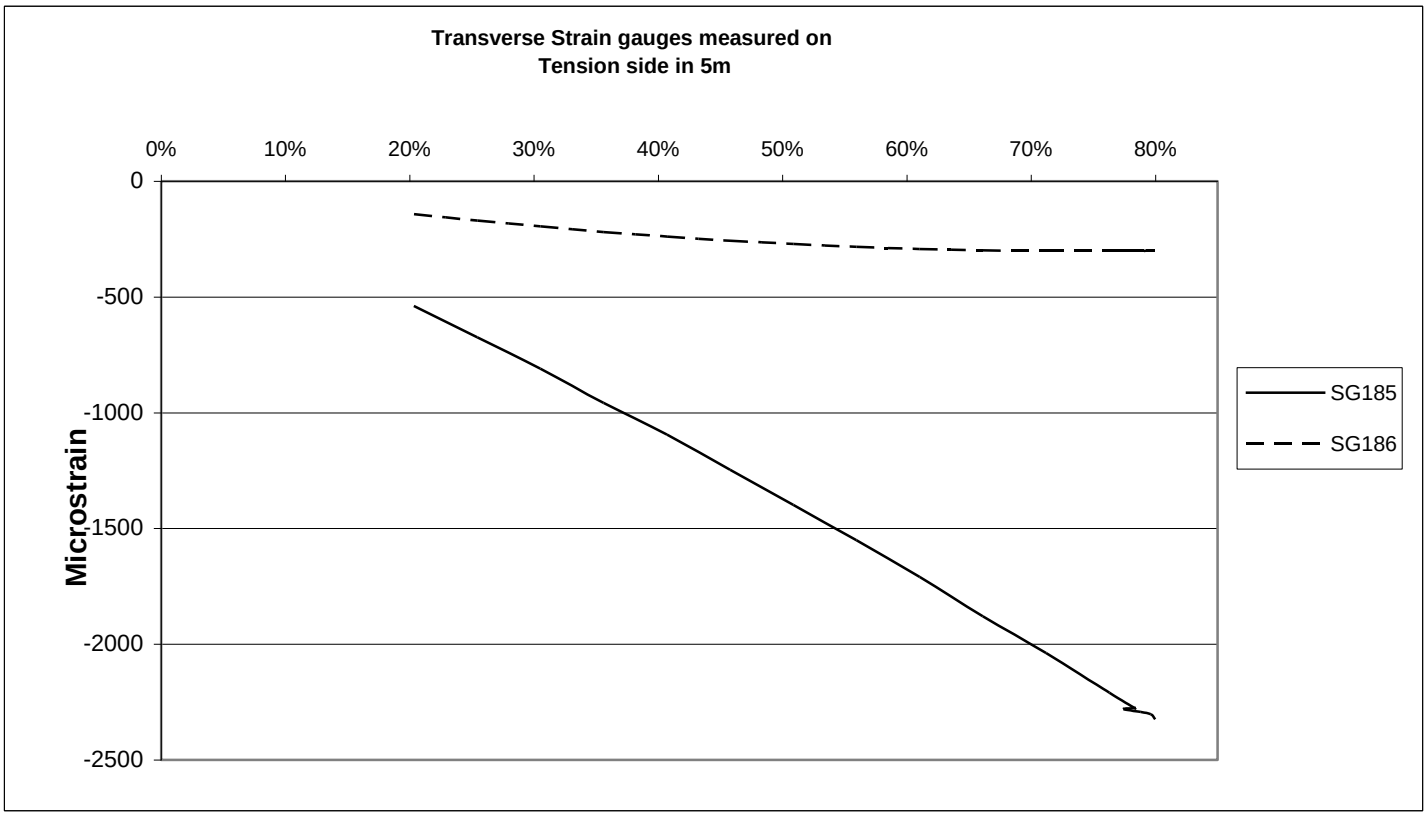
Transverse Strain gauges measured on
Tension side in 5m
0%
10%
20%
30%
40%
50%
60%
70%
80%
0
-500
-1000
-1500
-2000
-2500
Microstrain
SG185
SG186

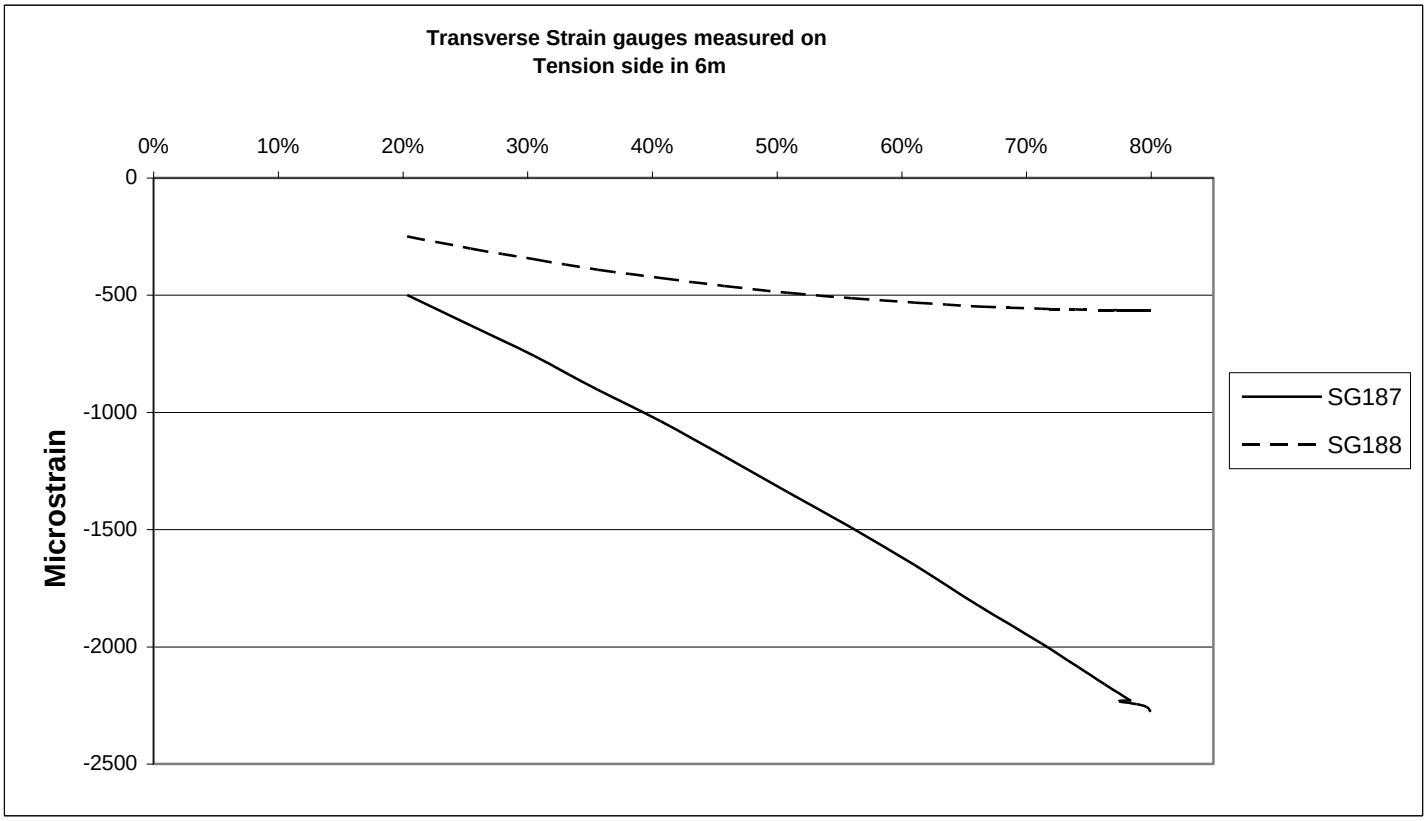
Transverse Strain gauges measured on
Tension side in 6m
0%
10%
20%
30%
40%
50%
60%
70%
80%
0
-500
-1000
-1500
-2000
-2500
Microstrain
SG187
SG188

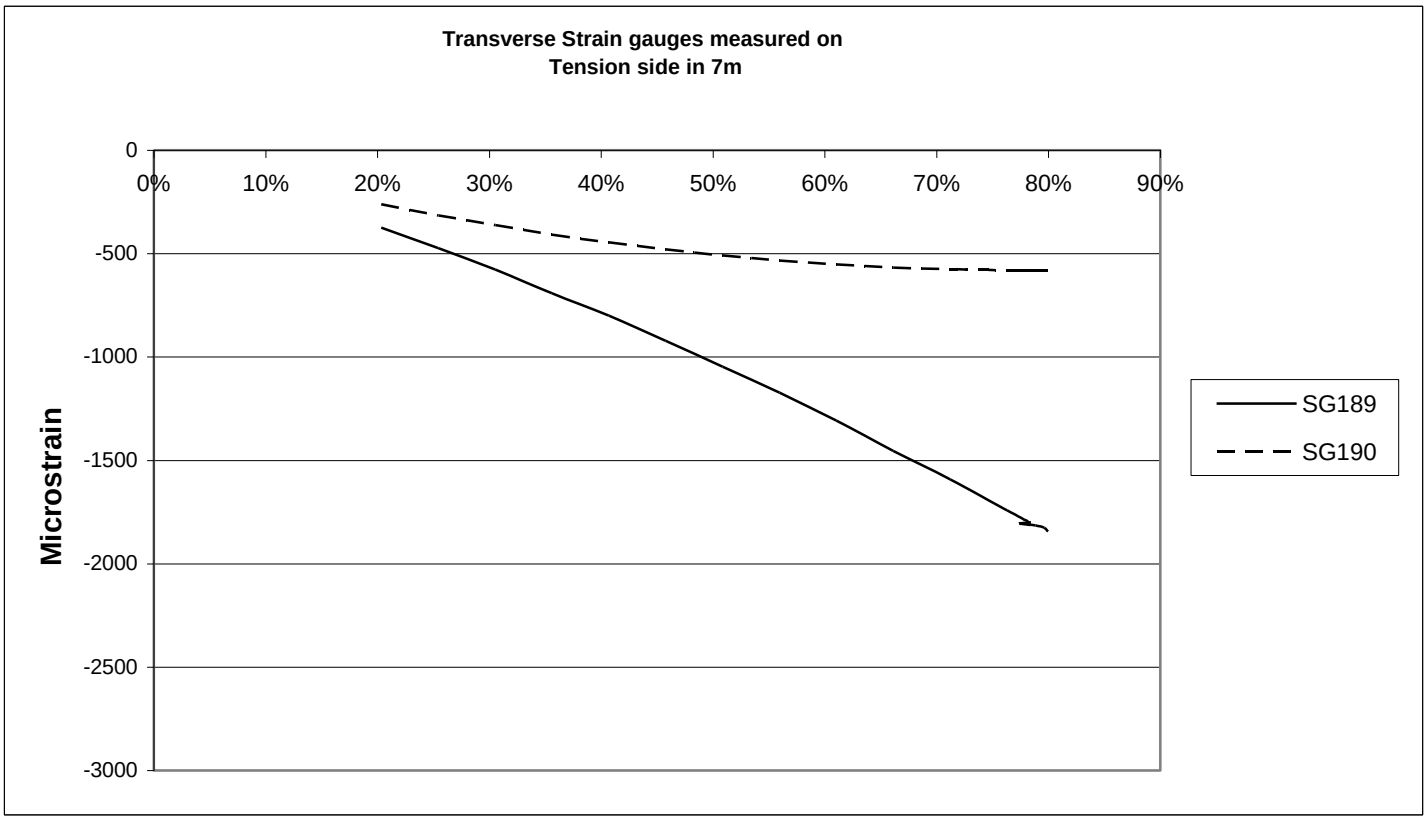
Transverse Strain gauges measured on
Tension side in 7m
0
0%
10%
20%
30%
40%
50%
60%
70%
80%
90%
-500
-1000
-1500
-2000
-2500
-3000
Microstrain
SG189
SG190

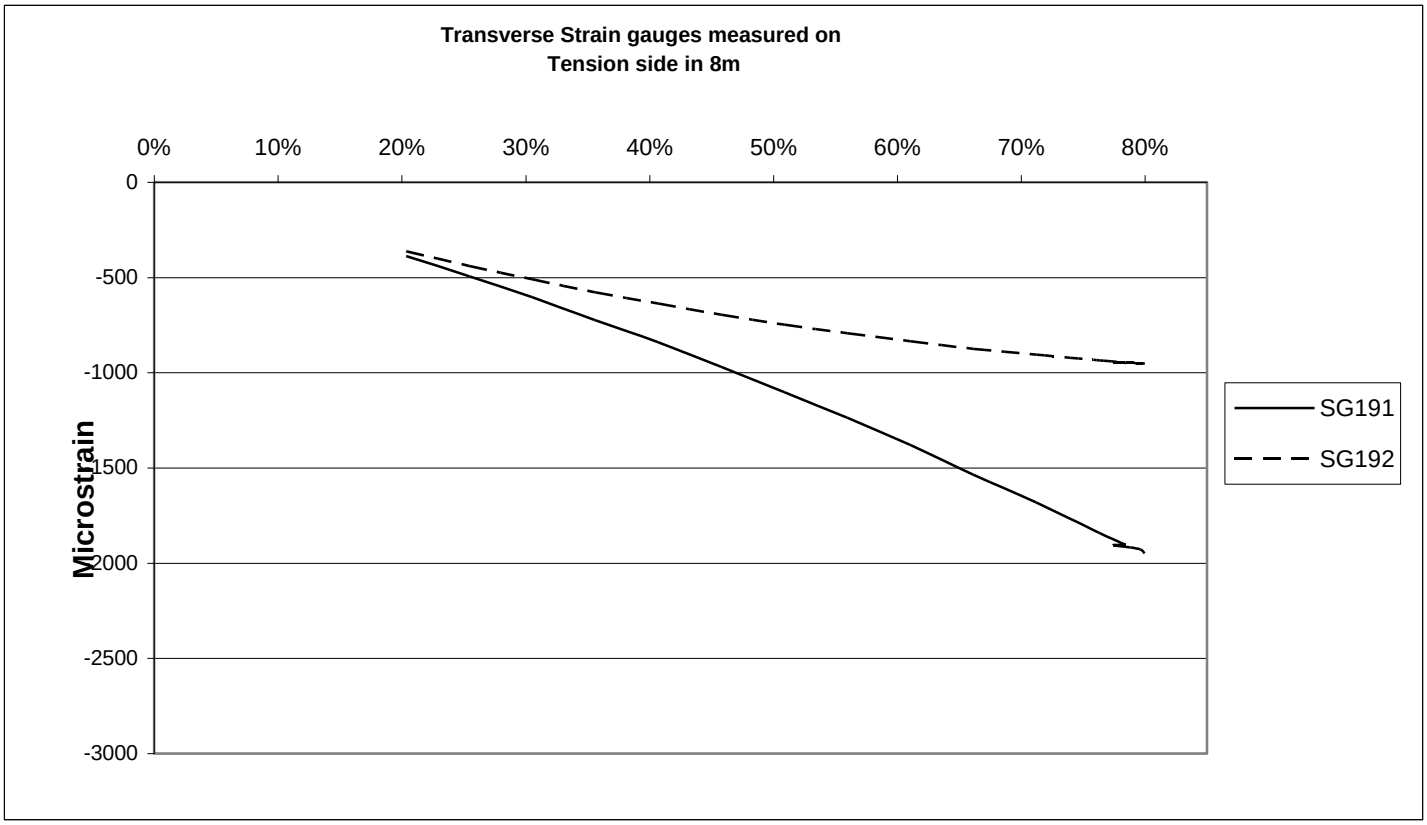
Transverse Strain gauges measured on
Tension side in 8m
0%
10%
20%
30%
40%
50%
60%
70%
80%
0
-500
-1000
-1500
-2000
-2500
-3000
Microstrain
SG191
SG192

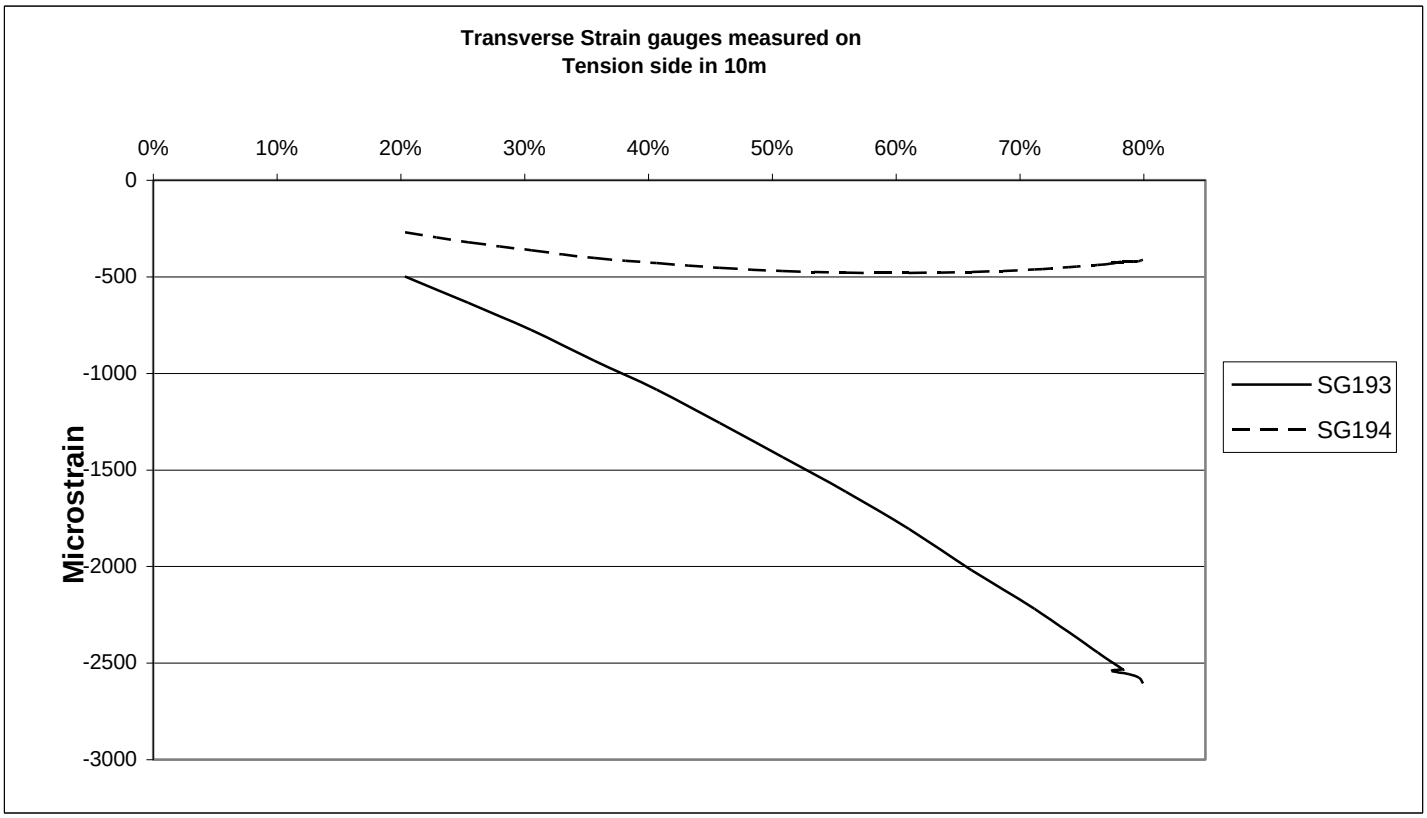
Transverse Strain gauges measured on
Tension side in 10m
0%
10%
20%
30%
40%
50%
60%
70%
80%
0
-500
-1000
-1500
-2000
-2500
-3000
Microstrain
SG193
SG194

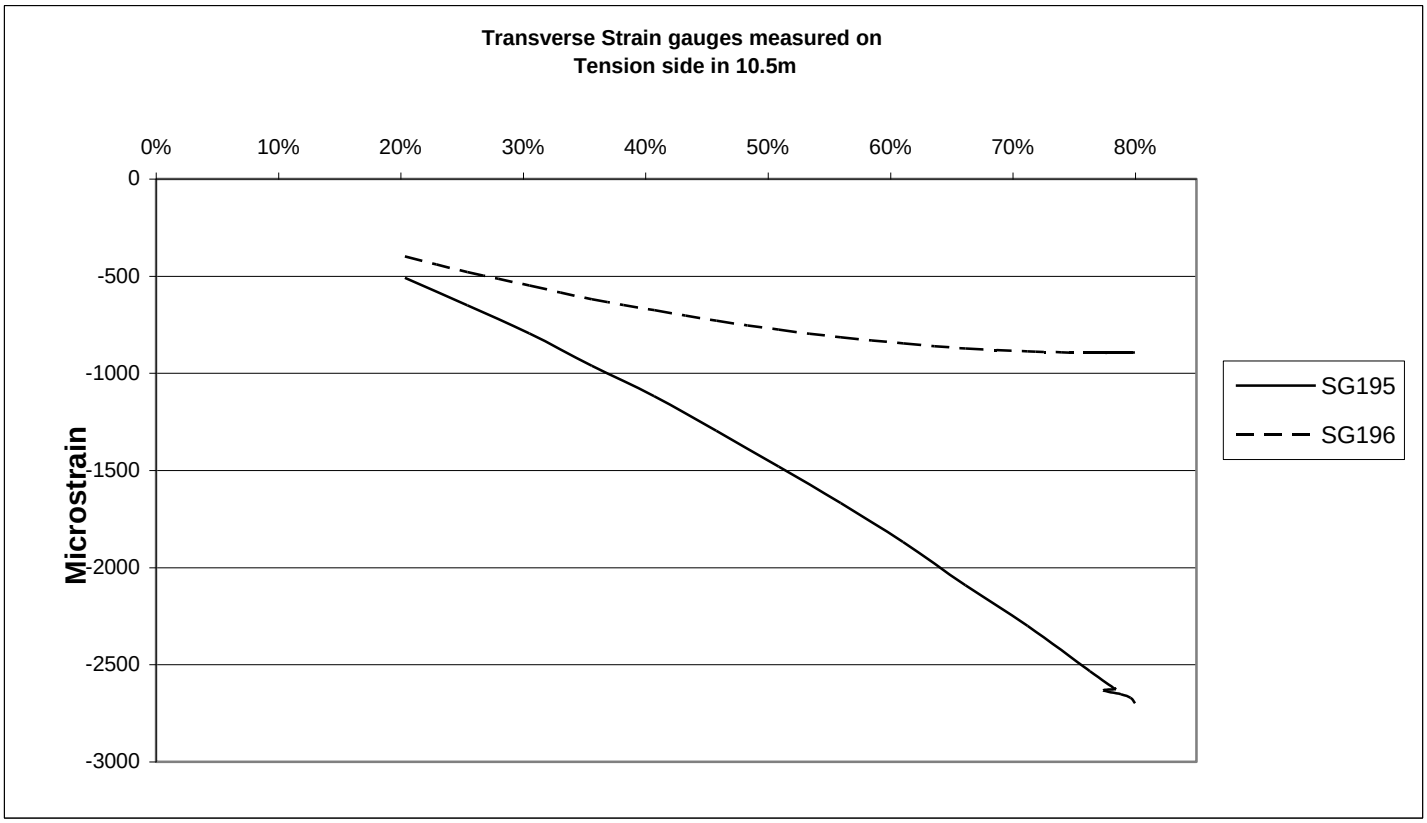
Transverse Strain gauges measured on
Tension side in 10.5m
0%
10%
20%
30%
40%
50%
60%
70%
80%
0
-500
-1000
-1500
-2000
-2500
-3000
Microstrain
SG195
SG196

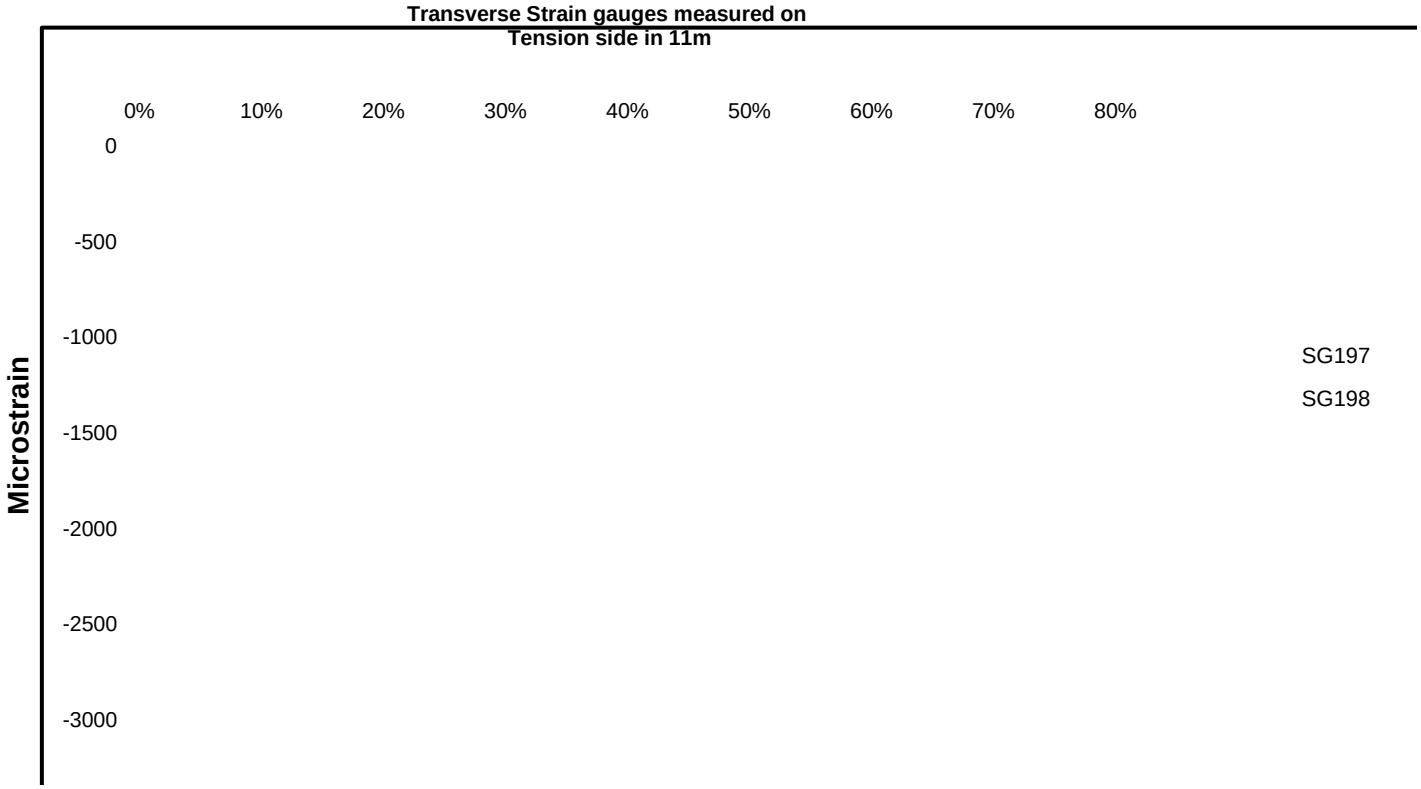
Transverse Strain gauges measured on
Tension side in 11m
0%
10%
20%
30%
40%
50%
60%
70%
80%
0
-500
-1000
-1500
-2000
-2500
-3000
Microstrain
SG197
SG198

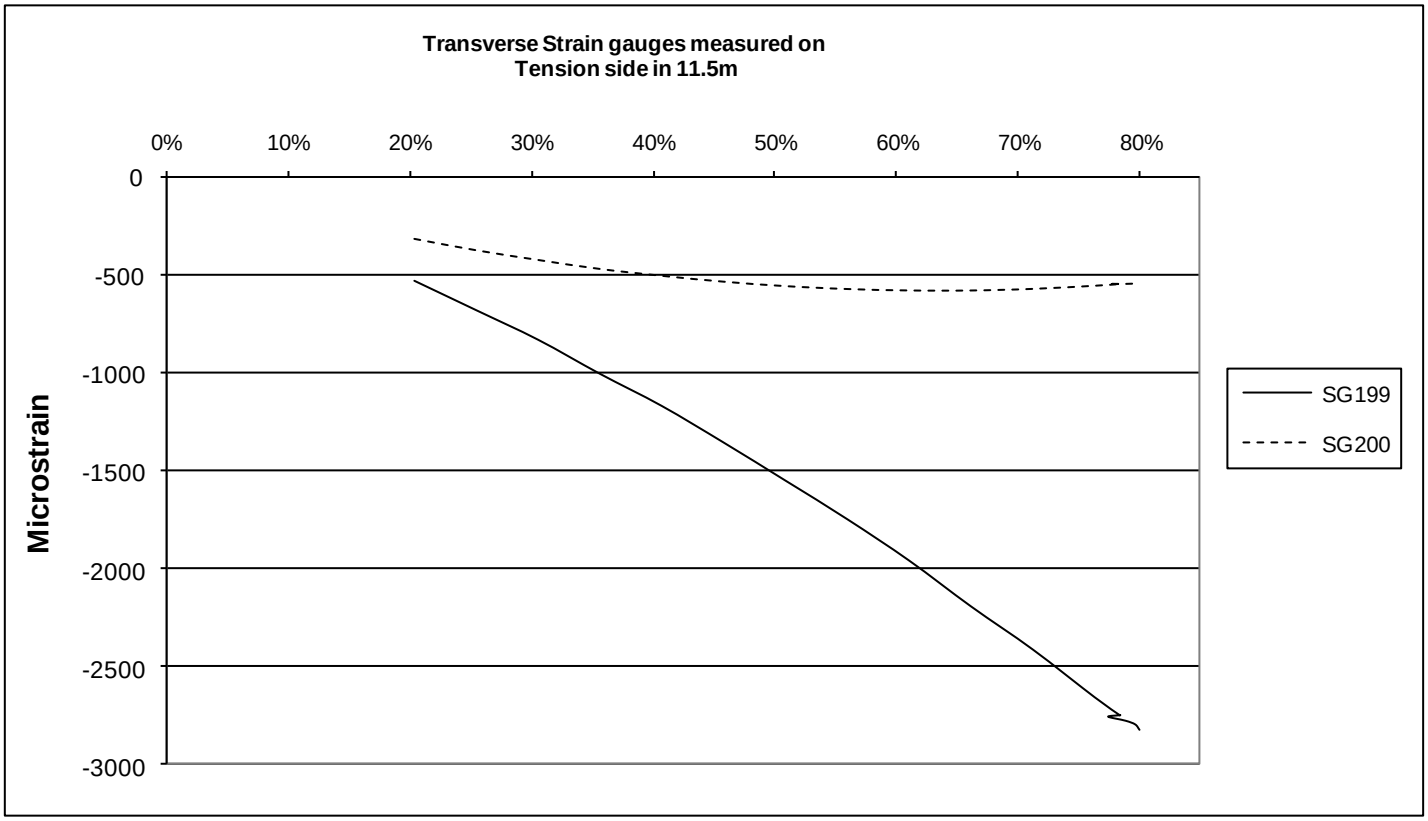
Transverse Strain gauges measured on
Tension side in 11.5m
0%
10%
20%
30%
40%
50%
60%
70%
80%
0
-500
-1000
-1500
-2000
-2500
-3000
Microstrain
SG199
SG200

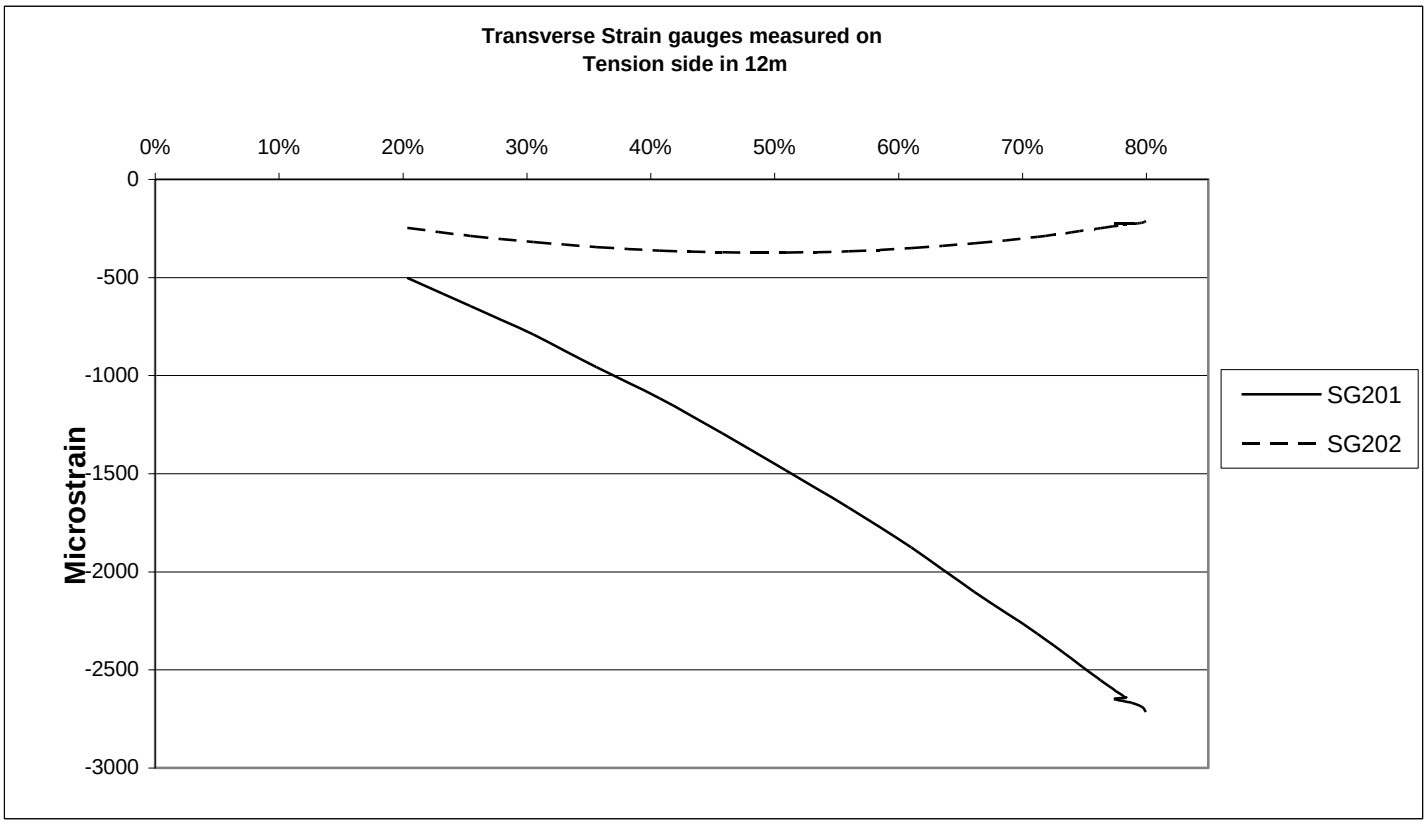
Transverse Strain gauges measured on
Tension side in 12m
0%
10%
20%
30%
40%
50%
60%
70%
80%
0
-500
-1000
-1500
-2000
-2500
-3000
Microstrain
SG201
SG202

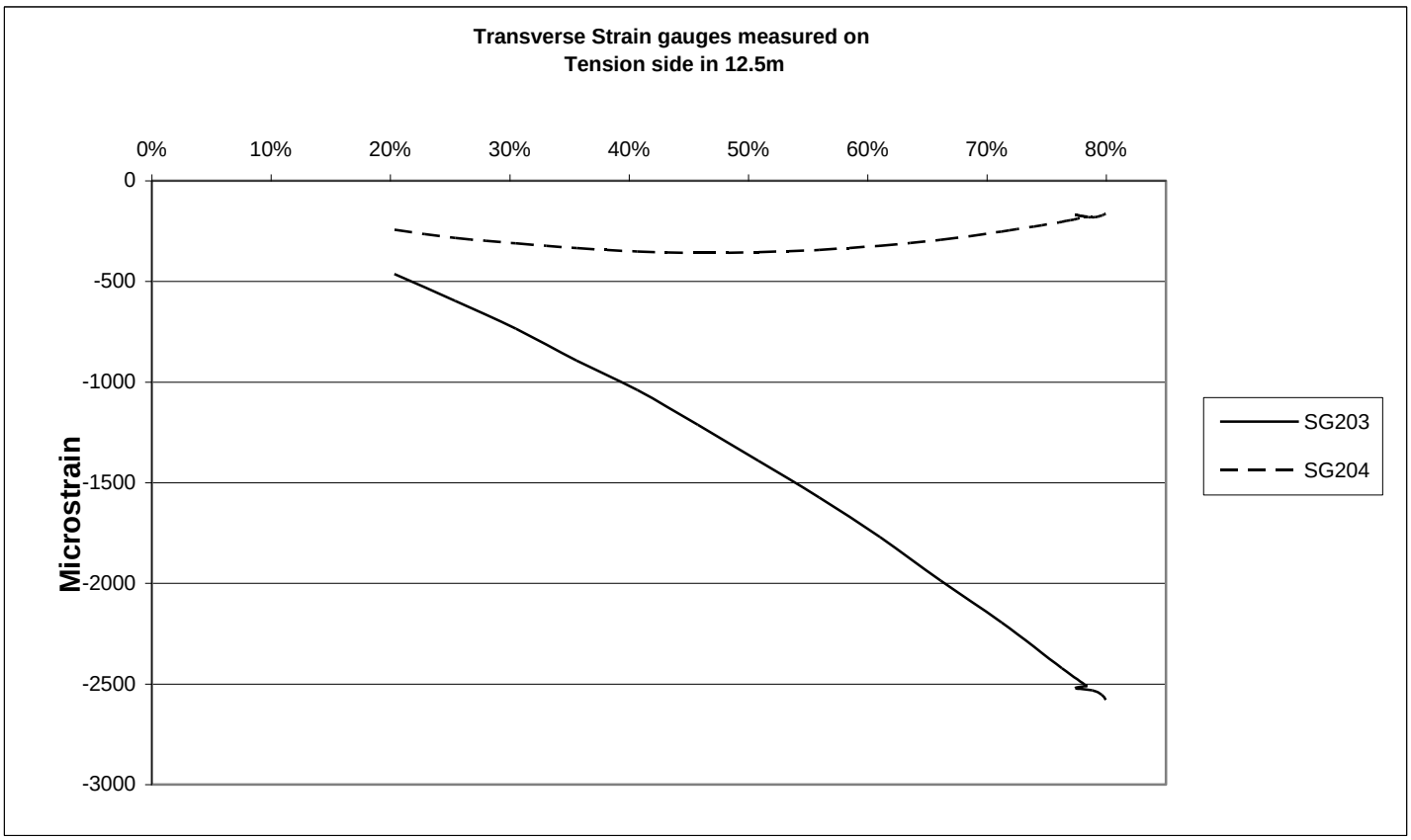
Transverse Strain gauges measured on
Tension side in 12.5m
0%
10%
20%
30%
40%
50%
60%
70%
80%
0
-500
-1000
-1500
-2000
-2500
-3000
Microstrain
SG203
SG204

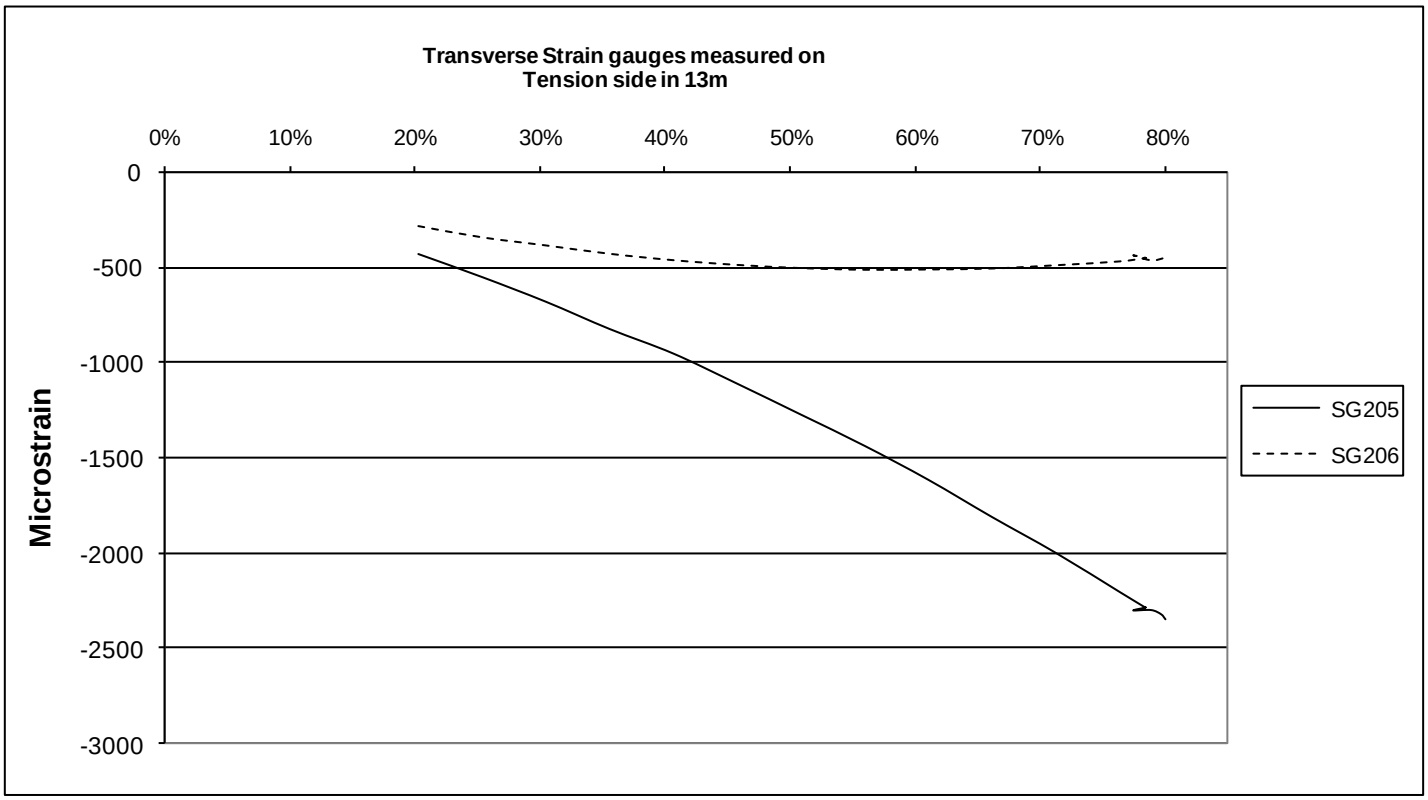

Graphs of Tophat Longitudinal Strain Gauges

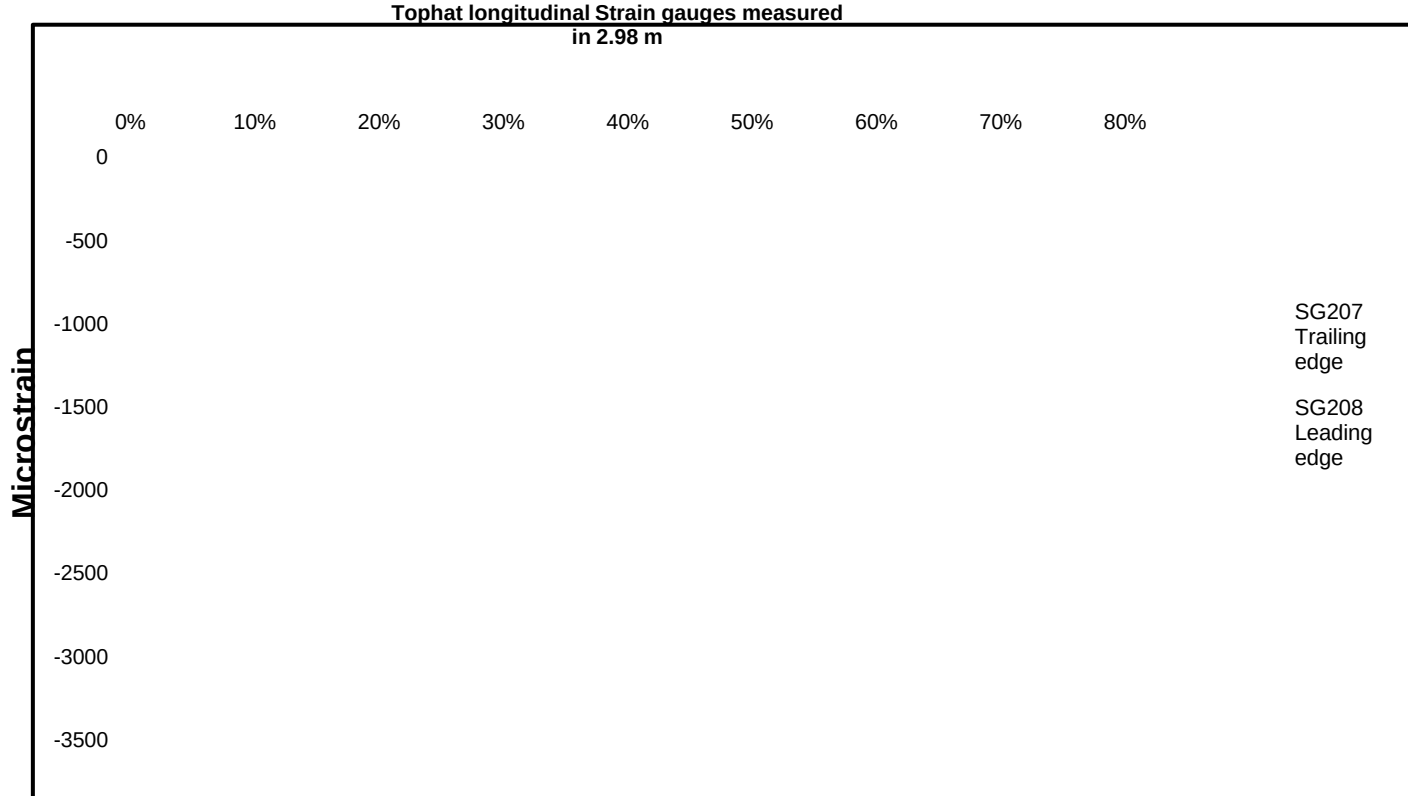

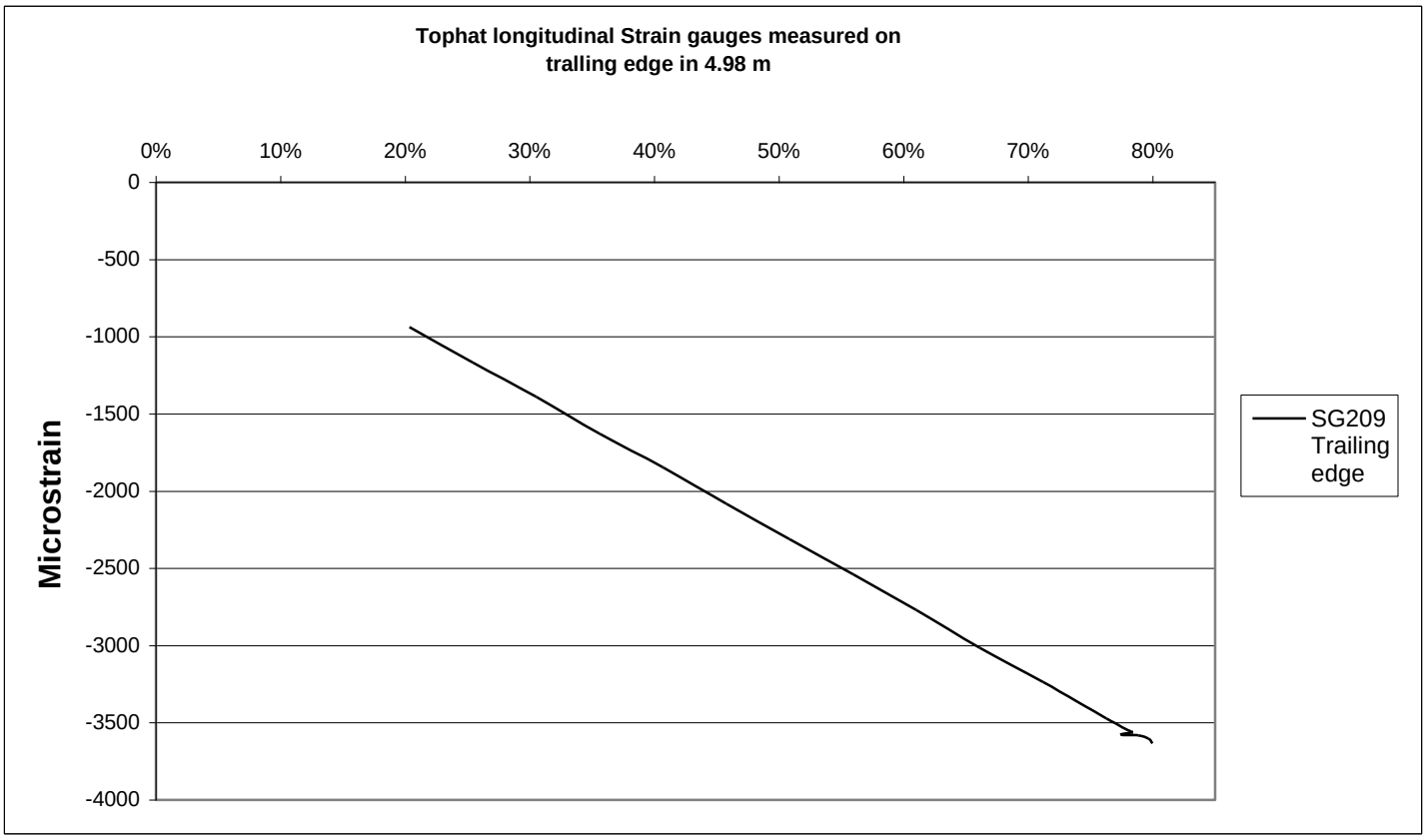
Tophat longitudinal Strain gauges measured on tralling edge in 4.98 m
0%
10%
20%
30%
40%
50%
60%
70%
80%
0
-500
-1000
-1500
-2000
-2500
-3000
-3500
-4000
Microstrain
SG209 Trailing edge

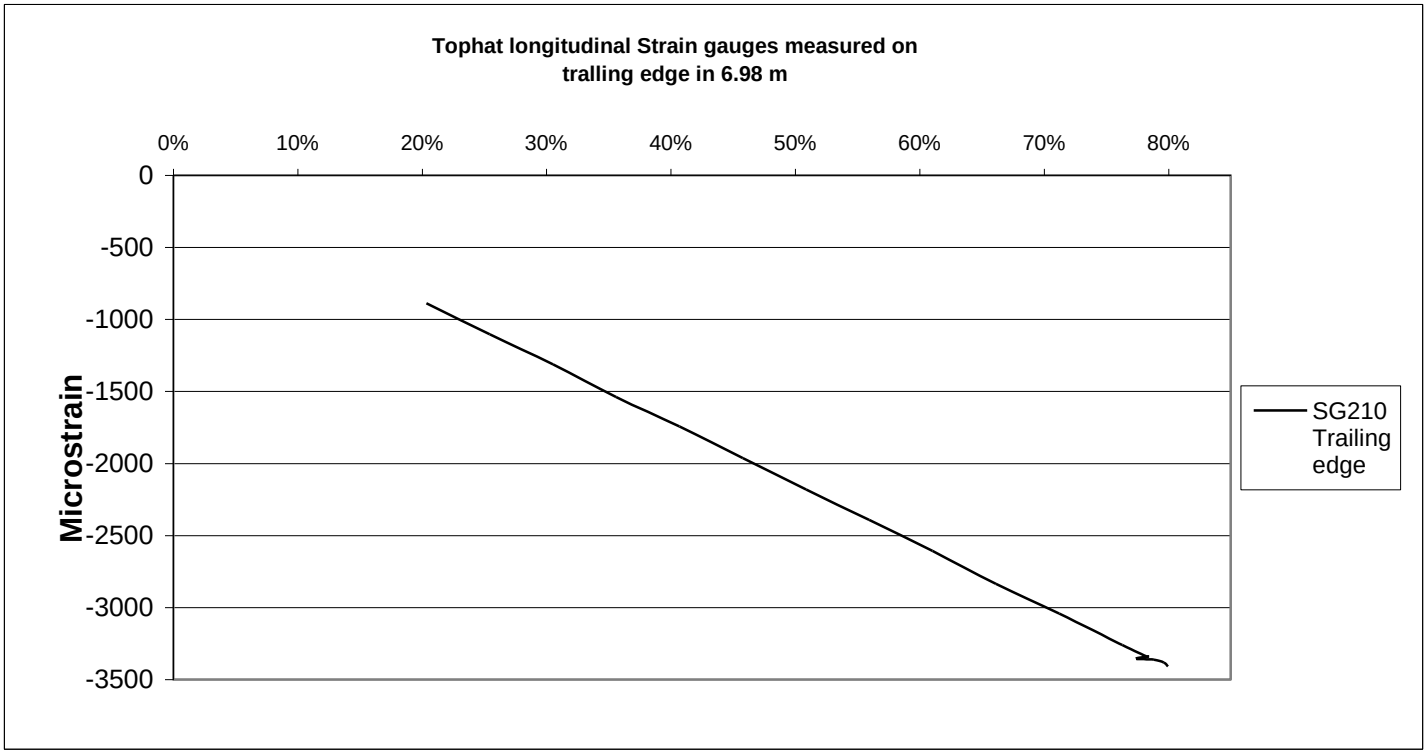
Tophat longitudinal Strain gauges measured on tralling edge in 6.98 m
0%
10%
20%
30%
40%
50%
60%
70%
80%
0
-500
-1000
-1500
-2000
-2500
-3000
-3500
Microstrain
SG210 Trailing edge

Graphs of Tophat 45º Strain Gauges

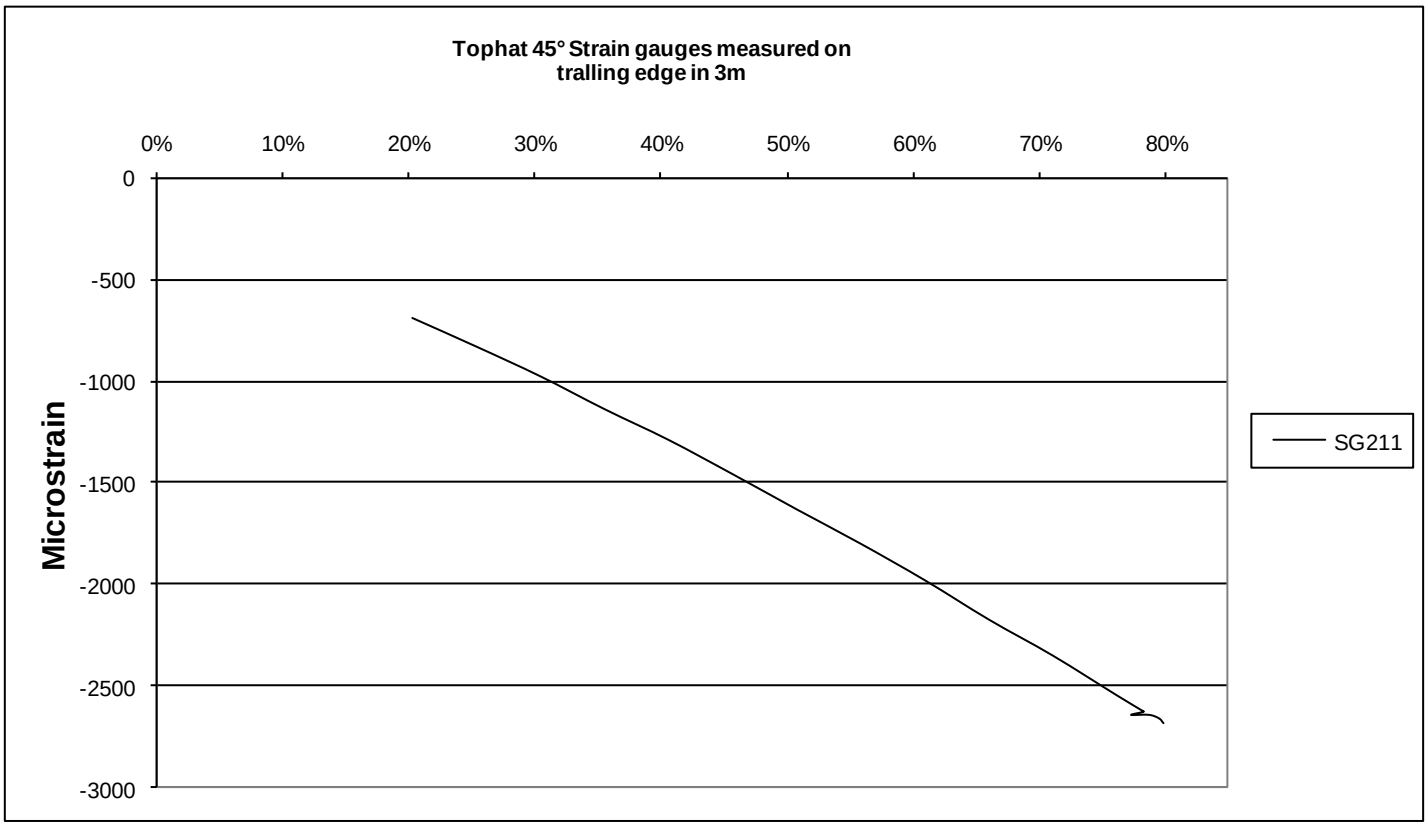

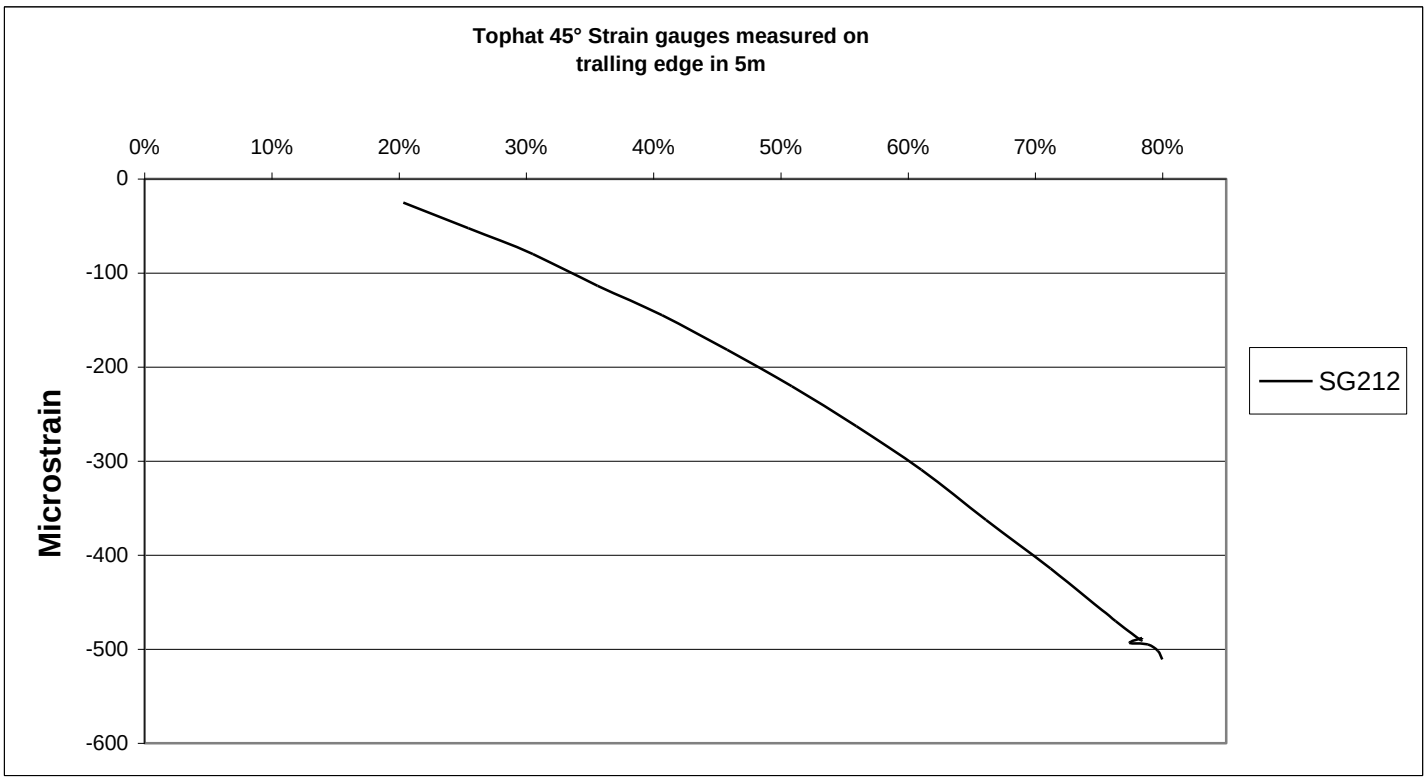

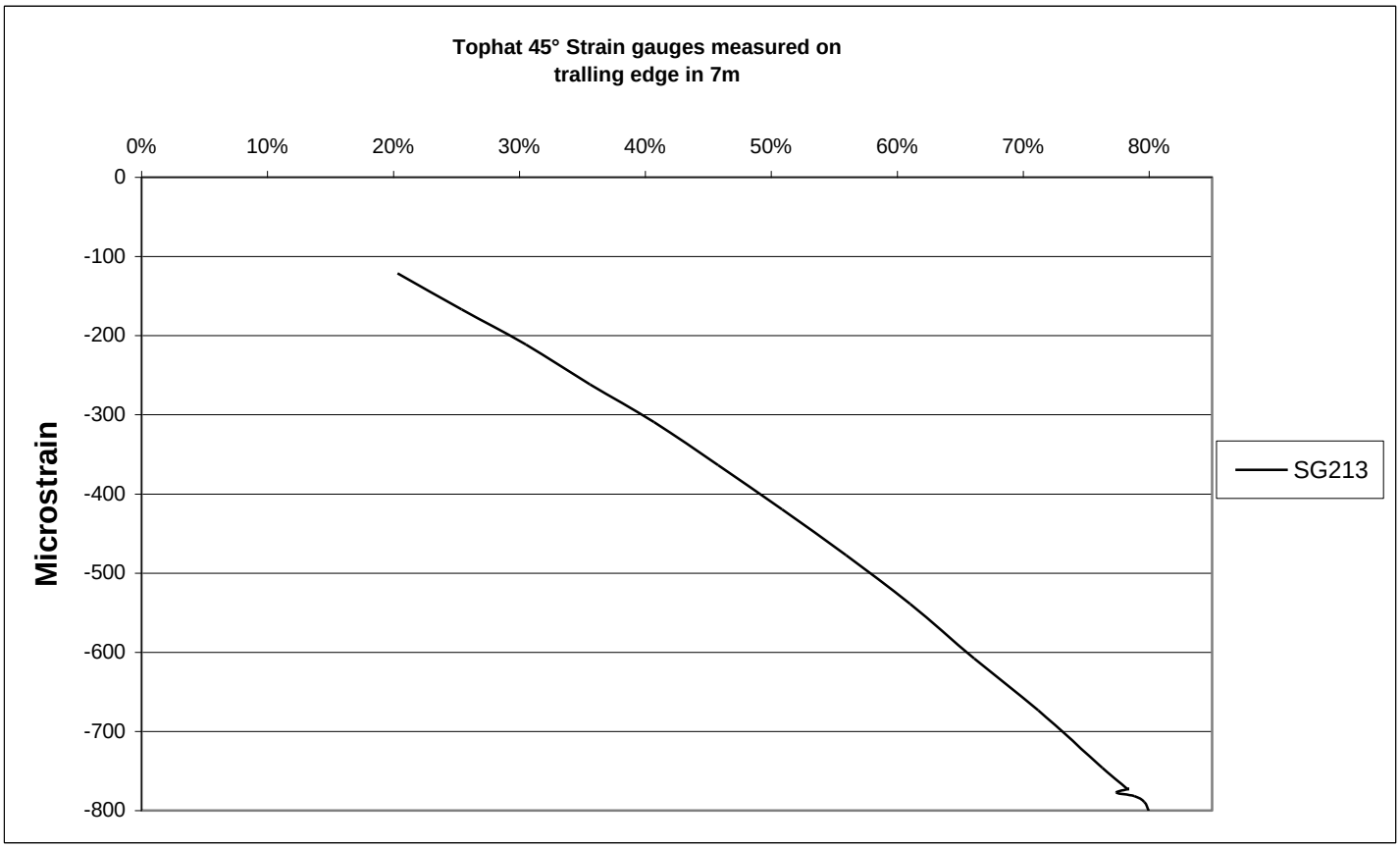

Graphs of 90º SG Strain

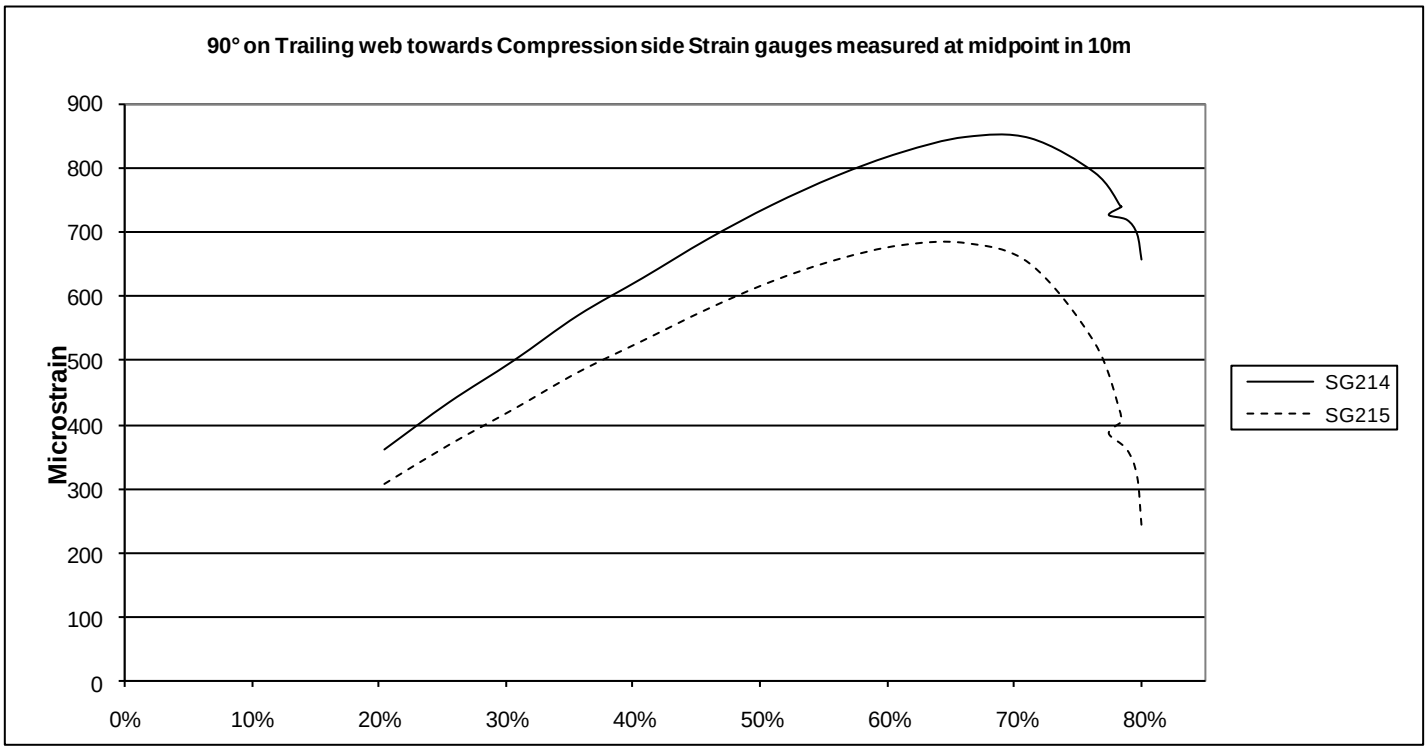

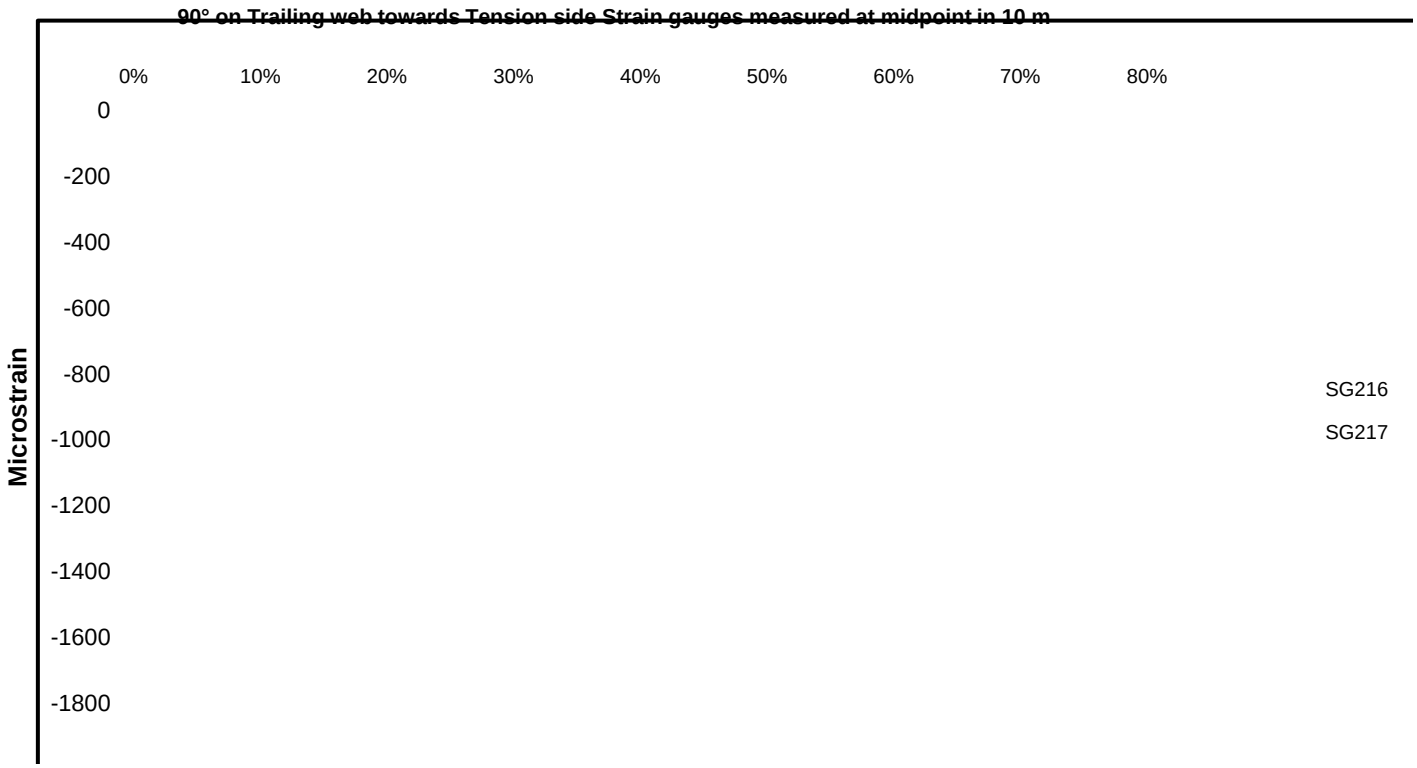
90° on Trailing web towards Tension side Strain gauges measured at midpoint in 10 m
0%
10%
20%
30%
40%
50%
60%
70%
80%
0
-200
-400
-600
-800
-1000
-1200
-1400
-1600
-1800
Microstrain
SG216
SG217

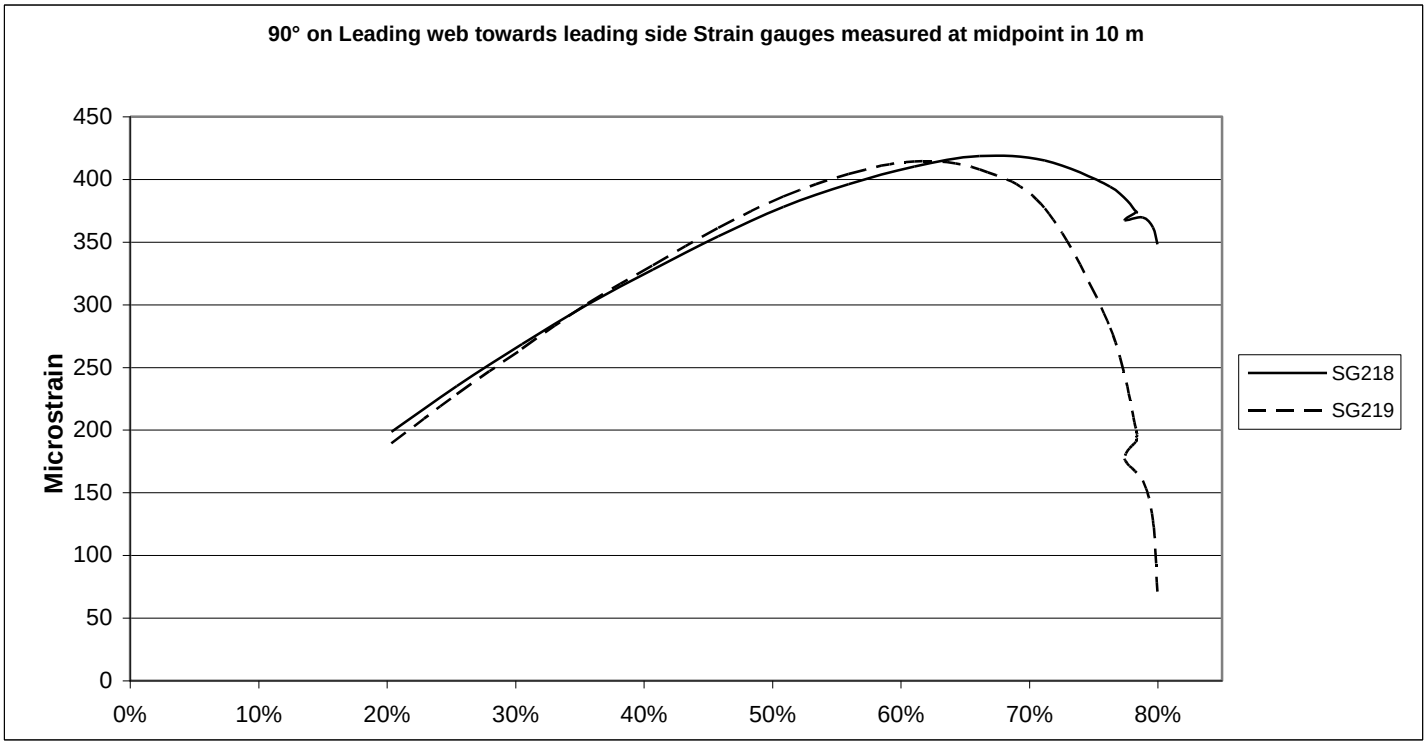
90° on Leading web towards leading side Strain gauges measured at midpoint in 10 m
450
400
350
300
250
200
150
100
50
0
0%
10%
20%
30%
40%
50%
60%
70%
80%
Microstrain
SG218
SG219


90° on Trailing web towards Tension side Strain gauges measured at midpoint in 10m
0%
10%
20%
30%
40%
50%
60%
70%
80%
0
-200
-400
-600
-800
-1000
-1200
-1400
-1600
-1800
Microstrain
SG220
SG221

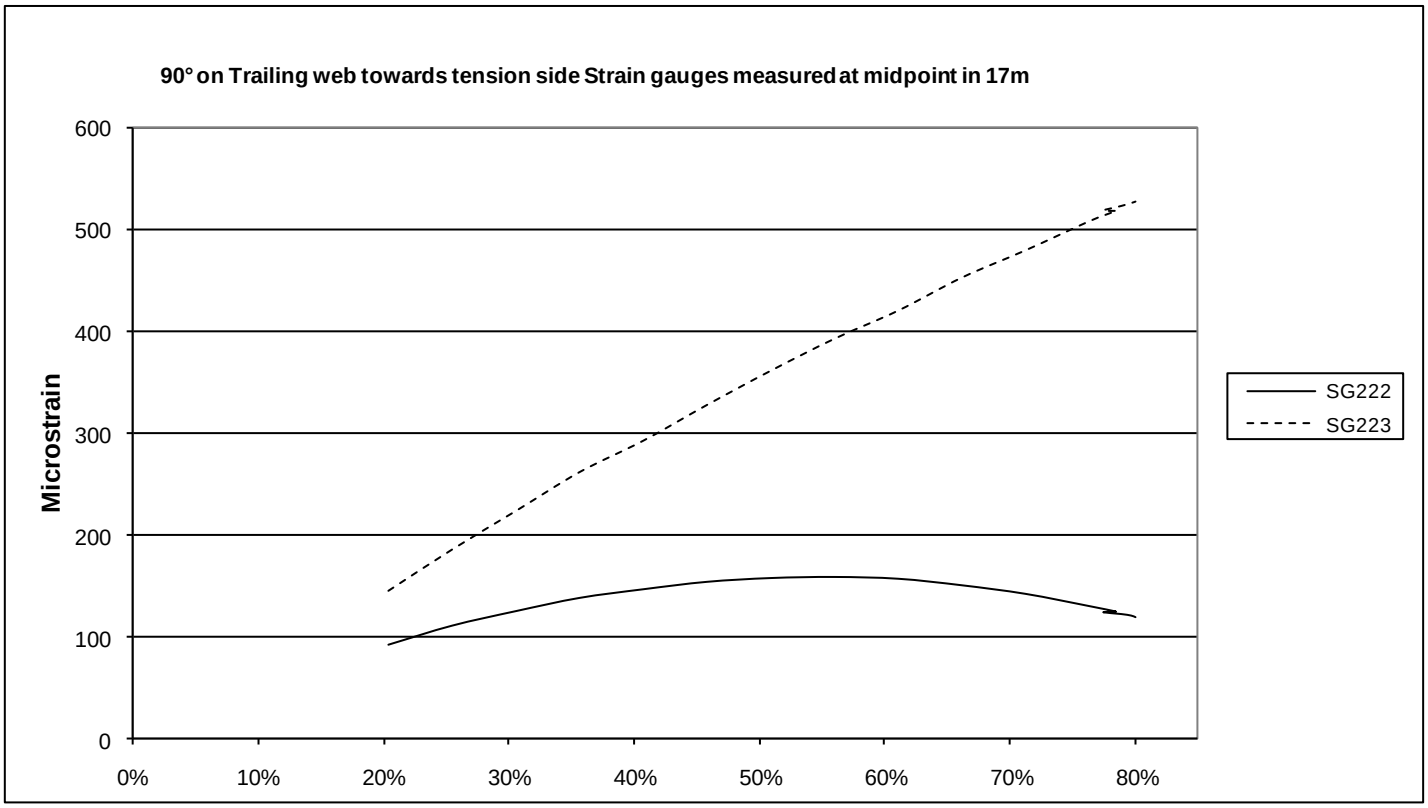
90° on Trailing web towards tension side Strain gauges measured at midpoint in 17m
600
500
400
300
200
100
0
0%
10%
20%
30%
40%
50%
60%
70%
80%
Microstrain
SG222
SG223

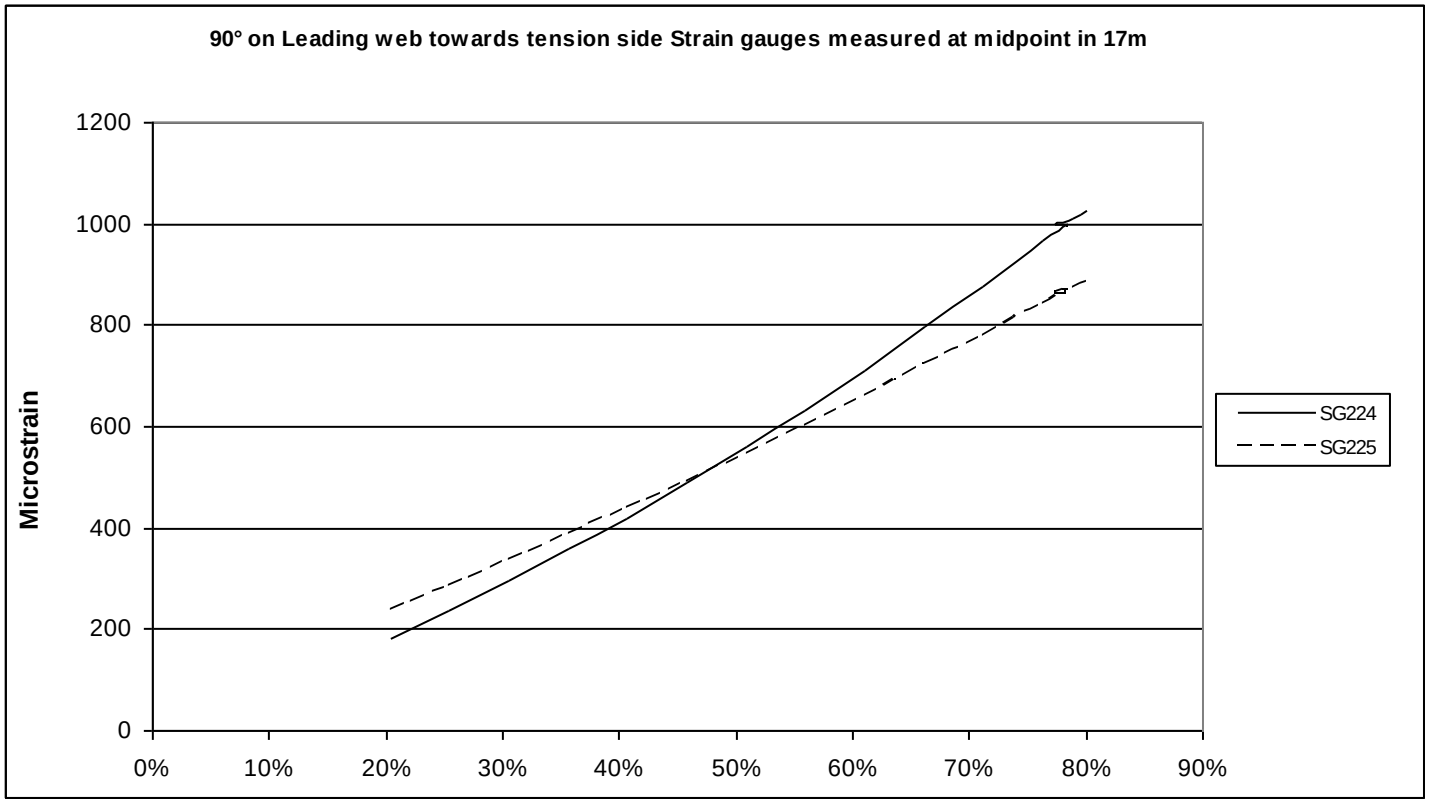

45° Strain Gauges on Trailing web towards Tension side Measurements

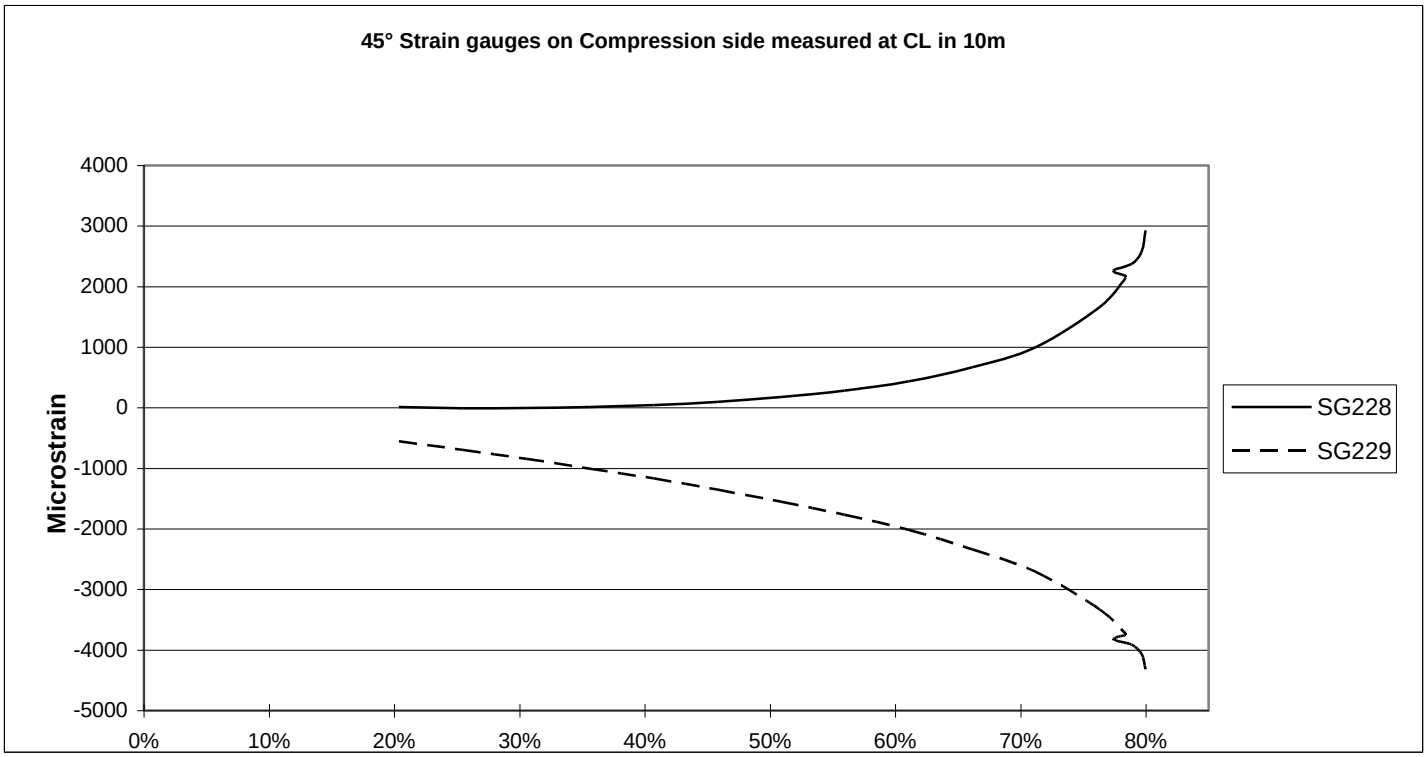

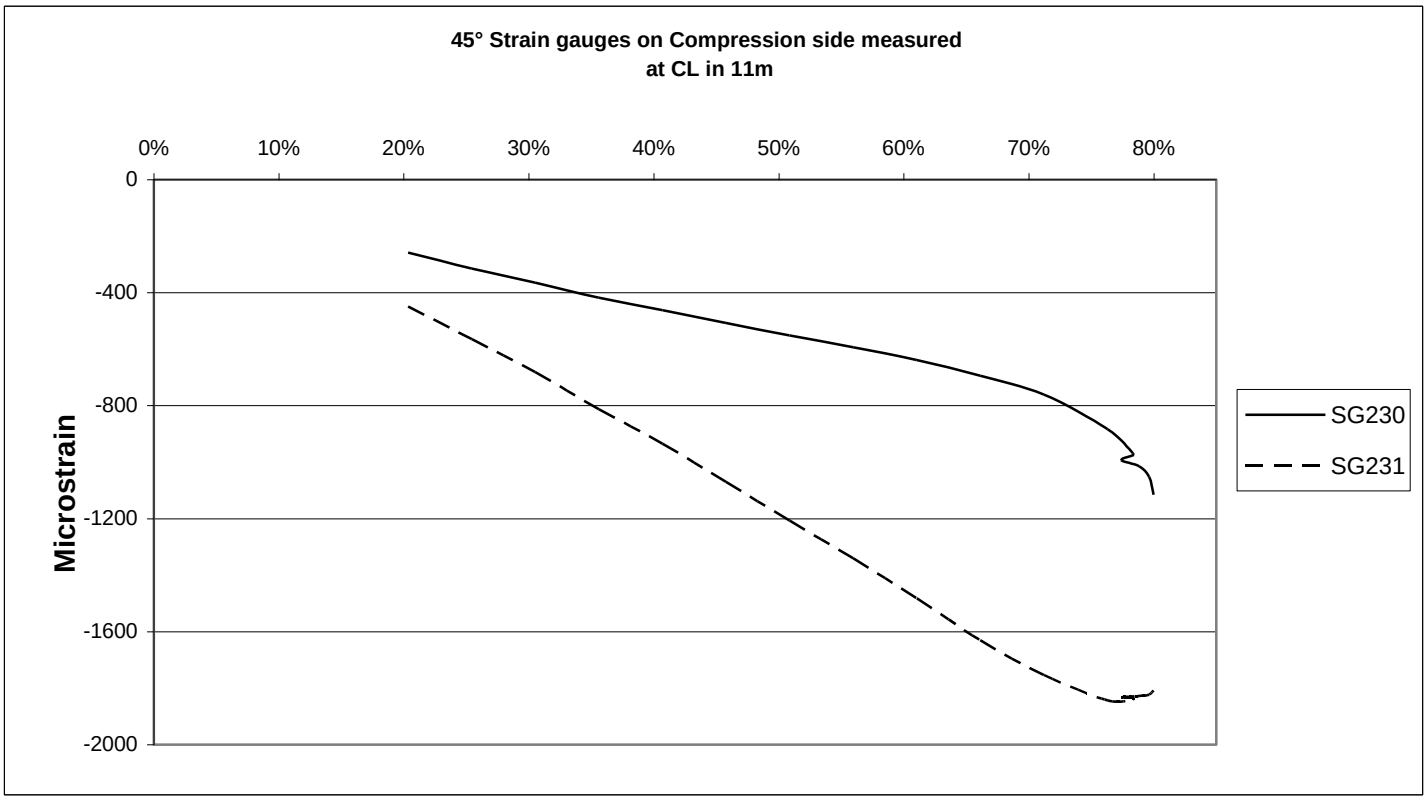
45° Strain gauges on Compression side measured
at CL in 11m
0%
10%
20%
30%
40%
50%
60%
70%
80%
0
-400
-800
-1200
-1600
-2000
Microstrain
SG230
SG231

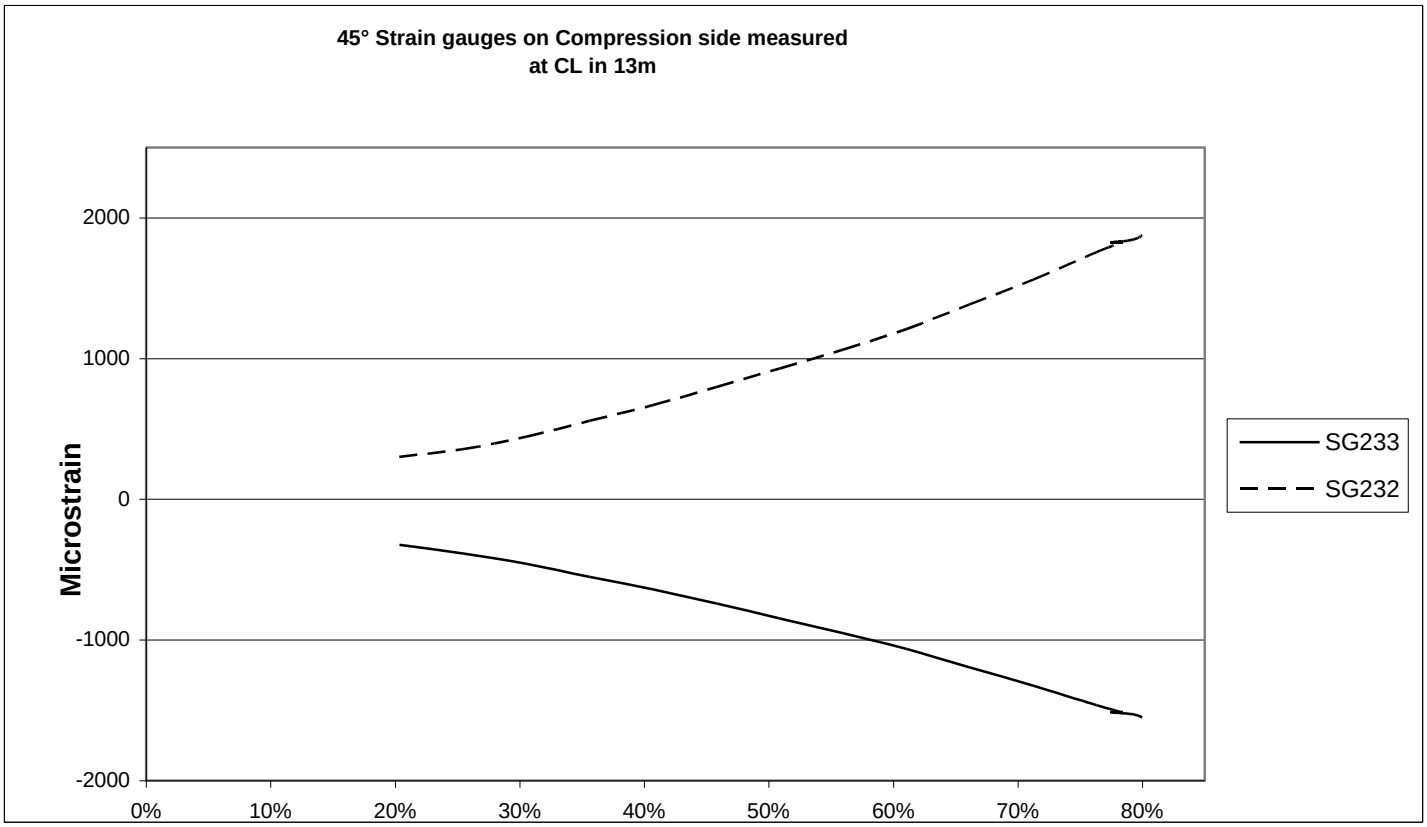
45° Strain gauges on Compression side measured
at CL in 13m
2000
1000
0
-1000
-2000
0%
10%
20%
30%
40%
50%
60%
70%
80%
Microstrain
SG233
SG232

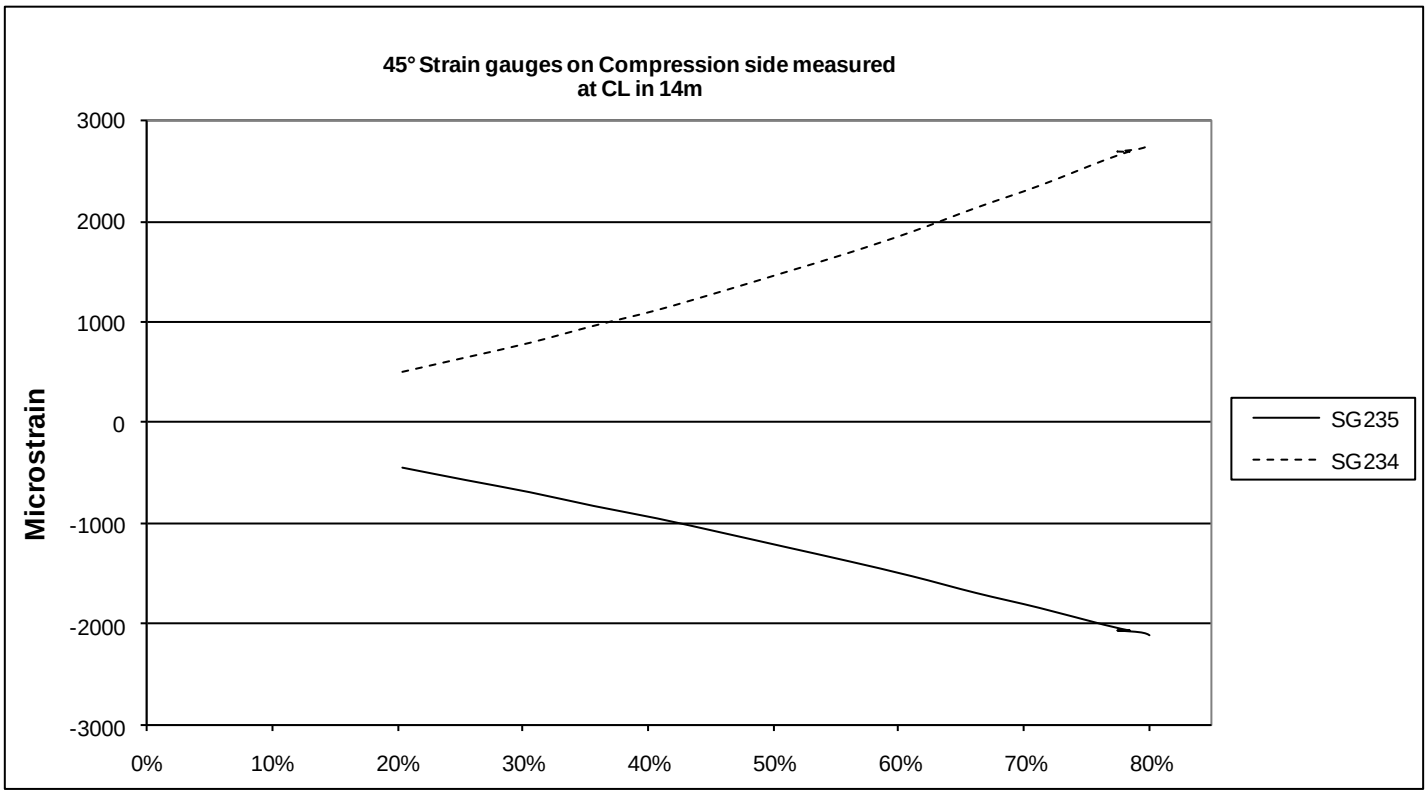
45° Strain gauges on Compression side measured
at CL in 14m
Microstrain
3000
2000
1000
0
-1000
-2000
-3000
0%
10%
20%
30%
40%
50%
60%
70%
80%
SG235
SG234

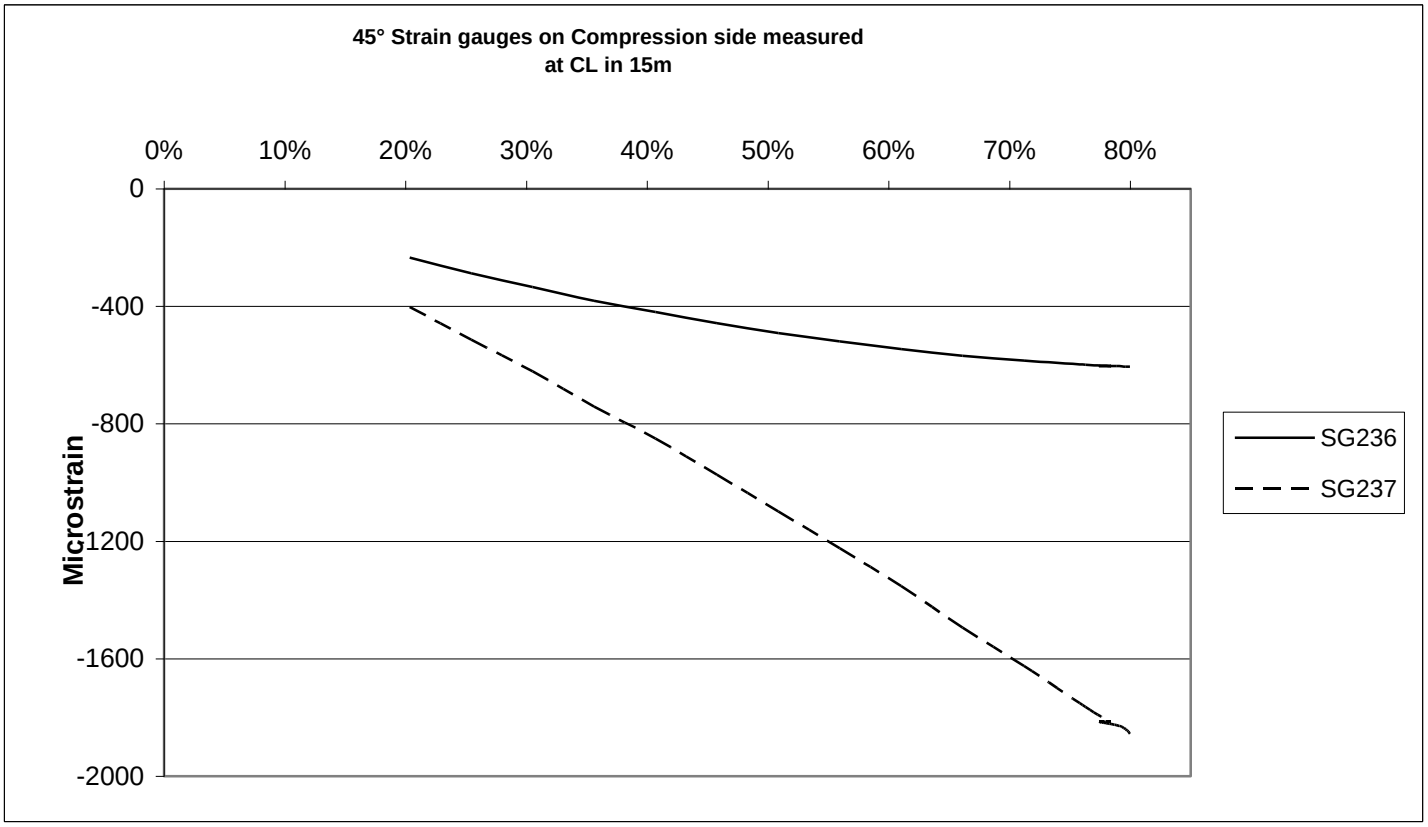
45° Strain gauges on Compression side measured
at CL in 15m
Microstrain
0%
10%
20%
30%
40%
50%
60%
70%
80%
0
-400
-800
-1200
-1600
-2000
SG236
SG237

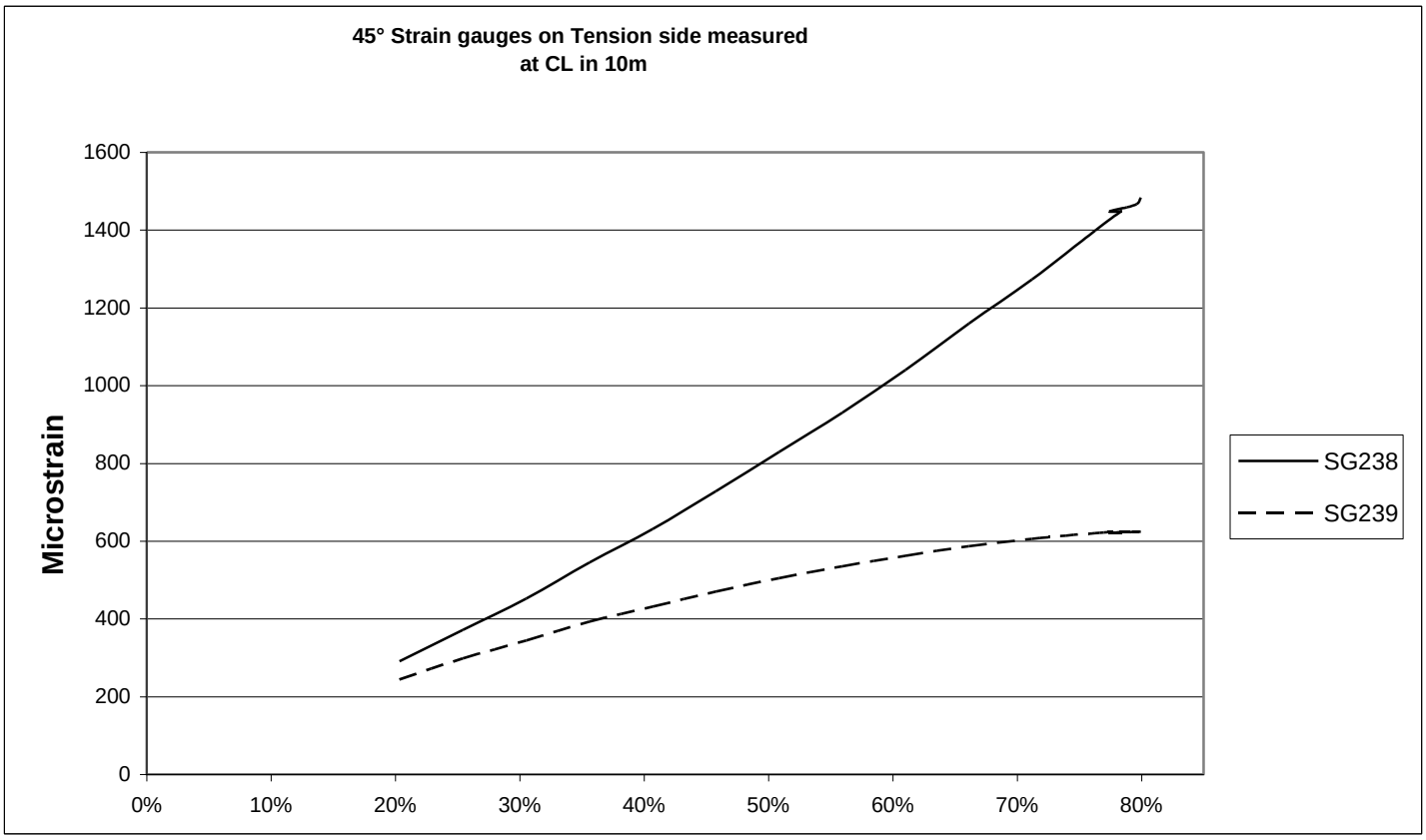
45° Strain gauges on Tension side measured
at CL in 10m
Microstrain
1600
1400
1200
1000
800
600
400
200
0
0%
10%
20%
30%
40%
50%
60%
70%
80%
SG238
SG239

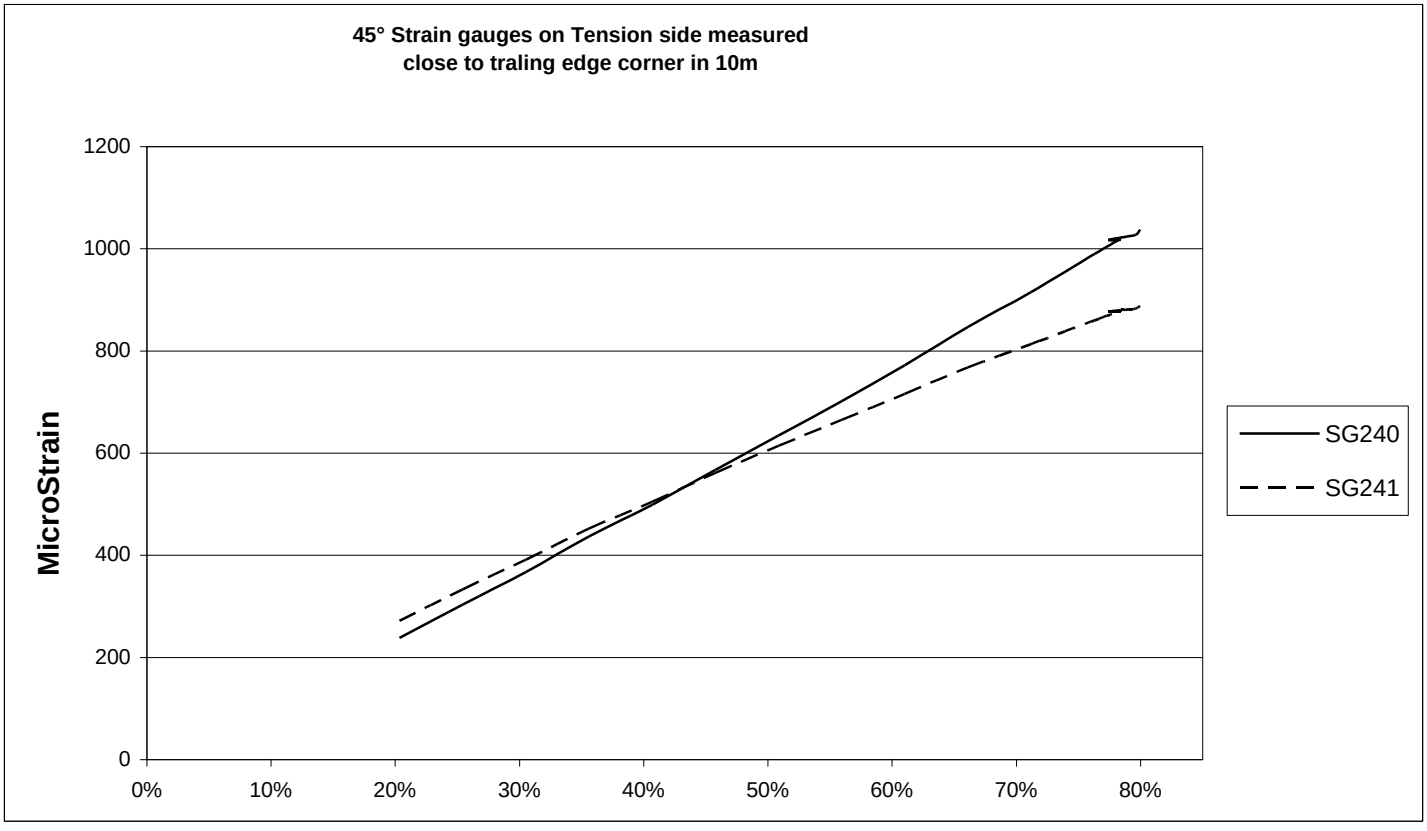
45° Strain gauges on Tension side measured
close to traling edge corner in 10m
MicroStrain
1200
1000
800
600
400
200
0
0%
10%
20%
30%
40%
50%
60%
70%
80%
SG240
SG241

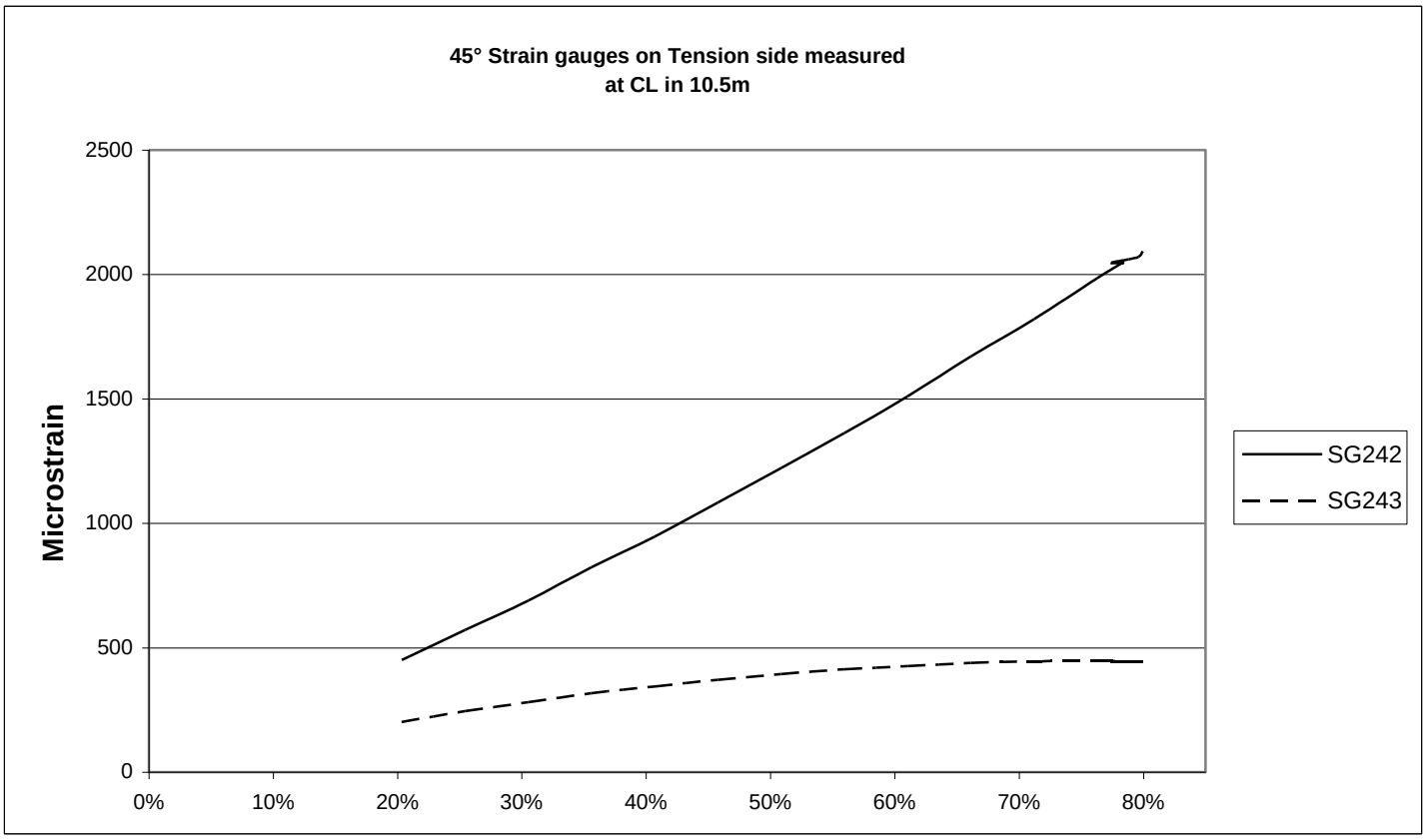
45° Strain gauges on Tension side measured
at CL in 10.5m
Microstrain
2500
2000
1500
1000
500
0
0%
10%
20%
30%
40%
50%
60%
70%
80%
SG242
SG243

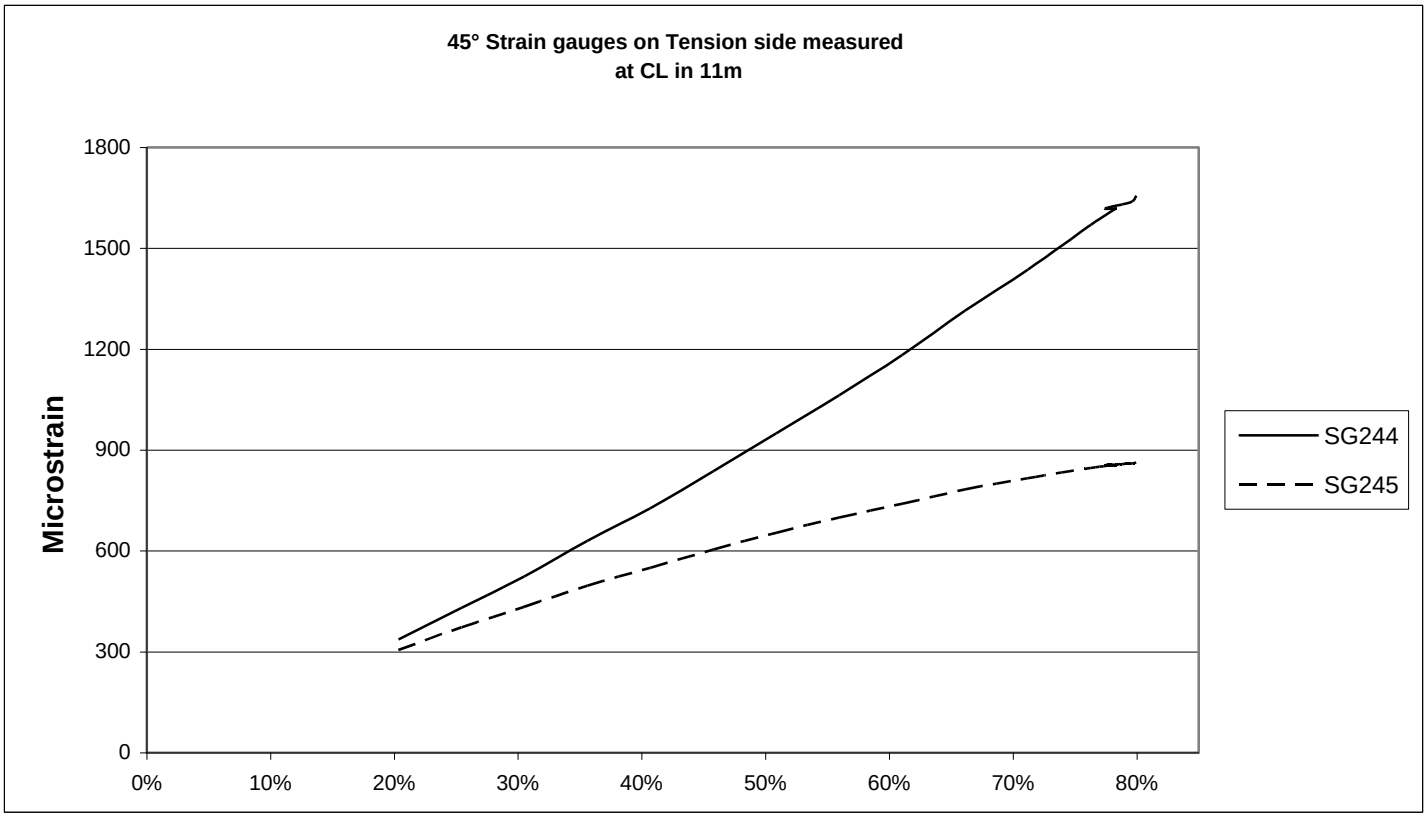
45° Strain gauges on Tension side measured
at CL in 11m
Microstrain
1800
1500
1200
900
600
300
0
0%
10%
20%
30%
40%
50%
60%
70%
80%
SG244
SG245

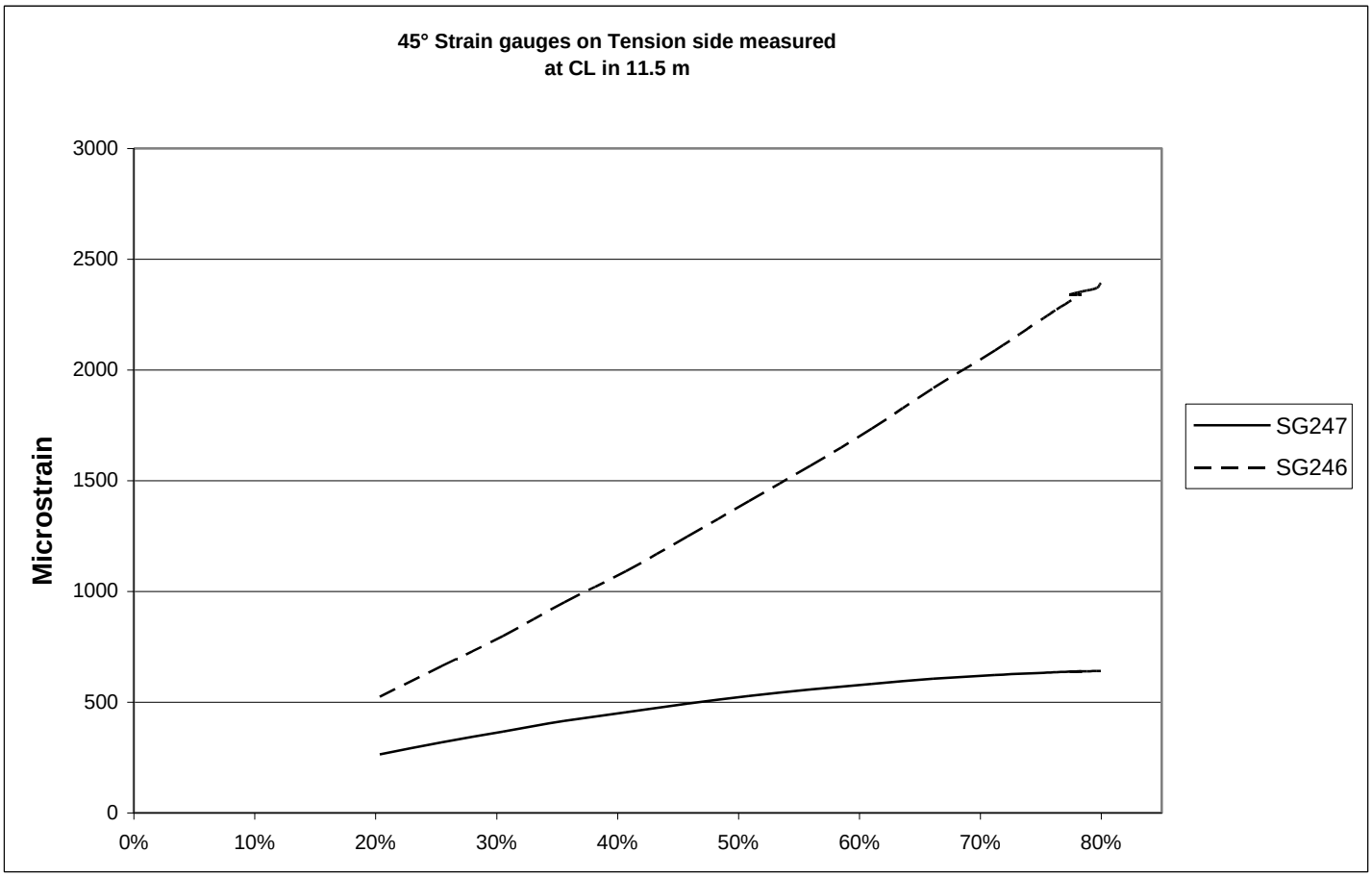
45° Strain gauges on Tension side measured
at CL in 11.5 m
Microstrain
3000
2500
2000
1500
1000
500
0
0%
10%
20%
30%
40%
50%
60%
70%
80%
SG247
SG246

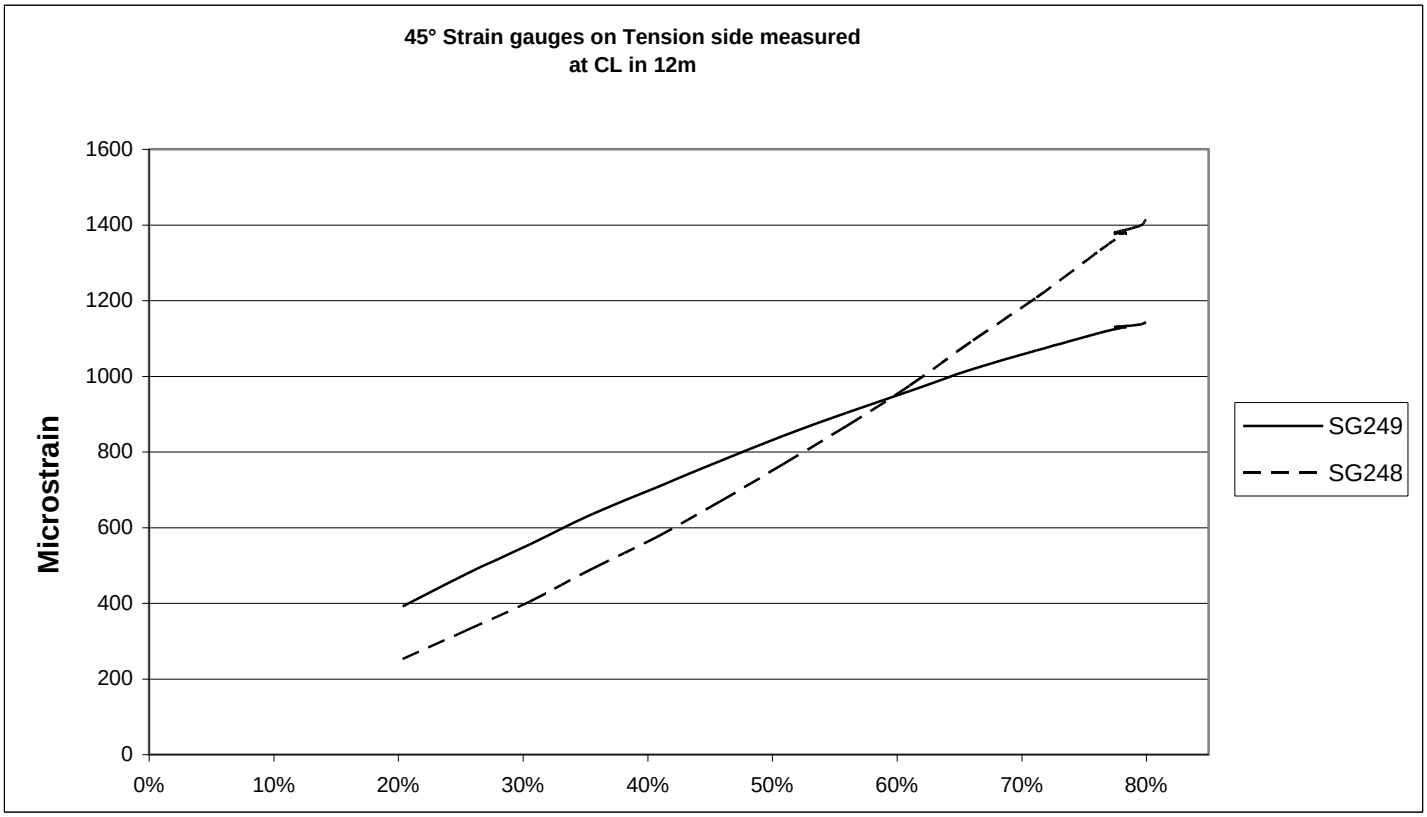
45° Strain gauges on Tension side measured
at CL in 12m
Microstrain
1600
1400
1200
1000
800
600
400
200
0
0%
10%
20%
30%
40%
50%
60%
70%
80%
SG249
SG248

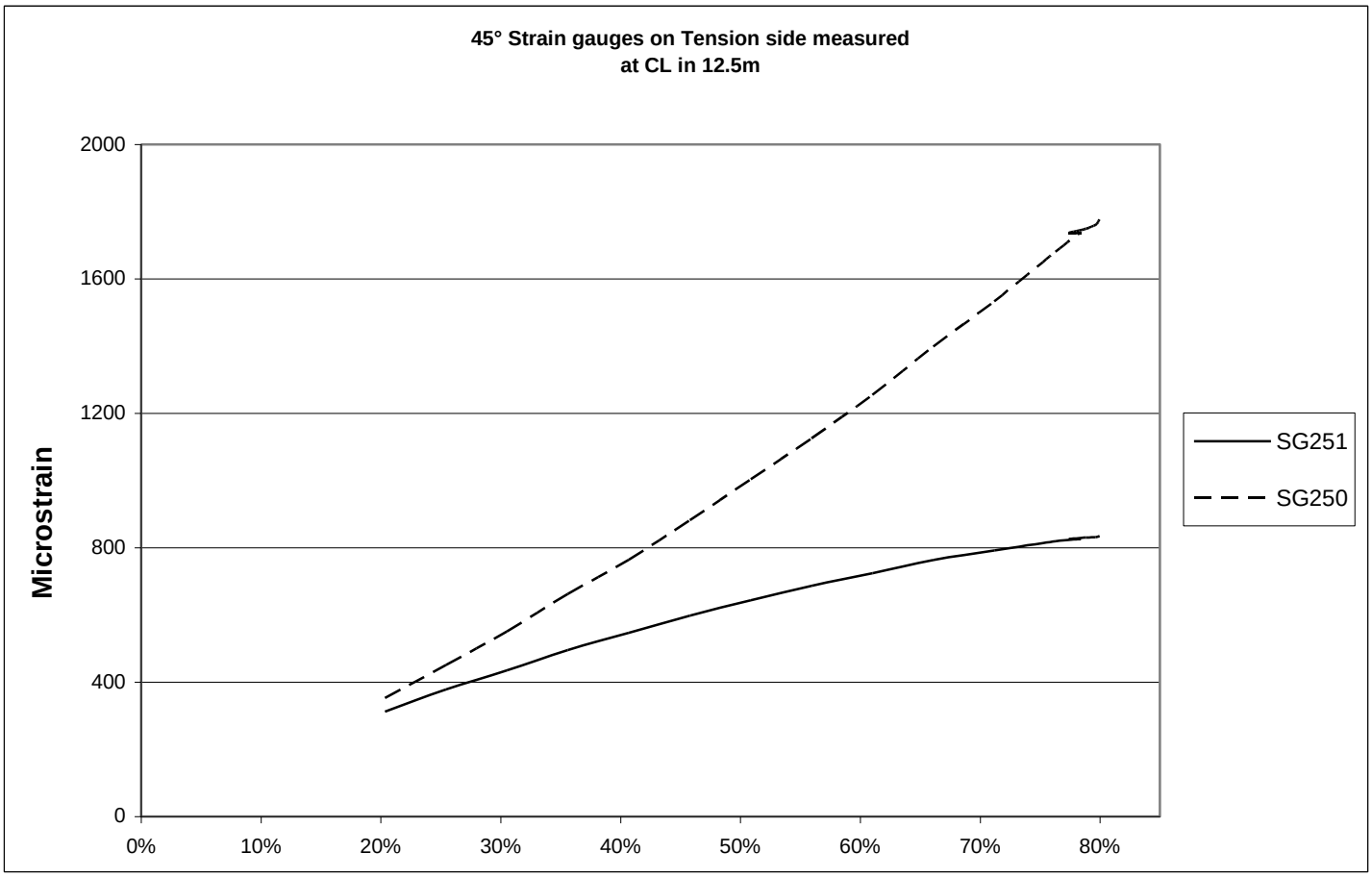
45° Strain gauges on Tension side measured
at CL in 12.5m
Microstrain
2000
1600
1200
800
400
0
0%
10%
20%
30%
40%
50%
60%
70%
80%
SG251
SG250

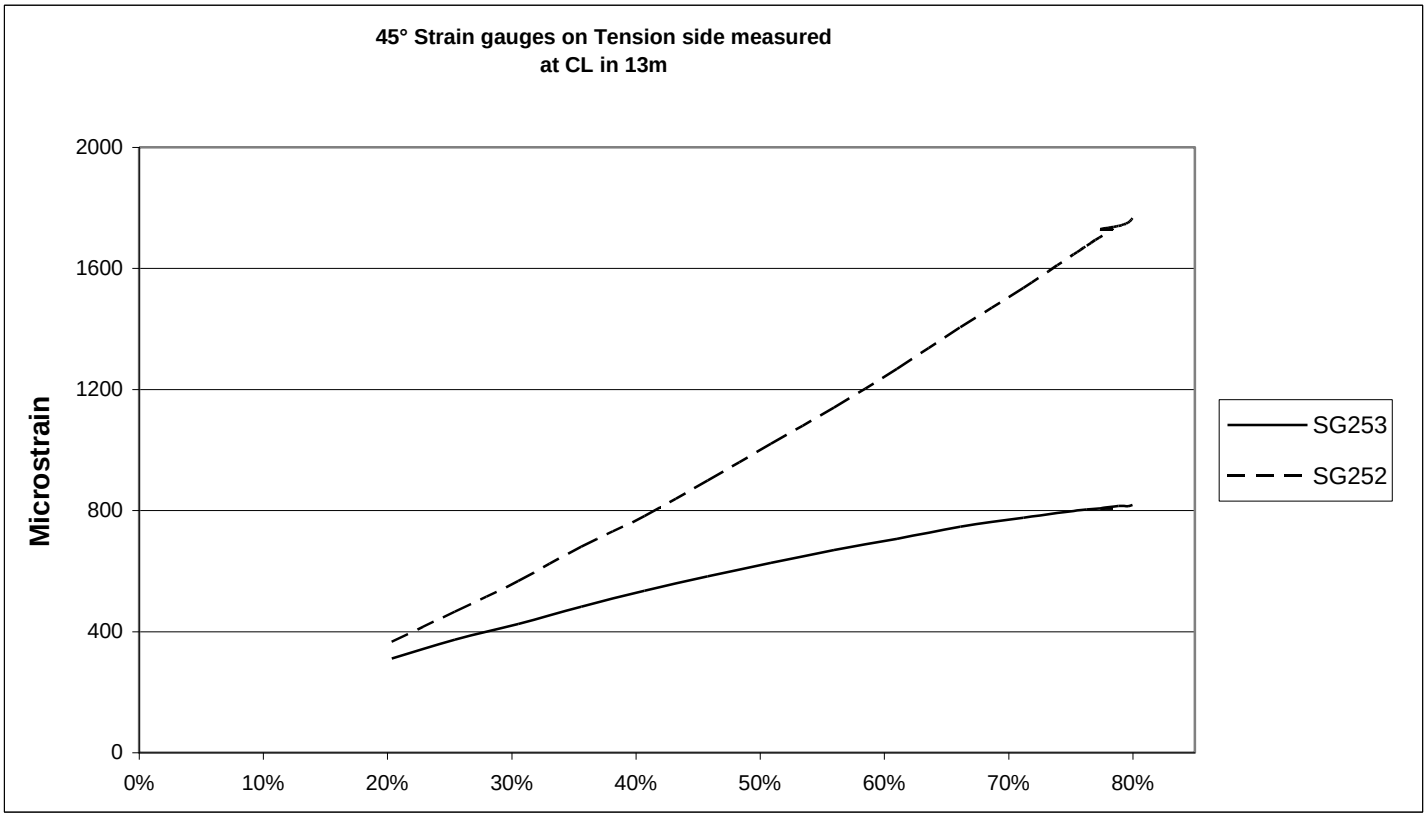
45° Strain gauges on Tension side measured
at CL in 13m
Microstrain
2000
1600
1200
800
400
0
0%
10%
20%
30%
40%
50%
60%
70%
80%
SG253
SG252

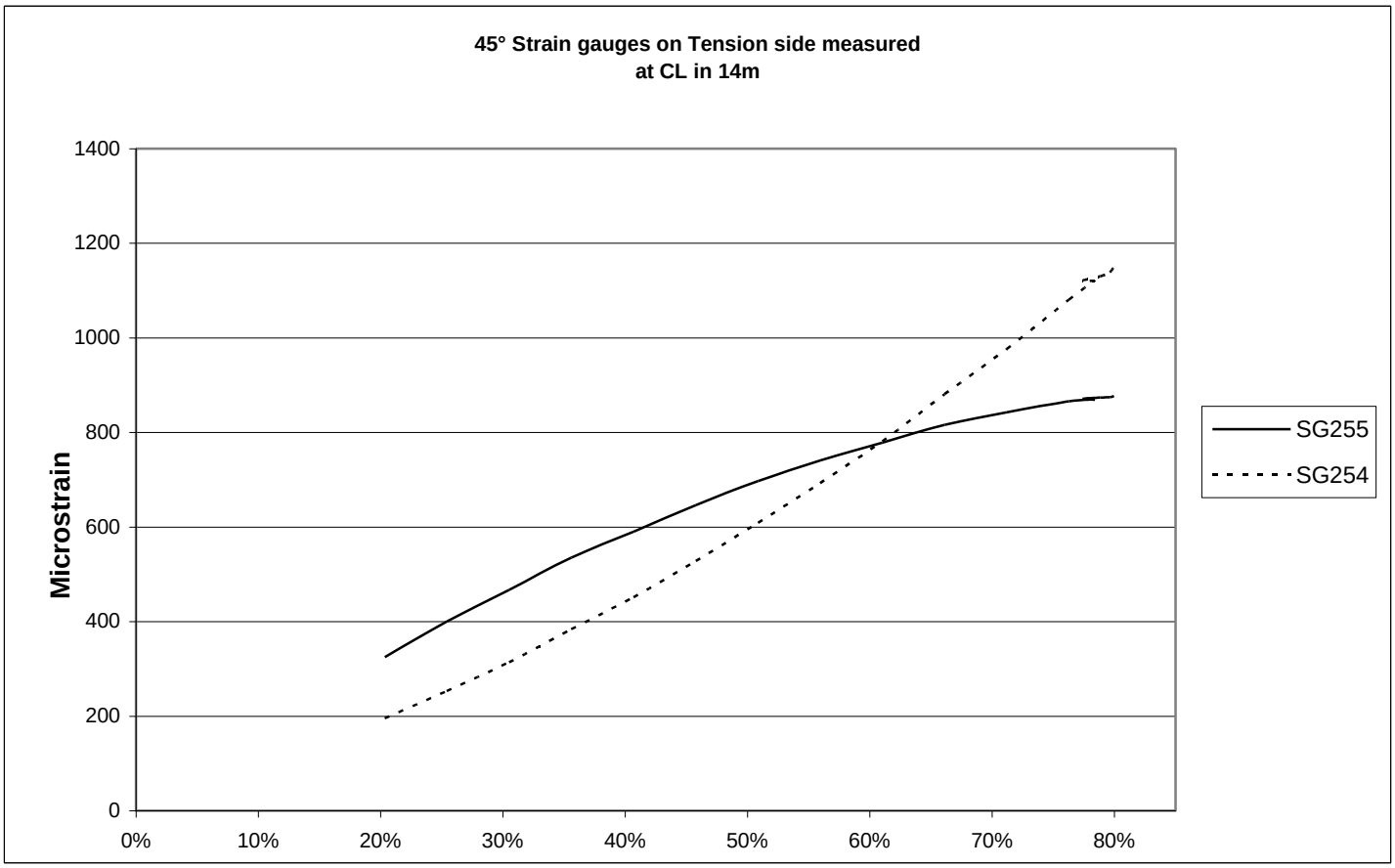
45° Strain gauges on Tension side measured
at CL in 14m
Microstrain
1400
1200
1000
800
600
400
200
0
0%
10%
20%
30%
40%
50%
60%
70%
80%
SG255
SG254

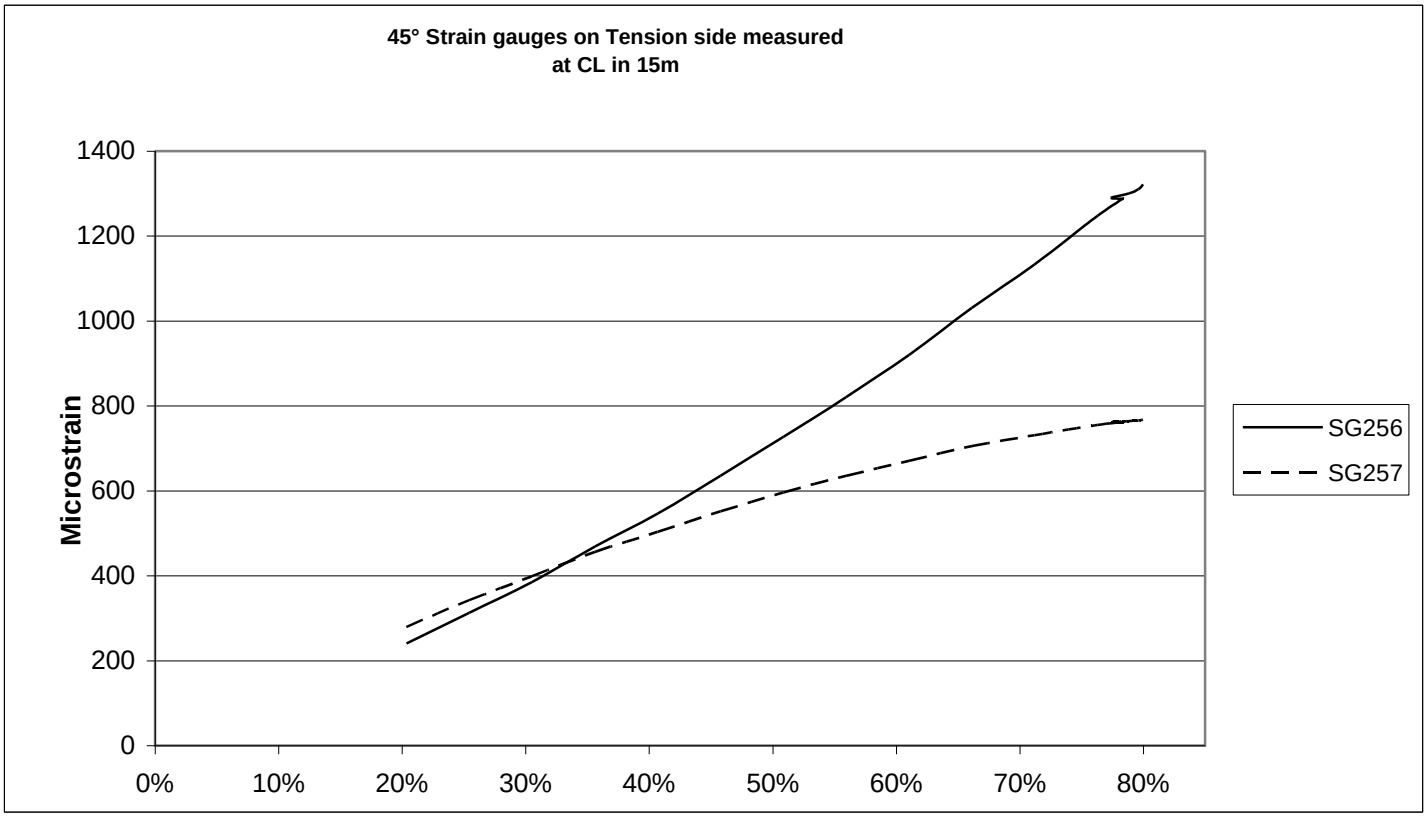
45° Strain gauges on Tension side measured
at CL in 15m
Microstrain
1400
1200
1000
800
600
400
200
0
0%
10%
20%
30%
40%
50%
60%
70%
80%
SG256
SG257

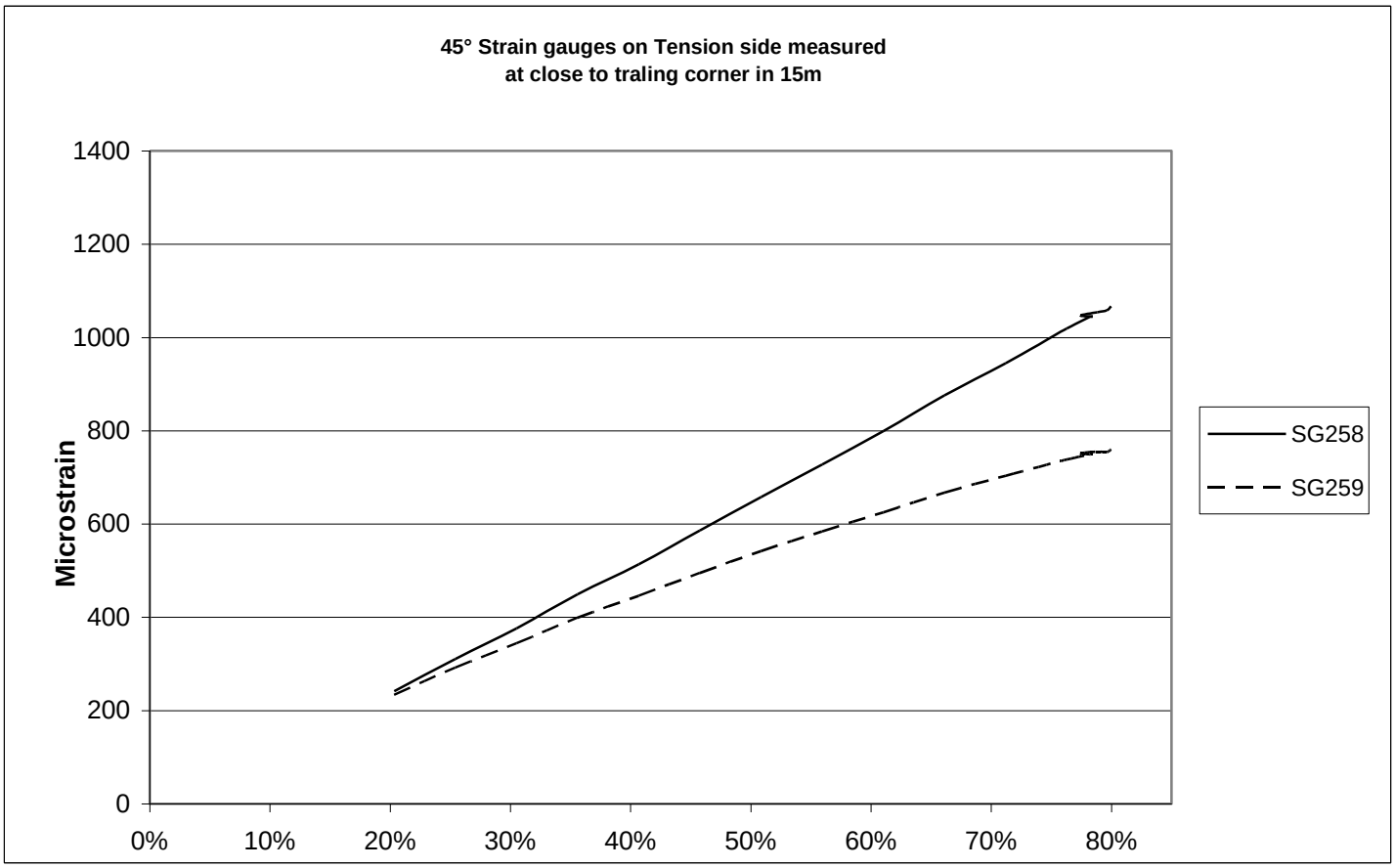
45° Strain gauges on Tension side measured
at close to traling corner in 15m
Microstrain
1400
1200
1000
800
600
400
200
0
0%
10%
20%
30%
40%
50%
60%
70%
80%
SG258
SG259

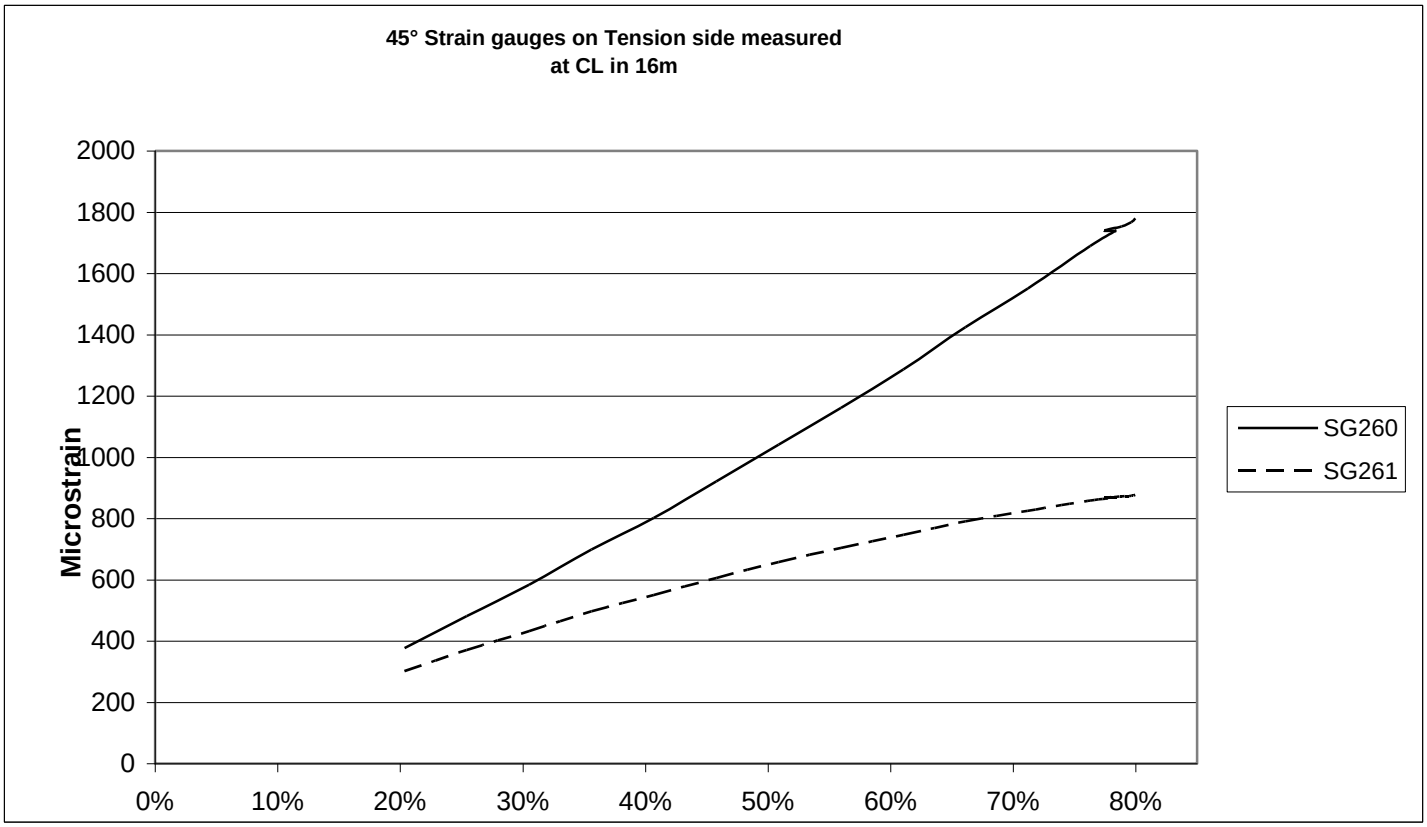
45° Strain gauges on Tension side measured
at CL in 16m
Microstrain
2000
1800
1600
1400
1200
1000
800
600
400
200
0
0%
10%
20%
30%
40%
50%
60%
70%
80%
SG260
SG261

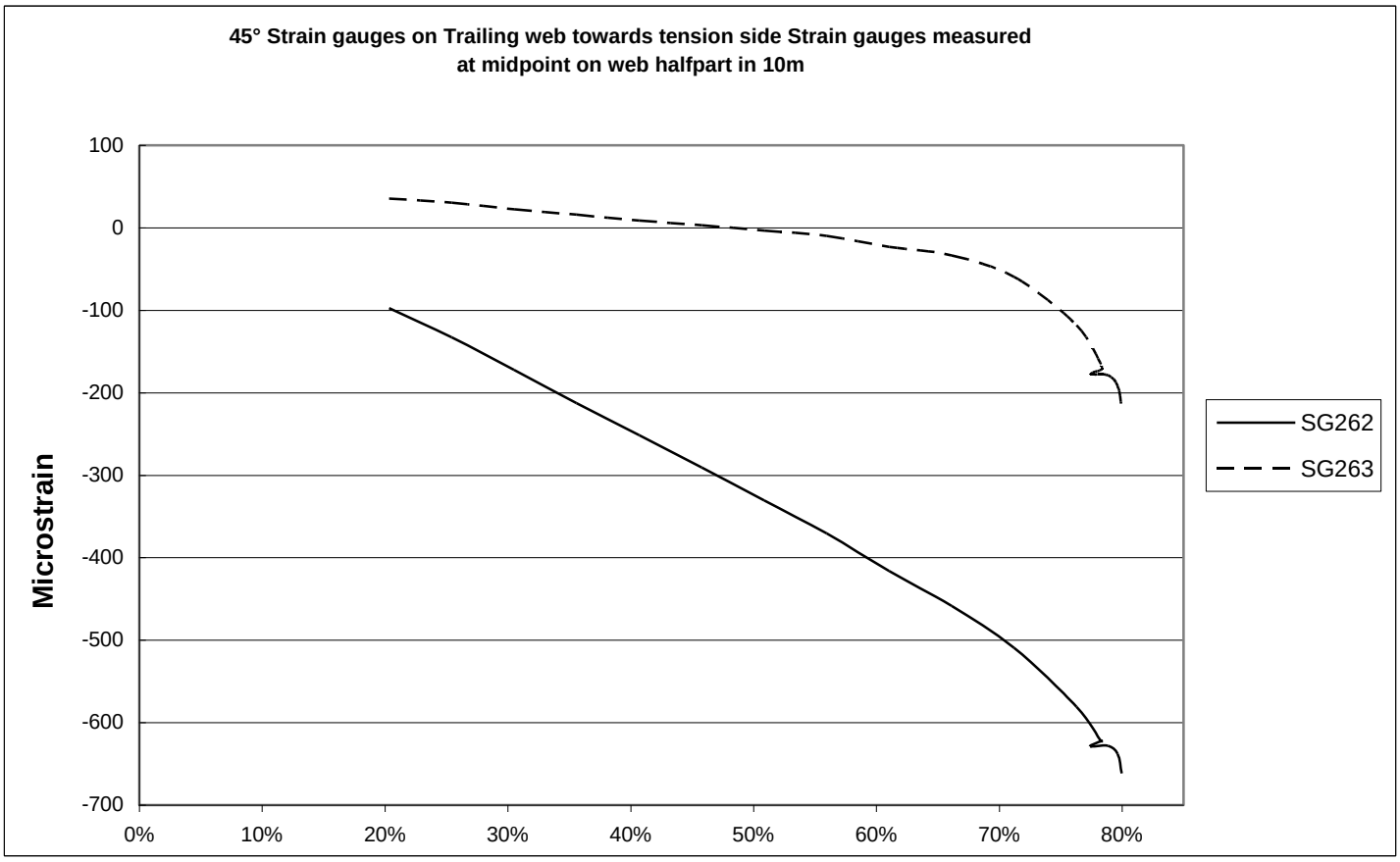
45° Strain gauges on Trailing web towards tension side Strain gauges measured at midpoint on web halfpart in 10m
Microstrain
100
0
-100
-200
-300
-400
-500
-600
-700
0%
10%
20%
30%
40%
50%
60%
70%
80%
SG262
SG263

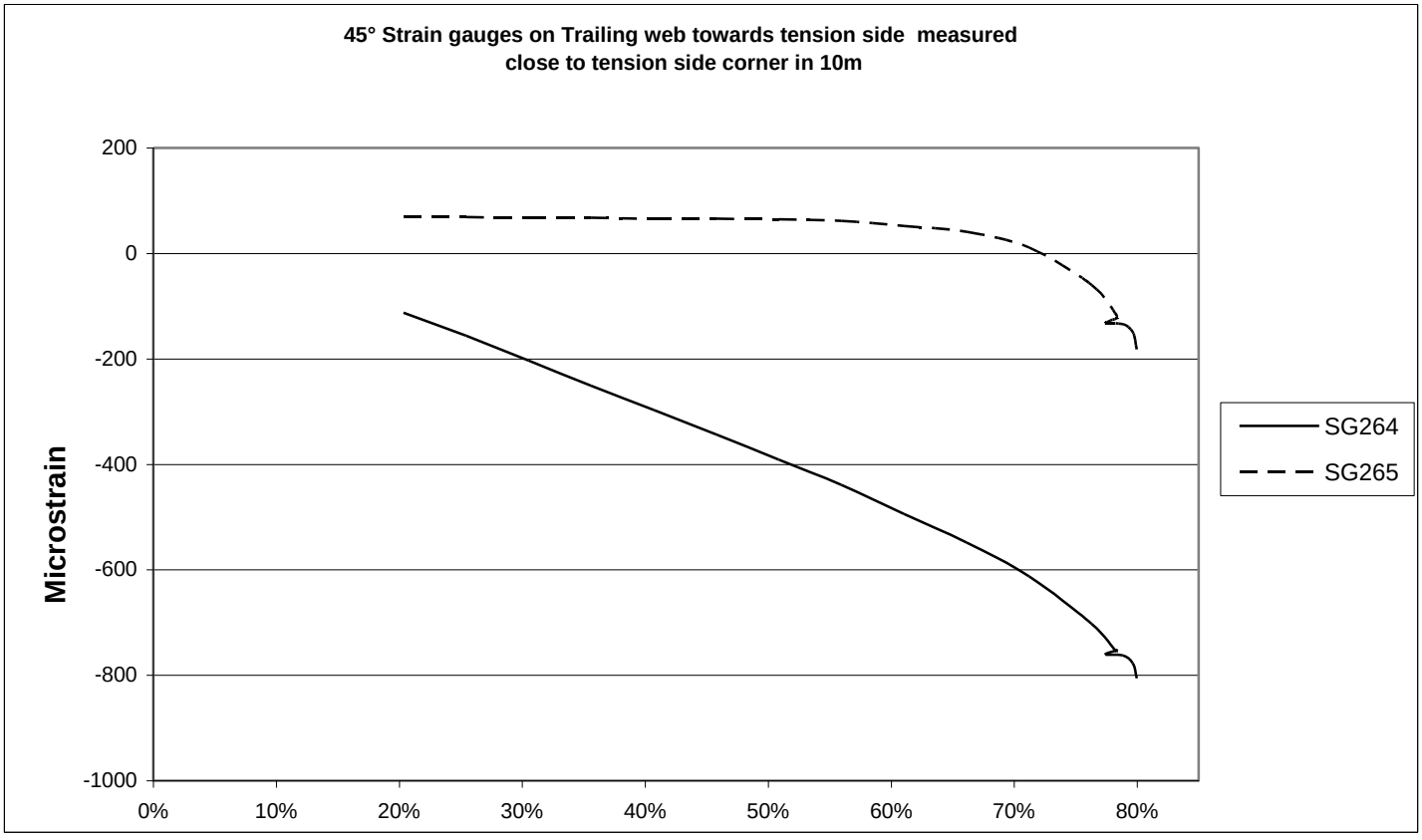
45° Strain gauges on Trailing web towards tension side measured close to tension side corner in 10m
Microstrain
200
0
-200
-400
-600
-800
-1000
0%
10%
20%
30%
40%
50%
60%
70%
80%
SG264
SG265

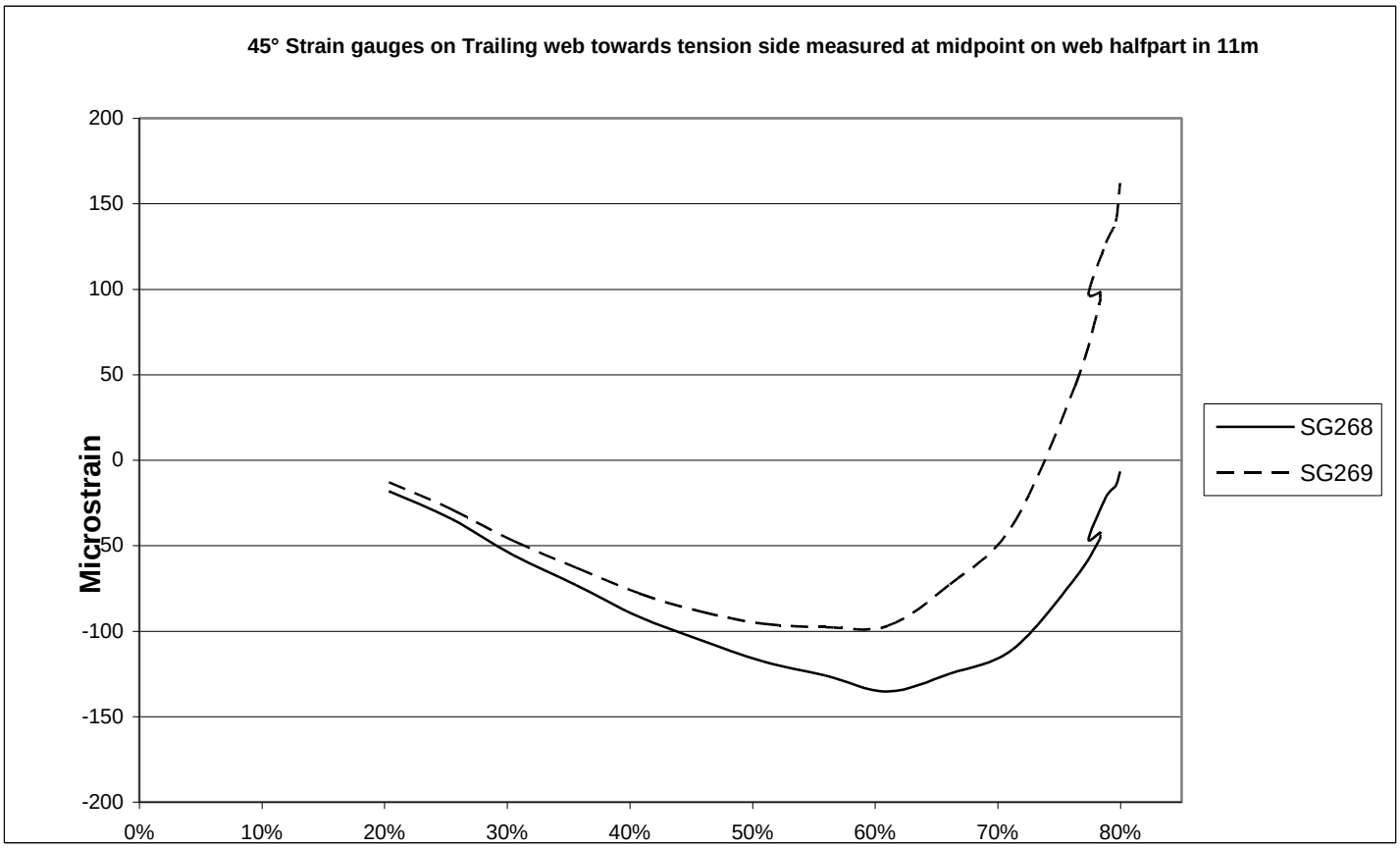
45° Strain gauges on Trailing web towards tension side measured at midpoint on web halfpart in 11m
Microstrain
200
150
100
50
0
-50
-100
-150
-200
0%
10%
20%
30%
40%
50%
60%
70%
80%
SG268
SG269

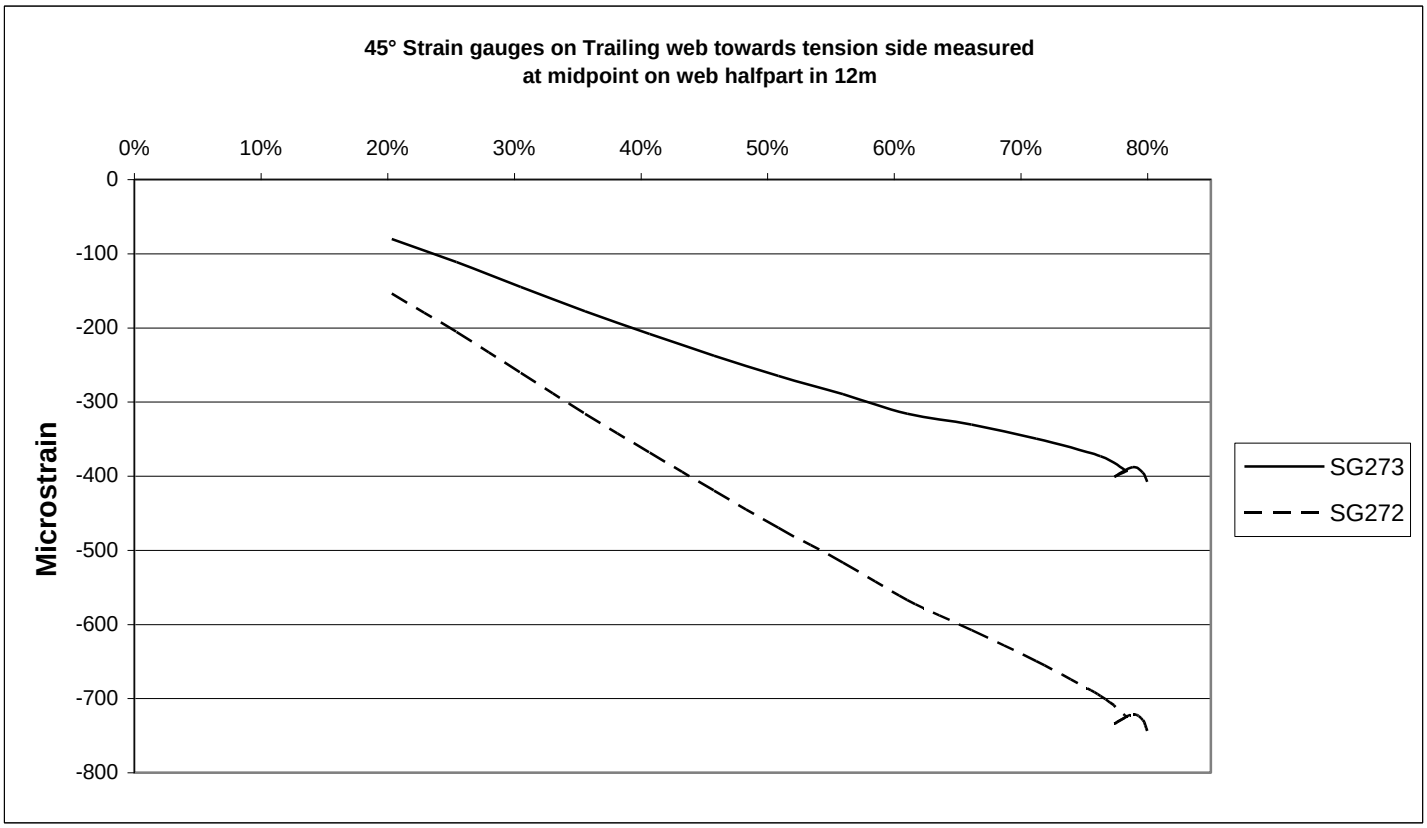
45° Strain gauges on Trailing web towards tension side measured at midpoint on web halfpart in 12m
Microstrain
0%
10%
20%
30%
40%
50%
60%
70%
80%
0
-100
-200
-300
-400
-500
-600
-700
-800
SG273
SG272

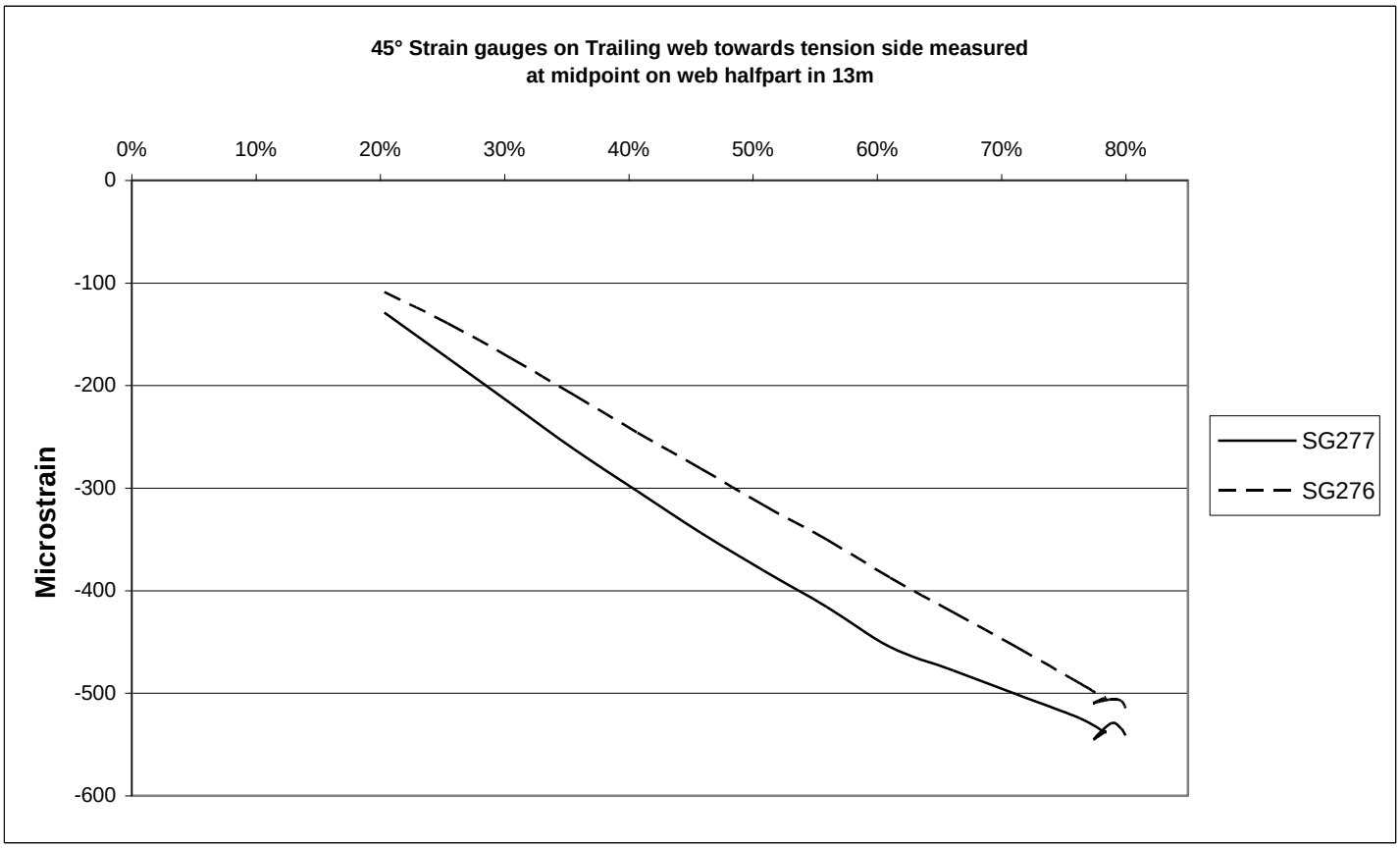
45° Strain gauges on Trailing web towards tension side measured
at midpoint on web halfpart in 13m
0%
10%
20%
30%
40%
50%
60%
70%
80%
0
-100
-200
-300
-400
-500
-600
Microstrain
SG277
SG276

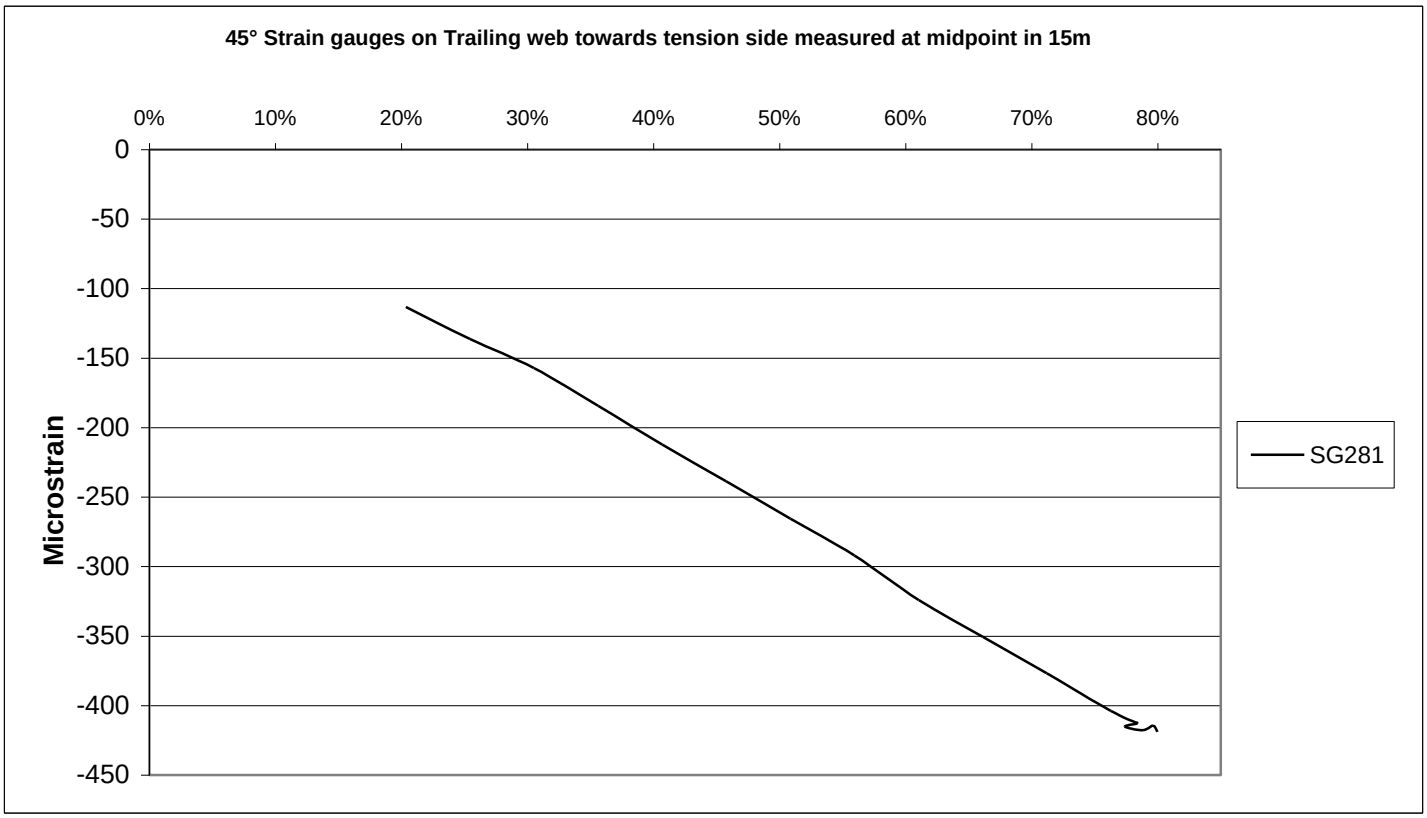
45° Strain gauges on Trailing web towards tension side measured at midpoint in 15m
0%
10%
20%
30%
40%
50%
60%
70%
80%
0
-50
-100
-150
-200
-250
-300
-350
-400
-450
Microstrain
SG281

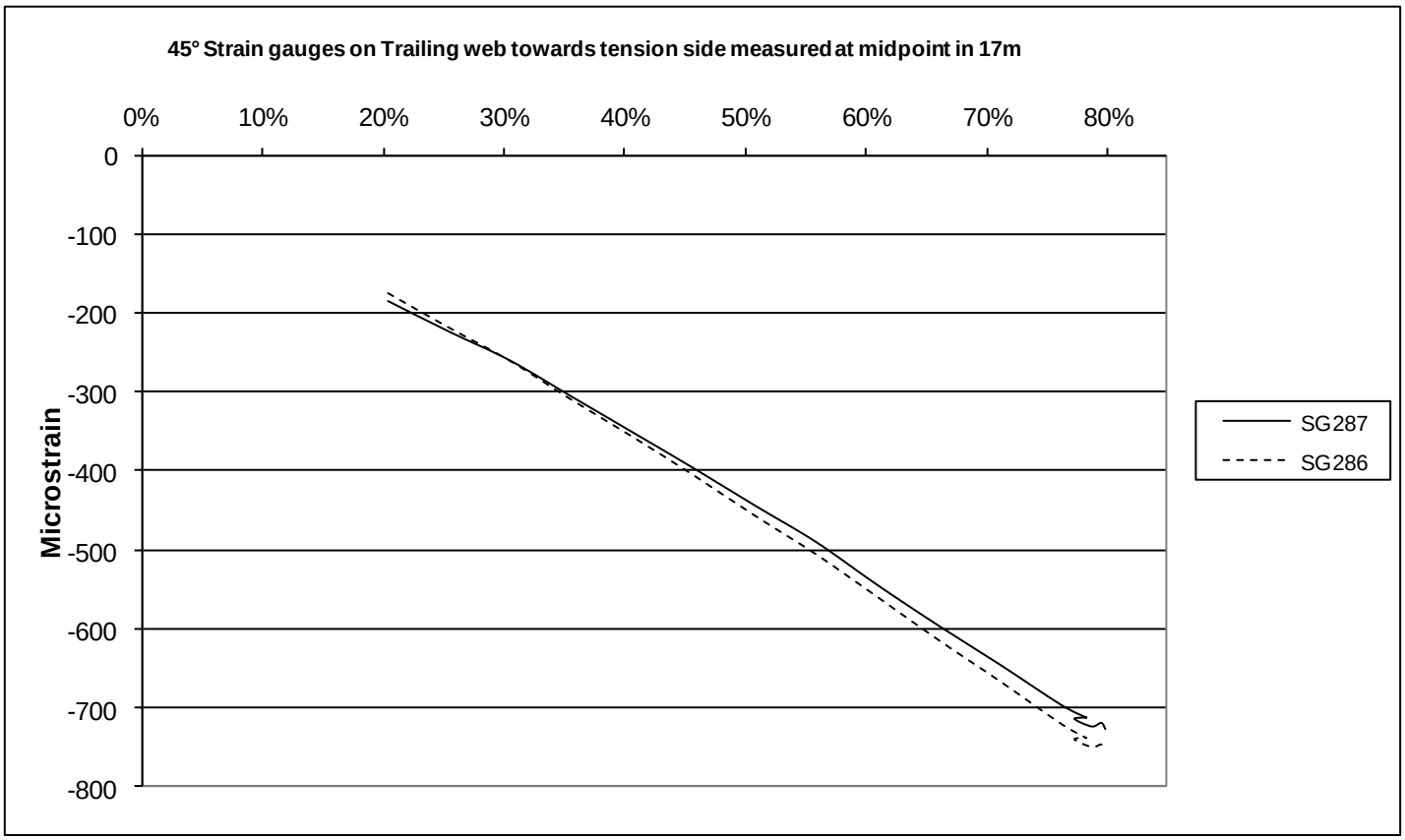
45° Strain gauges on Trailing web towards tension side measured at midpoint in 17m
0%
10%
20%
30%
40%
50%
60%
70%
80%
0
-100
-200
-300
-400
-500
-600
-700
-800
Microstrain
SG287
SG286

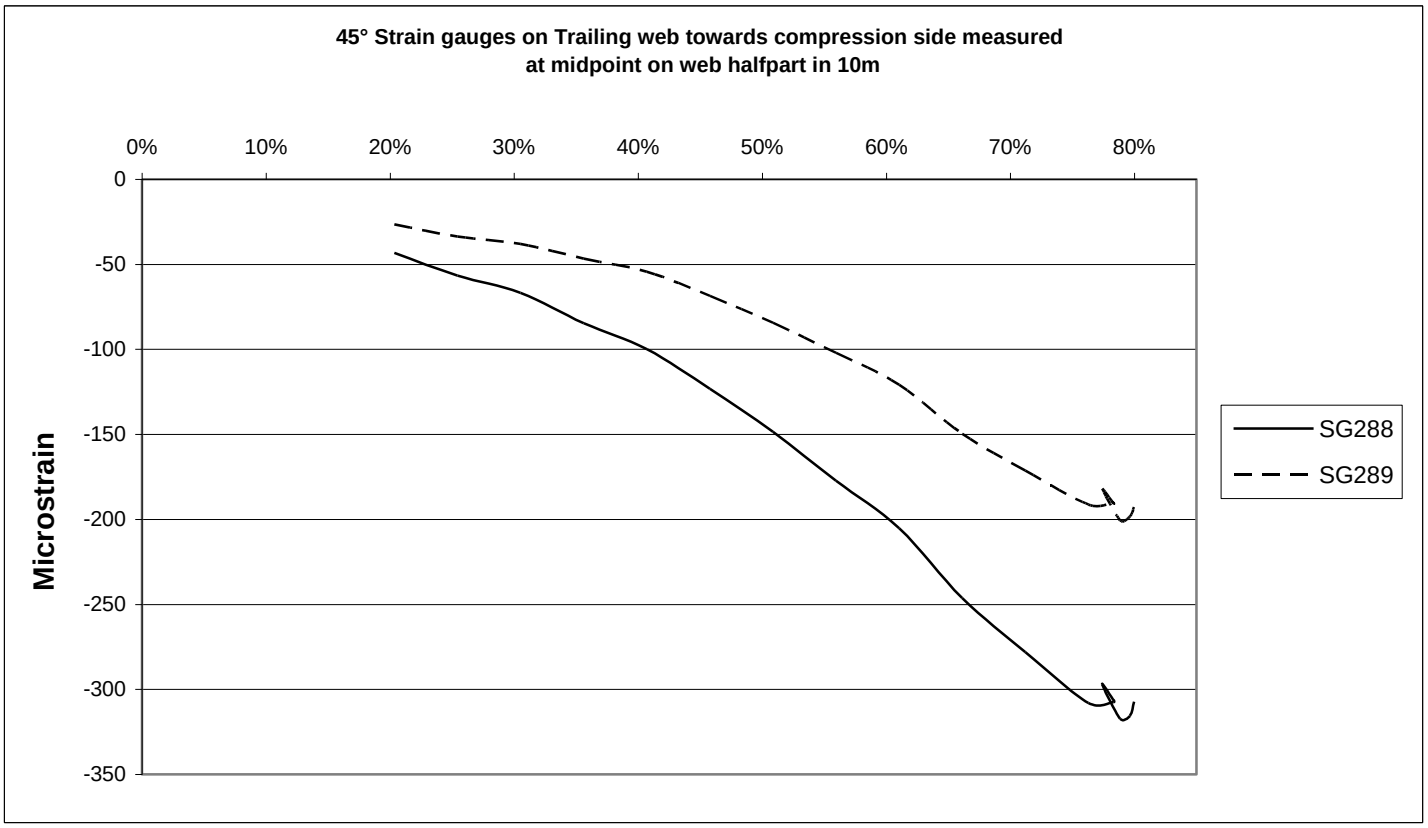
45° Strain gauges on Trailing web towards compression side measured
at midpoint on web halfpart in 10m
0%
10%
20%
30%
40%
50%
60%
70%
80%
0
-50
-100
-150
-200
-250
-300
-350
Microstrain
SG288
SG289

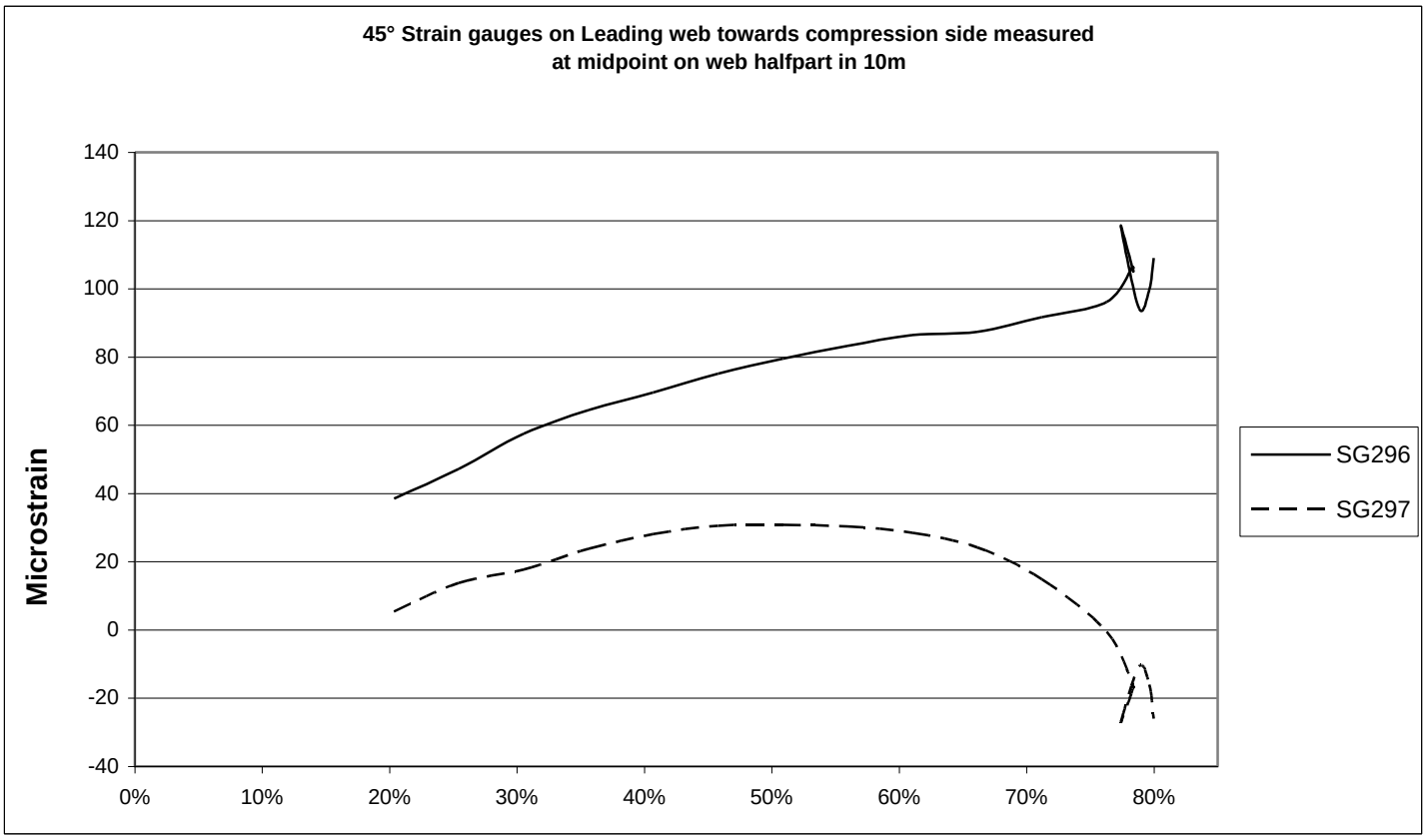
45° Strain gauges on Leading web towards compression side measured at midpoint on web halfpart in 10m
Microstrain
140
120
100
80
60
40
20
0
-20
-40
0%
10%
20%
30%
40%
50%
60%
70%
80%
SG296
SG297

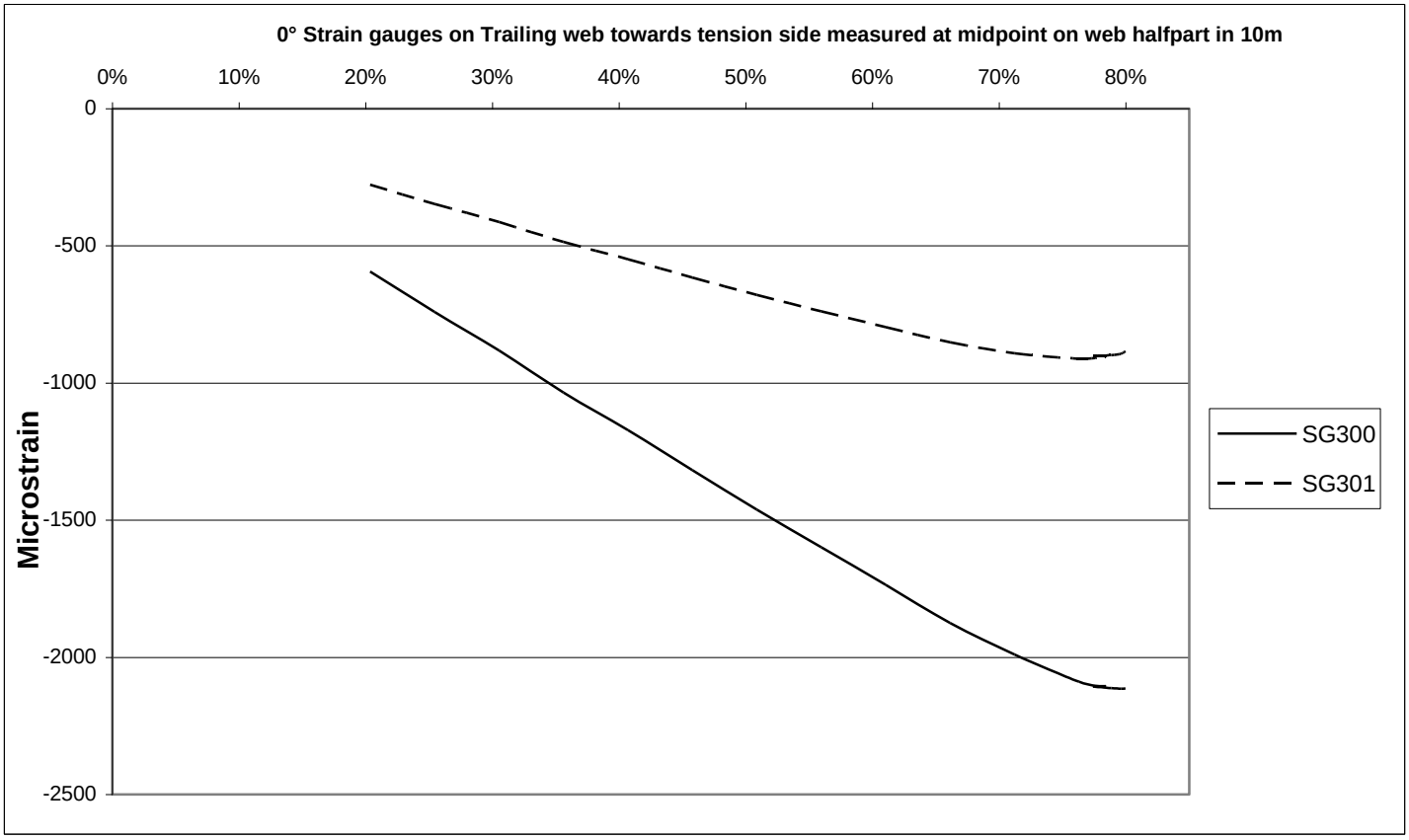
0° Strain gauges on Trailing web towards tension side measured at midpoint on web halfpart in 10m
Microstrain
0%
10%
20%
30%
40%
50%
60%
70%
80%
0
-500
-1000
-1500
-2000
-2500
SG300
SG301